
Geohydraulic Characterisation of Fractured Rock Flow Regimes

Regional Studies in Granite (Lindau, Black Forest, Germany) and Dolomite
(Tsumeb Aquifers, Northern Namibia)

Zur Erlangung des akademischen Grades
eines Doktors der Naturwissenschaften
an der Fakultät für Bauingenieur-, Geo- und Umweltwissenschaften
der Universität Karlsruhe (TH)
genehmigte

DISSERTATION

von
Dipl.-Hydrol. Roland Bäumle
aus Kehl

Karlsruhe 2003

Tag der mündlichen Prüfung: 05. Feb. 2003

Referent: Prof. Dr. Heinz Hötzl, Universität Karlsruhe (TH)

Korreferent: PD Dr. Thomas Himmelsbach, BGR Hannover

Geohydraulic Characterisation of Fractured Rock Flow Regimes
Regional Studies in Granite (Lindau, Black Forest, Germany) and
Dolomite (Tsumeb Aquifers, Northern Namibia)

Doctorate Thesis
by Roland Bäumlé

Windhoek, 05 February 2003

SUMMARY

The fundamental problem related to the characterisation of the regional groundwater flow in fractured rock is based on the difficulties in identifying and characterising hydraulically significant fractures on a regional scale. In this thesis, various geohydraulic approaches were applied in order to investigate the regional groundwater flow regime in two different fractured rock aquifers. The synthesis of the results from different geohydraulic methods is an important aspect and constitutes the principal methodological approach of this investigation. The case studies include fractured rock aquifers in Southwest Germany and Namibia. The Lindau fractured rock test site is situated within the north-eastern part of a granitic pluton in the Southern Black Forest. The Tsumeb Aquifers are located in the Otavi Mountainland, a dolomite rock massif that hosts one of the most valuable groundwater resources of northern Namibia.

The following five different geohydraulic methods were applied in the regional case studies: well hydrograph recession analysis, hydraulic tests, groundwater tracer techniques, hydrochemical investigations and groundwater modelling. The thesis includes a description of the state-of-the-art for each method and suggestions for further improvement of the analysis techniques. The applicability of each method to describe the flow pattern was assessed separately for each investigation area. The investigations resulted in the development of conceptual hydrogeological models for the fractured aquifers.

The study focuses on the assessment of the hydraulic impact of dominant fault and dyke structures, the regional distribution of different aquifer systems and the quantification of groundwater flow parameters. As the aquifers in both studies are characterised by a low primary porosity of the host rock the groundwater flow is mainly restricted to fractures, which are only abundant along dykes, faults and contact zones. The role of intrusive dykes and faults as conduits of groundwater flow could be demonstrated for both sites.

A highly permeable vertical dyke zone largely influences the groundwater flow pattern at Lindau. The ore dyke intersects the surrounding granite that has a much lower permeability. A drainage experiment was carried out in order to assess the hydraulic impact of the dyke on the regional groundwater flow. The groundwater system was artificially drained over a period of almost 14 months by opening a tapped borehole located in the observation tunnel. This borehole intersects the dyke some 80 m below the ground surface. The analysis of the hydraulic response at the observation wells was combined with the results of hydrochemical investigations and tracer tests. The results of the investigations were used to delineate the subterranean catchment of the dyke.

In addition, a well hydrograph recession analysis was performed at Lindau. This analysis, originally developed for streamflow and subsequently adopted for the evaluation of spring discharge and groundwater levels in karst aquifers, was for the first time applied to groundwater level data from wells in granitic rock. The analysis proved to be an effective tool to obtain a regional distribution of the mean residence time and the permeability of the rock from groundwater level data.

The presented study of the Tsumeb Aquifers included hydraulic testing and the development of a numerical groundwater flow model. It was an integral part of the comprehensive hydrogeological investigation program carried out in the framework of the *Tsumeb Groundwater Study*. The Tsumeb Aquifers proved to be one of the potential additional sources to meet the growing water demand of the Central Area of Namibia. The 3-D Tsumeb groundwater model has been established as a tool for the assessment of the groundwater resources and provided essential information for the establishment of environmentally sustainable groundwater management. As a result of this study, the regional groundwater potential of the area could be quantified for the first time. The groundwater model revealed the eminent importance of the dolomitic outcrops of the Otavi Mountainland for the replenishment of the groundwater resources.

KURZFASSUNG

Eines der Hauptprobleme bei der Charakterisierung der Grundwasserströmung im Festgestein beruht auf der Schwierigkeit, hydraulisch wirksame Klüfte zu identifizieren und deren räumliche Verbreitung und physikalische Eigenschaften zu ermitteln. Die vorliegende Forschungsarbeit beschreibt die Untersuchung der regionalen Grundwasserströmungsverhältnisse zweier Festgesteinsaquifere mittels unterschiedlicher geohydraulischer Ansätze. Die Synthese der Ergebnisse anhand der verschiedenen Methoden bildet den Schwerpunkt der Studie. Als Modellgebiete wurden Festgesteinsaquifere im nördlichen Teil Namibias und Südwestdeutschland ausgewählt. Dabei handelt es sich um das im südlichen Schwarzwald gelegene Felslabor Lindau, das sich im nordöstlichen Teil eines Granitplutons befindet, sowie das Tsumeb-Karstgebiet, ein dolomitisches Bergmassiv, das eines der bedeutendsten Grundwasservorkommen Namibias beherbergt.

In dieser Arbeit wurden fünf verschiedene geohydraulische Methoden angewandt: Grundwasserganglinienseparation, hydraulische Versuche, Grundwassermarkierungstechniken, hydrochemische Untersuchungen sowie eine Grundwassermodellierung. Die Arbeit enthält eine Zusammenfassung über den Stand der Forschung der Methoden und Vorschläge zur Optimierung der Auswertetechniken. Die Eignung der jeweiligen Methode zur Beschreibung der Strömungsverhältnisse wurde für beide Untersuchungsgebiete getrennt bewertet. Anhand der Ergebnisse der einzelnen Methoden erfolgte für jedes Modellgebiet eine geohydraulische Charakterisierung der Grundwasserfließsysteme innerhalb des geklüfteten Gesteins. Diese diente als Basis für die Entwicklung konzeptioneller hydrogeologischer Modelle für die Aquifere.

Schwerpunkte der Untersuchungen lagen in der Bewertung des hydraulischen Einflusses von dominierenden Störungssystemen und Gangstrukturen und in der Bestimmung der regionalen Verteilung verschiedener Grundwasserleiter. Da das Gebirge in beiden Untersuchungsgebieten eine geringe primäre Porosität besitzt, ist die Grundwasserströmung im wesentlichen auf Klüfte begrenzt, die hauptsächlich entlang von Erzgängen, Störungszonen und Kontaktbereichen auftreten. In beiden Fallstudien fungieren die intrusiven Erzgänge und Störungszonen nachweislich als präferentielle Fließwege.

Die Grundwasserströmung in Lindau wird maßgeblich durch einen hochdurchlässigen vertikalen Erzgang beeinflusst, der in das weitaus geringer durchlässige Granitgestein intrudierte. Mit Hilfe eines Drainage- Experimentes wurde der hydraulische Einfluss dieser Störungzone auf die Grundwasserströmung untersucht. Der Grundwasserleiter wurde dabei über einen Zeitraum von annähernd 14 Monaten durch Öffnen eines im Beobachtungstunnel gelegenen Bohrlochs künstlich drainiert. Dieses Bohrloch erschließt den Erzgang in ungefähr 80 m unterhalb der Geländeoberfläche. Die Auswertung der hydraulischen Reaktion an den Beobachtungsbohrlöchern wurde mit den Resultaten der Grundwassermarkierungsversuche und hydrochemischer Untersuchungen kombiniert. Anhand dieser Ergebnisse konnten die Grenzen des hydraulischen Einflusses des Erzganges bestimmt werden.

Darüber hinaus wurden in Lindau Rezessionsanalysen an Grundwasserganglinien durchgeführt. Dieses Verfahren, das ursprünglich für Oberflächenabfluss entwickelt und später auf die Auswertung von Trockenwetterfalllinien von Quellschüttungen und Grundwasserganglinien im Karst ausgedehnt wurde, wurde erstmalig für die Auswertung von Grundwasserganglinien in Granitgestein eingesetzt. Es konnte gezeigt werden, dass sich das Verfahren zur Bestimmung der regionalen Verteilung der mittleren Verweilzeiten des Grundwassers und der Gebirgsdurchlässigkeit eignet.

Die vorgestellte Studie der Tsumeb- Grundwasserleiter umfasst hydraulische Versuche und die Entwicklung eines numerischen Grundwassermodells. Die Untersuchung war Bestandteil eines umfassenden hydrogeologischen Untersuchungsprogramms im Rahmen der sogenannten *Tsumeb Groundwater Study*. Die Tsumeb- Grundwasserleiter haben sich als einer der potentiellen zusätzlichen Quellen herausgestellt, die den wachsenden Bedarf an Wasser in den zentralen Regionen Namibias in Zukunft decken könnte. Im Rahmen dieser Studie konnte das Grundwasserdargebot dieses Gebietes zum ersten Mal quantifiziert werden. Das entwickelte dreidimensionale Grundwassermodell ermöglicht eine nachhaltige Bewirtschaftung des Grundwasservorkommens. Es verdeutlicht zudem die herausragende Bedeutung der anstehenden Dolomite innerhalb des Otavi- Berglandes in Bezug auf die Erneuerung dieser Grundwasserressource.

ACKNOWLEDGEMENTS

This study was carried out in the framework of the on-going research program of the Hydrogeology Section at the Department of Applied Geology (University of Karlsruhe, TH) focussing on flow and transport processes in fractured rock aquifers. The study at the Lindau fractured rock test site was an integral part of the graduate program *Ökologische Wasserwirtschaft* at the University of Karlsruhe. This interdisciplinary program facilitated by the German Science Foundation (DFG) offered me a scholarship over a period of three years and provided funds for field trips and technical equipment. The Tsumeb Groundwater Study was mutually funded by the Namibia Water Corporation Ltd (NamWater), the Ministry of Agriculture, Water and Rural Development of Namibia (MAWRD) and the German Federal Ministry of Economic Cooperation and Development (BMZ), through the *Kreditanstalt für Wiederaufbau* (KfW).

I have received immense support during my research and not all that contributed to the successful completion of my thesis by means of scientific contributions, fruitful discussions or technical assistance can be listed individually. I would like to address my special thanks, however, to the following persons:

First, I would like to express my thanks to my promoter, Prof. Dr. Heinz Hötzel, for offering me the opportunity to carry out my research, for his continuous support and his amicable mentorship. I want to thank him particularly for his trust in my qualification when he appointed me to join the international group of experts of the Tsumeb Groundwater Study. He has also critically read this thesis and his valuable comments and suggestions are gratefully appreciated.

I would also like to thank my co-promoter, Dr. habil. Thomas Himmelsbach (*Bundesanstalt für Geowissenschaften und Rohstoffe*, Hannover) for his valuable comments and for supervising my work at Lindau and Tsumeb. I have greatly benefited from his extensive knowledge of the fractured rock system at Lindau and from his experience in developing conceptual hydrogeological models for complex geological set-ups. Our research assignments together in Namibia were just as pleasant as they were instructive.

My grateful thanks go to Mr. Greg Christelis from the Department of Water Affairs who, as an expert of the geology and hydrogeology of Namibia and a native speaker of English, thoroughly scrutinised my thesis and improved the English phrasing. His constructive comments and suggestions are very much appreciated and have been included.

Thanks to the whole team involved in the Tsumeb Groundwater Study, in particular Ralf Bufler, Arnold Bittner and Peter Ambs, for their encouraging and cheerful support during the study.

I would like to thank all my colleagues at the University of Karlsruhe for the frequent and productive discussions and their assistance during and with field and laboratory work. I would like to emphasise the contributions of Frank Reinert and Peter Witt to this study that carried out fieldwork under extreme weather conditions as part of their M.Sc. theses.

I also want to express my gratitude to the Department of Water Affairs under the Director of Resource Management, Mr. Piet Heyns for providing invaluable hydrogeological base data from former studies and the recent Tsumeb Groundwater Study. The Department of Water Affairs generously provided printing facilities.

I am grateful to my parents for supporting my academic education through all these years.

TABLE OF CONTENTS

1	INTRODUCTION	1
1.1	Problem statement.....	1
1.2	Investigation scope and targets	2
2	GEOHYDRAULIC METHODS	3
2.1	Methods for the geohydraulic characterisation of fractured rock aquifers.....	3
2.2	Well hydrograph analysis.....	3
2.2.1	<i>General concept</i>	3
2.2.2	<i>Determination of the mean residence time</i>	5
2.3	Hydraulic tests in fractured rock	8
2.3.1	<i>Overview and restrictions of hydraulic test procedures</i>	8
2.3.2	<i>Conceptual Models for fractured aquifer systems</i>	9
2.3.2.1	Homogeneously fractured, uniform aquifer	9
2.3.2.2	Double porosity concept	9
2.3.2.3	Single vertical fracture	10
2.3.2.4	Single horizontal fracture	13
2.3.3	<i>Aquifer test evaluation</i>	13
2.3.3.1	Diagnostic plots	13
2.3.3.2	Time-drawdown analysis	14
2.3.3.3	Recovery analysis.....	15
2.3.3.4	Bounded aquifers.....	16
2.4	Groundwater tracing techniques.....	16
2.4.1	<i>Principles of groundwater tracing</i>	16
2.4.2	<i>Analytical models</i>	17
2.4.2.1	Homogeneous aquifers.....	17
2.4.2.2	Aquifers with discrete fractures.....	18
2.4.2.3	Impact of non-instantaneous (retarded) injection	19
2.5	Hydrochemical and isotope studies	22
2.6	Groundwater modelling.....	23
3	TEST SITE DESCRIPTION	26
3.1	Lindau fractured rock test site.....	26
3.1.1	<i>Physiography</i>	26
3.1.2	<i>Climate</i>	27
3.1.3	<i>Geology</i>	28
3.1.4	<i>Hydrogeology</i>	29
3.1.5	<i>Hydrochemistry</i>	31
3.2	Tsumeb Aquifers.....	32
3.2.1	<i>Physiography</i>	32
3.2.2	<i>Climate</i>	33
3.2.3	<i>Geology</i>	36
3.2.4	<i>Hydrogeology</i>	42
3.2.5	<i>Hydrochemistry</i>	43
3.3	Comparison of the test sites	44

4 RESULTS.....	45
4.1 Lindau fractured rock test site.....	45
4.1.1 Well hydrograph recession analysis	45
4.1.2 Catchment drainage experiment.....	51
4.1.3 Hydrochemical study.....	63
4.1.4 Groundwater tracer tests	72
4.1.5 Classification of fractured aquifers.....	82
4.2 Tsumeb Aquifers.....	85
4.2.1 Hydraulic tests.....	85
4.2.2 Groundwater Model.....	93
4.2.2.1 General outline	93
4.2.2.2 Conceptual hydrogeological model.....	95
4.2.2.3 Model input data	100
4.2.2.4 Steady state calibration.....	104
4.2.2.5 Transient calibration.....	106
4.2.3 Assessing the groundwater potential.....	108
5 SUMMARY AND DISCUSSION	113
5.1 Assessment of potential and constraints of geohydraulic methods.....	113
5.2 Characteristics of fractured aquifers with dominant fault/dyke zones	116
5.3 Suggestions for future investigations.....	117
6 REFERENCES.....	119

NOMENCLATURE

A	[-]	Constant in analytical solution of Boonstra & Boehmer
C	[M/L ³]	Tracer concentration
D_L	[L ² /T]	Longitudinal dispersion coefficient
D_m	[L ² /T]	Molecular diffusion coefficient in free water
E	[L]	Elevation of spring outlet above datum in [m a.s.l.]
H	[L]	Water level above presumed elevation of spring outlet
K	[L/T]	Hydraulic conductivity
K_s	[-]	Chemical reaction constant (acid-base equilibrium)
L	[L]	Fracture half length
M	[M]	Tracer input mass
P	[L/T]	Rainfall
Pe	[-]	Peclet number
Q	[L ³ /T]	Spring or river discharge, pumping rate
R	[L/T]	Recharge rate
RF	[%]	Recharge factor
RR	[%]	Tracer recovery rate
S	[-]	Storage coefficient
T	[L ² /T]	Transmissivity
T_{rel}	[-]	Relative fracture transmissivity
V	[L ³]	Volume of water
X^2	[(M/L ³) ²]	Sum of the square deviations (between measured and calculated concentrations)
a_f	[L]	(Fracture) width, aperture
a_L	[L]	Longitudinal dispersivity
c	[-]	Intercept in graphical evaluation of E in a plot of h_{t+dt} against h_{dt}
d	[T] ⁻¹	Intercept in graphical evaluation of E in a plot of dh/dt against h
h	[L]	Water level above elevation of spring outlet
i	[%]	Hydraulic gradient
k	[T] ⁻¹	Constant in recession curve analysis
n	[-]	Number of values
n_e	[-]	Effective porosity
n_p	[-]	Porosity of the rock matrix
p	[-]	Probability (of rainfall occurrence)
r	[L]	Radial distance from pumping well
r_{im}	[L]	Radial distance to imaginary production well

s	[L]	Measured drawdown
s'	[L]	Corrected drawdown (trend, rainfall events)
s_f	[-]	Fracture skin
s_r	[L]	Residual drawdown (recovery)
s_w	[-]	Well skin
t	[T]	Time (since test started, since tracer injection)
t'	[T]	Time since start of recovery
t_0	[T]	Mean transit time of groundwater tracer
t_1	[T]	Tracer first arrival time
t_{Cmax}	[T]	Time of maximum concentration
v	[L/T]	Mean groundwater flow velocity
v_{max}	[L/T]	Maximum groundwater flow velocity
v_{med}	[L/T]	Median groundwater flow velocity
x	[L]	Distance (from injection to observation well, from observation to pumped well)
x, y	[L]	Cartesian co-ordinate
x_{im}	[L]	Linear distance to imaginary production well
α	[T ^{-1/2}]	Coefficient in SFDM and SFPFM (Diffusion parameter)
α_M	[T] ⁻¹	Retention ("Maillet"-) coefficient
$\delta(\tau)$	[1/T]	Dirac- delta function
ε	[-]	Constrictivity factor in SFDM and SFPFM
κ	[1/T]	Coefficient in input function of VI-ADM
λ	[1/T]	Coefficient in input function of EI-ADM
τ	[T]	Mean residence time of groundwater
τ_p	[-]	Tortousity factor for micropores in SFDM and SFPFM

SUBSCRIPTS

f	Single fracture or fractured dyke system
im	Imaginary well
m	Formation (host rock, rock matrix)
r	Residual (drawdown)
$real$	Real (actual) well
rel	Relative (transmissivity)
w	Well

ABBREVIATIONS

ADM	Ordinary A dvection- D ispersion M odel
CDF	C umulative D ensity F unction
DGPS	D ifferential G lobal P ositioning S ystem
DOC	D issolved O xygen C ontent
EC	E lectric C onductivity
EI-ADM	A dvection- D ispersion M odel with E xponential I ntput F unction
MIF	M agnetic- I nductive F lowmeter
MAR	M ean A nnual R ainfall
MRT	M ean R esidence T ime
OAA	O shivelo A rtesian A quifer
RWL	R est W ater L evel
SFDM	S ingle F issure D ispersion M odel
SFPFM	S ingle F issure P iston- F low M odel
SI	S aturation I ndex
TBC	T racer B reakthrough C urve
TDS	T otal D issolved S olids
TGWS	T sumeb G roundwater S tudy
VI-ADM	A dvection- D ispersion M odel with T ime- V ariable I ntput F unction
WHRA	W ell H ydrograph R ecession A nalysis
m a.s.l.	m eters a bove s ea l evel
m b.g.s.	m eters b elow g round s urface

DEFINITIONS

Gamma function:

$$\Gamma(p+1) = \int_0^{\infty} e^{-x} x^p dx$$

Complementary error function:

$$\operatorname{erfc}(x) = \frac{2}{\sqrt{\pi}} \int_x^{\infty} \exp(-t^2) dt = 1 - \frac{2}{\sqrt{\pi}} \int_0^x \exp(-t^2) dt$$

Well function

$$W(u) = \int_{r^2 s/4tT}^{\infty} \frac{e^{-x}}{x} dx$$

LIST OF TABLES

Table 1	Overview of the applied geohydraulic methods and their applicability	3
Table 2	Diagnostic plots for the assessment of flow characteristics of fractured aquifers	15
Table 3	Fitting parameters of transport models.....	22
Table 4	Stratigraphic succession	38
Table 5	Mean residence time obtained from the WHRA.....	50
Table 6	Results of the hydraulic test evaluation.....	60
Table 7	Comparison of the hydraulic test evaluations at Lindau	63
Table 8	Analysis methods and equipment.....	64
Table 9	Average chemical composition of open rainfall and groundwater at Bl. 17	65
Table 10	Tracer test design	73
Table 11	Tracer test results	75
Table 12	Transport modelling results	78
Table 13	Comparison of Lindau tracer test results.....	82
Table 14	Hydraulic test evaluation results.....	89
Table 15	Hydraulic test evaluation statistics.....	92
Table 16	Thickness of the model layers and the vertical differentiation of	
	T , K and S	100
Table 17	Comparison of the hydraulic parameters obtained from the hydraulic tests and the model calibration.....	105

LIST OF FIGURES

Figure 1	Sketch map defining the parameters h , H , E , E' and e	6
Figure 2	Normalised tracer input and corresponding breakthrough curves according to the EI-ADM	21
Figure 3	Normalised tracer input and corresponding breakthrough curves according to the VI-ADM	22
Figure 4	Site plan of the test site Lindau	26
Figure 5	Plan of the observation tunnel and the boreholes in the parallel pit	27
Figure 6	Locality map of the Lindau fractured rock test site	30
Figure 7	Locality map of the Tsumeb study area	33
Figure 8	Annual rainfall at the Tsumeb station from 1911-1998	34
Figure 9	Karstified surface features	36
Figure 10	Map of stratigraphic units in the study area	39
Figure 11	View of the southern study area from the farm <i>Ghaub</i>	40
Figure 12	Rose diagrams	40
Figure 13	Mud rotary drill cuttings of WW39992	42
Figure 14	The processed 1989 hydrograph data of B 130S as an example of the graphical fitting according to methods 1 and 2	46
Figure 15	Correlation of the WHRA results according to methods 1 and 2	47
Figure 16	WHRA performed at B 130S and B 68E for selected years	48
Figure 17	Regional distribution of mean residence time	51
Figure 18	Experimental set-up of the catchment drainage experiment	53
Figure 19	Daily rainfall at Lindau and Todtmoos	54
Figure 20	Groundwater level at B 132S and B 82E during the summer (April – October) for 6 individual years	56
Figure 21	Original drawdown data and trend correction at Bl. 15	57
Figure 22	Original recovery data and trend correction at Bl. 15	57
Figure 23	Evaluation of drawdown at Bl. 15	61
Figure 24	Evaluation of recovery at Bl. 15	62
Figure 25	Ternary Graphs	64
Figure 26	Histogram of fluoride concentration	66
Figure 27	Variation in the cation concentrations during the catchment drainage experiment	70
Figure 28	Variation in the anion concentrations during the catchment drainage experiment	71
Figure 29	Variation in the barium and strontium concentration during the catchment drainage experiment	71
Figure 30	Variation in the ion ratios during the catchment drainage experiment	72
Figure 31	Tracer concentration in the injection boreholes	74

Figure 32 Normalised TBC's of small-scale tracer tests	76
Figure 33 Analysis of tracer breakthrough and recovery curves for the bromide test at Bl. 15, and the chloride test at Bl. 18	79
Figure 34 Analysis of tracer breakthrough and recovery curves for the sulphorhodamine B test at Bl. 19, and the eosine test at Bl. 20	80
Figure 35 Schematic E-W profile through the ore dyke.....	83
Figure 36 The significance of the hydraulic test program within the study.....	85
Figure 37 Hydraulic test sites.....	86
Figure 38 Diagnostic semi logarithmic plot of the aquifer test carried out at WW39974	90
Figure 39 Modelling scheme	93
Figure 40 Geohydraulic units	96
Figure 41 Geohydraulic units as defined for the top layer (no. 1a) of the 3-D model	98
Figure 42 Cumulative density function (CDF) fitted to the annual rainfall at Tsumeb...	101
Figure 43 Recharge areas	102
Figure 44 Location of the calibration wells and hydrographs	103
Figure 45 Correlation between simulated and measured groundwater levels at wells with high-accuracy measurements	105
Figure 46 Schematic N-S profile	106
Figure 47 Groundwater balance and levels as obtained from the steady state model calibration.....	107
Figure 48 Rainfall data at Tsumeb and transient calibration of groundwater levels at Lake Otjikoto and WW10317	108
Figure 49 Total abstraction according to scenarios.....	110
Figure 50 Predicted decline of groundwater levels in the model area	112
Figure 51 Predicted accumulated change in groundwater storage	112

LIST OF APPENDICES

Appendix 1 Results of well hydrograph recession analysis according to Method 1	A-2
Appendix 2 Results of well hydrograph recession analysis according to Method 2	A-3
Appendix 3 Hydrochemical data.....	A-4
Appendix 4 Aquifer characterisation from pumping test analysis	A-5

1 Introduction

1.1 Problem statement

Over the last decade, the need for a better understanding and the development of new conceptual models of fluid flow and transport in fractured rock aquifer systems has been repeatedly emphasised. The hard rock hydrogeology has become a focus of research and played an important role at international conferences and in recent publications (National Research Council, 1996; Pointet, 1997; Annau et al., 1998; Seiler & Wohnlich, 2001).

The specific problems that are encountered during the application of fluid flow and transport analysis in fractured rock may be explained by the following reasons:

1. The extraordinary **heterogeneity** caused by the largely differing hydraulic parameters of single fractures, fracture sets and the rock matrix. In porous aquifers a similar heterogeneity can only be observed within delta deposits or alluvial sediments hosting paleo- channels.
2. The impact of the **physical properties of the fractures**, their geometry, position and interconnectivity, which largely determine the permeability, the anisotropy and the flow pattern of the formation.
3. The importance of the **scale** of the area under investigation and the resulting necessity to define representative geometric and hydraulic parameters.
4. The difficulty to investigate and to define these complex relationships in the field.

To cope with these particularities modern approaches must be considered and, if necessary, implemented during the investigations. This may be illustrated by the following simple examples: The cubic law proved to better describe the groundwater flow in fractures than Darcy's law. Double-porosity or single fracture models must be taken into consideration in order to evaluate hydraulic tests. For a more adequate characterisation of a fractured system, more sophisticated conceptual models such as multi-continuum, discrete fracture or fracture network models should be considered.

It is emphasised that a successful development of a conceptual model for a fractured aquifer system will hardly be possible without including interdisciplinary studies. Investigations that can lead to an accurate characterisation of the physical properties of the fractures are of particular importance. Prior to the application of the geohydraulic methods, a detailed geological survey should be performed. Apart from the stratigraphical and lithological description of the rock formations, such a survey should focus on the origin and the development of fracture systems and the physical characteristics of the fractures. Remote sensing and geophysical investigations can help to detect faults or dyke systems and to identify the hydraulic behaviour (conduit or barrier type) of such lineaments.

1.2 Investigation scope and targets

In this thesis, five different geohydraulic methods, namely well hydrograph recession analysis, hydraulic tests, groundwater tracer tests, hydrochemical investigations and groundwater modelling were applied in two regional case studies. The analysis techniques of each method are presented and improved. The usefulness of each method to describe the flow pattern is assessed separately for each investigation area. The results of the methods are combined with a geohydraulic characterisation of the fractured rock flow systems.

The **Lindau fractured rock test site** is situated within the north-eastern part of a granitic pluton in the Southern Black Forest, SW- Germany. The fractured rock aquifer system is characterised by a dominant vertical dyke zone that intersects the surrounding granite, which has a low permeability. The test site has been under hydrogeological investigation for more than three decades. It was used for research on fluid flow and transport by the Department of Applied Geology, University of Karlsruhe together with the Association of Tracer Hydrology - ATH (e.g. Ackermann, 1981; Himmelsbach, 1993; Veuillet, 1994; Himmelsbach et al., 1998; Witthüser, 2000). Most of the previous studies, however, focussed on small-scale investigations in the vicinity of the observation tunnel through which the dyke zone can be easily accessed. The objective of this study is to investigate the entire subterranean catchment of the dyke and to characterise the flow system as well as the interaction of the dyke and its host rock on a catchment scale ($>3 \text{ km}^2$).

The investigation of the **Tsumeb Aquifers**, included in this thesis, was carried out as part of the *Tsumeb Groundwater Study (TGWS)*. The KfW (*Kreditanstalt für Wiederaufbau*), Namibia Water Corporation Ltd and the Ministry of Agriculture, Water and Rural Development of Namibia jointly financed the international study.

Over the next decade, the water demand for the Central Area of Namibia will rise further. Therefore, it is necessary to develop and secure additional water resources from other areas. The Tsumeb Aquifers are considered to be one of the potential additional sources to meet the growing water demand. The dolomites of the Otavi Mountainland situated in the northern parts of Namibia host this valuable groundwater resource that could be linked to the existing water supply system of the Central Area.

The comprehensive investigation program was initiated in September 1999 and finalised in December 2002. It included a remote sensing and hydrocensus survey, a reconnaissance geophysical survey and an exploration drilling program as well as hydrochemical and isotope investigations. The hydraulic test evaluation and the development of a regional groundwater model form an integral part of this thesis. The overall objectives of the groundwater model are

1. to assess the impact of additional groundwater abstractions on the groundwater resources for different presumed hydrological conditions,
2. to quantify the sustainable yield of the investigation area,
3. to assess the available amount of contingency groundwater that can be directed towards the Central Area of Namibia during drought conditions, and
4. to provide essential information for the establishment of environmentally sustainable groundwater management.

2 Geohydraulic Methods

2.1 Methods for the geohydraulic characterisation of fractured rock aquifers

The geohydraulic methods presented and applied in this study are summarised in Table 1. Typical fields of application of each method are also given in the table. The methods aim at the development of a conceptual aquifer model, the quantification of aquifer parameters and water balance terms, and at the development of planning and management tools. To achieve a better understanding of the flow system, interdisciplinary studies are required which combine the various geohydraulic methods with geological, geophysical and other approaches.

Table 1 Overview of the applied geohydraulic methods and their applicability

Geohydraulic Method	Applicability
Well hydrograph recession analysis	Estimation of MRT Regional aquifer characterisation (permeability distribution) Determination of elevation of spring outlets
Hydraulic tests	Determination of hydraulic parameters (T , S) Aquifer characterisation (e.g. leakage, double porosity, conduits, barriers) Assessment of well performance (well loss)
Groundwater tracer tests	Assessment of groundwater flow direction/ divide Determination of groundwater flow velocities Detection of interconnected aquifer systems Determination of mass transport parameters (dispersion, diffusion, retardation) Developing of conceptual flow and transport models
Hydrochemical studies & isotope techniques	Estimation of MRT Estimation of recharge Developing of conceptual flow models Assessment of groundwater quality and risks
Groundwater modelling	Development and validation of conceptual models for groundwater flow and transport Assessment of the plausibility and the sensitivity of model assumptions Estimation of recharge Simulation of the groundwater flow pattern Quantification of the groundwater balance Scenario calculations (Planning and management tool)

2.2 Well hydrograph analysis

2.2.1 General concept

The hydrograph analysis was originally developed for surface runoff from rivers or springs. The **streamflow recession analysis** can be traced as far back as to studies carried out by Boussinesq in 1877 and Maillet in 1905. After a storm event, a hydrograph will typically show a rising limb, a crest segment and a falling limb. The shape of the rising limb is essentially controlled by the characteristics of the storm event, whereas the shape of the recession limb is largely independent of the specific nature of the storm (Linsley et al., 1982). The falling limb is termed a recession or depletion curve. Three different segments can commonly be distinguished in a recession limb, each of them

representing a different reservoir and residence time. The three segments are related to surface runoff, interflow from the upper soil layers and baseflow from aquifers (Barnes 1940; Linsley, et al., 1982). The **baseflow recession analysis** focuses on the evaluation of the baseflow segment and has been applied to estimate the groundwater recharge of a river catchment (Rorabaugh, 1964) and the effective fracture porosity of rock formations (Toussaint, 1981; Schräber & Szymczak, 1984).

The fundamental principle describing the recession is the exponential equation

$$[1] \quad Q = Q_0 \cdot \exp(-\alpha_M t)$$

The discharge Q curve plots on a straight line with a slope α_M in a semilogarithmic plot of $\log(Q)$ against t . The so-called “Maillet-coefficient” α_M was alternatively termed the “retention coefficient” by Boussinesq and the “exhaustion coefficient” by Shevenell (1996). Large values of α_M indicate a fast depletion of a reservoir due to its low storage properties.

The **mean residence time (MRT)** in a reservoir τ , alternatively termed “response time” by Shevenell (1996), is defined by (Hoehn, 1979):

$$[2] \quad \tau = 1/\alpha_M$$

Making use of the principle of superposition, the existence of n (parallel) reservoirs with distinct storage properties can be expressed as following:

$$[3] \quad Q = \sum_{i=1}^n Q_{0i} \cdot \exp(-\alpha_{M_i} t)$$

The **well hydrograph recession analysis (WHRA)** investigates the groundwater level measurements versus time. This technique was first described and applied by Shevenell (1996) and since then by Powers & Shevenell (2000) for a karst aquifer. Shevenell investigated the recession limbs of the hydrographs after storm events. She found that the most useful hydrographs for wells in the karst aquifer were obtained during sudden, intense storm events. Up to three straight-line segments with characteristic values of α_M could be distinguished in semilogarithmic plots of the water levels versus time. As with the streamflow recession, the three segments of the recession limbs were attributed to different reservoirs with characteristic types of storage and residence times. The fastest response stems from discharge from large conduits, whereas the second segment was allocated to discharge from fractures. The third segment represents the drainage of small fissures or the rock matrix.

Similar to equation [1] the recession limb of a well hydrograph can be expressed by

$$[4] \quad h = h_0 \cdot \exp(-\alpha_M t).$$

h is hereby defined as the water level above the static water level. In a mountainous area, the static water level will most likely equal the elevation of the spring outlet. The curve of h plots on a straight line of slope α_M in a semilogarithmic plot of $\log(h)$ against t .

The superposition of n (parallel) reservoirs with distinct storage properties results in the following equation:

$$[5] \quad h = \sum_{i=1}^n h_{0i} \cdot \exp(-\alpha_{Mi} t)$$

The method implies that the storage characteristics of the reservoirs are distinct and that the drainage of each reservoir will dominate a section within the recession limb. If the segments of the recession limb are curvilinear rather than that of a straight-line, a non-linear recession equation may be more appropriate (Tallaksen 1995; Wittenberg & Sivaplan, 1999).

It will be illustrated in this thesis that hydrograph analysis can also be applied to fractured aquifers in granitic rock in a humid climate. Due to the low permeability of granite, the WHRA is not performed on recession limbs after storm events but on the seasonal decline of the water levels during the drier summer period. **The WHRA is a fairly simple and cheap method to obtain information on the regional variation of MRT and permeability provided that groundwater level records are available.**

2.2.2 Determination of the mean residence time

In principle, α_M and the MRT τ can be determined from the slope in a semilogarithmic plot of $\log(h)$ against t . In practice, however, the recession limb is typically interrupted by rising limbs caused by rainfall. In the **matching strip method** (Toebe & Strang, 1964) the individual recession limbs are plotted and shifted horizontally until they overlap. The best fit to the joined individual segments can be regarded as the mean recession curve commonly referred to as the **master recession curve** (Tallaksen, 1996). The matching strip method has often been criticised for depending too much on subjective judgements. Therefore, advanced graphical shifting methods and recession selection algorithms have been presented in the literature (see Tallaksen, 1996, for an excellent review of these techniques).

Another problem that is encountered during a WHRA is the definition of the water level h . Shevenell (1996) proposed a consistent method of determining the water level. She defined the water level as the height of the water column above the inserted pressure probe that was placed at the same height above the presumed static water level for all wells in a catchment. In many cases, however, the static water level or the elevation of the spring outlet may not be known with sufficient accuracy. Since the definition of the water level dramatically influences α_M , highly erroneous values for the MRT may be obtained.

The two different methods described in the following sections help overcome this problem. **By applying these methods, the correct residence time can be determined even if the precise static water level (or elevation of spring outlet) is unknown.** Furthermore, once the residence time is known, the elevation of the spring outlet can be determined with these techniques.

Method 1

This method has been referred to as the **correlation method** in the streamflow recession analysis (Tallaksen, 1995). The principle of this method is based on the fact that equation [4] can be written in the alternative form:

$$[6] \quad h = h_0 \cdot k^{-t}, \text{ where } \alpha_M = \ln(k).$$

Two succeeding water levels h_1 and h_2 are then defined by

$$h_1 = h_0 \cdot k^{-t_1} \text{ and } h_2 = h_0 \cdot k^{-t_2}.$$

It can be easily shown that h_2 can be expressed in terms of h_1 as

$$[7] \quad h_2 = h_1 \cdot k^{t_1 - t_2} = h_1 \cdot k^{-dt}$$

It follows from equation [7] that h_{t+dt} vs. h_{dt} will plot as a straight line with slope k' if the water level measurements are taken at equal time intervals dt (Tallaksen, 1995), where

$$[8] \quad k' = k^{-dt}.$$

Hence, k and α_M can be determined from such a plot using the relationships

$$[9] \quad k = \sqrt[-dt]{k'} = (k')^{1/dt} \text{ and } \alpha_M = \ln(k)$$

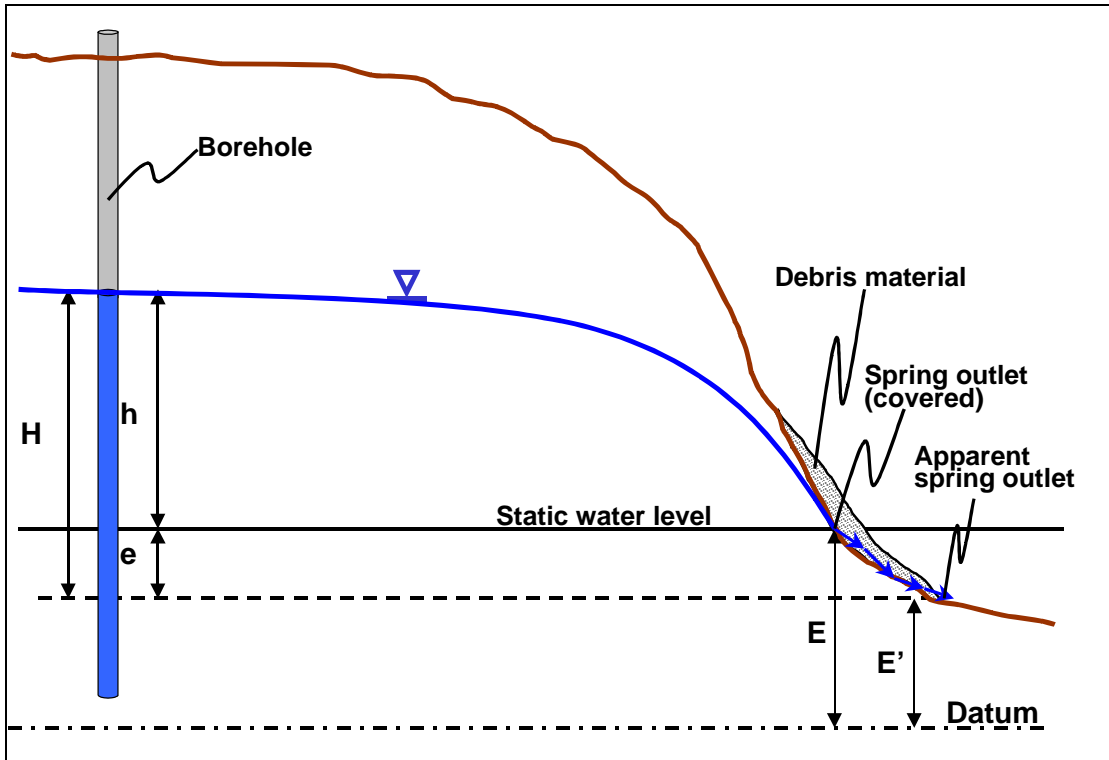


Figure 1 Sketch map defining the parameters h , H , E , E' and e

If we assume that the static water level corresponds with the elevation of the spring outlet E , but that the presumed elevation of the spring outlet E' diverges by the amount of e (see Figure 1), i.e.

$$[10] \quad E = E' + e$$

the equation governing H becomes

$$[11] \quad H = h + e = h_0 \cdot k^{-t} + e$$

Considering two subsequent water levels H_1 and H_2 , taken at the time interval dt , and making use of equation [7], H_2 can be expressed as follows:

$$H_2 = h_2 + e = h_1 \cdot k^{-dt} + e = (H_1 - e) \cdot k^{-dt} + e = H_1 \cdot k^{-dt} + e(1 - k^{-dt})$$

Since dt is constant, H_{t+dt} vs. H_{dt} will again plot as a straight line with slope k' and the intercept c , where

$$[12] \quad c = e(1 - k^{-dt})$$

Using equation [10] and [12], the corrected elevation of the spring outlet can be calculated as follows:

$$[13] \quad E = E' + \frac{c}{(1 - k^{-dt})}$$

Method 2

Equation [4] can be regarded as the solution of the differential equation

$$[14] \quad \frac{dh}{dt} = -\alpha_M \cdot h, \text{ with the initial condition: } h(0) = h_0$$

Hence, the derivative dh/dt against h plots on a straight line with slope α_M .

In the case where the precise elevation of the spring outlet is unknown, H instead of h will be erroneously inserted in the differential equation. The error caused by these assumptions can be expressed mathematically as

$$[15] \quad \frac{dH}{dt} = -\alpha_M \cdot (H - e) = -\alpha_M \cdot H + \alpha_M \cdot e \quad ^1)$$

The curve of dH/dt against H plots on a straight line of slope α_M with the intercept d . Consequently, the value for α_M is not affected by the wrong assumptions and can be determined graphically from the plot. The error e in the assumed elevation can be gained thereafter from the equation:

$$[16] \quad e = d / \alpha_M$$

Using equation [10], the correct elevation of the spring outlet can be calculated by

$$[17] \quad E = E' + d / \alpha_M$$

¹⁾ The initial condition then becomes: $H(0) = H_0 - e$. Equation [15] is non-homogeneous. By replacing h and h_0 with H and $(H_0 - e)$, respectively, equation [4] becomes a solution of the homogeneous problem of equation [15]. It can easily be shown that $H(t) = e$ is a specific solution of the non-homogeneous problem. It is well known that a general solution of the inhomogeneous differential equation can be obtained by the superposition of the solution of the homogenous problem with any specific solution of the inhomogeneous problem. The general solution hence takes the form: $H(t) = (H_0 - e) \cdot \exp(-\alpha_M t) + e$.

2.3 Hydraulic tests in fractured rock

2.3.1 Overview and restrictions of hydraulic test procedures

Hydraulic test procedures are the classical approach to determine hydraulic aquifer parameters and to assess the well efficiency. Equally important, they can be interpreted in order to define the flow regime and to characterise the aquifer. Among the most common hydraulic test procedures applied in fractured rock are slug & bail tests, pulse tests, fluid logging and pumping tests including step tests and constant discharge tests. The selection of the most adequate hydraulic test procedure will be based on the objective of the study, the transmissivity of the formation and the available budget. Step tests are usually carried out to assess the performance of a well and are therefore commonly called well tests. The objective of a constant discharge test is to characterise an aquifer and to quantify its hydraulic properties. Constant discharge tests are therefore referred to as aquifer tests. Hekel (1994) provides a good comparison of the applicability and restrictions between the various test procedures.

It follows from the heterogeneity of fractured rock that hydraulic test results will only provide small-scale information. The hydraulic parameters gained are only representative for the volume of rock formation that has been tested. For a pumping test, the tested rock volume will be in the order of $Q \cdot t/n_e$ (Schulze-Makuch et al., 1999). The aquifer test incorporates the largest rock volume among the hydraulic tests due to the extended period of pumping and should therefore produce the most reliable information on the hydraulic properties of the formation. Only a large number of tests will enable a statistical analysis of the hydraulic parameters to be performed. The high costs of hydraulic tests will inevitably cause conflicts during regional studies of heterogeneous formations. By carefully selecting representative test sites, however, it should be possible to determine at least the range of potential aquifer values within a study area.

Single fractures can act either as conduits or barriers, which largely affect the flow pattern. Fracture networks can combine to form a double porosity system within the rock matrix. These aquifer systems must be treated differently from homogenous systems. Analytical solutions considering a fracture specific flow pattern, however, have only been developed for pumping tests. Furthermore, single fracture type analytical solutions have not yet as been widely used and are currently not incorporated in commercial software packages such as AQTESOLV, AquiferTest Pro or HydroSolve.

The original papers dealing with single fractures generally use petroleum-engineering units and are barely transparent to hydrogeologists. An examination of existing reviews in the hydrogeology literature showed that the published equations frequently contain errors. It was therefore considered beneficial to summarise the concepts and analytical solutions of hydraulic test evaluation methods for fractured rock using a consistent nomenclature. Previous summaries of hydraulic test methods in fractured rock aquifers were provided by Stober (1986), Kruseman & de Ridder (1991) and Strayle et al. (1994).

2.3.2 Conceptual Models for fractured aquifer systems

2.3.2.1 Homogeneously fractured, uniform aquifer

The conventional analysis of pumping tests assumes a homogeneous and isotropic aquifer. A fractured aquifer will most likely fulfil this assumption if a dense network of uniform fractures intersects the rock. If for instance the average fracture spacing is small compared to the expected cone of depression, the fracture network likely builds a continuum comparable to a porous aquifer. Theis (1935) and Cooper & Jacob (1946) described the unsteady-state radial convergent flow around the pumping well in a confined homogeneous and isotropic aquifer. Agarwal et al. (1970) have included the wellbore storage and skin effects in the analysis. The drawdown s in a well at a radial distance r from the pumped well is as follows:

$$[18] \ s(r, t) = - \frac{Q}{4 \pi T_m} W(u),$$

$$\text{where } u = \frac{r^2 S}{4 T_m t} \text{ and } W(u) \text{ is known as the well function.}$$

Slug test

During a slug test, the water-level response due to the instantaneous injection or withdrawal of water from a well in a confined homogeneous and isotropic aquifer is measured. The straight-line analysis according to Cooper et al. (1967) and the type curve analysis according to Bouwer & Rice (1976) can be applied for the evaluation of the tests.

2.3.2.2 Double porosity concept

The principles of a double-porosity system were originally developed by Barenblatt et al. (1960). The aquifer is regarded to be composed of fractures and matrix blocks. The fractures are assumed to be of high permeability but low (secondary) porosity and storage capacity. The matrix blocks, however, are of low permeability but possess a high (primary) porosity and storage capacity. Only the fractures produce a flow directly to the well. The flow from the fracture into the well is radial. This implies a dense, homogeneous and continuous fracture network. The matrix blocks act as a source, which feeds water into the fractures.

The drawdown in the pumped well and the observation wells is characterised by two parallel straight lines in a semi-logarithmic plot of s vs. $\log(t)$ which are separated from each other by a transition zone. The first straight line corresponds to the radial flow of water that originates solely from the fractures, and the second straight line coincides with the radial flow of water produced by the total system (fractures + matrix blocks). During the transition zone, the induced pressure difference between the fractures and the matrix blocks stabilises until steady state conditions are reached.

Numerous solutions have been presented to describe the transient flow from a double-porosity formation into a well. They can be distinguished by the way the shape of matrix blocks (blocks, spheres, plates etc.) is idealised. Originally, a pseudo-steady state flow

from the matrix blocks into the fractures was assumed, i.e. no variation in head within the matrix was considered (Warren & Root 1963; Kazemi 1969; Mavor & Cinco, 1979). Later solutions include transient interporosity flow (de Swan, 1976; Boulton & Streltsova, 1977; Bourdet & Gringarten 1980; Moench, 1984). Wellbore storage and skin effects were first introduced by Mavor & Cinco (1979) and Bourdet & Gringarten (1980). Moench (1984) presented the most complete solution including pseudo-steady state and transient interporosity flow including wellbore storage, well skin and fracture skin. Fine reviews on the interpretation of hydraulic tests in double-porosity aquifers are given by Gringarten (1984), Streltsova (1988) and Kruseman & de Ridder (1991).

2.3.2.3 Single vertical fracture

The concept assumes that a set of vertical fractures or a dyke can be idealised by a single vertical fracture with an aperture a_f and a length $2 L_f$ which fully penetrates the confined and otherwise homogeneous aquifer. The pumping well intersects the fracture that feeds to the well. The unsteady-state flow towards the well follows, in principle, four distinct flow phases (Cinco & Samaniego, 1981):

1. Fracture linear flow
2. Bilinear flow
3. Formation linear flow
4. Pseudo-radial flow

The term linear flow refers to a flow field with parallel flowlines within the fracture or the host rock. The fracture linear and the bilinear flow phase will only be developed in fractures with a low permeability. In terms of the relative fracture transmissivity T_{rel} , these initial flow phases can be observed if the following relationship is fulfilled (Cinco et al., 1978):

$$[19] T_{rel} = (T_f \cdot a_f) / (T_m \cdot L_f) < 300$$

In this case, the solutions of Cinco & Samaniego (1981) for fracture linear and bilinear flow can be applied. For a composite dyke-aquifer system, the method of Boonstra & Boehmer (1986) can be used. If $T_{rel} \geq 300$, the storage in the fracture can be neglected. The fracture acts as a high permeable conduit and the head difference within the fracture is very small or zero. The methods of Gringarten et al. (1974) and Jenkins & Prentice (1982) are appropriate for this type of flow (Bardenhagen, 2000).

Fracture linear and bilinear flow

The fracture linear flow occurs within a vertical fracture of finite conductivity at early times during which the groundwater is almost exclusively abstracted from the fracture itself. The drawdown within the fracture at a distance x from the pumped well was derived by **Cinco & Samaniego (1981)**:

$$[20] s(x, t) = \frac{Q}{T_f a_f} \sqrt{\frac{T_f t}{S_f}} \left\{ \frac{e^{-b}}{\sqrt{\pi}} - b \operatorname{erfc}(b) \right\}, \quad b = \frac{x}{\sqrt{4 \frac{T_f}{S_f} t}}$$

For the pumped well ($x = 0$) the equation simplifies:

$$[21] s|_{x=0} = \frac{Q}{a_f} \sqrt{\frac{t}{\pi T_f S_f}}$$

The bilinear flow follows the linear flow phase and indicates that the water is now supplied from the rock formation. No water is supplied from storage in the fracture. The flowlines within the fracture are parallel and directed towards the abstraction well. The flow pattern within the formations is also parallel but oblique to the axis of the fracture and the flowlines within the fracture. Cinco & Samaniego (1981) derived the following equation for the drawdown at the pumped well:

$$[22] s(0, t)|_{t \gg 0} = \frac{Q}{\Gamma(1,25) \sqrt{8 T_f a_f \sqrt{T_m S_m}}} t^{1/4} \approx \frac{0.39 \cdot Q}{\sqrt{T_f a_f \sqrt{T_m S_m}}} t^{1/4}$$

Boonstra & Boehmer (1986) and **Boehmer & Boonstra (1987)** developed a relationship for a well that pumps from a vertical dyke of infinite extent but finite conductivity. The dyke is characterised by its width a_f , transmissivity T_f and storage coefficient S_f . The dyke fully penetrates the host rock, which is characterised by its infinite areal extent, the transmissivity T_m and the storage coefficient S_m . Their solutions cover the fracture linear flow phase (parallel flow within the dyke) at early times, the bilinear flow phase (parallel flow within both the dyke and the formation) at intermediate times as well as the pseudo-radial flow at late times. The drawdown within the dyke at a distance x from the pumped well is (Boonstra & Boehmer, 1986):

$$[23] s(x, t) = \frac{Q}{2A \sqrt{\pi T_f T_m S_m / S_f}} \exp(-2 \sqrt{\tau}) \int_0^{\sqrt{\tau}} \exp\left(2\sqrt{\tau^2 - \zeta^2} - \frac{A^2 T_m S_m x^2}{a_f^2 T_f S_f \tau^2}\right) d\zeta$$

$$\text{where } \zeta \text{ is the integration variable, } \tau = \sqrt{\frac{4 A^2 T_m S_m}{(a_f S_f)^2}} t \text{ and } A = \sqrt{0.88}$$

For the production well ($x=0$) the solution reduces to

$$[24] s(0, t) = \frac{Q}{2A \sqrt{\pi T_f T_m S_m / S_f}} \exp(-2 \sqrt{\tau}) \int_0^{\sqrt{\tau}} \exp\left(2\sqrt{\tau^2 - \zeta^2}\right) d\zeta$$

The fracture linear flow phase ends at approximately $\tau = 0.003$. The drawdown at the pumped well during this phase is characterised by a straight line with a slope of 0.5 in a log-log plot. The bilinear flow period starts at approximately $\tau = 100$ and develops a straight line with a slope of 0.25 in a log-log plot.

For observation wells within the rock formation ($y \neq 0$) the following solution applies according to Boehmer & Boonstra (1987):

$$[25] s(x, y, t) = s(x, 0, t) \left[\exp(-z^2) - \sqrt{\pi z} \operatorname{erfc}(z) \right],$$

$$\text{where } z = \frac{y}{2} \sqrt{\frac{S_m}{T_m t}}$$

Formation linear flow

Gringarten et al. (1974) developed an analytical solution to describe the unsteady-state linear flow from the rock formation into a well that fully penetrates a highly permeable vertical fracture zone. They considered a plane (zero-thickness) vertical fracture with negligible storage. It is assumed that the water is solely supplied by the host rock even at early times. They proposed two analytical solutions, which they referred to as the “*infinite conductivity*”, and the “*uniform flux*” solution. Their solutions are applicable if the fracture has very high or infinite conductivity.

The **infinite flux solution** assumes that the fracture conductivity is infinite. The drawdown in a well at a vertical distance y from the fracture axis can be calculated by

$$[26] \ s(y, t) = \frac{Q}{4\pi T_m} \frac{\sqrt{\pi}}{2} \int_0^\tau \exp\left(-\frac{(y/L_f)^2}{4v}\right) \left[\operatorname{erf}\left(\frac{0.134}{\sqrt{v}}\right) + \operatorname{erf}\left(\frac{0.866}{\sqrt{v}}\right) \right] \frac{dv}{\sqrt{v}}$$

where v is the integration variable and $\tau = \frac{T_m}{(S_m L_f)^2} t$.

According to this equation, the drawdown is independent of the distance x along the fracture axis. This means that there will be no pressure drop along the fracture. Consequently, the drawdown is identical at any position within the fracture.

The **uniform flux solution** assumes an equal flux at any position along the fracture. The solution can be written as

$$[27] \ s(x, y, t) = -\frac{Q}{4\pi T_m} \frac{\sqrt{\pi}}{2} \int_0^\tau \exp\left(-\frac{(y/L_f)^2}{4v}\right) \left[\operatorname{erf}\left(\frac{1-x/L_f}{2\sqrt{v}}\right) + \operatorname{erf}\left(\frac{1+x/L_f}{2\sqrt{v}}\right) \right] \frac{dv}{\sqrt{v}}$$

Note that equation [27] is identical to [26] if x/L_f is set to 0.732. The uniform flux solution implies a very high, but finite fracture conductivity, which creates a small but non-zero pressure drop along the fracture.

Based on the uniform flux solution, **Bardenhagen (1999)** introduced a method to detect and determine the well losses caused by skin effects. The skin effects may occur at the contact between the well and the fracture (well skin) as well as between the fracture and the formation (fracture skin).

Independent of Gringarten et al., **Jenkins & Prentice (1982)** proposed a similar analytical solution for formation linear flow. They set up a one-dimensional boundary value problem in the direction y perpendicular to the fracture axis. It is presumed that the fracture length is sufficiently long so that its edges have no effect on the drawdown of the observation well. The fracture has infinite conductivity and consequently acts like an “*extended well*”. The drawdown at any point within the fracture is therefore equal to drawdown at the well ($y = 0$). The drawdown at an observation well at a distance y from the fracture axis is defined by

$$[28] \ s(y, t) = \frac{Q}{(2L_f)T_m} \sqrt{\frac{T_m t}{S_m}} \left\{ \frac{e^{-b}}{\sqrt{\pi}} - b \operatorname{erfc}(b) \right\}, \text{ with } b = \frac{y}{\sqrt{4 \frac{T_m t}{S_m}}} = \sqrt{\frac{S_m y^2}{4 T_m t}}$$

For large values of t , their solution can be approximated by the simplified equation:

$$[29] \quad s(y, t)|_{t \gg 0} = \frac{Q}{(2L_f)T_m} \left\{ \sqrt{\frac{T_m t}{\pi S_m}} - \frac{y}{2} \right\}$$

It is important to note that only the product $T_m \cdot S_m$ can be obtained from a least square fit since the solution is not unique. However, Jenkins & Prentice describe how the hydraulic diffusivity T/S can be obtained from a graphical analysis. Firstly, t_0 has to be determined from the relationship $s(y, t = t_0) = 0$. The time t_0 is the value of t in the plot of s vs. $t^{1/2}$ for which the drawdown s becomes zero. It follows that the diffusivity equals ²⁾

$$[30] \quad \frac{T_m}{S_m} = \frac{\pi y^2}{4 t_0}$$

2.3.2.4 Single horizontal fracture

Gringarten & Ramey (1974) developed an analytical solution of the unsteady-state linear flow from the formation towards a well that intersects a high permeable “penny-shaped” horizontal fracture zone. They assumed negligible storage and uniform flux within the fracture.

2.3.3 Aquifer test evaluation

2.3.3.1 Diagnostic plots

The so-called diagnostic plots are an indispensable tool for the evaluation of pumping tests in heterogeneous aquifers. They can be applied to identify the aquifer type and flow regime from pump test data. Kruseman & de Ridder (1991: 48) emphasised that

“the choice of theoretical model is a crucial step in the interpretation of pumping tests. If the wrong model is chosen, the hydraulic characteristics calculated for the real aquifer will not be correct.”

The most useful diagnostic plots comprise

- ❑ the drawdown s versus time t in a log-log plot ($\log s$ vs. $\log t$)
- ❑ the drawdown versus the logarithm of time (semi-log plot: s vs. $\log t$)
- ❑ the drawdown versus the square root of time (s vs. $t^{1/2}$)
- ❑ the drawdown versus the fourth root of time (s vs. $t^{1/4}$)
- ❑ the time derivative of the drawdown versus the time in a log-log plot

The derivative plot is defined as

²⁾ Due to the resemblance of equation [20] to equation [28], the hydraulic diffusivity of the fracture T_f/S_f can be determined in a similar way. The drawdown data representing the fracture linear flow phase has to be plotted for the graphical analysis. The hydraulic diffusivity is calculated

$$\text{using } \frac{T_f}{S_f} = \frac{\pi x^2}{4 t_0}$$

$$[31] \frac{\partial s}{\partial t} \cdot t \approx \frac{s_{i+1} - s_i}{t_{i+1} - t_i} \cdot \frac{t_i + t_{i+1}}{2},$$

where s_i and s_{i+1} represent the drawdown at two subsequent time steps t_i and t_{i+1} .

Table 2 gives a summary how the flow regime and the aquifer type can be identified from the diagnostic plots. The formation linear flow e.g. is characterised by a straight line with a slope 0.5 in a log-log plot of the drawdown as well as the derivative versus time. It can also be identified from a straight-line in a plot of s vs. $t^{1/2}$. Bardenhagen (1999) pointed out that this line only intersects the origin if skin effects are negligible.

2.3.3.2 Time-drawdown analysis

The aquifer and well parameters are obtained from an inverse curve-fitting procedure. In principle, the best match of the measured time-drawdown data to an analytical solution has to be found by either a graphical or computer-operated method. Most commercial software packages use fitting algorithms to achieve the best match of the theoretical curves with the measured data.

As a summary of the presented methods and evaluation techniques, the following procedure for the evaluation of an aquifer test is proposed:

1. Develop a conceptual aquifer model from geological evidence.
2. Create the diagnostic plots from pumping test data and define the flow regime according to Table 2.
3. Choose the appropriate analysis method(s) and determine the aquifer and well parameters from the curve fitting of the drawdown and the recovery data.
4. If different flow regimes can be identified during a test, each section can be evaluated using the corresponding analysis method. For instance, the bilinear and the formation linear flow phase are likely to be succeeded by a pseudo-radial flow. The late time data can hence be evaluated with the Theis or Cooper & Jacob method.
5. Since the analytical solutions for fractured aquifer systems contain more than two fitting parameters, it is essential to obtain parameter estimates from independent methods. The geometric properties of the fracture such as the fracture half-length L_f and aperture a_f , for instance, can be obtained or verified from geological or geophysical investigations. Some of the hydraulic parameters can frequently be obtained from additional tests within the formation or from the evaluation of distinct sections of the drawdown. The hydraulic parameters of the rock formation, T_m and S_m , can be evaluated from hydraulic tests which are not influenced by the lineament. They can also be obtained from late time data corresponding to the pseudo-radial flow phase, which is also independent of the lineament. By inserting these values, the equation describing the fracture type flow regime can be solved for the remaining parameters.

Table 2 Diagnostic plots for the assessment of flow characteristics of fractured aquifers

Aquifer type	Flow regime	Diagnostic plots		References
		Drawdown	Derivative	
Homogeneous, isotropic	Radial symmetric	semi-log : straight line	log-log : horizontal line	Theis (1935) Cooper & Jacob (1946)
Double porosity	Radial symmetric	semi-log : two parallel straight line sections	—	Barenblatt et al. (1960) Warren & Root (1963) Bourdet & Gringarten (1980) Moench (1984)
Single vertical fracture or dyke	Fracture linear flow	log-log : straight line with ½ slope	log-log : straight line with ½ slope	Cinco-Ley et al. (1978) Cinco-Ley & Samaniego (1981)
	Bilinear flow	s vs. $t^{1/4}$: straight line log-log : straight line with ¼ slope	log-log : straight line with ¼ slope	Boonstra & Boehmer (1986) Boehmer & Boonstra (1987)
	Formation linear flow	s vs. $t^{1/2}$: straight line log-log : straight line with ½ slope	log-log : straight line with ½ slope	Gringarten et al. (1974) Jenkins & Prentice (1982) Bardenhagen (1999)
	Pseudo-radial flow	semi-log : straight line	log-log : horizontal line	Theis (1935) Cooper & Jacob (1946)
Single horizontal fracture	Storage type flow	log-log : straight line with 1/1 slope	—	Gringarten & Ramey (1974)
	Linear flow	log-log : straight line with ½ slope	log-log : straight line with ½ slope	
	Pseudo-radial flow	semi-log : straight line	log-log : horizontal line	

2.3.3.3 Recovery analysis

The recovery of a pumped aquifer can be interpreted in the same way as the drawdown by using diagnostic plots. The recovery analysis is achieved by applying the principle of superposition. The analysis is based on the assumption that the pumped well continues to be pumped at a constant rate once the pump has been shut off and that the equal rate of water is simultaneously injected into the well. Hence, the following equation applies for the residual drawdown s_r after a pumping test:

$$[32] \quad s_r(t) = \int_0^t s(\tau) d\tau - \int_{t'}^t s(\tau - t') d\tau = \int_0^t s(\tau) d\tau - \int_0^{t-t'} s(\tau) d\tau = \int_{t-t'}^t s(\tau) d\tau,$$

where τ is the integration variable, t' is the time since pumping stopped and s is the drawdown $s(x,y)$ at the well or the piezometer (space co-ordinates are omitted in [32] for the sake of simplicity).

The residual drawdown after a pumping test at a radial distance r from the well in a homogeneous isotropic aquifer is

$$[33] \quad s_r(r, t) = -\frac{Q}{4\pi T_m} [W(u) - W(u')], \text{ with } u' = \frac{r^2 S}{4T_m t'}$$

Applying equation [32] to the uniform flux solution of Gringarten et al. (1974) for formation linear flow, the following equation for the residual drawdown can be derived:

$$[34] s_r(x, y, t) = -\frac{Q}{4\pi T_m} \frac{\sqrt{\pi}}{2} \int_{\tau'}^{\tau} \exp\left(-\frac{(y/L_f)^2}{4v}\right) \left[\operatorname{erf}\left(\frac{1-x/L_f}{2\sqrt{v}}\right) + \operatorname{erf}\left(\frac{1+x/L_f}{2\sqrt{v}}\right) \right] \frac{dv}{\sqrt{v}}$$

where v and τ are defined as in equation [26], and $\tau' = \frac{T_m}{(S_m L_f)^2} t'$.

2.3.3.4 Bounded aquifers

The general assumption of an infinite aquifer is violated if either a recharging boundary or a barrier boundary is located in the vicinity of the pumped well. Such hydraulic boundaries are treated by introducing an imaginary well (Stallman, 1963, in Langguth & Voigt, 1980) which is located on the point of reflection across the hydraulic barrier and pumped at the same rate as the actual production well. Again, the principle of superposition is applied. The drawdown of a well or a piezometer at a distance of r_{real} from the actual pumped well and at a distance of r_{im} from the imaginary well is given by

$$[35] s(t) = s_{real}(r_{real}, t) \pm s_{im}(r_{im}, t)$$

2.4 Groundwater tracing techniques

2.4.1 Principles of groundwater tracing

The groundwater tracing techniques described in this chapter imply the application of artificial tracers. Tracer studies furthermore include investigations of naturally occurring main and trace constituents of groundwater or of substances, which have been accidentally released into the groundwater. A summary of the analysis of geochemical data is presented in chapter 2.5.

The classical field of application for artificial tracer tests in groundwater studies is the **detection of flow paths and flow directions**. Tracer tests have been widely used to determine the extent of subterranean catchments or to examine a presumed interconnection between aquifers.

Another important purpose of tracer tests is to determine groundwater **flow velocities**. The maximum flow velocity v_{max} is defined by the time of first tracer arrival whereas the median flow velocity v_{med} is determined from the time of maximum tracer concentration. Both velocities can be readily obtained from a tracer breakthrough curve (TBC). In either case, no assumptions concerning the type of flow system and the transport mechanisms have to be made. The mean groundwater flow velocity v , however, is defined by the appropriate transport equation (see chapter 2.4.2). It can only be accurately determined from field experiments if the experimental set-up fulfils the assumptions on which the transport equation is based. Tracer tests are often analysed in terms of the mean transit time of groundwater rather than the mean flow velocity. It is defined by

$$[36] t_0 = \frac{x}{v}$$

The comparison of flow velocities (or transit time) within an investigation area may lead to a distinction between different flow systems within the formation. Large variations may be associated with flow within conduits, fracture sets and the rock matrix.

The **effective porosity** n_e is defined as the fraction of the volume of the mobile groundwater over the volume of rock:

$$[37] n_e = \frac{V_{mobile\ groundwater}}{V_{rock}}$$

It can be determined from a tracer test by replacing the volume of mobile groundwater in equation [37] by

$$[38] V_{mobile\ groundwater} = Q \cdot t_0$$

The **kinematic dispersion** is a mixing process associated with the variations of flow velocities inside the medium. The amount of heterogeneity of flow velocities can be expressed in terms of the dispersion coefficient in the direction of flow, D_L . Representative values of D_L only exist for each flow system such as conduits, fracture sets and the rock matrix. It is therefore recommended to determine dispersion coefficients for each flow system separately. It is convenient to replace D_L in analytical solutions of the transport equation by the Peclet number

$$[39] Pe = \frac{v t_0}{D_L}$$

The Peclet number can be interpreted as the ratio between the advective component and the dispersive component of groundwater flow.

The dispersivity in the direction of flow a_L is defined as

$$[40] a_L = \frac{D_L}{v}$$

Finally, groundwater tracer techniques are also applied to analyse **mass transport mechanisms**. Since this thesis aims at the characterisation of fluid flow, however, the role of transport mechanism is only treated marginally.

2.4.2 Analytical models

2.4.2.1 Homogeneous aquifers

Ordinary advection-dispersion models

Ordinary advection-dispersion models have been developed for the evaluation of tracer tests in homogenous porous aquifers. Analytical solutions are derived from the fundamental partial differential equation for mass transport:

$$[41] \frac{\partial C}{\partial t} = \vec{D} \cdot \frac{\partial^2 C}{\partial x^2} - \vec{v} \cdot \vec{\nabla} C \quad (3-D)$$

$$\frac{\partial C}{\partial t} = D_L \frac{\partial^2 C}{\partial x^2} - v_x \frac{\partial C}{\partial x} \quad (1-D)$$

The equation implies that the tracer behaviour is ideal, i.e. that neither sorption nor degradation or chemical reactions will considerably affect the tracer transport.

Additionally, density effects are considered negligible, an assumption, that is sometimes violated by high tracer input concentrations. Diffusive processes are considered negligible compared to transport by advection and dispersion.

Analytical solutions based on ordinary advection-dispersion models can provide reasonable test results only if the fractured system can be regarded as an equivalent porous medium. The rock must be densely fractured, the hydraulic properties of the fractures must be rather uniform and diffusion of fracture into matrix water must be of minor importance.

Ogata & Banks (1961) developed an analytical solution of the partial differential equation [41] for experiments with a **step input** of the tracer. The one-dimensional advection-dispersion model introduced by Lenda & Zuber (1970) applies for convergent flow tracer tests. It assumes an **instantaneous tracer injection**, which is mathematically expressed by the Dirac (delta) function

$$[42] C(t=0)|_{x=0} = \frac{M}{Q} \delta(t)$$

The concentration C at the sampled site can be calculated for any time t since the tracer injection using the analytical solution

$$[43] C(t) = \frac{M}{Q t_0} \frac{1}{\sqrt{\frac{4\pi}{Pe} \left(\frac{t}{t_0}\right)^3}} \exp \left(- \frac{\left(1 - \frac{t}{t_0}\right)^2}{\frac{4t}{Pet_0}} \right)$$

Q represents the average production rate and M the injected tracer mass. The **ordinary Advection-Dispersion Model** of Lenda & Zuber is abbreviated by **ADM** in the following chapters.

2.4.2.2 Aquifers with discrete fractures

The discrete fracture transport models assume that the fracture system can be substituted by either a single fracture (single fissure models) or by a set of identical parallel fractures with uniform aperture (parallel fissure models). Moench (1995) developed a fracture transport model with sphere-shaped matrix blocks. The models assume that the fractures and the surrounding porous matrix can be represented by two orthogonal coupled one-dimensional systems. Advection and dispersion dominate the transport within the fracture whereas the transport in the rock matrix is governed by molecular diffusion due to its very small permeability. The models account for diffusion processes from the fracture(s) into the adjacent rock matrix. The diffusive mass flux from the fracture into the matrix is perpendicular to the fracture axis and proportional to the concentration gradient in the direction perpendicular to the fracture. Although fractures are seldom parallel and uniform, experimental data could be successfully interpreted by means of these models.

Step input

Grisack & Pickens (1981) were the first to derive an analytical solution for solute transport through a single discrete fracture for the case of a step input of the tracer and one-dimensional convergent flow experiments. They considered the diffusive mass flux into the matrix, but neglected dispersion within the fracture. Tang et al. (1981) found a solution for the case of a single discrete fracture and a step input considering advection and dispersion within the fracture and a diffusive mass flux into the matrix. Sudicky & Frind (1982) developed an equivalent solution for a set of parallel fractures.

Instantaneous tracer injection

Maloszewski & Zuber (1985) found an analytical solution for the diffusive mass flux from a set of parallel fractures into the rock matrix for convergent-flow experiments with an instantaneous tracer injection. The same authors developed the equivalent solution for a single discrete fracture that was referred to as the **Single Fissure Dispersion Model (SFDM)** (Maloszewski & Zuber, 1990). The model accounts for diffusion processes into the adjacent infinitely extended matrix. The concentration C can be expressed in terms of the mean transit time t_0 , the Peclet number Pe and a third fitting parameter α .

$$[44] C(t) = \frac{\alpha M}{2\pi Q} \sqrt{Pe t_0} \int_0^t \exp\left(-\frac{Pe(t_0 - \tau)^2}{4t_0 \tau} - \frac{(\tau \alpha)^2}{(t - \tau)}\right) \frac{d\tau}{\sqrt{\tau(t - \tau)^3}}$$

where τ is the integration variable. The model parameter α incorporates the matrix diffusion and is defined in terms of the matrix porosity n_p , the fracture width a_f , the molecular diffusion coefficient in free water D_m , the tortuosity factor for micropores, τ_p and the constrictivity factor ε by:

$$[45] \alpha = \frac{n_p}{a_f} \sqrt{\frac{\varepsilon D_m}{\tau_p}}$$

The SFDM has been applied successfully in earlier studies at the Lindau rock test site (e.g. Himmelsbach et al. 1992, 1998; Witthüser, 2000; Bäuml et al., 2001).

If dispersion within the fractures is neglected, the identical assumptions made within the SFDM lead to the following analytical solution of the **Single Fissure Piston Flow Model (SFPFM)** (Maloszewski, 1994).

$$[46] C(t) = \frac{\alpha M}{Q \sqrt{\pi t_0 \left(\frac{t}{t_0} - 1\right)^3}} \exp\left(-\frac{\alpha^2 t_0}{\left(\frac{t}{t_0} - 1\right)}\right)$$

2.4.2.3 Impact of non-instantaneous (retarded) injection

The ADM, SFDM and SFPFM described above assume an instantaneous tracer injection. It is, however, sometimes difficult to fulfil this assumption in practice. This may lead to errors in the test evaluation. The assumption of an instantaneous injection may be violated by the following reasons:

- The tracer may be forced to emanate in all directions from the injection borehole. This problem will arise in particular if the tracer volume is large and the porosity of the rock formation is small. It may be further enhanced if a large amount of chase fluid is applied after injection of the tracer volume (Guvanasen & Guvanasen, 1987).
- The tracer may be pushed into dead-end pores during injection. Thereafter the tracer will re-enter the active flow channels by a slow backward-directed diffusion (Witthüser, 2000).
- At least a portion of the tracer volume is only slowly released from the borehole into the formation due to different hydraulic properties of the formation and the immediate surrounding of the borehole (Carrera & Walter, 1989; Nowakowski, 1992). Such a slow decrease of the solute concentration at the injection borehole has recently been reported by Goldscheider et al. (2001) for a long distance tracer test in a Karst area. This effect leads to errors in the evaluation of tracer tests especially if the ratio of the mean transit time to the time needed for tracer injection is small. The borehole dilution may be minimised if a larger amount of chase fluid is applied; this, however, may severely disturb the flow field and enlarge the initial volume of the tracer plume.

The described effects will most likely lead to a stronger tailing of the TBC. The tailing will then be mistakenly attributed to either dispersive mixing or to the effect of matrix diffusion. This will lead to incorrect estimates of the model parameters t_0 , Pe and α . Several authors applied semi-analytical or numerical methods to take into account a non-Dirac type injection (Nowakowski, 1992; Moench, 1995; Carrera & Walter, 1989; Brouyère, 2000). Van Genuchten & Alves (1982) proposed an analytical solution for the case when the tracer input can be approximated by an exponential decay function. Tsang et al. (1991) applied their solution for the evaluation of field experiments. Bäümle (2001) introduced two analytical solutions with a time-variable input concentration, which are less cumbersome for evaluation purposes than the previously existing approaches. The solutions account for a non-instantaneous, i.e. a retarded release of the tracer solution from the injection borehole into the formation. In a similar approach as proposed by Van Genuchten & Alves, Bäümle assumed that the dilution of the tracer concentration in the injection well follows the exponential decay function given as

$$[47] \quad C(t=0)_{x=0} = \frac{\lambda M}{Q} e^{-\lambda t}$$

The solution of the 1-D transport equation [41] with respect to the boundary condition [47] was found by application of the Laplace transform method and reads (Bäümle, 2001):

$$[48] \quad C(t) = \frac{M \lambda}{Q t_0} \int_0^t \frac{1}{\sqrt{\frac{4\pi}{Pe} \left(\frac{\tau}{t_0}\right)^3}} \exp \left\{ - \left[\lambda(t-\tau) + \frac{\left(1 - \frac{\tau}{t_0}\right)^2}{\frac{4\tau}{Pe t_0}} \right] \right\} d\tau$$

Equation [48] describes the advective-dispersive mass transport in a convergent flow field for the case of an exponential input function. This model will be referred to as the **Advection-Dispersion Model with Exponential Input Function (EI-ADM)**.

In some cases, mixing and dispersion in the injection instrumentation and the well substantially influences the tracer input. The measured concentration in the well will then rather follow the relationship:

$$[49] \quad C(t=0) \Big|_{x=0} = \frac{\kappa^2 M}{Q} t e^{-\kappa t}$$

The corresponding analytical solution for the TBC is given by (Bäumle et al., 2000; Bäumle, 2001):

$$[50] \quad C(t) = \frac{M \kappa^2}{Q t_0} \int_0^t \frac{(t-\tau)}{\sqrt{\frac{4\pi}{Pe} \left(\frac{\tau}{t_0}\right)^3}} \exp \left\{ - \left[\kappa(t-\tau) + \frac{\left(1 - \frac{\tau}{t_0}\right)^2}{\frac{4\tau}{Pet_0}} \right] \right\} d\tau$$

Equation [50] describes the advective-dispersive mass transport in a convergent flow field for the case that the tracer input follows the time variable function [49]. This model will be referred to as the **Advection-Dispersion Model with Time-Variable Input Function (VI-ADM)**.

Figure 2 and 3 illustrate examples of tracer-input curves and the corresponding TBC's for the EI-ADM and the VI-ADM, respectively. The smaller the values of λ and κ , the more the injection is retarded. The graphs show that the retardation causes a shift of the peak arrival and an enhanced tailing of the TBC's. It can be concluded that the mean flow velocity will be underestimated if the retardation within the injection well is neglected.

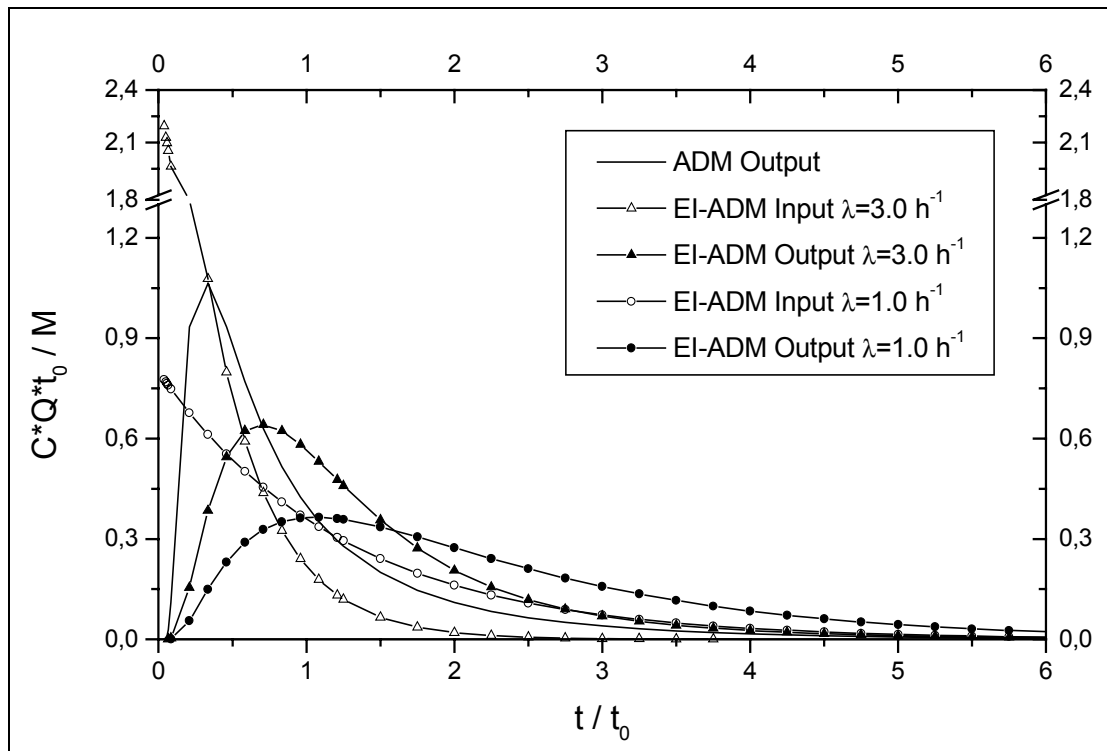


Figure 2 Normalised tracer input and corresponding breakthrough curves according to the EI-ADM for $Pe = 2.0$ and $t_0 = 0.8$ h

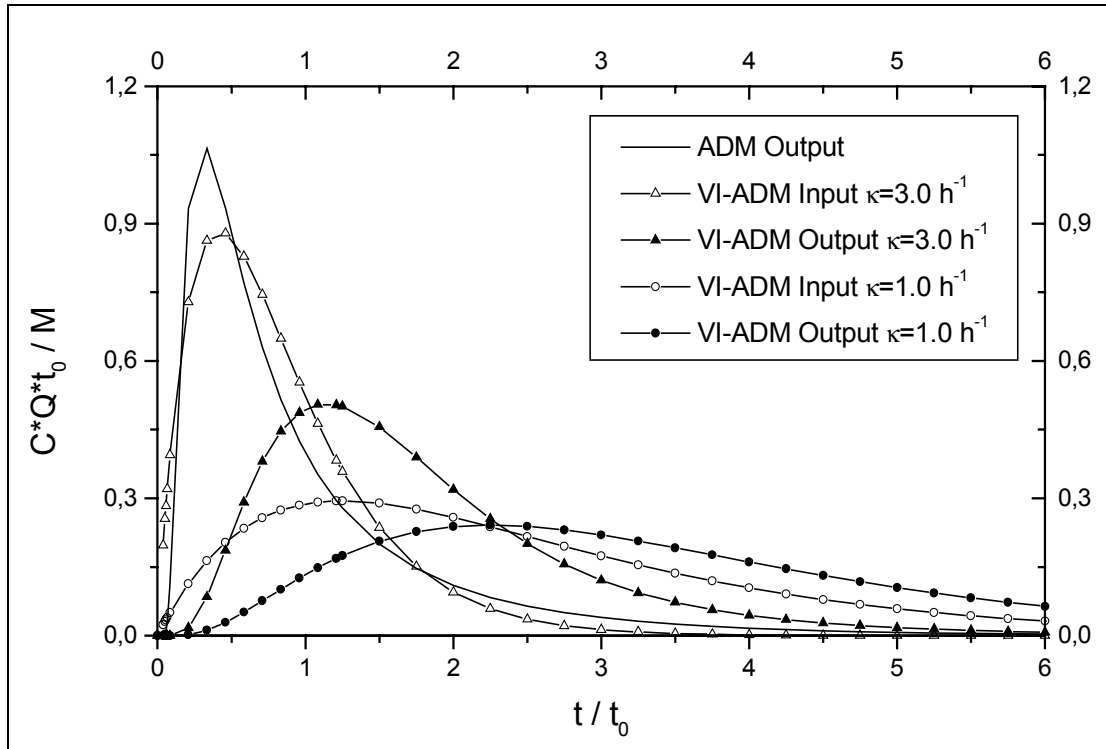


Figure 3 Normalised tracer input and corresponding breakthrough curves according to the VI-ADM for $Pe = 2.0$ and $t_0 = 0.8$ h

Table 3 summarises the transport models applied in this thesis. The models contain two or three parameters, which can be determined from fitting the measured TBC's.

Table 3 Fitting parameters of transport models

Transport Model	Equation for $C(t)$	Fitting parameter		
		1 st	2 nd	3 rd
ADM	[43]	t_0	Pe	---
SFDM	[44]			α
SFPFM	[46]			---
EI-ADM	[48]			λ
VI-ADM	[50]			κ

2.5 Hydrochemical and isotope studies

Hydrochemical and isotope studies, although strictly speaking not a geohydraulic method, are often included in hydraulic tests and regional groundwater investigations. Thus, they often give valuable additional information on the structure of the aquifer system.

Physico-chemical parameters are recorded during pumping tests as a standard procedure because the lowering of the hydraulic head might alter the geochemical conditions. The measuring procedure typically includes temperature, electric conductivity (EC), pH, Eh and dissolved oxygen content (DOC). Additionally, water samples can be taken at certain intervals and analysed to determine their chemical composition. Besides characterising the groundwater quality, the measurements can be used to ascertain the

origin of the pumped water. Changes in the groundwater composition during a test are often an indication of leakage from adjacent groundwater reservoirs or surface water.

In regional studies, hydrochemical and isotope data can be used to distinguish different aquifers. They are also useful for the detection of zones of interaction (mixing). Trace elements and environmental isotopes often provide a signature to a particular water type. Graphical procedures are particularly useful for interpretation (see e.g. Lloyd & Heathcote, 1985). Piper, Durov, Schoeller and ternary diagrams, for instance, can be used for identifying and classifying groundwater types within the study area (Hötzl & Witthüser, 1999). The distribution of different aquifers or the change in the groundwater composition along the flow path can be visualised by means of pie, radial or stiff charts by plotting them on a map of the study area at each sampling site.

Geochemical methods are widely used in arid and semi-arid areas to gain estimates of recharge. The chloride mass balance method has been successfully applied in many studies in semi-arid regions of Southern Africa (refer to Selaolo, 1998 and Külls, 2000 for a review). An estimate of direct groundwater recharge can be obtained by comparing the chloride content of groundwater with the chloride concentration of rainfall.

Hydroisotope measurements taken along a vertical profile can be used to determine the moisture flux and vertical flow velocities in the unsaturated zone. Furthermore, the recharge rate can be calculated from such a vertical distribution of the tracer (Scanlon et al., 2002). Radioisotopes such as tritium, ^{13}C and ^{14}C are used to determine the MRT of groundwater. The accuracy of reliable dating of water is however often limited by the uncertainty surrounding the initial radioisotope concentration (e.g. Moser & Rauert, 1982; Bredenkamp et al., 1995). The MRT is an important measure of the dynamics of groundwater flow since it can be used to determine transit times and groundwater velocities. If estimates of the aquifer thickness and porosity are available, the MRT can be used to quantify the groundwater recharge (e.g. Bredenkamp & Vogel 1970; Bredenkamp, 1995). Permeability estimates can also be derived from the MRT (Moser, 1979).

2.6 Groundwater modelling

The development of a numerical groundwater model was outlined by the National Research Council (1996: 14) as follows:

“Development of a conceptual model should be an iterative process. It begins with development of a conceptual model, which in turn, is used to formulate a numerical model of the flow system. The parameters of the numerical model are determined through the collection of field data, and the numerical model is used to predict the behaviour of the flow system. The predicted behaviour is compared to the actual behaviour of the flow systems as determined from field observations. If the predicted and observed behaviours do not match, the conceptual model is re-evaluated and updated, and the process is repeated.”

Groundwater modelling of the complex aquifer systems should commence with the development of a **conceptual hydrogeological model** (FH-DGG, 1999). The development of the conceptual model aims at a simplification of the stratigraphical setting and the fracture pattern. The model should nevertheless adequately delineate the overall

hydraulic characteristics of the investigation area. The process of developing a conceptual model of a fractured aquifer system includes

- ❑ the definition of **geohydraulic units** which combine rock formations with rather similar lithological and hydraulic properties,
- ❑ the detection of the most important features such as dominant faults and fracture zones,
- ❑ the identification of the hydraulic properties of such features and the assessment of their impact on the flow regime at the scale of interest,
- ❑ the identification of the geometry of fractures or fracture populations and their hydraulic characteristics such as porosity, permeability and anisotropy,
- ❑ the identification of exchange processes between the fractures and rock matrix.

Overall, the following types of conceptual models have been distinguished (National Research Council, 1996; Kolditz, 1997):

Equivalent continuum models

The heterogeneity is modelled by dividing the model area in geohydraulic units with rather uniform hydraulic characteristics. The fractures should be well connected. Individual fractures are not explicitly treated, although their integrated effect on the flow field caused by preferential orientation can be considered by assigning anisotropy factors to the units. Areally extensive faults and fracture zones can be treated as individual geohydraulic units with distinct permeability and porosity.

Multi- equivalent continua models

Multi- equivalent continua models are applicable if the heterogeneous reservoir is composed of two or more homogeneous equally distributed media. One or more fracture sets and the rock matrix are each treated as a single equivalent continuum. A mathematical relation couples the various continua and defines exchange processes between them. Commonly, the fractures represent the conductive system whereas the rock matrix has the higher storage capacity. The fractures are typically simulated as parallel plates or as lattices. The modelling approach is equivalent to the double porosity concept developed for the evaluation of pumping tests (see chapter 2.3.2.2) and the fracture type analytical solutions of tracer tests (see chapter 2.4.2.2).

Discrete fracture network models

A fracture network approach is required if the heterogeneity of the individual fractures or fracture populations does not justify an equivalent continuum approach. Groundwater flow is assumed to be mainly restricted to the fractures whose hydraulic properties largely differ from the properties of the rock matrix. The cubic law most accurately describes the flow within the fractures. The geometry and the degree of interconnectivity of the fractures substantially determine the flow field and the transport processes at the scale of interest. Fracture network applications therefore require information on the permeability and the geometry of the fractures including aperture, orientation, density and length. The in situ determination of the fracture properties, however, is cumbersome and information

on the spatial variability of the fracture characteristics will be generally limited. A deterministic evaluation of the fracture characteristics is therefore, if at all, only feasible for a combination of a very few single fractures. Sometimes, the fracture pattern may be idealised by an array of parallel or lattice shaped fractures. A more general approach is to gain statistical information on the fracture characteristics and to randomly generate different realisations of the fracture networks. The prediction of flow and mass transport parameters can then be expressed in terms of the mean and the standard deviation of the results from consecutive model runs.

Hybrid models

Hybrid models can be regarded as a combination of discrete fracture and equivalent continuum model.

3 Test site description

3.1 Lindau fractured rock test site

3.1.1 Physiography

The Lindau fractured rock test site is situated in the Southern Black Forest, Germany (Figure 4). The study area of 3.5 km² comprises parts of the catchments of the *Schwarzenbächle* and the *Höllbach*. The lowest point within the study area is defined by the confluence of the *Schwarzenbächle* and *Ibach* rivers at 765 m a.s.l. The rivers are surrounded by hills with topographic elevations ranging from 930 to 1000 m a.s.l. Fluvial erosion has created steep slopes on both sides of the *Schwarzenbächle* valley. Flat areas within the study area represent erosion surfaces that can be linked to various recessional stages of the glaciers during the Würmian (Weichselian) glacial period. During the cold and humid climatic conditions moors developed in these areas since the low permeable glacial deposits inhibit the rapid drainage of rainfall and seepage water.



Figure 4 Site plan of the test site Lindau

The test site is situated near the intended reservoir area of a formerly-planned hydrostation. The foundation area of the planned dam falls on a hydrothermally mineralised fault zone, known as the **ore dyke Hermann**. The permeability of the dyke is much higher than that of the undisturbed granite. More than 200 boreholes were drilled to investigate the geological situation and to assess the hydraulic impact of the dyke on the planned reservoir. The plan to build the reservoir has subsequently been abandoned because of economic and ecological reasons. About 40 of these surface boreholes are presently preserved. Additionally, a 450 m long observation tunnel was excavated in the granite. From the parallel pit, the dyke can be investigated via 19 boreholes that were drilled into the ore body (Figure 5). The parallel pit is located at a height of approximately 840 m a.s.l. or some 80 m b.g.s. After the exploration drilling, 1100 tons of cement were

injected into the fault zone as a vertically oriented fan in order to prevent seepage underneath the dam.

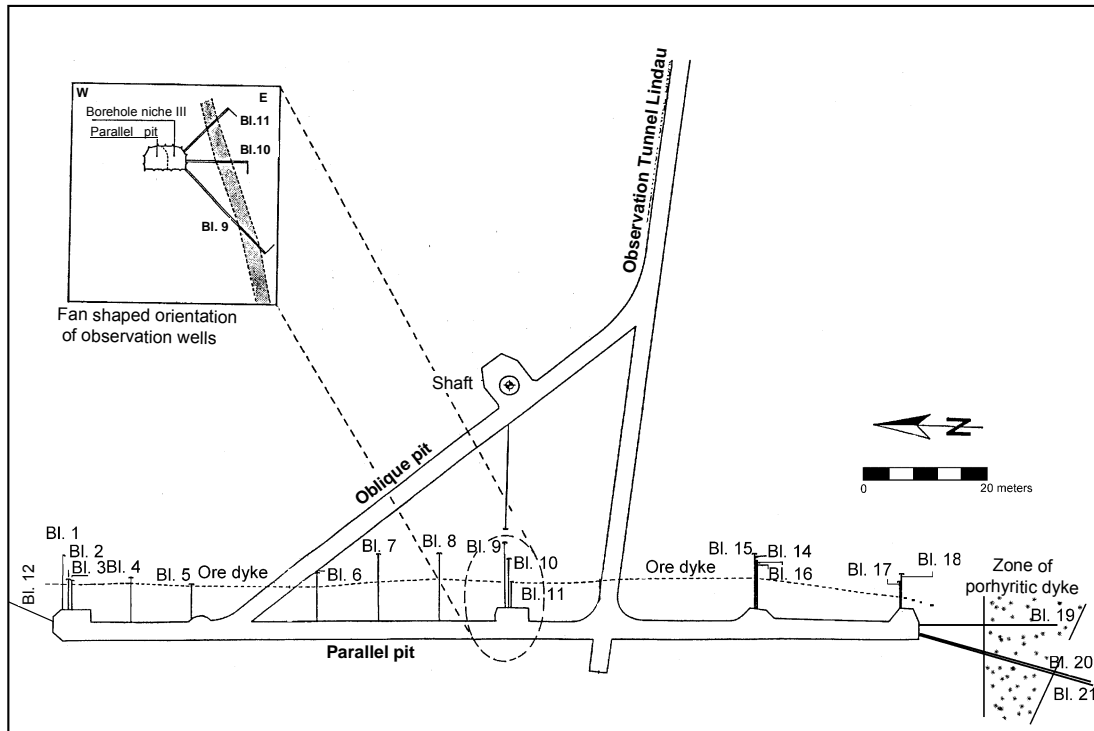


Figure 5 Plan of the observation tunnel and the boreholes in the parallel pit (after Himmelsbach, 1993)

3.1.2 Climate

The study area has a temperate to cold-humid climate. The mean annual temperature at *St. Blasien* (795 m a.s.l.) that is situated approximately 10 km north-east of the test site is 6.2°C. The mean monthly minimum of -2.2°C occurs during January and the mean maximum of 15.1°C is encountered in July (Mühr, 2002). The actual mean annual evaporation is between 550 and 600 mm (Armbruster, 2002).

The mean annual rainfall at *St. Blasien* amounts to 1704 mm. The highest rainfall occurs during the winter months from November to March with a mean monthly rainfall of 150 to 209 mm. A secondary maximum is developed in June amounting to 125 mm (Mühr, 2002). Summer precipitation is commonly associated with thunderstorms. Precipitation frequently falls as snow between November and April. Warm Atlantic fronts, however, may carry warmer air masses and rain even during the winter months. The winter season is therefore characterised by an intermission of rain, snowfall, snowmelt and dry periods.

Groundwater recharge

Regular groundwater level measurements taken in the years 1988-1992 and 1999-2000 typically show a recession from May to October. This indicates that direct groundwater recharge typically commences at the beginning of November. No recharge at all may be encountered during the summer months and early autumn, like in 1989. High intensity rainfall especially in May and June, however, commonly generates recharge, which

interrupts the recession. Except for the Höllbach catchment, the recharge has not been quantified in the study area until now.

3.1.3 Geology

The Black Forest is part of the Central European Variscan belt. The Variscan orogen is marked by the collision of two continental protoplates, Laurasia in the North and Gondwana in the South. The orogenesis lasted from the Silurian to the Lower Permian, but reached its peak during the Lower Carboniferous (360-265 Ma).

The Palaeozoic rocks of the Southern Black Forest comprise the *Badenweiler-Lenzkirch-Zone* in the north, a weakly metamorphic zone consisting of a series of Upper Viséan clastic sediments and volcanic rocks, and the *Hotzenwaldkomplex* in the south, a gneissan terrain intruded by a series of granitoid plutons. After the period of strongest convergence and intensive uplift and overthrusting, a system of wrench faults and extensional faults developed which led to the emplacement of four plutons in the *Hotzenwaldkomplex*. The plutons comprise the *Albtalgranite*, the *Bärhaldegranite*, the *Schluchseegranite* and the *St. Blasien granite*. According to Schaltegger (2000) the volcanic activity associated with the formation of the Southern Black Forest is subdivided into two phases, the Lower Carboniferous (Viséan) volcanism and the Upper Carboniferous (Namurian) volcanism. The intrusion of the granitoid plutons can be allocated to the second phase. Recent radiological dating resulted in an age of 334 ± 3 Ma for the *Albtalgranite*, 333 ± 2 Ma for the *St. Blasien granite* and of 332 ± 3 Ma for the *Bärhaldegranite* (Schaltegger, 2000).

The test site is located in the north-eastern part of the *Albtalgranite*, which covers an area of 125 km². The *Albtalgranite* shows normal granitoid composition in the western and central part of its distribution. It contains remarkable kalifeldspar-porphyroblasts up to 3 cm long. Towards the east, the *Albtalgranite* has a more granodioritic composition, which Emmermann (1977) explains by the assimilation of the neighbouring rock consisting of hybrid gneiss-anatexite.

Continuous divergence during the Carboniferous led to the development of **granite-porphyrific and rhyolitic dykes** with a preferential NW-SE strike direction. Schaltegger (2000) determined an age of 332 Ma (+2/-4 Ma) for a dyke within the *Badenweiler-Lenzkirch-Zone* close to the village of *Präg* using the U-Pb dating technique. The period of the dyke intrusions presumably extended into the Permian (Schleicher, 1978). The Lindau test site is intersected by three granite-porphyrific dykes, which are often associated with rhyolitic dykes at their margins. The rhyolitic dykes also occur as isolated features (Himmelsbach, 1993). The thickness of these dykes may reach up to 100m. They show a strike of 120-140° and dip at an angle of 60-85° in a north-eastern direction.

The porphyritic and rhyolitic dykes intersect the almost north-south (5°) striking **ore dyke Hermann**. The development of the hydrothermally mineralised dykes is associated with a period of volcanic activity during the transition from the Carboniferous to the Lower Permian. The exact age of these dykes in the Black Forest has not yet been determined. The dyke dips at an angle of 70-85° in north-eastern direction. Its thickness varies between a few decimetres and >3 m.

According to Metz (1980), Renk (1981) and Ritter (1994) the ore dyke minerals comprise mainly quartz and barite and to a lesser degree fluorite. Among the minor constituents

are galena and pyrite. The ore body owes its cavernous structure to the dissolution of fluorite by descending water. Quartz has subsequently partially replaced fluorite by pseudomorphosis.

The ore dyke *Hermann* is associated with a fault zone that runs parallel to the strike direction. A remarkable wrench fault with a NNW-SSE strike direction has dislocated the most southern of the three porphyritic dykes within the test site by about 100 m. The displacement extends from the *Krai Woog Gumpen* to the confluence of the *Schwarzenbächle* and the *Ibach*. Another SW-NW striking wrench fault dislocates the ore dyke and the two northern porphyritic dykes by 10 m in the area north of the observation tunnel (see structural map, Fig. 3.4 in Himmelsbach, 1993).

3.1.4 Hydrogeology

According to Himmelsbach (1993) four aquifers can be distinguished: The porous aquifer and the fractured aquifers which can be further subdivided into the granitic rock, the ore dyke, and the porphyritic and rhyolitic dykes. The porous aquifer consists of moraine deposits, talus deposits and the weathering product of the granite, the so-called *Berglesand*.

The **moraine deposits** are only present at an altitude of below 940 m a.s.l. and reach a thickness of up to 7 m. Their permeability is usually low and they form the confining layer in the northern part of the study area near the *Schwarze Säge*. Himmelsbach (1993) gives *K*-values of 3 to $7 \cdot 10^{-5}$ m/d for the moraine deposits.

The thickness of the ***Berglesand*** is highly variable ranging from a few meters to 25 m according to the borehole completion reports. The transition of the *Berglesand* to the granite is rather diffuse. The *Berglesand* is the product of the granite that has transformed to grit by in situ weathering processes and consists mainly of medium to coarse-grained sand. Consequently, the permeability of the *Berglesand* is good. According to Himmelsbach (1993) the *K*-values are in the range of 1 to $7 \cdot 10^{-4}$ m/d.

The host rock consists of the so-called ***Albtalgranite*** that has a low permeability. The pluton is characterised by a fairly regular, orthogonal fracture network, which developed during the cooling of the magma. The permeability of the granite is related to these fissures since the rock matrix is virtually impermeable. Wittek (1991) determined *K*-values in the order of 10^{-6} m/d to 10^{-7} m/d from the inflow rate of matrix water into suction cups under a given pressure difference. Mercury porosimetry carried out on more than 60 core samples indicated that the porosity of the granite is less than 1%. The ore body yielded porosities in the order of 2%. The highest porosities of up to 7% were found in the intensively fractured and hydrothermally altered parts of the contact zone (Himmelsbach & Maloszewski, 1997).

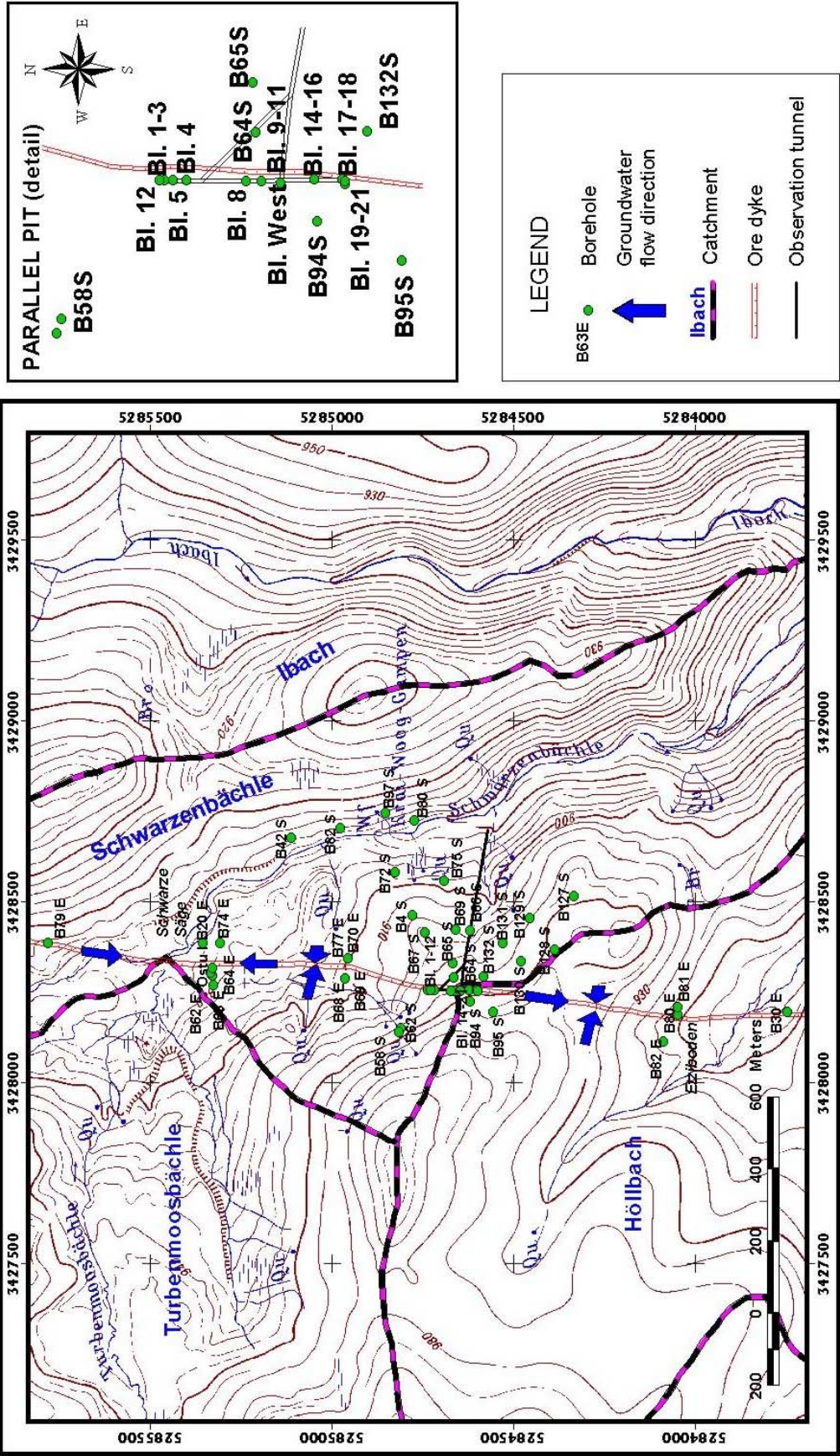


Figure 6 Locality map of the Lindau fractured rock test site

The **ore dyke Hermann** including the highly fractured contact zone adjacent to the undisturbed rock has locally a very high permeability that can be explained by fractures with apertures of up to 1 cm and the cavernous structure of the ore body. The intensive fracturing parallel to the dyke can be explained by the fault zone associated with the dyke, by the thermal strain during intrusion of the ore body as well as by the intensified weathering by descendant aqueous solutions. The permeability of the dyke and its contact zone is some magnitudes higher than the permeability of the adjacent granite but varies tremendously. The observation tunnel, for instance, intersects the dyke where it is virtually impermeable while a huge water flux was reported during the drilling of the boreholes from the parallel pit. The permeability of the dyke averages $4 \cdot 10^{-4}$ m/d according to Himmelsbach (1993). His results were obtained for the dyke section north of the observation tunnel. The results of former hydraulic tests will be reviewed and compared to the recent hydraulic test results in Chapter 4.1.2. The results are combined to obtain a regional distribution of the permeability.

The dyke system consisting of the ore dyke and its contact zone act as a conduit within the basement rock. Due to contrast in permeability, the dyke system drains the catchment and creates a narrow trough with a depression in the hydraulic head and with steep hydraulic gradients on both sides. The hydraulic head within the dyke zone is some 30 m below the groundwater level in the adjacent undisturbed rock. The cement injection acts as an artificial groundwater divide within the dyke system. The groundwater in the southern section of the parallel pit (Bl. 14-18) flows southward towards the *Höllbach*. The groundwater north of the cement injection (Bl. 1-12) follows the ore dyke in a northern direction and eventually drains into the *Schwarzenbächle*. The groundwater is assumed to exfiltrate close to the bridge across the *Schwarzenbächle* just 300 m north of the *Schwarze Säge* where the dyke intersects the river.

The **porphyritic and rhyolitic dykes** are intensively fractured at the contact with the adjacent rock due to high temperature differences during the intrusion and the subsequent shrinking during the cooling. It can hence be assumed that the dykes combine to form a drainage network orientated along their strike directions. Currently, however, there is little information on the permeability and the regional connectivity of such high permeable zones within the porphyritic and rhyolitic dykes.

3.1.5 Hydrochemistry

The groundwater of the study area usually fits in the Ca-HCO₃ or the Ca-Na-HCO₃ type. It is characterised by a low mineralisation indicated by an EC of generally less than 40 µS/cm. Only groundwater originating from stagnant regions within the sparsely fractured granite shows a higher mineralisation with the EC typically between 50 and 160 µS/cm (Stenzel, 1997). The groundwater in these zones is enriched by Na and K at the expense of Ca and Mg, which Himmelsbach (1993) explains by cation exchange processes controlled by the specific chemical environment (pH, Eh) within the stagnant zones. The groundwater originating from the ore dyke is characterised by increased barium concentrations of up to 0.5 mg/l and a higher fluoride content of up to 1 mg/l.

Himmelsbach (1993) investigated the vertical variation of the ³H and ¹⁸O content of the groundwater. He distinguished two vertical zones with strongly varying MRT's. The upper zone consists of the porous aquifer and the more intensively fractured and weathered upper section of the granite, and is characterised by a MRT of less than one year. This

zone is mainly drained by shallow and often intermittent springs. It reaches down to at the most 30 m and is sharply separated from the less permeable lower zone. The lower zone consists of granite, but excludes the dyke system. Himmelsbach determined a higher MRT ranging from 2 to 5 years and observed a somewhat increased mineralisation for this zone.

3.2 Tsumeb Aquifers

3.2.1 Physiography

The study area is located in northern Namibia (Figure 7) and covers an area of about 11,500 km². The study includes the northern Otavi Mountainland (OML) between the towns of Otavi, Grootfontein and Tsumeb and the flat Kalahari foreland up to an imaginary line from the south-eastern edge of the Etosha pan to Oshivelo and Tsintsabis.

Morphology and surface runoff

The **Kalahari** foreland is a peneplain, which dips gently to the north from a topographic height of 1150 m a.s.l. in the Tsumeb area to 1080 m a.s.l. at Oshivelo and Etosha. A surface drainage pattern within the Kalahari has generally not developed in the study area. Only at its northern boundary the intermittent river *Omuramba Owambo* drains westward into the Etosha Pan. Surface ponds commonly form in shallow depressions after strong rainfall.

The **OML** is a dolomitic massif dominated by a pronounced rugged relief with hills rising some 500 m above the surrounding plain. The highest peaks in the study area are found in the south reaching 1800 m a.s.l. The OML is intersected by a series of major broad west-east trending valleys and only a few minor lateral valleys, which drain into the main valleys. The OML represents a radial watershed draining westward into the *Ugab* catchment, northward into the Etosha and *Okavango* catchments, and southward and eastward into the *Omatako* catchment. The generation of surface runoff is unlikely since the area is characterised by a marked absence of a surface drainage system (Van der Westhuizen, 1984; DWA, 1990). The high evaporation and the predominance of underground drainage can explain this phenomenon, which is distinctive for karst areas.

Vegetation and land use

The study area lies within the thorn country vegetation belt of Namibia and Botswana. The typical vegetation is low thorny tree and scrub savannah. Open grasslands are not commonly developed, which is partly caused by overgrazing on cattle farms resulting in the development of bush encroachment. The dolomitic hills are largely covered by low tree savannah, which comprise both evergreen and deciduous types. Agriculture is restricted to comparatively small areas north-east and east of Tsumeb (on the farms *Mannheim*, *Heidelberg* and *Ludwigshafen*) and to areas close to Lake Otjikoto and Lake Guinas. The irrigation nevertheless causes an increased demand of groundwater.

Soils

The soils on the Kalahari sediments are very poorly developed lithosols. They are often sandy, but commonly contain interstratified layers of clay. Calcrete is extremely common

in the soil profile and is frequently more than 10 m thick. Külls (2000) suggests that recharge can be enhanced where the calcrete is thin and cracks and solution channels offer preferred pathways or where they mechanically prevent roots from abstracting water from greater depths. In the study area, however, vertical drainage through the calcrete is considered poor, and large flat areas become waterlogged during a good rainy season.

The dolomitic hills are generally barren or have a thin soil cover. The valleys are generally better covered but soil profiles of more than 2 m are uncommon.

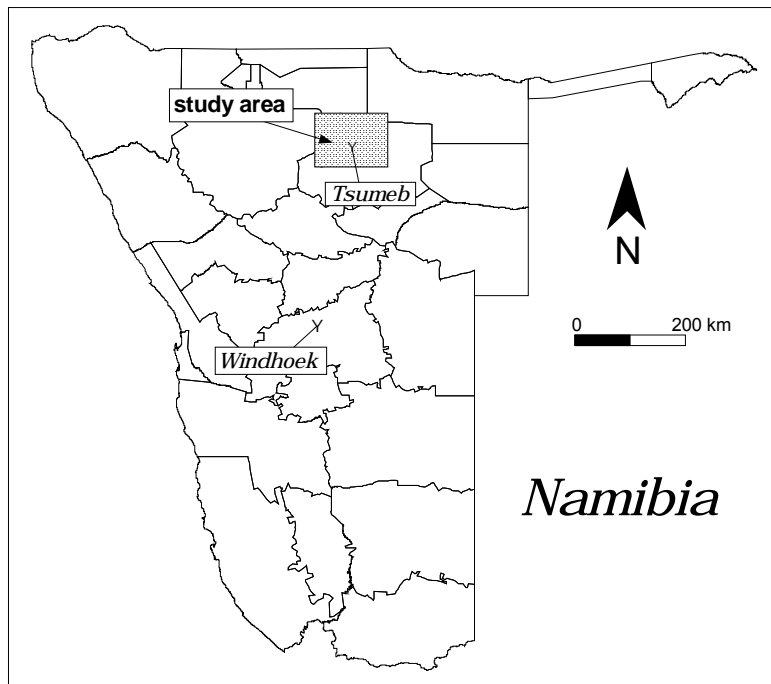


Figure 7 Locality map of the Tsumeb study area

3.2.2 Climate

The climate of the study area is semiarid to sub-tropical. The mean annual temperature at Tsumeb is 22°C with a mean monthly minimum of 15°C and a maximum of 29°C. The humidity averages at 46%. The mean annual potential evaporation of the Otavi Mountainland is between 2800 and 3000 mm (Christelis & Struckmeier, 2001). Wrabel (1999) determined lower evaporation values from Pan A records at Grootfontein. The mean annual potential evaporation from the years 1951 to 1985 amounts to 2314 mm. The highest evaporation of 2724 mm was recorded in 1962 and the minimum of 1852 mm occurred in 1974.

Rainfall

The rainfall is characterised by a distinct seasonal pattern. Virtually no rainfall occurs during the dry season from May to September. During the hot summer period from October to April the rainfall occurs mainly as short but strong convective thunderstorms. The mean annual rainfall (MAR) at stations within or in the close vicinity of the study area varies between 444 and 605 mm. Higher rainfall is encountered in the most elevated areas of the Otavi Mountainland in the south of the study area whereas the lowest rainfall

occurs in the flat Kalahari Basin in the north. The records at the Tsumeb rainfall station span the period from 1911-2001 (Figure 8). The average annual rainfall at Tsumeb amounts to 524 mm. The model calibration period that covers the previous 30 years is characterised by exceptionally high precipitation in the mid 1970's, with remarkably low rainfall in the 1980's and 1990's. A statistical analysis of the annual rainfall at Tsumeb was performed as part of this study (see Chapter 4.2.2.3).

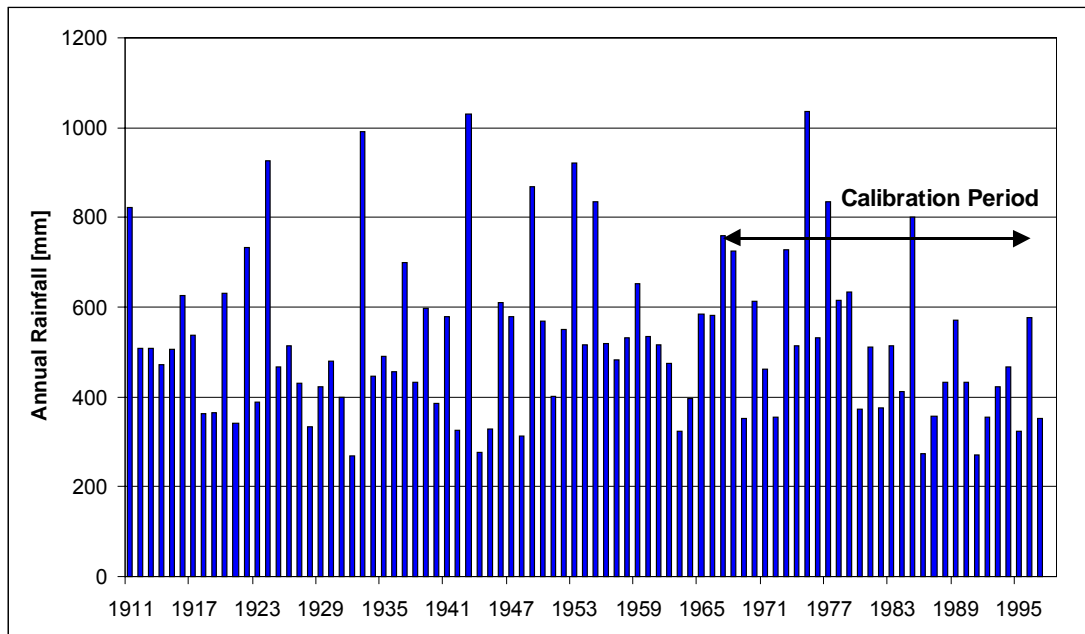


Figure 8 Annual rainfall at the Tsumeb station from 1911-1998

Groundwater recharge

The groundwater recharge of the **Kalahari Basin** has been investigated in numerous studies throughout Botswana and Namibia successfully applying the chloride mass balance method, isotope techniques or methods relevant to the unsaturated zone (soil profiles). For the eastern fringe of the Kalahari in Botswana, the recharge was found to vary between 1 and 15 mm or 0.2 and 3.5% of the MAR amounting to 450-500 mm (Vogel, 1974; Gieske et al., 1995; Verhagen, 1995; Sealaolo, 1998). Small recharge rates ranging from 0.6 to 5 mm or 0.2 to 1.4% of the MAR were published for the drier Central Kalahari in Botswana (Beekmann et al., 1996; Verhagen, 1999). Edmunds & Verhagen (1999) found a maximum recharge of 4.9 mm/a or 1.6% of the MAR (300 m) for the southern extent of the Kalahari in South Africa using the chloride mass balance method in hand auger profiles. An equally scattered range of values has been obtained for the Kalahari areas in Namibia. Dachroth & Sonntag (1983) assigned a recharge of 4 to 8 mm or 0.8 to 1.7% of the MAR (475 mm) to the Central Area of Namibia with a thin Kalahari cover. Klock et al. (2001) considered a recharge as low as 1 mm/a or 0.2% of MAR (425 mm) as a representative value for the north-eastern Kalahari in Namibia. Külls (2001) determined a recharge of 0.4 to 9.6 mm with an average of 4.5 mm or 1.1% of the MAR from soil profiles ('grey sand') within the same region. Wrabel found recharge values between 1.4 and 42 mm or 0.3 – 10.4% of the MAR (450 mm) for the *Hochfeld* area. In this area, however, the Kalahari consists mainly of a thin veneer that covers

marble and schist of Damaran age. Mainardy (1999) obtained a recharge of 8.5 to 14 mm or 2 to 3.3% of the MAR for the transition zone between Kalahari sediments and the Waterberg sandstone. The Kalahari aquifer in the south-western Kalahari, covering the so-called Stampriet Artesian Basin is characterised by a considerably lower MAR of 214 mm. According to the recently accomplished groundwater study (JICA, 2002) the recharge of 1.5 mm/a or 0.7% of the MAR, using a groundwater balance approach, was obtained. In the 1999/2000 rainy season, however, during which the rainfall exceeded the MAR by more than 100% the average recharge throughout the basin was estimated to be about four times higher.

The results of the different studies carried out in the Kalahari cannot readily be compared with each other since different methods for recharge estimates were applied. The chloride mass balance and soil profile methods provide local and present day recharge rates at the sampling site whereas basin-averaged values are derived from the water balance approach and isotope studies of the saturated zone. The recharge obtained from isotope studies of the saturated zone represents long-term average climatic conditions. These methodological differences explain the large variation of the recharge rates described in the literature.

The actual recharge largely depends on the lithology and thickness of the Kalahari, rainfall amounts and intensity and vegetation cover. **The existing studies suggest that recharge occurs only locally, and it was often assumed that the recharge is negligible in areas where the sand cover exceeds 6 m. High recharge values above 5 mm/a are apparently only representative for small areas and are often associated with the transition zone between the Kalahari sediments and hard rock formations. It is hence recommended to assume a conservative value of 1 to 2 mm/a for large-scale studies within the Kalahari.**

The recharge in the **Otavi Mountainland** is presumably larger than in the Kalahari due to the higher elevation and rainfall, and the exposure of the fractured or karstified dolomite (Figure 9). Comparatively few investigations to date have focussed on the quantification of the recharge in this area. Seeger (DWA, 1990) assumed a recharge at 6% of the MAR. Other estimates of the groundwater potential of this area at the Department of Water Affairs were based on a more conservative value of 11 mm or 2% of the MAR (Hoad, 1992). The BGR (1996) developed a groundwater model for the southern parts of the Otavi Mountainland. The model calibration resulted in a recharge of 1 to 2% of the MAR (566 mm) during years with normal or above average rainfall. After several years of below average rainfall, however, the recharge may drop to zero according to this study. The evaluation of radiocarbon data ($^{13}\text{C}/^{14}\text{C}$) resulted in highly variable recharge values ranging from 0.4 to 9 mm or 0.1 to 1.7% at the sampled wells (DWA et al., 2002d). These values are based on typical values of porosity for dolomites, which have not yet been measured in the field.



Figure 9 Karstified surface features: Exposed dolomite of the Elandshoek formation with low tree savannah near the road B1 south of Tsumeb (left) and Lake Otjikoto (right).

3.2.3 Geology

Tectonic evolution

The geological structure of Namibia is dominated by the **Damara Orogen** that occurred during the Late Precambrian (1000 – 545 Ma) and the Cambrian (545 – 510 Ma). The Damara Sequence traverses the central part of Namibia in a 400 km wide north-easterly direction. It also branches to the north, parallel to the coast, from its south-western portion. This geological period is characterised by phases of intracontinental rifting, continental break up, spreading, convergence and different stages of continental collision.

The early phase of the Damara Orogen was characterised by intracontinental rifting and continental erosion (Miller, 1983). Clastic sediments known as the Nosib Group were deposited in the rift valleys. The further drifting apart of the continental plates eventually created oceans between the Congo Craton in the north and the Kalahari Craton in the south. Deposits of mainly dolomite and limestone accumulated on the shelf that formed on the southern edge of the northern craton, which today is the Cuvelai-Etoshia Basin³⁾.

During the Late Precambrian (~650 – 630 Ma) the direction of crustal movement reversed and the oceanic crust separating the cratons, the so-called Damaran Mobile Belt, was pushed further and further under the plate of the Congo Craton. The continental collision and the subduction of the oceanic crust culminated in the formation of Alpine-type mountain belts 650 – 550 Ma ago. The dolomite and limestone along the edge of the Cuvelai-Etoshia Basin were folded and tilted upwards to form a rim to the basin. Seeger (DWA, 1990) subdivided the OML based on the geological structures into (from south to north) the eastern half of the *Otavi Valley-Uitkomst Syncline* (Area I), the *Grootfontein-Berg Aukas Syncline* (Area II), the *Harasib-Olifantsfontein Syncline* (Area III) and the *Tsumeb-Abenab Synclinorium* (Area IV). The study area comprises the Area IV

³⁾ The Cuvelai-Etoshia Basin covers the North-Central Regions of Namibia and was formerly called the Owambo Basin

(syncline) and the northern continuation, as well as the so-called **Nosib anticline** between Areas III and IV.

The orogenesis was followed by a long period of terrestrial erosion, which persisted from about 290 Ma until present (Buch & Trippner, 1997). The OML is considered as the remnants of the Otjiwarongo branch of the Damara Orogen. The Cuvelai-Etосha Basin has been a topographic depression in which sediments were deposited. It was the depository for a northern molasse, the Mulden Group, during the earliest phase of continental collision (650 – 570 Ma). Throughout the Permian and the Mesozoic, the Karoo Sequence was deposited in the basin. The Karoo is overlain by the Tertiary and Quaternary sediments of the Kalahari Sequence.

Stratigraphy

The stratigraphical succession comprises rocks ranging from the Proterozoic Grootfontein basement complex to the recent aeolian sands of the Kalahari Group (see Table 4). A distribution map of the stratigraphic units is shown in Figure 10.

The **Grootfontein Basement Complex** includes granite and gneiss, emplaced around 1600 Ma ago (Hedberg, 1979). Basement outcrops are found as isolated small outcrops in the southern study area (Nosib anticline).

Approximately 6000 m of sediments of the **Damara Sequence** have been accumulated upon the Grootfontein Basement Complex (Hedberg, 1979; Lombaard et al. 1986; Miller, 1997). The folded sediments of the Damara Sequence form the OML. The Sequence includes the Nosib Group (up to 1500 m) overlain by the dolomitic rocks of the Otavi Group (up to 3000 m) and the upper clastic sediments of the Mulden Group (>700 m).

The **Nosib Group** comprises the Nabis and Ghaub Formations with a variety of meta-sedimentary and extrusive rocks. At the southern boundary of the project area, the rocks of the Nosib Group are exposed. The predominantly dolomitic rocks of the **Otavi Group** have been stratigraphically subdivided into the (upper) Tsumeb Subgroup and the (lower) Abenab Subgroup. The dolomitic rocks contain interbedded layers of limestone, marl and shale. The **Mulden Group** is a molasse facies comprising mainly sandstone and shale. Only the younger Tschudi Formation has been deposited in the synclines of the central and western study area.

The **Karoo Sequence** consists of basal glaciogenic rocks overlain by clastic sediments. It overlies the Damara Sequence unconformably. Extrusive basalts were emplaced during late Karoo times, locally overlying and intermingled with the continental deposits. The presence of the Karoo in the study area was proven for the first time by the drilling and the geophysical survey included in the TGWS (DWA et al., 2002b). It underlies the Kalahari at depths of >170 m some 40 km north of Tsumeb.

The **Kalahari Sequence** forms an extensive cover of terrestrial origin. Its thickness at the transition to the OML, however, amounts to only some tens of meters and seldom exceeds 200 m in the northern part of the study area. Lime-cemented sands and conglomerates are followed by calcareous sand, clay and calcrete. Unconsolidated aeolian sand covers most of the Kalahari Sequence (Miller, 1992 & 1997).

Table 4 Stratigraphic succession (after Bäumle et al., 2001^{*)})

System	Sequence	Group	Subgroup	Formation	Lithology	Average Thickness
Quaternary		Kalahari			Aeolian sands	
Tertiary				Andoni	Sands, clay, calcrete	
				Olukonda	Sands, calcrete	
				Beiseb	Gravel, sandstone	
Cretaceous	Karoo 280 Ma			Unconformity		
Jurassic				undifferentiated: Etjo / Etendeka / Dwyka and equivalent	Sandstone, shale, basalt, dykes	
Triassic						
Permian to Cambrian	Unconformity (280-450 Ma)					
Namibian	Damara	Mulden (570- 650 Ma)		Tschudi	Shale, phyllite, siltstone, sandstone, conglomerate	>700 m
		Unconformity (570-760 Ma)				
		Otavi (700- 730 Ma)	Tsumeb	Hüttenberg	Dolomite, shale, chert	840 m
				Elandshoek	Dolomite	>1200 m
				Maieberg	Dolomite, limestone, shale beds	880 m
				Chuoss	Quartzite, tillite, shale	200 m
			Unconformity			
			Abenab	Auros	Dolomite, limestone, marl, shale	350 m
				Gauss	Dolomite	750 m
				Berg Aukas	Dolomite, limestone, shale	550 m
		Unconformity (830-840 Ma)				
		Nosib (900 Ma)		Ghaub	Phyllite, tuff, quartzite	750 m
				Nabis	Quartzite, conglomerate	
Mokolian		Unconformity (950~1500 Ma)				
		Grootfontein Basement Complex			Granite, gneiss, shist	

^{*)} based on BGR (1997), Miller (1997), Dierkes (1996), DWA (1993), Lombaard et al. (1986), Hedberg (1979) and TCL (1979);

Mining activities

The OML is well known for its occurrence of abundant base metals such as vanadium, copper, zinc, silver and lead. The ore deposits are associated with hydraulically favourable structures such as paleo-karst cavities and fault conduits (Lombard et al., 1986; Christelis & Struckmeier, 2001). Mining has taken place at Tsumeb, Abenab, Abenab West and Tschudi within the study area.

The mines at Abenab and Abenab West have been in operation from 1923 to 1947 and from 1947 to 1958, respectively. The Tsumeb mine was operational from 1907 to 1996 and then was temporarily closed until 2000, when it was re-commissioned. Huge amounts of water were abstracted during the mining process. The mining at Abenab reached a maximum depth of 215 m b.g.s. An amount of 3 to 4 Mm³/a was pumped from the open cast and the mineshaft. Abenab West is located only 300 m south of the Abenab Mine. The water table at Abenab West was lowered to a depth of 380 m b.g.s. with a maximum abstraction rate of 4.4 Mm³/a. The maximum depth of mining at Tsumeb reached 1800 m b.g.s. The water abstraction at the Tsumeb mine varied between 6 and 9 Mm³/a from 1961 to 1970 (BGR, 1995).

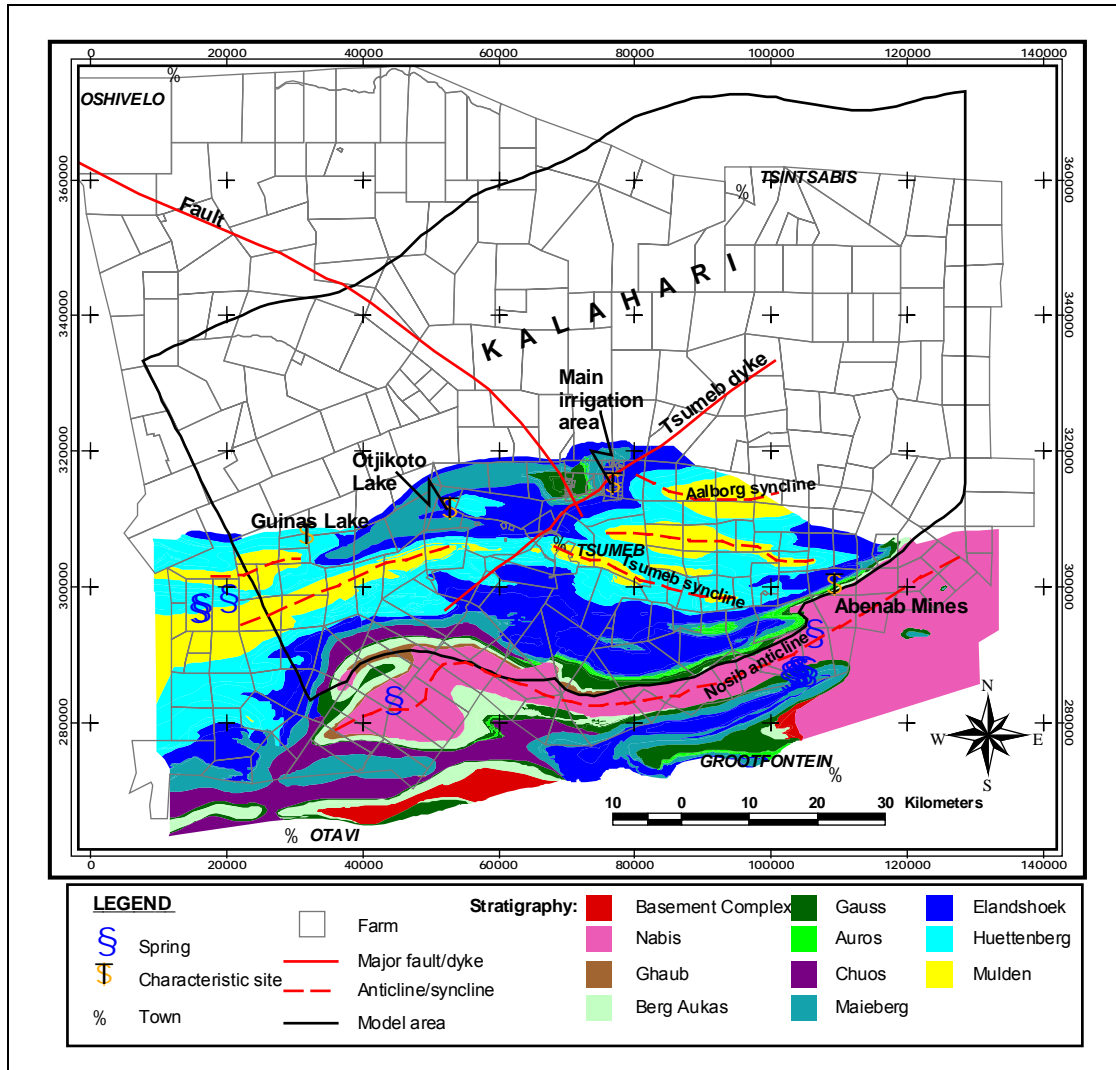


Figure 10 Map of stratigraphic units in the study area

Structural characteristics

The geological field study of the TGWS included an analysis of dominant structure types such as joints and fractures, karst features and surface weathering textures (DWA et al., 2002b). In general, the structure is controlled by the host rock (carbonate or clastic rock, massive or bedded), the structural regime (tensional or compressional) and by secondary effects, notably the solution of carbonate.

The **joint directions** on the surface and within the recently drilled boreholes were measured and statistically evaluated. Rose diagrams have been constructed for four areas to detect variations of the joint directions across the study area (Figure 12). In the western area, the fracture directions accumulate in a SW-NE direction whereas in the eastern area NNW-SSE directions prevail. In the central and central-east a more complex joint direction pattern can be observed. In the central area, the NNW-SSE and NE-SW directions predominate. In the central-east area, N-S and E-W joint directions are most abundant.



Figure 11 View of the southern study area from the farm *Ghaub*. The plain in the front is formed by the Nabis formation, which is exposed along the anticline between Areas III and IV. The mountain ranges in the background reach 1800 m a.s.l and consist of the rocks of the Ghaub Formation and the Abenab Subgroup.

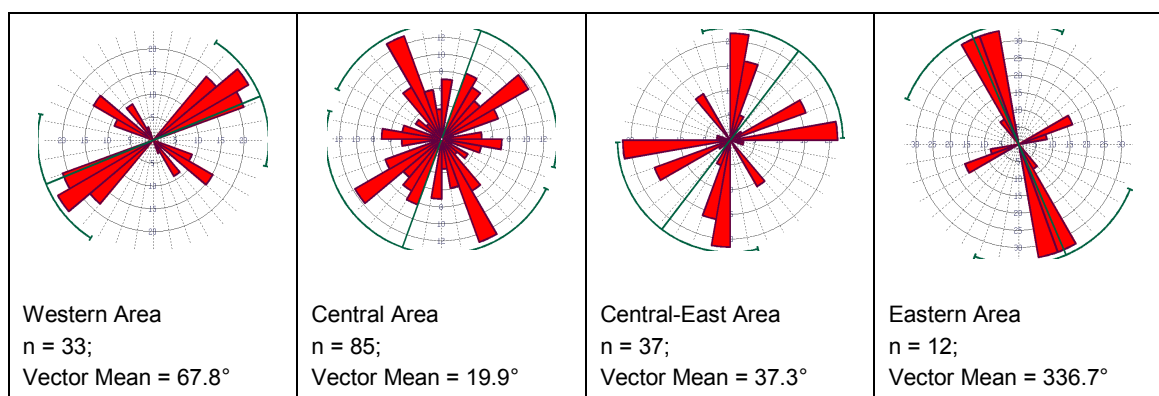


Figure 12 Rose diagrams (after DWA et al., 2002b)

It is concluded that N-S joint directions prevail in the study area except for the western part. Water strikes are mainly related to this structural direction. The prevailing joint direction also corresponds with the regional groundwater flow direction.

Regional faults have developed during the Cambrian (580-450Ma) and were mostly rejuvenated during the continental break-up in the Jurassic (180-130Ma) as Southern Africa began to separate from Australia and India. Therefore, the study area is

intersected by N-S trending faults along cross-warped axes and NNW-SSE trending conjugate faults. These faults are open tensional structures that are potentially good water carriers.

The NE-SW trending faults are however compressional closed structures. Only where **doleritic dykes** have intruded these structures, during the Jurassic, are they open and can carry water. From aeromagnetic data, three dyke swarms could be found in the Cuvelai-Etosa Basin, one trending NW, one N-S and one NE. The dykes all converge southwards on the *Etaneno Ring Complex* south of the Paresis Mountains. In the study area NE trending dykes and dyke swarms with extensions of several kilometres could be detected by lineament analysis using both satellite images and reconnaissance geophysical surveys (DWA et al., 2002a). The Tsumeb dyke is such a doleritic intrusive body.

Karstification

Four karstification periods of the dolomitic rocks of the Otavi Group have been delineated. The first and oldest period of karstification lasted presumably from 760 Ma to 570 Ma in a period of uplift and erosion during the peak of the Damaran orogenesis (Lombaard et al., 1986; BGR, 1997a). A second karstification period interrupted by glaciation and sedimentation lasted from 450 Ma to 280 Ma. The third karstification period occurred during early Tertiary (Van der Westhuizen et al., 1988). The last major phase of karst processes developed during the Pleistocene from approximately 34,000 to 14,000 years BP according to Geyh (1995).

Predominant karst features are the lakes Otjikoto and Guinas, the Ghaub Cave and the Karst chimneys of the Tsumeb mine and the Abenab mines. Minor karst features include sinkholes and circular structures and the widespread lapiés and pinnacles. Seeger (DWA, 1990) distinguished between karstification in inter- and intraformational fractured zones. The latter developed due to competency contrasts of the rocks (concordant features) and fractured zones along faults and dykes (discordant features). Open fractures with abundant open small karst voids and breccias with ferrous oxide coatings were encountered in the vicinity of the Tsumeb dyke on the farm *Scott* (DWA et al., 2002b) - see Figure 13. It can hence be assumed that karst fracture zones are associated with folding and faulting or aligned with intrusive dykes.

Despite the occurrence of these karstic features, most authors assume that karstification is of minor importance within the carbonates of the Otavi Group. Van der Westhuizen et al. (1988) stated that the preservation of pre-Tertiary karst features is unlikely since erosion has largely removed older karstified units within the sedimentary succession. Consequently, only deep karst features such as the Tsumeb chimney could endure. The BGR (1997) stated that karstification in the OML is relatively poor and that deep-reaching cavities such as lakes and caves are relatively rare. They justify their findings by the smooth groundwater contour plan throughout the OML and the well hydrographs, which show a smooth decline of the groundwater levels during the period from 1985-1992. It can be concluded from these investigations that the karstification has only limited impact on the regional groundwater flow pattern. However, effective karstification may be present along structurally weak zones, where chemical solution could advance.



Figure 13 Mud rotary drill cuttings of WW39992 show breccias with ferrous oxide coatings within the dolomite (Hüttenberg formation).

3.2.4 Hydrogeology

The **Tsumeb Aquifers** form an important regional groundwater resource for the water supply of the adjacent municipalities and the irrigation and cattle farming. Three different aquifer types can be distinguished within the study area, i.e. the Dolomite Aquifer, the Kalahari Aquifer and aquifers associated with dyke and fault zones.

The **Dolomite Aquifer** of the Tsumeb and the Abenab Group have been described as low to medium permeable fractured aquifers (DWA, 1990; Bäuml et al. 2000; DWA et al. 2002c). The carbonate rocks have only little primary porosity. The permeability of the Dolomite Aquifer may, however, be locally enhanced due to intense karstification at contact and tectonic shear zones. The transmissivity of the heterogeneous rocks may vary between 1 to several 100 m²/d and reach more than 1000 m²/d locally.

The **Kalahari Aquifer** consists of unconsolidated gravel and sands with intermittent layers of clay or calcrete. The Kalahari Aquifer is generally considered a porous aquifer although recent hydraulic tests indicate that the formation is locally compacted and fractured. The thickness and the transmissivity of the Kalahari Aquifer increase towards the northern edge of the study area. The highest transmissivity values, in the order of 5000 m²/d, are found in the Oshivelo Artesian Aquifer at the north-western edge of the study area according to recent pumping test results (DWA, 2002).

Fractured dykes and fault systems of different geological provenance form the third aquifer type. The hydraulic properties of these dykes are mostly unknown although their influence on the entire hydraulic regime cannot be neglected. For instance, the Tsumeb and the Abenab mines are situated near such dyke and fault systems.

The clastic and metamorphic sediments of the Nosib and the Mulden Group generally act as **aquitards**. Within the Abenab Subgroup intermittent layers of quartzite, tillite, marl and shale have a low permeability. The Karoo deposits also proved to have a low permeability and this separates the Kalahari Aquifers from the Dolomite Aquifer in the northern part of the study area. A more comprehensive investigation of the hydraulic properties of the various formations forms part of this thesis and is presented in Chapter 4.2.1.

The **springs** within the study area are intermittent and generally related to the contact zones between relatively impermeable and more permeable formations. The discharge from these springs, however, is so low that they become negligible for the water budget calculations.

The groundwater flow is generally directed from south to north. Steeply dipping formations and compressional closed structures with a low permeability can locally dissect and divert the general **groundwater flow** direction as for example within the Abenab formation in the south-eastern part of the study area (see modelling results in Chapter 4.2.2.4). The Dolomite Aquifer dips underneath the Kalahari Aquifer north of Tsumeb. The Kalahari Aquifer is therefore fed by direct recharge and by groundwater originating from the adjacent or underlying Dolomite Aquifer.

3.2.5 Hydrochemistry

The groundwater in the Dolomite Aquifer generally fits in the Ca-Mg-HCO₃ groundwater type. Ca-HCO₃, Mg-HCO₃ and Ca-Mg-Na-HCO₃-Cl-SO₄ groundwater types are of minor significance according to data from Huyser (1982) and DWA et al. (2000). The composition of the groundwater is characteristic for dolomitic rock. A high hardness of the groundwater is apparent. The groundwater composition of the Kalahari Aquifer shows a transition from Ca-Mg-HCO₃ groundwater type in the southern area close to the Dolomite Aquifer to Mg-Na-HCO₃-Cl-SO₄ type further north and Na-Cl-HCO₃ or Na-Cl groundwater type at the northern boundary of the investigation area.

Isolated, increased nitrate concentrations occur throughout the study area, indicating intensive use of fertiliser or infiltrating water contaminated with faeces from livestock. Nevertheless, the majority of analyses for major ions and physical parameters show group A (excellent) and B (good) groundwater quality according to the Namibian Guidelines for the Evaluation of Drinking Water for Human Consumption (DWA, 2002a).

The **vertical distribution** of oxygen and sulphate indicates a zone of oxidising milieu down to approximately 150 m b.g.s according to DWA et al. (2002a). Between 150 m b.g.s. and 350-450 m b.g.s. the hydrochemical environment becomes increasingly reducing. Hydrochemical data from depths below 350 m b.g.s. is extremely scarce, but a further increase in reducing conditions is most likely. Measurements of sulphate in the Tsumeb mineshaft showed a sharp decrease of the sulphate concentration at mining levels between 1200 m b.g.s. and 1600 m b.g.s. (Marchant, 1980). Hence, a highly reducing hydrochemical environment prevails at depths below 1200 m b.g.s. even in the tectonically disturbed zone around the mine.

3.3 Comparison of the test sites

By comparing the two investigation areas, their difference in the geology, the lithology and the vegetation becomes evident. They are situated in different climate zones that are characterised by largely different amounts of precipitation and evaporation and a very dissimilar rainfall pattern. Furthermore, the amount of recharge and the renewal rate of groundwater at the Lindau test site largely exceed those of the Tsumeb Aquifers.

Nevertheless, there are some obvious and interesting similarities between the two study areas. Firstly, both the granite and the dolomites have a low primary porosity, and groundwater flow is therefore almost entirely restricted to fractures. The groundwater systems are divided both laterally and vertically, in zones of distinct residence times. Furthermore, individual fault and dyke systems such as the ore dyke *Hermann* at Lindau and the Tsumeb dyke act as conduits, which noticeably influence the groundwater flow regime. The impact of these lineaments, however, differs in magnitude, which is basically due to the differing scale of the investigation. The ore dyke *Hermann* is the predominant hydraulic feature within the study area of 3.5 km². The Tsumeb dyke would be of equal importance if the investigation area were comparable (e.g. for investigations towards the development of a well field). However, because of the scale of interest of this study, with an investigation area of 11,500 km², its impact will be considerably smaller.

4 Results

4.1 Lindau fractured rock test site

4.1.1 Well hydrograph recession analysis

The WHRA was carried out at the 27 boreholes with available groundwater level records including the flooded exploration shaft *Östu I*. Additionally, the hydrographs of 4 boreholes in the observation tunnel could be analysed using pressure gauge (manometer) measurements. A conventional recession analysis that uses runoff measurements could be performed at the artesian borehole B 30E located in the very south of the study area. During 1999, the runoff at the borehole dropped from 3.3 l/s in April to 2.4 l/s in late September.

The available groundwater levels cover the years 1988 to 1992 and 1999 to 2000. Consequently, the WHRA could be individually performed for a maximum number of 7 years at each site. For most of the boreholes, however, the number of years that could be analysed is smaller (see Appendix 1 and 2). For example, at boreholes B 69E, B 70E and B 74 E no recent data is available since they collapsed after 1992.

The Hydrological Year in Central Europe is defined as the period from 01 November to 31 October, as the lowest river and spring discharge (base flow) is typically observed during fall. The recession of the groundwater levels generally occurred during the second half of the Hydrological Year, i.e. from May to October. A maximum in the groundwater levels was mostly encountered during April or May and served as the starting point for the WHRA. The most useful hydrographs are those for the years with little precipitation and negligible direct groundwater recharge during summer. The year 1989 with virtually no recharge during summer and the year 1992 with little recharge are therefore the most suitable for the analysis. The high rainfall associated with thunderstorms during May and June of 1999 (see Figure 19) made the analysis more difficult. The failure of the WHRA for individual years was due to high fluctuations in the groundwater levels within the recession period or, in some cases, sparse data.

As a first step, the recession segments had to be identified in a semilogarithmic plot of the water level h against time. The matching strip method, as described in Chapter 2.2.2, was used to create the master recession curve out of the individual straight-line segments for each year with groundwater level records. Thereafter the method 1 and method 2 presented in Chapter 2.2.2 were applied to the data of the master recession curve. According to the evaluation procedure of method 1, the water levels h_{t+dt} were plotted against h_t and the line of best fit was determined (Figure 14 left). The retention coefficient α_M and the elevation of the spring outlet E were calculated with equations [9] and [13], respectively. With reference to method 2, the derivative dh/dt was plotted against h (Figure 14 right). The retention coefficient is equal to the slope of the line of best fit according to equation [14]. The elevation of the spring outlet was calculated using equation [17]. Finally, the MRT τ was determined for both methods with equation [2].

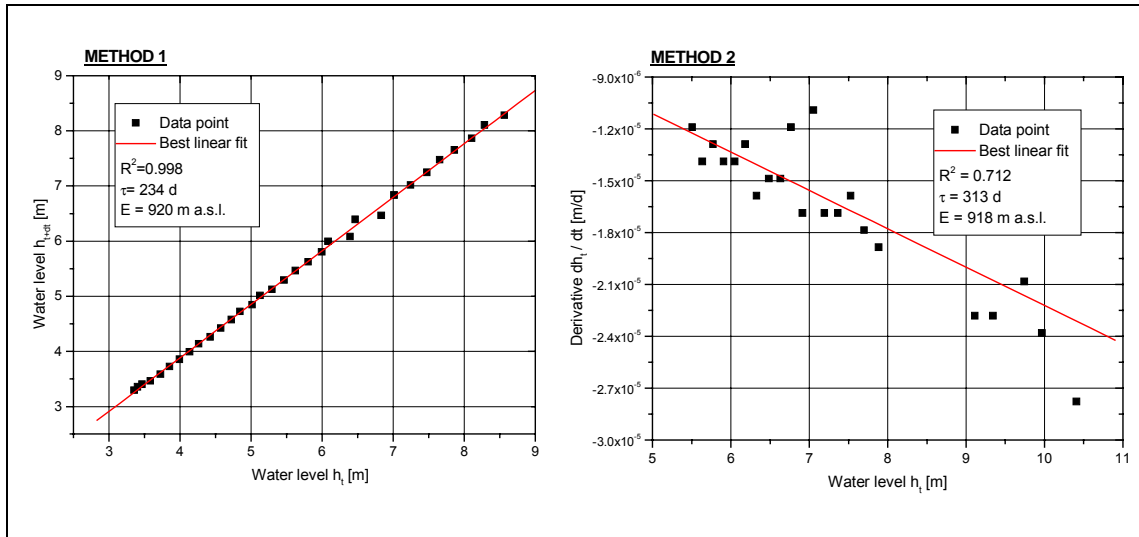


Figure 14 The processed 1989 hydrograph data of B 130S as an example of the graphical fitting according to method 1 (left) and method 2 (right).

Appendix 1 contains the results obtained from method 1 for each borehole including the maximum, minimum and median values of both the MRT and the elevation of the spring outlet. The analogous results of method 2 are presented in Appendix 2. The elevation of the spring outlets varies between 860 and 940 m a.s.l. according to the WHRA. These values match the elevation of the *Schwarzenbächle* (850 – 875 m a.s.l.) and the line of springs along the western valley side at 880 – 920 m a.s.l., delineated on the topographic map (see Figure 6). The fact that they typically exceed the mapped elevation by 10 to 20 m is a clear indication that the actual spring outlet is covered by debris.

Figure 15 shows the correlation between the results of methods 1 and 2. Both methods produce very similar elevations for the spring outlets as indicated by the slope of the regression line of 1.0. The MRT shows higher discrepancies, in particular for values larger than 400 d. Various reasons contribute to this fact: The MRT obtained from method 1 is highly sensitive with respect to the slope of the line of best fit. The data of the derivative plot in method 2 is generally quite scattered. Furthermore, the separation of the recession segments is a difficult task in years with a repeated occurrence of recharge events and often depends on subjective judgements. Yet, because of these difficulties, it is even more important to apply both methods for as many years as possible.

Figure 16 shows three examples of the WHRA. The hydrograph at B130S shows the excellent fit to the recession curve (equation [4]) in 1989. The MRT equals 234 d. During 1999, the initial groundwater level was some 3 m higher compared to 1989. Two linear segments can be distinguished and associated with the depletion of two reservoirs with distinct storage properties. The recession curve represents the best fit to equation [5], which describes the superposition of two reservoirs.

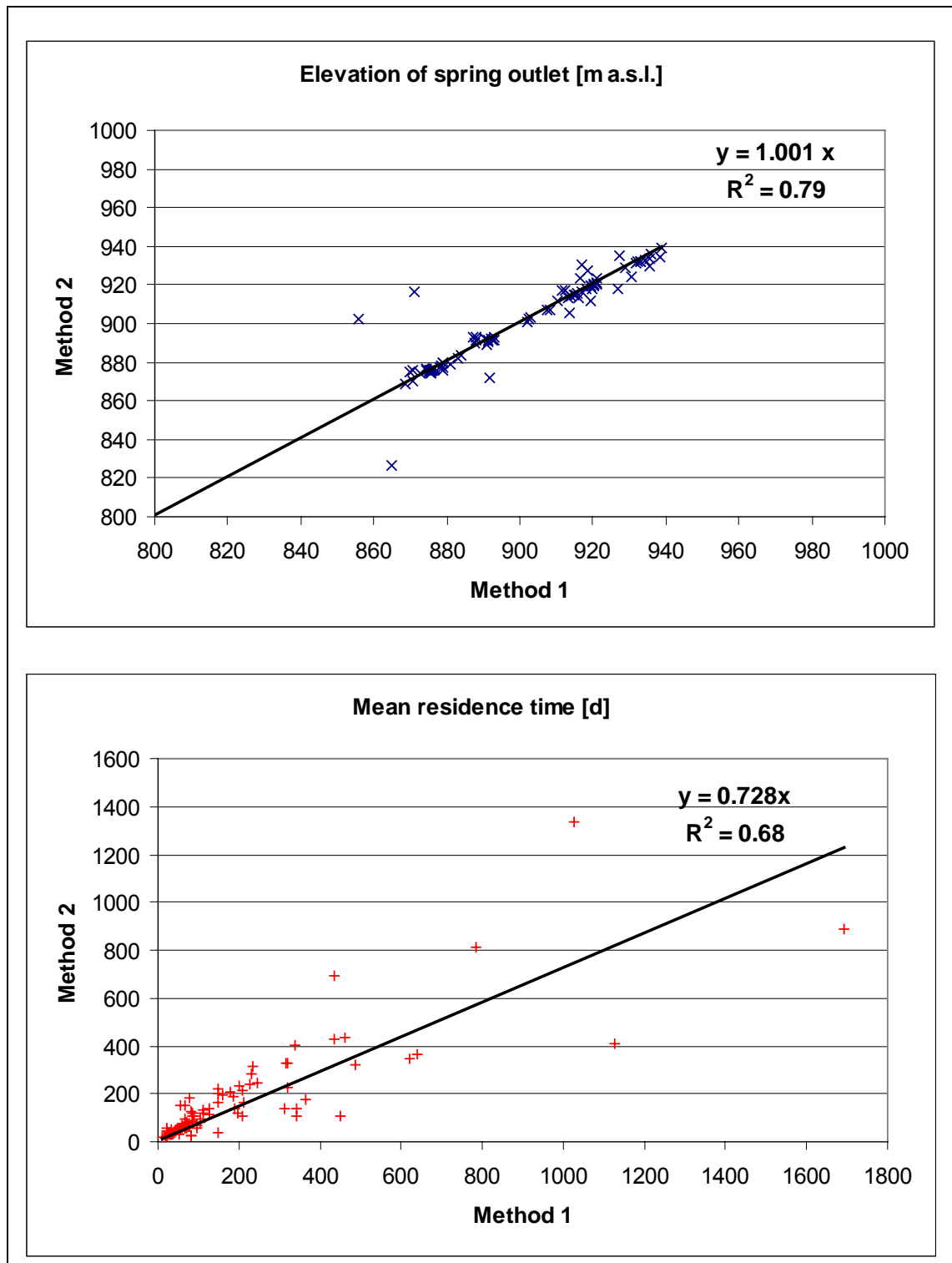


Figure 15 Correlation of the WHRA results according to methods 1 and 2

The analysis results in a MRT of 25 d for the first segment and 179 d for the second segment. A similar pattern was observed at B 68E for the same year. The MRT of the two reservoirs yields 9.5 d and 83 d, respectively. Such an additional reservoir with a fast response (1st recession segment) was identified for a number of boreholes, but the quantification of the corresponding MRT proved to be inaccurate since the first straight-line segment was generally of very short duration.

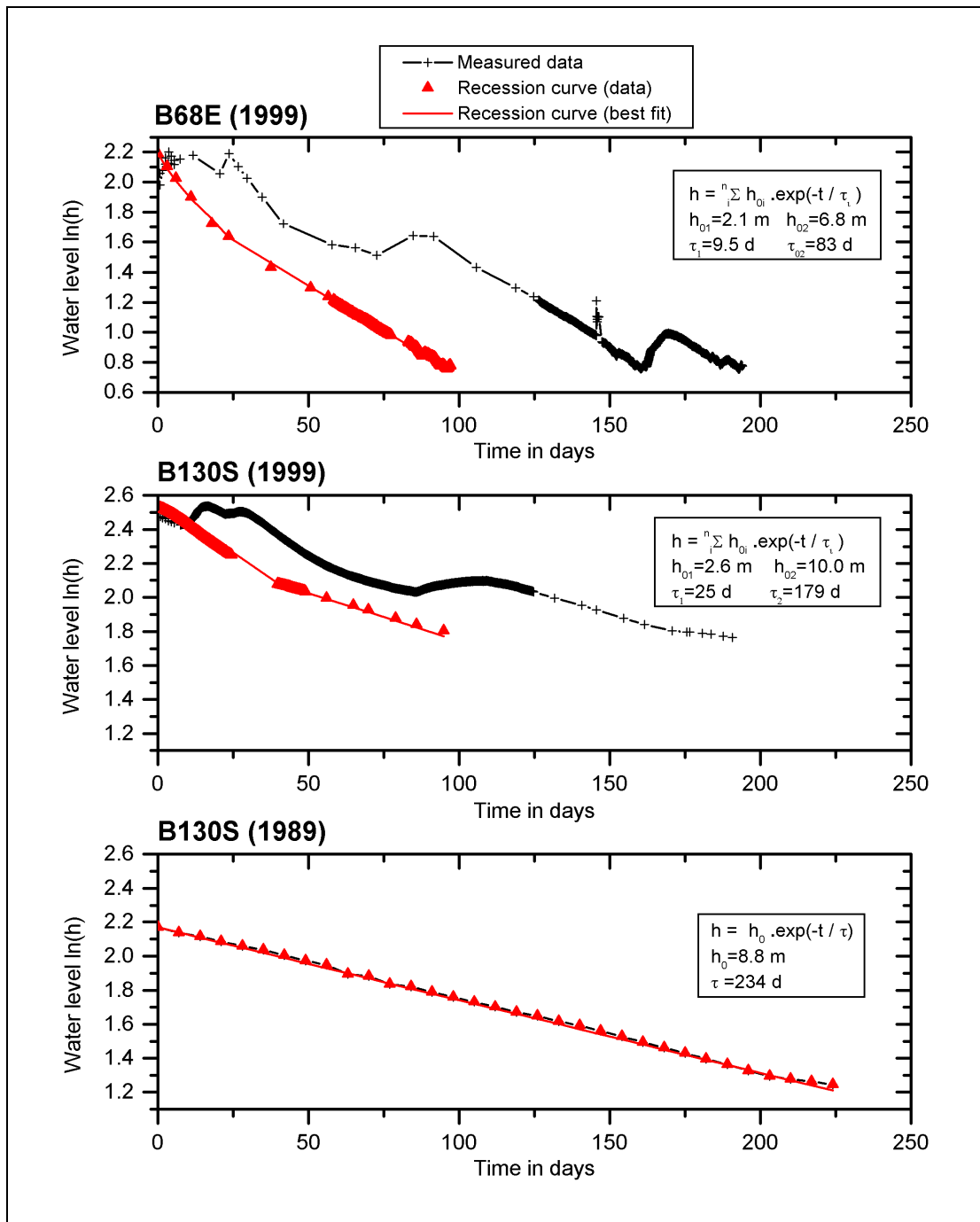


Figure 16 WHRA (method 1) performed at B 130S and B 68E for selected years

The fact that two reservoirs with different mean residence times were only observed in exceptionally wet years with above-average groundwater levels indicates that the aquifer is subdivided in distinct vertical layers. The **first recession segment** represents an upper reservoir with a fast response consisting of *Berglesand* or the unconsolidated strongly fractured and weathered upper section of the granite. This upper reservoir probably belongs to the vadose zone unless it is replenished by strong rainfall events. After replenishment, it will be quickly depleted due to its high permeability and the increased hydraulic gradients along the steep slopes of the mountainous terrain. Most of the runoff produced from this reservoir can be attributed to interflow. Biehler (1995)

analysed the runoff records over three consecutive years at three tunnels in the Southern Black Forest and also identified a multi-layered aquifer system from a recession analysis. The recession limbs showed a first straight-line segment with a MRT of 33 to 50 d and a second segment with a MRT of 333 to 1000 d. He allocated the first segment to the upper highly weathered zone and the second segment to the lower, less permeable granite and gneiss.

The MRT's obtained from the analysis of the **2nd recession segment** are summarised in Table 5. The high range of values that vary by an order of magnitude reflects the heterogeneity of the fractured rock system. The MRT's that were obtained range from 13 d at Bl. 12 to 637 d at B 30E. Interestingly, the MRT seems to be clearly linked to the catchment area as well as to the geology and lithology encountered at the investigated site. The average MRT amounts to 61 (± 72) d in the northern catchment, i.e. the area north of the cement fan within the observation tunnel. In the southern catchment, which drains towards the *Höllbach*, the average MRT amounts to 256 (± 152) d. It is unlikely that this remarkable difference is due to a non-representative distribution of the boreholes. It follows that the northern catchment is characterised by a much higher permeability and an immediate drainage of the groundwater reservoir. This result is illustrated by the regional distribution of the MRT depicted in Figure 17. Within each catchment, the geological setting largely controls the MRT. It is evident that except for B 30E the lowest MRT is associated with the dykes and their contact zones. A high MRT occurs in the undisturbed granite. This finding confirms that groundwater flow within the granite massif is largely restricted to fractured and tectonically disturbed zones.

It is likely that additional groundwater reservoirs with larger MRT's exist over and above the two reservoirs identified by the well hydrograph analysis. The reservoir with the lower MRT (2nd recession segment) presumably corresponds to the shallow upper aquifer (± 30 m) within the *Berglesand* and the weathered granite, for which Himmelsbach (1993) obtained a MRT of less than 1 year from vertical profiles of the ^3H and ^{18}O content (Chapter 3.1.5). It additionally includes deeper zones in the vicinity of the dykes. For the undisturbed granite at greater depths, Himmelsbach determined a MRT of 2 to 5 years. Such a reservoir would create a third, flat segment of the recession curve during late times. However, since the period of recession will always be less than 180 d due to the heavy winter rains, it is not possible to detect this reservoir from the WHRA.

Table 5 Mean residence time obtained from the WHRA (combined results for methods 1 & 2)

Borehole	MRT τ [d]	Catchment area	Geology
Bl. 12	13	North	ore dyke, contact zone
Bl. 3	18	North	ore dyke, contact zone
B 42S	25	North	Albtalgranite
B 77E	25	North	Porphyritic dyke, contact zone
Östu I	33	North	ore dyke, contact zone
Bl. 11	39	North	ore dyke, contact zone
B 74E	41	North	Albtalgranite, contact zone
B 68E	42	North	Porphyritic dyke
B 64S	48	North	Porphyry grit, Albtalgranite
B 64E	48	North	Albtalgranite, contact zone
B 62E	49	North	Albtalgranite, contact zone?
B 63E	52	North	Albtalgranite, contact zone
B 67S	55	North	Albtalgranite
B 69S	61	North	Albtalgranite
B 70E	65	North	Porphyritic dyke, ore dyke
B 69E	72	North	Porphyritic dyke
B 65S	73	North	Berglesand, Albtalgranite
B 66S	105	South	Albtalgranite
B 94S	124	South (?)	Albtalgranite
Bl. West	130	South (?)	Albtalgranite
B 129S	138	South	Berglesand, Albtalgranite
B 81E	158	South	Albtalgranite
B 95S	174	South	Albtalgranite, quartz porphyry
B 82E	199	South	Albtalgranite, contact zone
B 80E	204	South	Berglesand, Albtalgranite
B 127S	248	South	Albtalgranite
B 130S	267	South	Berglesand, Albtalgranite
B 4S	340	North	Berglesand, Albtalgranite
B 131S	377	South	Berglesand, Albtalgranite
B 132S	410	South	Albtalgranite
B 128S	412	South	Porphyry grit, Porphyritic dyke
B 30E	637	South	ore dyke, contact zone

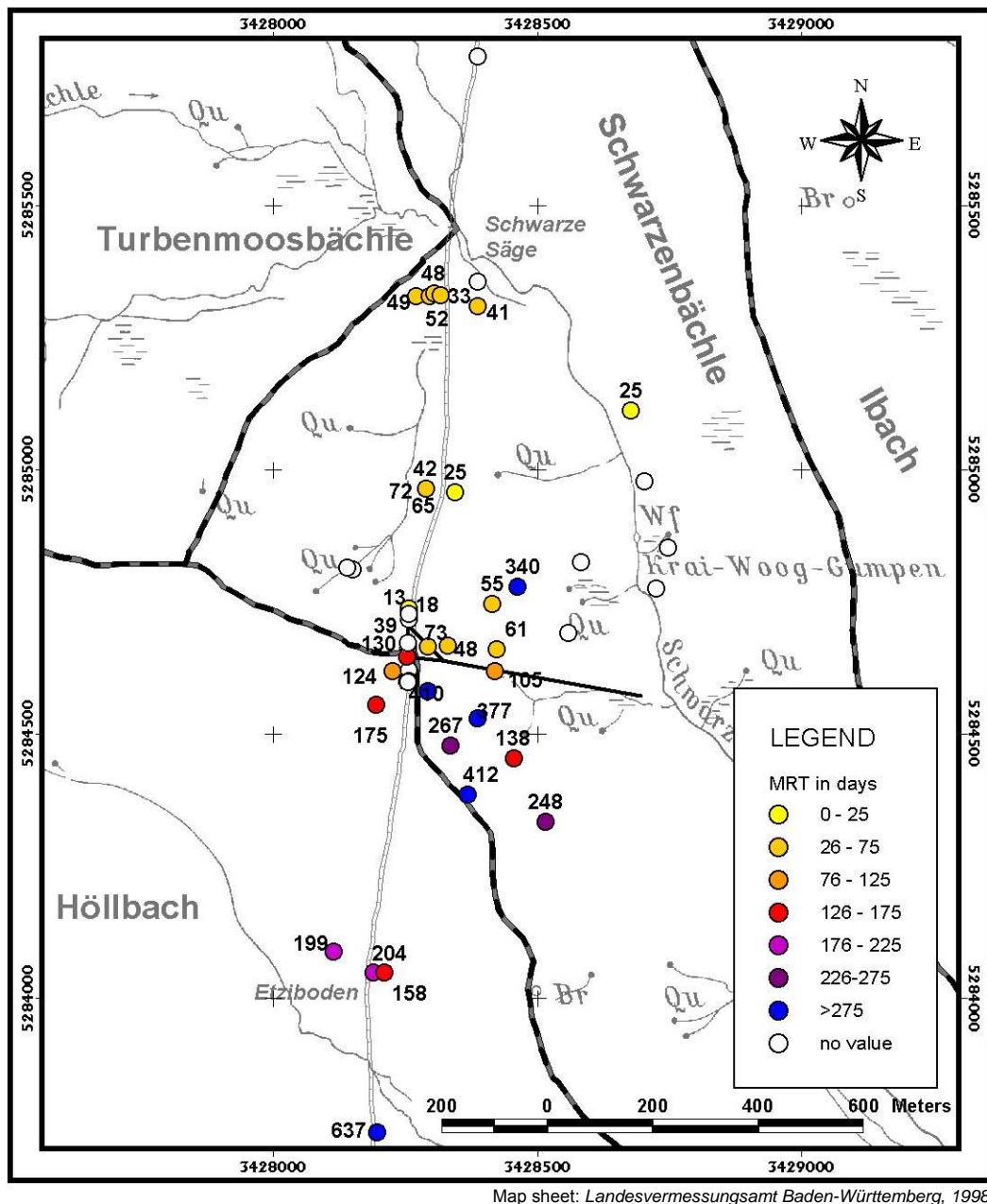


Figure 17 Regional distribution of mean residence time

4.1.2 Catchment drainage experiment

The so-called catchment drainage experiment stood in the centre of the investigations at the Lindau test site. The artificial drainage of the catchment was achieved by opening the tap of the horizontal borehole Bl. 17, which is situated in the southern part of the parallel pit and intersects the ore dyke at a depth between 2 to 5 m. The borehole that intersects the ore dyke discharged at a rate ranging from 7.8 to 15.0 l/s over a period of more than one year. The outflow from Bl. 17 created a narrow catchment along the strike direction of the dyke, which drained towards the observation tunnel. The natural (undisturbed) groundwater flow direction was thus reversed.

The catchment drainage experiment can be regarded as a long-term hydraulic test. The experiment was combined with hydrochemical investigations and tracer tests, which will

be described in the later sections. The main objective of the experiment is to characterise the hydraulic system consisting of the water-carrying dykes, the slightly permeable host rock and the overlying more permeable weathered zone. It is of particular interest how the aquifer in the undisturbed granite responds to the hydraulically stimulated conditions.

Experimental set-up

Figure 18 contains photos of the experimental set-up. The production rate was measured with a magnetic-inductive flowmeter (MIF). The water levels at boreholes Bl. 15, Bl. 19 and Bl. 20 in the observation tunnel were determined from high accuracy measurements ($\pm 0.1\%$) with digital pressure transducers. Bl. 15 intersects the ore dyke *Hermann* whereas Bl. 19 and Bl. 20 were drilled into the porphyritic dyke that intersects the ore dyke irregularly in a zone 20 – 40 m south of the production borehole. The interval of the continuous measurements varied between 3 s and 1 h depending on the stage of the experiment. The drawdown at the remaining boreholes in the parallel pit was determined from regular readings of the permanently installed manometers. The accuracy of the manometer readings, however, equals 0.05 bar or 0.5 m only.

A preliminary test that included two steps with a production rate of 1.8 l/s and 4.8 l/s, respectively, was carried out between the 08 – 15 April 1999. The catchment drainage experiment commenced on the 20 April 1999 at 23:23 and ended on the 26 May 2000 at 16:00. The total duration of the experiment amounted to 413 d. During the first step, which was terminated after 24 days, the production rate stayed fairly constant with an average yield of 9.7 l/s and a minimum and maximum of 9.4 l/s and 10.4 l/s, respectively. On the 04 May 1999 at 16:16, a second step with an increased production rate was initiated. The new rate of 15 l/s, however, dropped almost continuously to 7.8 l/s during late September since the sustainable yield of the groundwater system was apparently exceeded (Figure 21, upper graph). The production rate could not be measured with the MIF over the winter period due to the lack of power supply. It was, however, observed that the production rate increased after the strong winter precipitation. From the beginning of the second step, the borehole behaved like a natural spring. The production rate was clearly linked to the groundwater levels, with high discharge corresponding to high groundwater levels.

The tap at Bl. 17 was closed on the 26 May 2000 at 16:00. Immediately before the shut-off, the production rate amounted to 8.4 l/s. The recovery of the groundwater levels was measured over a period of approximately 160 d until late October/early November at both the surface boreholes and the boreholes in the parallel pit.

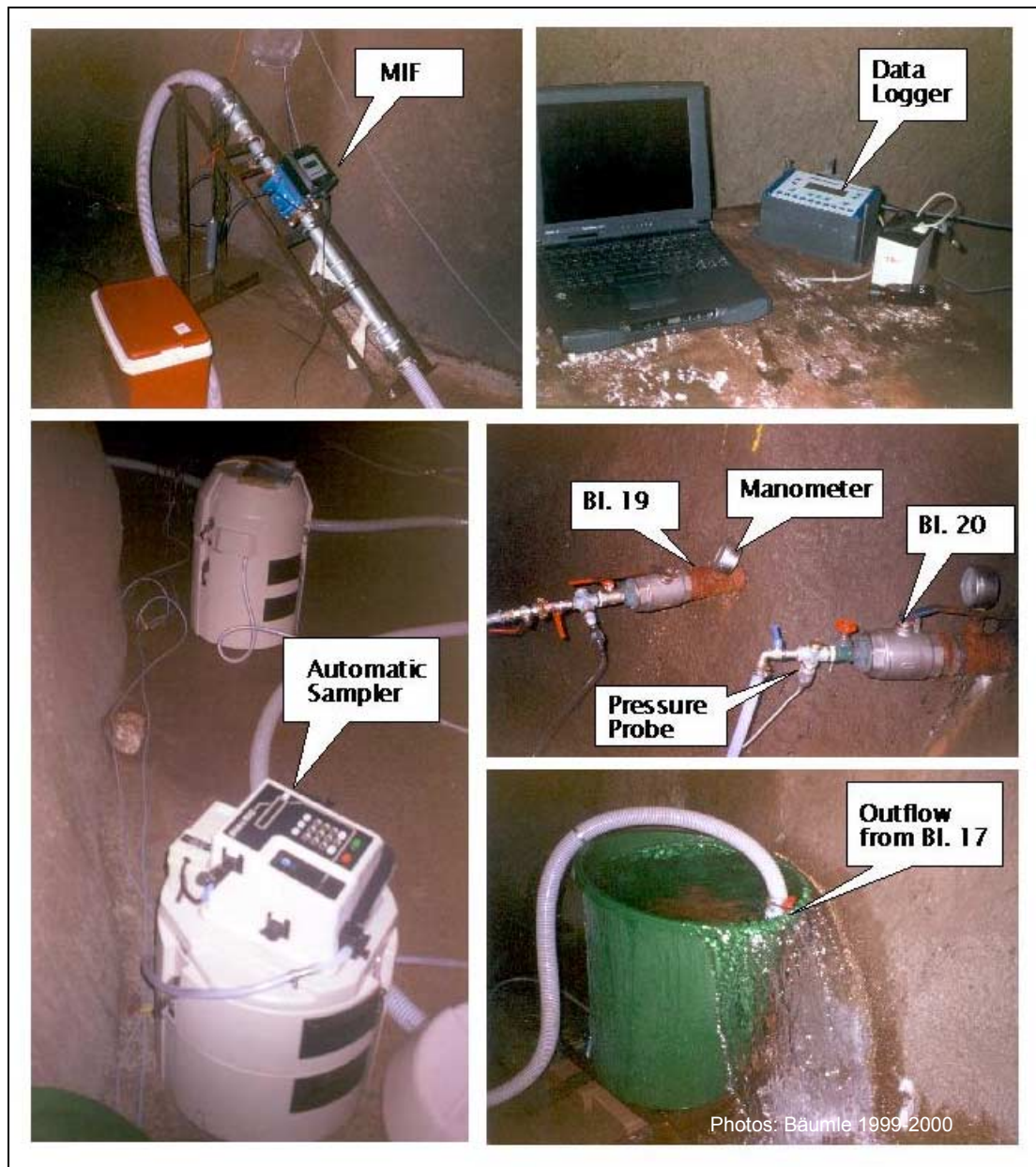


Figure 18 Experimental set-up of the catchment drainage experiment

Hydraulic response

The **boreholes in the southern pit** showed an immediate and clear response to the drainage experiment. The drawdown at Bl. 15 amounts to 20 m at the end of the first step and to >50 m after the second step during October (Figure 21). The drawdown at Bl. 19 and Bl. 20 was very similar. The drawdown was repeatedly disturbed by recharge periods. Rainfall together with snowmelt produced recharge during April. The monthly rainfall in May and June amounts to 165 mm and 212 mm, respectively, but only the precipitation during May caused a rise in the groundwater table. Another recharge event was observed after a period of thunderstorms between the 05 – 14 July 1999 with 107 mm of rainfall measured at the *Schwarze Säge* (Figure 19). The winter precipitation led to a strong rise of the groundwater levels everywhere.

The recovery at Bl. 15 was completed within 35 d (Figure 22). The additional rise in the groundwater levels after ~50 d was caused by the exceptionally high monthly rainfall during July 2000 amounting to 287 mm at *Todtmoos*. The high residual drawdown at Bl. 15 of approximately 20 m can be explained by the seasonal lowering of the groundwater levels.

None of the **boreholes in the northern pit** showed a response to the drainage experiment proving that the cement injection separates the two dyke sections.

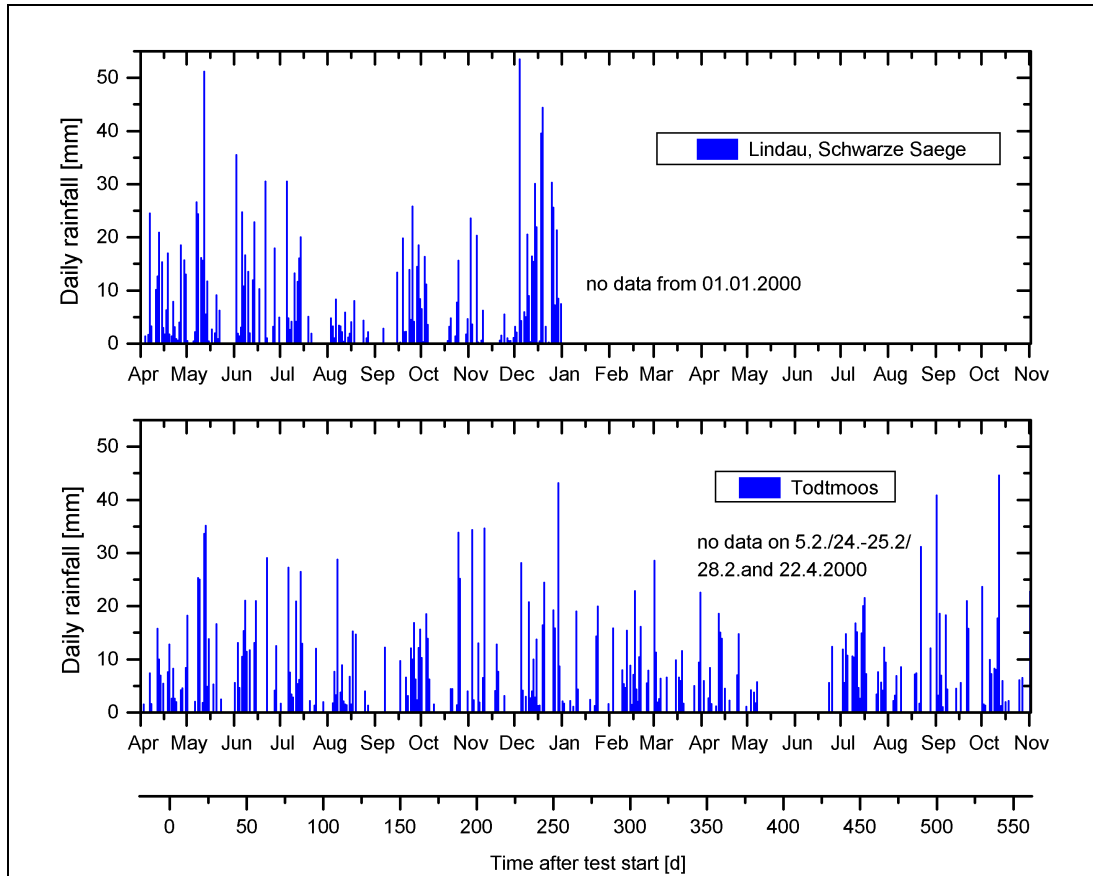


Figure 19 Daily rainfall at Lindau and Todtmoos from 01 April 1999 until 01 November 2000 (Rainfall data from Todtmoos were kindly provided by the *Landesanstalt für Umweltschutz Baden-Württemberg*)

The expected reaction of the **surface boreholes** in the vicinity of the observation tunnel could not be proved. The boreholes B 132S, B 94S and B 95S are located only 30 to 60 m away from the dyke axis, but a drawdown could be observed in neither of them. The upper graph in Figure 20 depicts the groundwater levels over the summer period at Bl. 132 for 6 different years. During 1999, the groundwater levels did not show any variation to previous years. The slight increase in the groundwater levels during early June 2000 may be interpreted as the recovery that was initiated a week earlier. **Surprisingly, the boreholes B 80E, B 81E and B 82E at the *Etziboden* clearly showed a response to the drainage experiment. The boreholes intersect the contact zone of the ore dyke but are situated 550 m south of the observation tunnel.** The highest drawdown and clearest recovery could be observed at B 82E (Figure 20, lower graph). The groundwater levels during 1999 are clearly below the levels

of previous years and the occurrence of the recovery at the end of May 2000 is unquestionable.

The hydraulic response to the drainage experiment can be summarised as follows: The natural southward-directed groundwater flow within the dyke was reversed by the experiment. The drainage created a narrow trough of less than 60 m in width along the dyke axis. The drawdown reached 50 m in the vicinity of the production borehole and even 550 m south of the observation tunnel, a drawdown in the order of 10 m could be observed.

Analysis

The drawdown and recovery data had to be corrected for a seasonal trend due to the general recession of the groundwater levels during the summer. It is assumed that the seasonal trend can be described by a recession curve according to the principles outlined in chapter 2.2. However, the seasonal depletion of the reservoir will cease as soon as the groundwater levels in the observation tunnel fall below the static water level⁴⁾. Unfortunately, no well hydrograph data are available for the boreholes in the southern part of the parallel pit. Therefore, the MRT of the groundwater and the static water level had to be estimated. The values obtained for the dyke systems in the northern catchment, ranging from 12 to 73 d (see Table 5), are probably too low since the southern catchment is believed to be less permeable. A MRT of 80 d seems therefore to be a reasonable estimate for the southern ore dyke. The elevation of the static water level was obtained from the WHRA at B 80E, B 81E and B 82E and amounts to 892 m a.s.l. This elevation corresponds to the point of intersection of the *Höllbach* and the dyke (see Figure 6). The red curve in Figure 21 shows that the original drawdown data at Bl. 15 (black curve) had to be corrected by a maximum amount of 5.5 m. The blue curve depicts the corrected data. The evaluated drawdown is hence up to 5.5 m lower than the measured drawdown. After approximately 40 d, when the water level in the borehole dropped below 892 m a.s.l., the further increase in the drawdown was no longer affected by the seasonal trend. A similar correction applies for the recovery analysis once the groundwater level exceeds the elevation of the static water level. The correction of the seasonal trend at Bl. 15 is shown as an example in Figure 22.

⁴⁾ The correction c_s for the seasonal trend can be expressed mathematically as follows:

$$c_s = \begin{cases} h_0 - s'_{i-1} + h_{i-1} \exp[-\alpha_M(t_i - t_{i-1})] & h_i > 0 \\ s_{i-1} - s'_{i-1} & h_i \leq 0 \end{cases}$$

i number of time step

t time

s measured drawdown

s' corrected (actual) drawdown

h water level above static water level

h_0 water level above static water level at start of the test

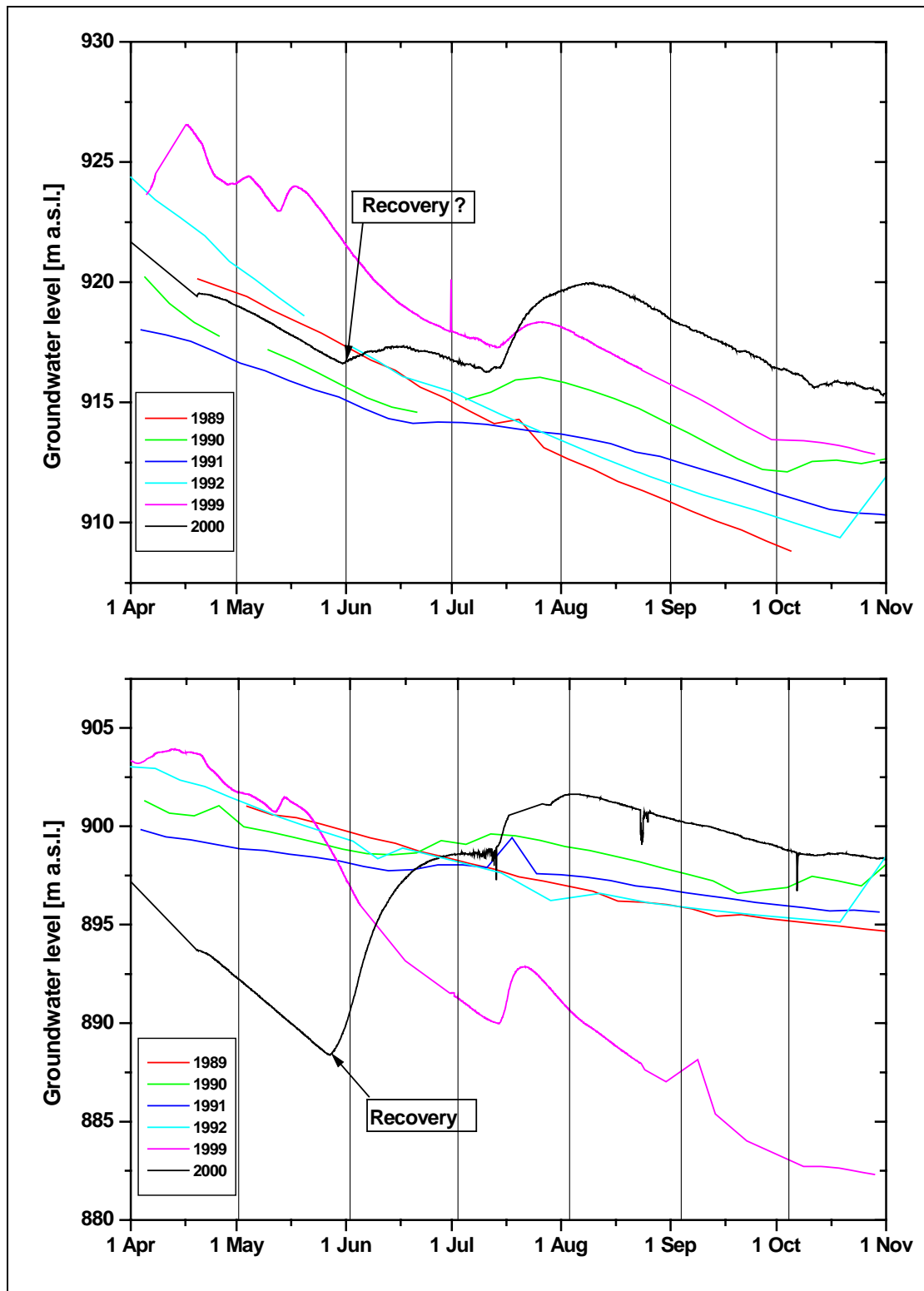


Figure 20 Groundwater level at B 132S (top) and B 82E (bottom) during the summer (April – October) for 6 individual years

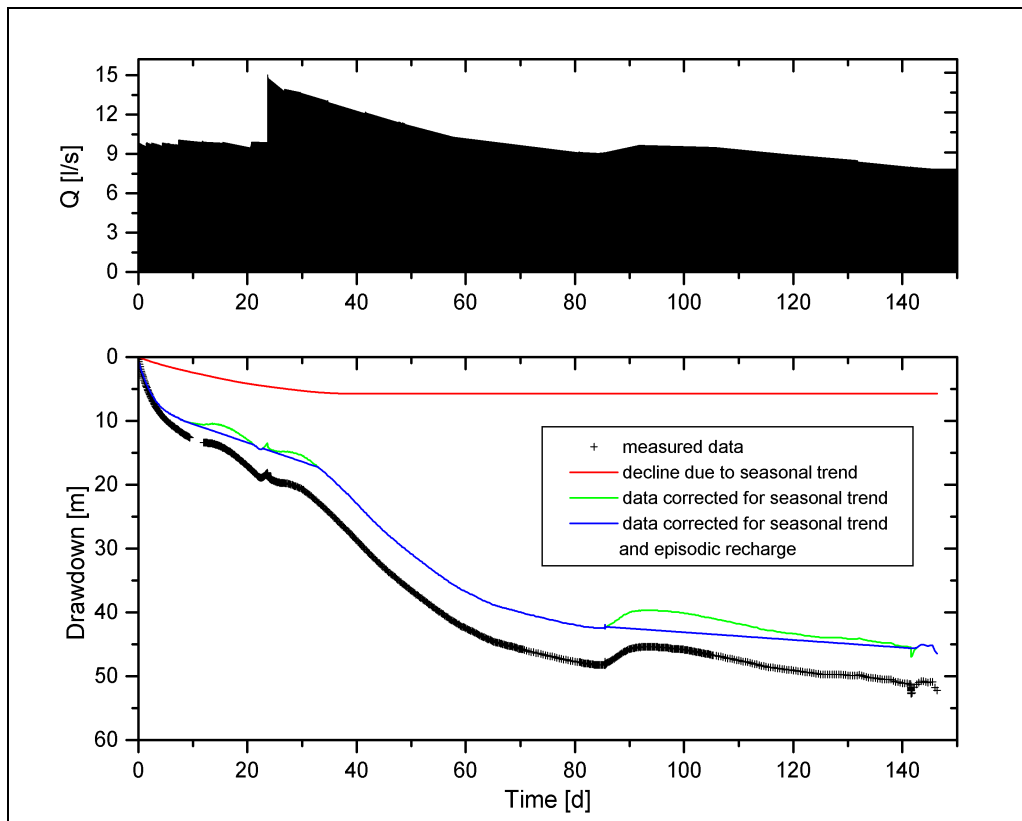


Figure 21 Original drawdown data and trend correction at Bl. 15

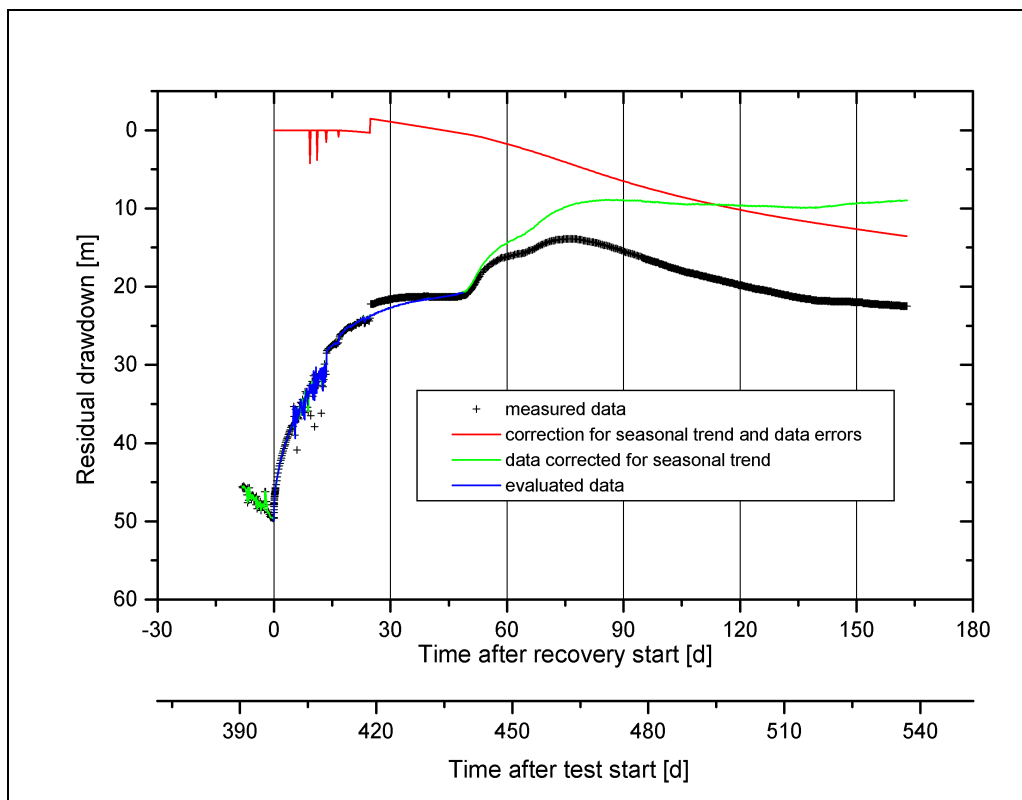


Figure 22 Original recovery data and trend correction at Bl. 15

Results

The analysis of the catchment drainage experiment follows the recommendations given in chapter 2.3.3. The drawdown and recovery data are plotted in the diagnostic plots. Figure 23 and Figure 24 show the analysis of the test data at Bl. 15 as an example. Only the first 30 days of the drawdown period and the first 50 days of the recovery period were considered as the subsequent recharge events seriously disturbed the test. The lines with a $\frac{1}{2}$ slope are clearly visible in the double-logarithmic plots of the drawdown and the derivative. The plots of s against the square root of time unmistakably show a straight-line segment. **There is hence no doubt that the ore dyke together with the contact zone acts as a vertical conduit within the low permeable host rock.**

The curves were fitted to analytical solutions using the method of least squares fit. Algorithms were developed in the C++ programming code. The implemented numerical methods include a *Romberg*-scheme to approximate the integrals in the equations and a *Levenberg-Marquardt*-scheme to determine the least squares fit solution.

The methods of Cinco et al. (equations [20] to [22]), Boonstra & Boehmer (equations [23] to [25]), Gringarten et al. (equation [27]) and Jenkins & Prentice (equation [28]) have been applied to analyse the tests. All methods assume that the pumped well is located in a highly permeable vertical fracture or dyke zone. It is interesting to note that the pseudo-radial flow phase has not been reached during the evaluation period. It is therefore not permitted to apply the methods of Theis and Jacob. The recovery has been evaluated according to the principle of superposition outlined in chapter 2.3.3.3. Equation [34] applies for the recovery analysis with the method of Gringarten et al. The average width of the dyke and the contact zone is taken to be 3 m. It is assumed that the length $2L_f$ of the dyke can be approximated by the range of the hydraulic depression that equals approximately 700 m. The cement injection separates the ore dyke between the southern and northern section of the parallel pit and acts as a hydraulic barrier. It is obvious that the cement fan influences the drawdown since it is located only 80 m south of the production borehole. Nevertheless, the hydraulic boundary was not considered in the preliminary evaluation. This approach is partly justified as the evaluation methods above do not consider boundary effects and generally assume that the production well is situated in the centre of the vertical fracture. In a second evaluation, the boundaries were included in the analysis by introducing an imaginary well (see chapter 2.3.3.4). In this case, the length of the dyke is taken to be 1400 m. The barrier type boundary is situated at half the distance from the production and imaginary wells.

Examples of the curve fittings at Bl. 15 for the second evaluation are given in Figure 23 and 24. The fits are regarded as good, especially if the uncertainties regarding the data are taken into consideration, which stem from the seasonal trend correction and the recharge event shortly after the beginning of the drawdown period. Table 6 summarises the results of the hydraulic test evaluation. The results considering the hydraulic boundary (lower table) better represent the hydraulic conditions within the dyke and are therefore considered more accurate. The transmissivity T_m of the host rock (fractured granite) ranges from 24 to 35 m²/d; its storage coefficient S_m varies between $1 \cdot 10^{-4}$ and $4 \cdot 10^{-4}$. The transmissivity T_f of the dyke and its contact zone ranges from 9000 to 15000 m²/d and is thus two to three orders of magnitude higher than the host rock. Similarly, the storage coefficients of between $1 \cdot 10^{-1}$ and $4 \cdot 10^{-1}$ exceed the values obtained for the host rock by two orders of magnitude.

Table 7 contains the transmissivities obtained from this study and from former hydraulic tests. **The results show the very distinct hydraulic properties of the dyke zone and the adjacent fractured granite.** Pohl (1994) carried out a similar but much shorter drainage experiment in the northern section of the parallel pit. He obtained a transmissivity in the order of $22000 \text{ m}^2/\text{d}$ for the dyke from data at the production borehole BI. 2 and the artesian borehole B 20E using the method of Boonstra & Boehmer. B 74E is located a few meters away from the dyke zone, which may explain its smaller transmissivity. **These results suggest that the permeability of the dyke north of the observation tunnel is about twice as high as the permeability of the southern dyke section and consequently, that the northern catchment is drained more efficiently.** This finding coincides with the results of the WHRA (chapter 4.1.1) which generally provided smaller MRT's for the northern catchment.

The transmissivity of the host rock obtained from former studies varies between 1 and $500 \text{ m}^2/\text{d}$. The wide range of values can partly be seen as a result of the heterogeneity of the fractured granite. Most of the tested wells are located within or close to the contact zone around the dyke which results in exceptionally high transmissivities, e.g. for B 20E and B 74E. It is emphasised that the given values are only applicable to the fractured and weathered granite and do not represent the much less permeable rock matrix. It is pointed out in chapter 4.2.1 that a high well loss is often encountered in fractured wells. The additional drawdown in the abstraction well caused by the fracture and well skin often makes it impossible to obtain accurate values for both T and S from single well tests. The results from single well tests are therefore considered less reliable and may explain the variation of the results for some wells such as B 62E.

Table 6 Results of the hydraulic test evaluation

Drawdown, no boundary												
Borehole	Input data				Jenkins & Prentice (1982)				Gringarten et al. (1974)			
	x [m]	y [m]	L _r [m]	a _r [m]	T _m [m ² /d]	S _m [-]	T _m *S _m [m ² /d]	T _m /S _m [m ² /d]	T _m [m ² /d]	S _m [-]	T _f /S _f [m ² /d]	
Bl. 14	24	0.0	700	3.0	--	--	0.045	--	16.8	1.9E-03	9085	
Bl. 15	24	0.0	700	3.0	--	--	0.048	--	12.0	3.1E-03	3866	
Bl. 16	24	0.0	700	3.0	--	--	0.039	--	12.2	2.7E-03	4562	
Bl. 18	3.0	0.0	700	3.0	--	--	0.039	--	17.8	1.4E-03	12942	
Bl. 19	34	0.0	700	3.0	22.5	2.7E-03	0.058	8320	13.3	3.4E-03	3925	
Bl. 20	34	14	700	3.0	7.3	9.8E-03	0.071	743	14.2	3.6E-03	3942	
Bl. 21	34	15	700	3.0	15.6	4.7E-03	0.074	3309	16.4	3.4E-03	4782	
B 82 *)	563	0.0	700	3.0	--	--	(3.8)	--	(26.2)	(1.2E-01)	(213)	

Borehole	Input data				Cinco et al. (1981)				Boonstra & Boehmer (1986)			
	x [m]	y [m]	L _r [m]	a _r [m]	T _f [m ² /d]	S _f [-]	T _f *S _f [m ² /d]	T _f /S _f [m ² /d]	T _f [m ² /d]	S _f [-]	T _f /S _f [m ² /d]	
Bl. 14	24	0.0	700	3.0	7811	3.1E-01	2437	25034	3361	2.2E-01	15162	
Bl. 15	24	0.0	700	3.0	7258	3.6E-01	2613	20160	2365	3.7E-01	6336	
Bl. 16	24	0.0	700	3.0	6774	3.1E-01	2127	21572	2252	3.6E-01	6304	
Bl. 18	3.0	0.0	700	3.0	--	--	--	--	3778	2.6E-01	14381	
Bl. 19	34	0.0	700	3.0	--	--	--	--	2586	3.3E-01	7846	
Bl. 20	34	14	700	3.0	--	--	--	--	2822	3.4E-01	8372	
Bl. 21	34	15	700	3.0	--	--	--	--	3054	3.7E-01	8231	
B 82 *)	563	0.0	700	3.0	--	--	--	--	--	--	--	

Note: *) x = 282m, 0.5*x/L_r = 0.80 assumed

Recovery, no boundary												
Borehole	Input data				Gringarten et al. (1974)			Boonstra & Boehmer (1986)				
	x [m]	y [m]	L _r [m]	a _r [m]	T _m [m ² /d]	S _m [-]	T _m /S _m [m ² /d]	T _f [m ² /d]	S _f [-]	T _f /S _f [m ² /d]		
Bl. 15	24	0.0	700	3.0	7.4	1.6E-03	4600	2402	1.1E-01	22016		
Bl. 19	34	0.0	700	3.0	8.8	1.0E-03	8710	3568	7.6E-02	46839		
Bl. 20	34	14	700	3.0	8.2	1.6E-03	5042	2815	1.2E-01	24328		

Drawdown, boundary												
Borehole	Input data					Gringarten et al. (1974)			Boonstra & Boehmer (1986)			
	x [m]	x _{im} [m]	y [m]	L _r [m]	a _r [m]	T _m [m ² /d]	S _m [-]	T _m /S _m [m ² /d]	T _f [m ² /d]	S _f [-]	T _f /S _f [m ² /d]	
Bl. 14	24	62	0.0	1400	3.0	34	9.3E-04	36363	13457	2.4E-01	57250	
Bl. 15	24	62	0.0	1400	3.0	24	1.6E-03	15472	9346	4.1E-01	22986	
Bl. 16	24	62	0.0	1400	3.0	24	1.3E-03	18254	8896	3.9E-01	23027	
Bl. 18	3.0	83.0	0.0	1400	3.0	35	6.9E-04	51680	14612	1.7E-01	85337	
Bl. 19	34	120	0.0	1400	3.0	26	1.7E-03	15555	10153	3.2E-01	32050	
Bl. 20	34	120	14	1400	3.0	27	2.1E-03	12554	10329	3.9E-01	26649	
Bl. 21	34	120	15	1400	3.0	31	2.0E-03	15451	11156	4.2E-01	26386	
B 82	563	649	0.0	1400	3.0	(9.3)	(4.0E-01)	(23)	--	--	--	

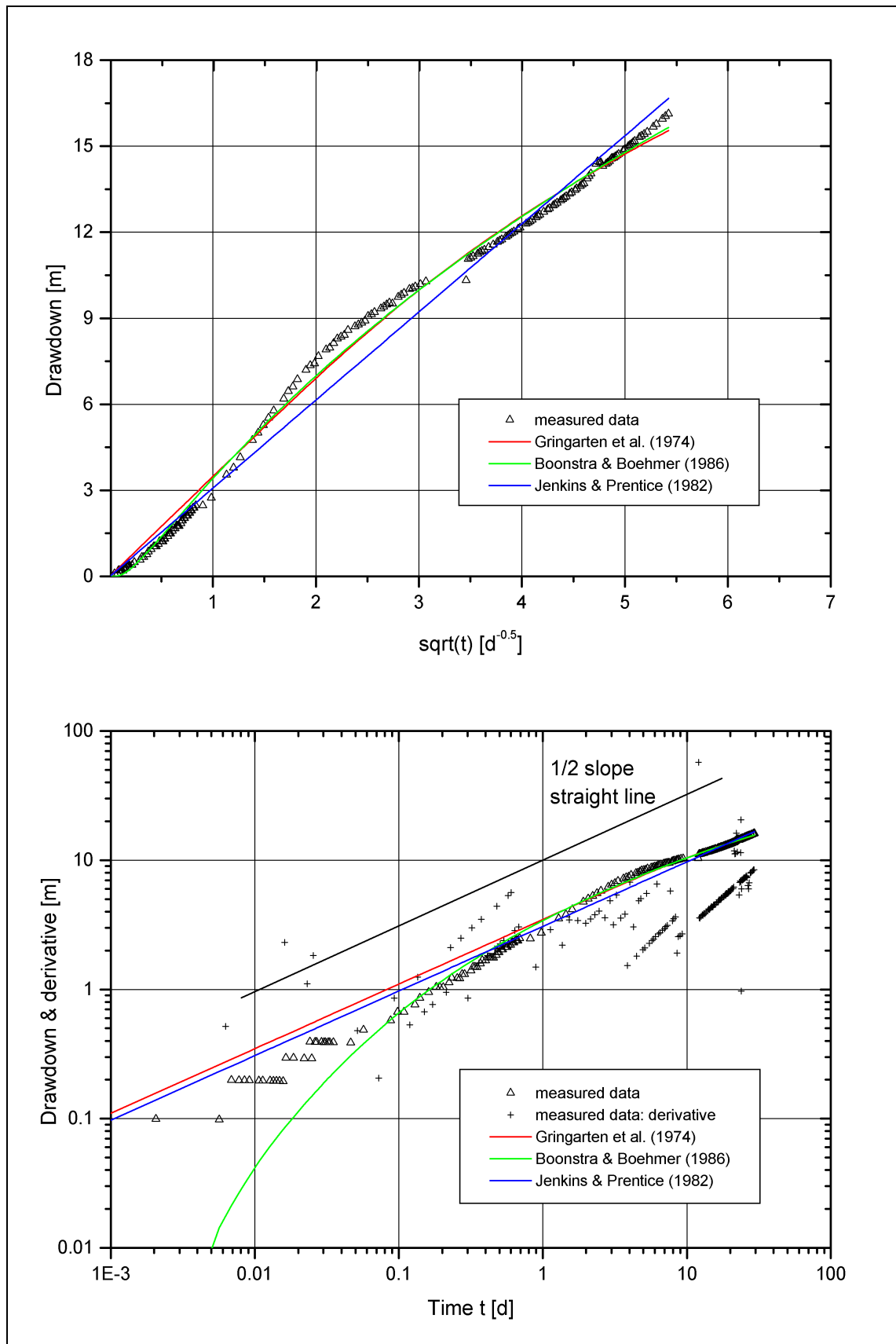


Figure 23 Evaluation of drawdown at BI. 15

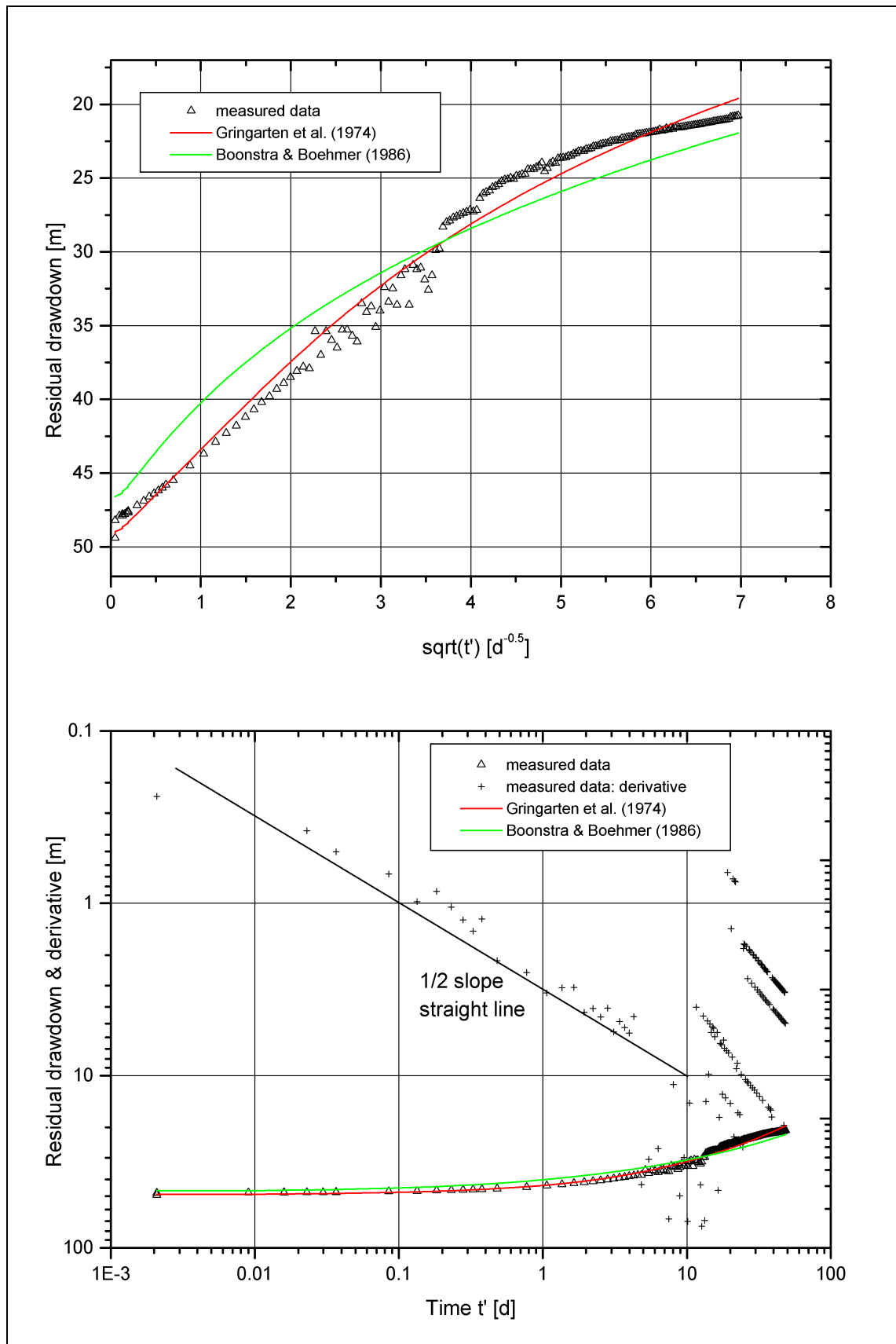


Figure 24 Evaluation of recovery at Bl. 15

Table 7 Comparison of the hydraulic test evaluations at Lindau

Borehole	T_m [m ² /d]			T_f [m ² /d]	Remarks
	Cooper & Jacob (1946)	Agarwal et al. (1970)	Gringarten et al. (1974)	Boonstra & Boehmer (1986)	
B 20E	501		496	22032	P
B 42S	1.5	5.3			H
B 62E	1.8	21			H
	0.7				R
	235				W
B 63E	1.0	5.9			H
B 64E		49			H
			14		R
	100				W
B 65S					
B 69E	231		256		P
B 74E	314			3456	P
B 77E	200		183		W
B 80E	79				H
B 82E	18	18			R
			(9)		*)
Östu I	191				W
Bl. 2	190	154		21859	P
Bl. 3		274			W
Bl. 5		183			W
Bl. 12		131			W
Bl. 14			34	13457	*)
Bl. 15			24	9346	*)
Bl. 16			24	8866	*)
Bl. 18			35	14612	*)
Bl. 19			26	10153	*)
Bl. 20			27	10329	*)
Bl. 21			31	11156	*)

Notes: P: Pohl, 1994, catchment drainage experiment
H: Himmelsbach 1993, hydraulic tests (after Troscke 1990 and Mellert 1989)
R: Reinert 1999, pumping tests
W: Witt 2000, catchment drainage experiment
*) catchment drainage experiment, boundary considered, this study

4.1.3 Hydrochemical study

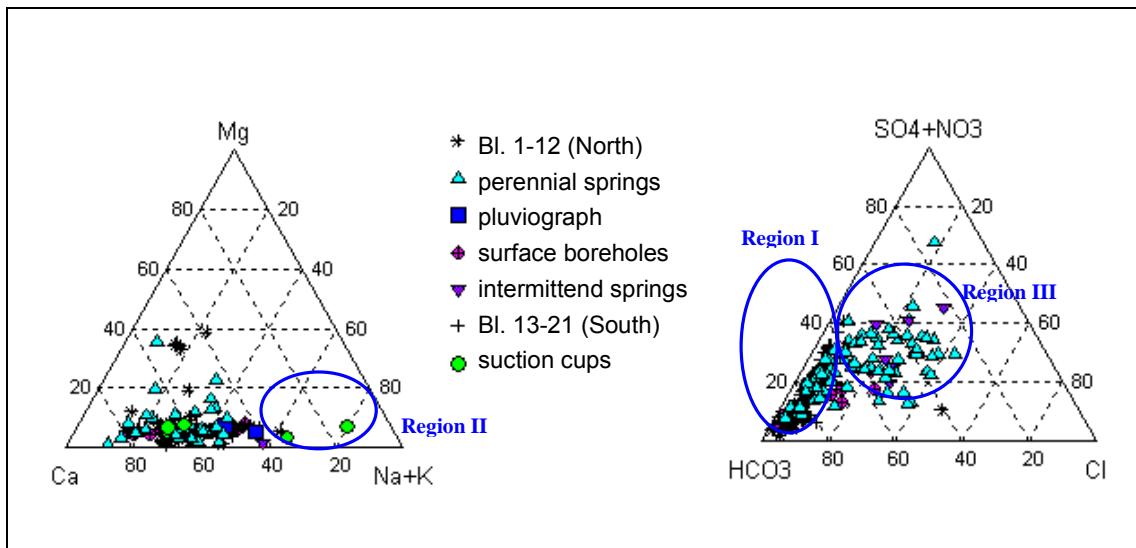
Characterisation of the hydrochemical composition of groundwater

During the catchment drainage experiment the physical parameters temperature, pH, EC and the O₂-content were regularly measured from 08 April 1999 to 09 September 1999 and groundwater samples were taken during the period from 08 April 1999 to 18 May 2000 at the outlet Bl. 17. Additional samples were taken from the adjacent boreholes Bl. 15, Bl. 18, Bl. 19 and Bl. 20 on the 15 July 1999 and from the pluviograph (Lindau, *Schwarze Säge*) on the 20 and 25 May 1999. The samples were analysed for the major cations Na, K, Ca and Mg, the major anions Cl, F, SO₄, NO₃ and PO₄ and for the minor constituents Fe, Ba, and Sr. The analyses methods and the equipment utilised are listed in Table 8.

Table 8 Analysis methods and equipment

Constituent	Method	Analysis Equipment
pH, T	in situ measurement	WTW pH 197 S
O ₂	in situ measurement	WTW Oxi 196
Na, K, Ca, Mg, Fe	Atomic Absorption Spectro-Photometry (AAS), (acetylene/air)	Perkin Elmer Model 3030 B
Ba, Sr	Inductively Coupled Plasma Mass Spectrometry (ICP-MS)	Thermo Jarrel Ash ICPMS PQ3
Cl, SO ₄ , F, NO ₃ , PO ₄	Ion Chromatography (suppressor technique)	IC Model 500, anion separation columns Dionex "AS-14", Dionex "AG14"

Figure 25 shows the composition of the groundwater with respect to the main constituents in ternary diagrams. This type of diagram is more meaningful compared to a Piper diagram in this study since either magnesium or bicarbonate measurements are not available for a number of samples. The diagrams comprise chemical analysis of rainwater, episodic and perennial springs and groundwater obtained from boreholes. The samples have been gathered during this study and during former investigations at the Lindau fractured rock test site (Ackermann, 1981; Stenzel, 1997; Witt, 2000).

**Figure 25** Ternary Graphs

In general, the groundwater fits in the Ca-Na-HCO₃ type. Table 9 shows the average values of the analysed parameters at BI. 17 during the catchment drainage experiment. The complete hydrochemical data is presented in Appendix 3. Relative to rainfall the groundwater is enriched in the major cations by an order of magnitude and by a factor of 2 in sulphate.

Despite the difference in MRT the groundwater sampled from episodic springs and presumably older groundwater from perennial springs, boreholes and the observation tunnel are similar with respect to their major ion composition and can therefore hardly be distinguished from each other (Region I in Figure 25). The perennial springs may contain a fair amount of younger water that is mixed with older groundwater at or close to the outlet. Only the samples gained from suction cups within the observation tunnel show a distinct chemistry. These samples represent virtually immobile groundwater and are

characterised by a higher amount of total dissolved solids (TDS) since the ion content could come close to equilibrium concentrations due to the long reaction time. In particular, the sodium and sulphate content are considerably higher compared to more mobile groundwater (Region II). Several of the spring samples show a higher chloride content and fit in the Ca-Na-HCO₃-Cl type (Region III). These samples were taken between May and July 1978 and showed lower chloride contents in a subsequent sampling campaign that was carried out during September 1978. It is therefore likely that the increased chloride content was caused by human activities, e.g. by application of salt during the cold season.

Table 9 Average chemical composition of open rainfall and groundwater at Bl. 17

Site	T [°C]	pH [-]	EC [mS/m]	O ₂	Na	K	Mg	Ca	Fe	Sr	Ba	Cl	F	SO ₄	NO ₃	PO ₄
Bl. 17	6.2	5.8	2.7	10.9	2.46	.61	.40	4.35	<.25	.027	.25	.94	.46	1.65	2.25	<.03
Rain-fall	-	-	-	-	.25	.02	.04	.28	-	-	-	.95	.04	.81	1.44	<.03

Note: Values are in mg/l if not otherwise stated

Since it proved difficult to distinguish the groundwater components from its major constituents, minor elements were additionally investigated. Himmelsbach (1993) and Biehler (1995) have pointed out that groundwater originating from the dyke systems is characterised by a higher content of barium and fluoride. Similarly, the Ba:Sr ratio will be increased and may serve as an environmental tracer.

According to Biehler (1995), the fluoride concentration in basement rock aquifers of the Southern Black Forest varies between 0.1 and 5.5 mg/l and the barium concentration between 0.02 and 1.03 mg/l. The histogram of the fluoride concentration measured in the Lindau test site (Figure 26) clearly shows a bimodal distribution with the first peak representing spring water with a fluoride content of less than 0.1 mg/l and the second peak representing the water from the dyke systems with values of 0.5 mg/l and above.

The mineralisation of the groundwater is very low, even if compared to similar basement rock aquifers of the Southern Black Forest, as indicated by the EC of only 27 µS/cm. Nevertheless, a relatively high barium content of 0.25 mg/l and a fluoride concentration of 0.46 mg/l were observed. The fluoride content corresponds to approx. 6% of the equivalent concentration of the anions. These values clearly demonstrate the influence of mineral dissolution within the ore dyke.

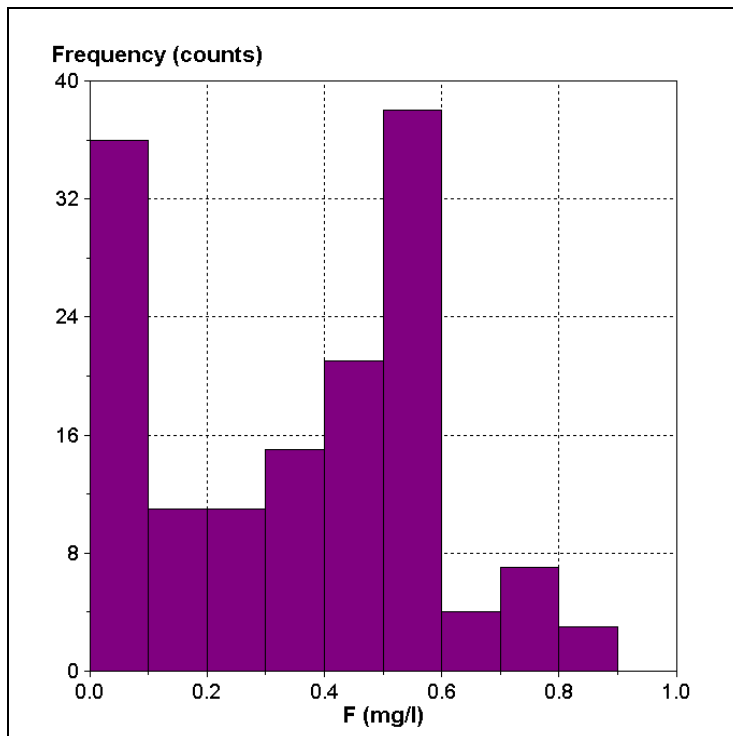


Figure 26 Histogram of fluoride concentration

Evolution of the hydrochemical composition of groundwater

Three different phases can be distinguished from the evolution of the hydrochemical composition of the groundwater during the experiment:

1. an initial phase at the very beginning of the experiment until 21 April 1999
2. phase 2 which roughly covers the second half of the 1999 hydrological year (May - October)
3. phase 3 which covers the second half of the 2000 hydrological year (November – April)

Phase 1

Phase 1 covers the first step of the pilot test carried out between 08 – 13 April 1999 ($Q = 1.8$ l/s), the subsequent second step from 13 – 15 April 1999 ($Q = 4.8$ l/s) and the beginning of the main test from 20 – 21 April 1999 ($Q = 9.7$ l/s).

Prior to the commencement of the test, the northern pit was situated at the outer (northern) edge of the subterranean catchment drained by the dyke. The northern catchment boundary is formed by the cement injection. Opening the BI. 17 suddenly reversed the hydraulic gradient and the direction of groundwater flow. During phase 1, stagnant groundwater that was not or only to a small extent incorporated in the hydrological cycle was replaced by water originating from a zone with active groundwater circulation.

The stagnant groundwater is characterised by a higher nitrate content (0.080 - 0.085 meq/l), slightly increased calcium concentrations (0.22 - 0.23 meq/l), low fluoride

values (0.013 meq/l) and a low concentration of the trace element barium (0.0025 meq/l). The stagnant water also shows a comparatively low Ba:Sr ratio of approximately 4 and a small Na:Cl ratio of approximately 3.5 (Figure 27 to 30).

During phase 1, the nitrate concentration drops sharply from its original concentration of 0.080 - 0.085 meq/l to values ranging from 0.04 - 0.05 meq/l. The calcium content decreases to 0.20 meq/l and the rising fluoride concentration reaches values of 0.018 meq/l towards the end of phase 1. Consequently, the Ca:F ratio shows a significant drop from 16 - 19 to approximately 11. The Na:K ratio also decreases from 2.5 to 2.0.

According to Biehler (1995) the measured nitrate concentration of rainfall in the Southern Black Forest ranges from 1 to 11 mg/l (0.016-0.177 meq/l). The nitrate content at the *Schwarze Säge* rainfall gauge observed on 20.05.1999 and 25.05.1999 equalled 1.4 mg/l (0.023 meq/l) and 2.0 mg/l (0.032 meq/l), respectively. They clearly fall within the lower range of the values given by Biehler. Similar concentrations found in the fractured rock aquifers can hence to a large extent be explained by atmospheric deposition. Some nitrate, however, may also stem from the microbiological activity (nitrification) within the unsaturated zone. The increased nitrate concentration of the stagnant water can be explained by a contamination during drilling and construction of the tunnel or by local percolation of seepage water with a somewhat higher nitrate content. The higher calcium values are most likely due to corrosion of the injected cement. The low content in barium and fluoride indicates that barite and fluorite, minerals associated with dissolved barium and fluoride within the dyke, were less abundant in the zone of stagnant groundwater adjacent to Bl. 17.

Phase 2

The phase 2 covers the summer period until the early fall. The strong rainfall during mid-May was followed by a regional rise in the groundwater table and was hence associated with groundwater recharge. The strong rainfall events encountered during the first half of July and in November, however, seem to have only locally contributed to groundwater recharge.

Phase 2 is characterised by an overall increase in TDS. The EC rises from 25 $\mu\text{S}/\text{cm}$ during late April to 30 $\mu\text{S}/\text{cm}$ during mid-September. In particular the following changes in the groundwater composition were observed (Figure 27 to 30):

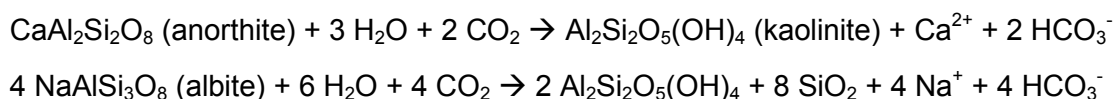
- ❑ A continuous rise in the calcium concentration by 30% from 0.20 to 0.26 meq/l (the single value of 0.38 meq/l presumably represents a contaminated sample)
- ❑ A similar increase in magnesium from 0.03 to 0.04 meq/l
- ❑ A continuous increase in the sodium concentration by 40% from 0.085 to 0.12 meq/l
- ❑ A continuous increase in the barium concentration by 130% from 0.0025 to 0.0058 meq/l
- ❑ A continuous rise in the fluoride concentration by 140% from 0.018 to 0.043 meq/l
- ❑ A sharp drop in the nitrate concentration from approximately 0.03 meq/l to below the detection limit between 28 October and 05 November 1999

Due to the rise in the sodium content, the Na:K ratio increases by 67-100% (from 5-6 to almost 10) and the Na:Cl ratio increases by 25% (from 4 to 5). The Ba:Sr ratio increases

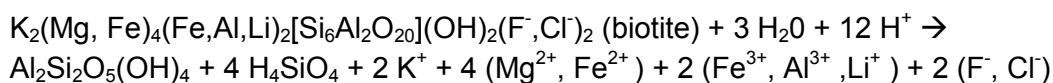
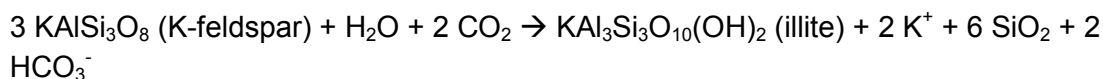
by 225 % (from 4 to 9) as the strontium concentration remains fairly stable during the experiment. The content of the remaining major ions, notably potassium, show no or insignificant variations. The sulphate concentration rises temporarily by 30% after mid-August and the chloride content increased slightly during October/November.

The bicarbonate concentration was not directly measured. It can be assumed from the ion balance, however, that the bicarbonate concentration doubled from 0.2 to 0.4 meq/l during phase 2. Hydrochemical analysis of the spring water sampled consecutively during early summer (May-July) and in September by Ackermann (1981) confirms the general increase in calcium and bicarbonate during the summer season.

The increase in calcium, sodium and bicarbonate can be explained by enhanced hydrolysis of feldspars and mica. Only a small portion of the increased calcium content can be attributed to the dissolution of fluorite. The hydrolysis of the feldspars produces calcium, sodium and bicarbonate according to the equations given by Stober & Bucher (2000):



Potassium and magnesium may originate from the hydrolysis of K-feldspar and biotite:



According to Biehler (1995) a Na:Cl ratio of well above 1 indicates that the sodium is produced mainly by hydrolysis of albite or cation exchange processes whereas a ratio close to 1 indicates that the groundwater composition is mainly influenced by rainfall. A ratio of 1 and a high content of sodium and chloride are usually related to the application of salt during winter for the prevention of slippery road conditions. The observed ratios of 4 to 5 hence indicate the geogenic origin of sodium.

The enhanced hydrolysis is likely to be caused by an input of organic acids and carbon dioxide during the summer season while the microbiological activity is highest. This indicates that a component of younger shallow groundwater reaches the deeper levels at the observation tunnel. This also explains the observed vanishing of the nitrates in mid-October since microbiological activity ceases abruptly due to low temperatures within the soil during early fall. Sorption and the lower solubility of K-feldspar may explain the fact that the potassium content remains quite constant during the experiment. The solubility of K-feldspar is small compared to anorthite and albite (Stober & Bucher, 2000). Furthermore, potassium is easily sorbed on clay minerals which form the coatings on fractures within the ore dyke (Witthüser, 2000). The sorption of potassium in the soil and the saturated zone results in the low potassium content and the high Na:K ratio generally observed in the basement rock aquifers of the Southern Black Forest (Biehler, 1995; Stenzel, 1997).

For a more detailed investigation of the hydrochemical data, saturation indices (*S_i*) as defined by Lloyd & Heathcote (1985) were calculated with Phreeqcl V. 2.2. The analysis

results of the sample dated 09 September 1999 were used as input data for the simulations. The calculations showed that the groundwater is still strongly undersaturated with respect to fluorite (SI = -2.32) but almost in equilibrium with the poorly soluble barite (SI = -0.05). It was formerly suggested that sulphate partially stems from the oxidation of sulphide such as pyrite (Biehler 1995; Himmelsbach 1993). In the investigated system, however, sulphides appear to be absent. According to the simulations, the oxidation of sulphides would lead to the precipitation of barite and to lower than observed barium concentrations.

The increase in the concentration of barium and fluorite during phase 2 can be explained by an enhanced dissolution of barite and fluorite, which is described by the following equilibrium equations (Parkhurst, 1996):



Apparently, regions with a higher content in these two minerals are progressively incorporated in the groundwater circulation whereas regions, which are already depleted in barite and fluorite, contribute mainly to the outflow at the earlier stage. This explanation is reasonable since the natural flow direction was reversed and formerly poorly connected zones may thereby be drained more efficiently during the experiment.

Phase 3

Phase 3 covers the winter period and commences with strong precipitation and a sharp regional rise in the groundwater table after 02 December 1999. Groundwater recharge is caused either by intense rainfall or snowmelt and occurs mainly during December 1999/January 2000 and during March/April 2000.

Due to the mixing of formation water with low mineralised rainwater or seepage water, the calcium and the sodium content decreases to 0.20 meq/l and 0.10 meq/l, respectively. These concentrations are close to the original values observed at the beginning of phase 2. Due to the decrease in sodium, the Na:K ratio reduces to 6 and the Na:Cl ratio to 4. Similarly, a drop in the barium (0.004 meq/l), sulphate (0.035 meq/l) and the fluoride (0.025 meq/l) concentrations and of the Ba:Sr ratio (6-7) is observed. These values represent intermediate levels compared with the concentrations observed during phase 2.

The nitrate content suddenly recovers during March 2000 to values close to the concentrations measured during phase 2.

The dilution of calcium, barium and fluoride is most evident. The concentrations drop after 08.12.1999 and decline further until early January 2000 (Figure 27 to 29). The time lag between rainfall and dilution is hence in the order of one week. If it is assumed, for the sake of simplicity, that the seepage water has a similar ion composition as rainwater, a simple mixing calculation yields a percentage of 25-40% of seepage water within the total outflow. This percentage is unexpectedly high and proves the high vertical permeability within the ore dyke.

From the hydrochemical analysis no indication was found that significant amounts of old groundwater from the adjacent low permeable granite at greater depths enters the ore dyke system. The increase in TDS is seasonal and hence more likely

associated with a surface related groundwater component. The increase in the barium and fluoride contents is associated with the dissolution of barite and fluorite minerals, which are solely found within the dyke. **This shows that water reaches the outlet via the highly permeable zones within the ore dyke.** The increase in calcium, magnesium, sodium and bicarbonate during the warm summer season indicate that a fair amount of shallow, surface-related groundwater contributes to the outflow at greater depths. This shallow water presumably percolates vertically through the higher permeable ore dyke that reaches to or close to the surface as illustrated in Figure 35. The sudden decrease in nitrate during October and the equally abrupt increase during spring as well as the observed dilution effect after strong rainfall and snowmelt during the winter season are further indications of such a surface-related component. The surface-related groundwater apparently reaches the deep aquifer levels within approximately a week. This result is only at first contradictory to the findings of Himmelsbach (1993) who obtained mean residence times from tritium measurement in the order of 1.5 and 5.5 years. He, however, investigated seepage (dripping) water within the tunnel under undisturbed hydraulic conditions. The higher residence times can be explained by the considerably lower vertical hydraulic gradients and the much smaller permeabilities within the less disturbed granite. **As a main result of the hydrochemical study, the flow velocities may vary within several orders of magnitude both laterally and vertically depending on the permeability of single flowpaths.**

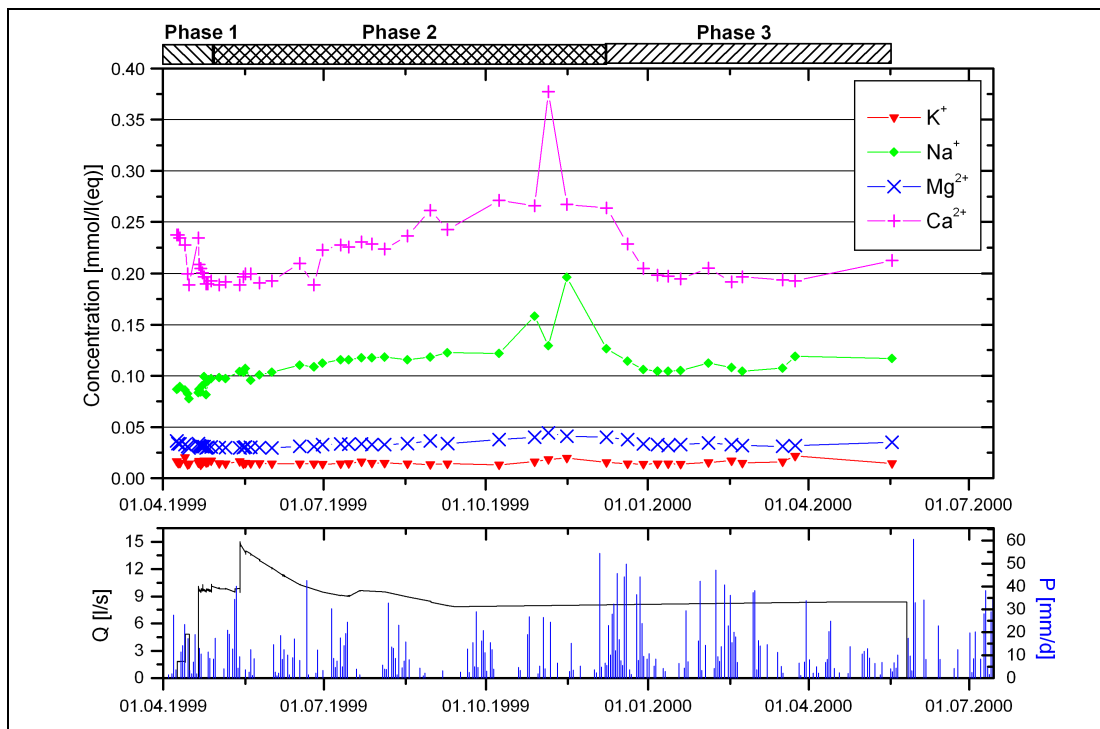


Figure 27 Variation in the cation concentrations during the catchment drainage experiment

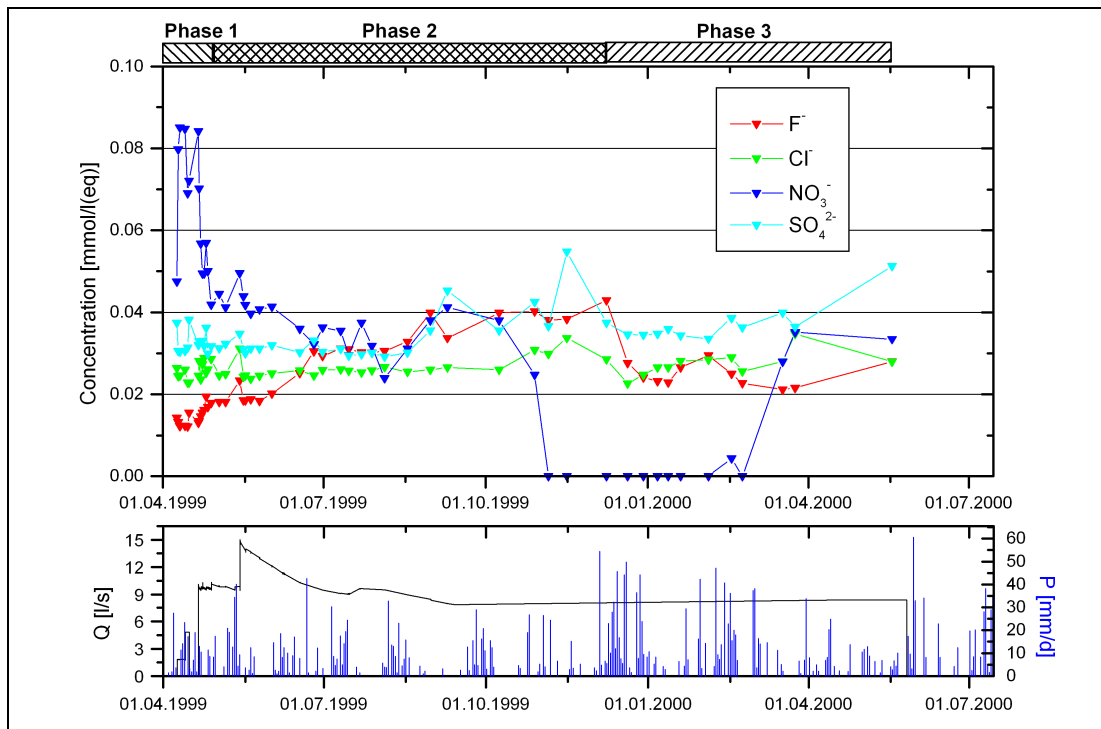


Figure 28 Variation in the anion concentrations during the catchment drainage experiment

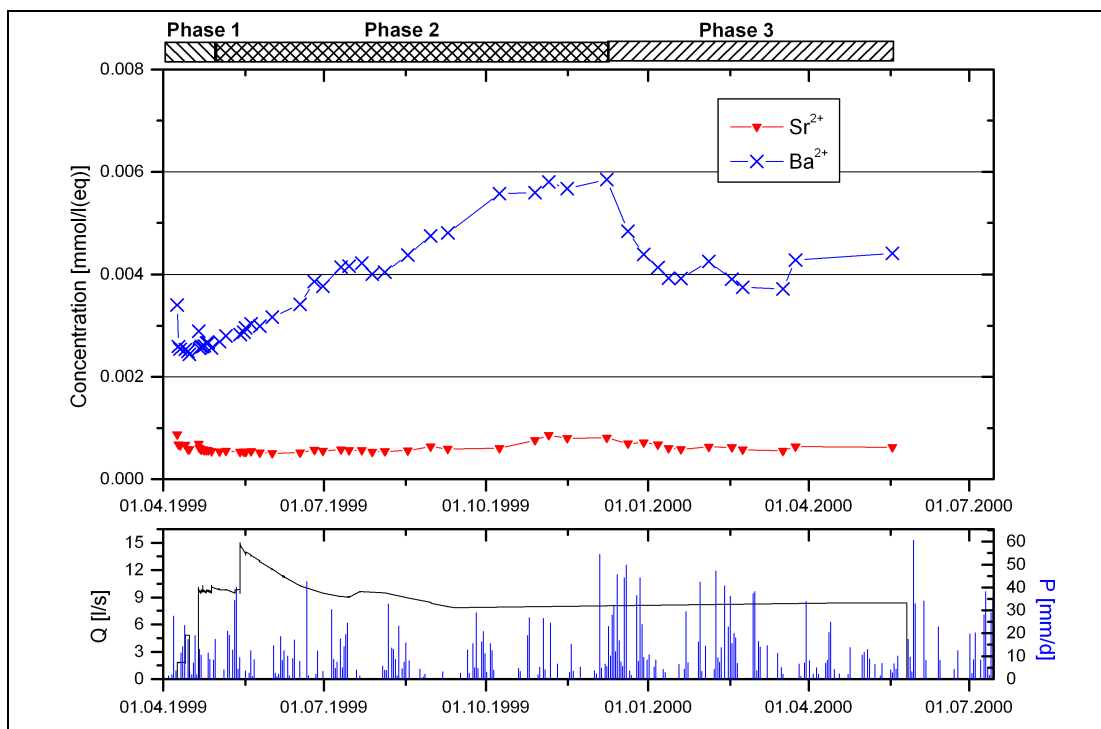


Figure 29 Variation in the barium and strontium concentration during the catchment drainage experiment

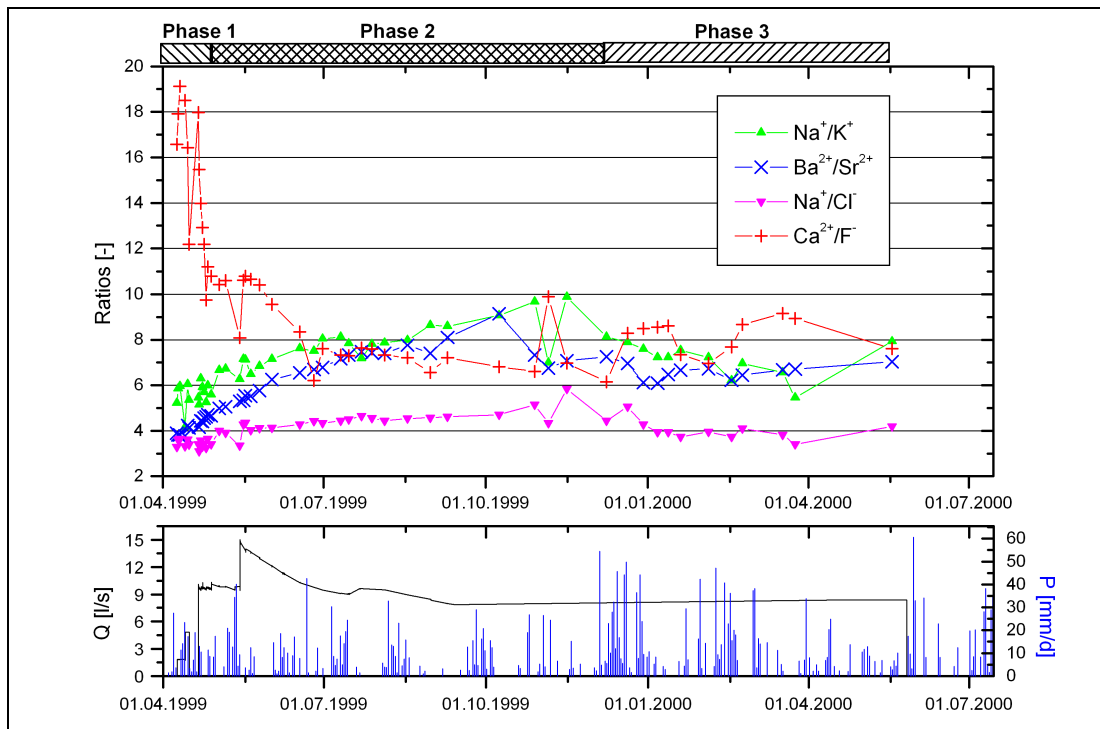


Figure 30 Variation in the ion ratios during the catchment drainage experiment

4.1.4 Groundwater tracer tests

Test design

Various tracer tests of different scale were performed during the catchment drainage experiment. Due to the drawdown created by the experiment, the tracer tests were carried out under forced-gradient conditions. The flow towards the production borehole BI. 17 can be assumed radial-convergent along the vertical plane of the ore dyke, but is linear (parallel) and directed towards the dyke within the host rock and the porphyritic dykes.

Fluorescent dyes and salts were used as tracers. The injected fluorescent dyes comprised amidorhodamine (sulphorhodamine G, C.I. Acid Red 50), eosine (C.I. 45 380), fluoresceine (uranine, C.I. Acid Yellow 73), pyranine (C.I. Solvent Green 7), sulphorhodamine B (C.I. Acid Red 52) and sodium naphthionate. The salt tracers bromide and chloride were injected as dissolved NaBr and KCl, respectively.

Small-scale experiments with distances from 3 to 25 m were performed in the dyke sections that can be accessed via the observation tunnel. It can be concluded from the strong and uniform drawdown at the boreholes in the southern pit that the injection boreholes and the outlet are connected by a discrete set of highly permeable fractures. The injection boreholes BI. 15 and BI. 18 intersect the ore dyke whereas BI. 19 and BI. 20 run parallel to the ore dyke and intersect the porphyritic dyke at various depths between 10 and 60 m south of the pit according to the borehole completion reports. BI. 18 was drilled next to BI. 17 with an upward inclination of 45°. The flow from this borehole is hence vertical, with a distance of only 3 m within the ore dyke. The first tracer tests were carried out on 15 July 1999. BI. 17 produced at an average rate of 9.1 l/s over the test

period. Due to the short distance, it can be assumed that a steady state radial-convergent flow field was established around the production borehole within the ore dyke. The tests at Bl. 19 and Bl. 20 were repeated on 09 September 1999, since the original input mass of 2 g of eosine and sulphorhodamine B proved to be too small. The average production rate during these tests amounted to approximately 8.0 l/s. The dissolved tracers were carefully poured into a tube and pushed into the borehole as a short pulse by a pressurised chase fluid. The short pulse injections were accomplished within less than one minute. The tracer volume and the volume of the chase fluid were reduced to the smallest possible amount in order to minimise the initial spreading of the tracer plume around the injection borehole. The total injection volume of 0.02 to 0.06 m³ is small compared to the production rates. It is hence unlikely that the flow field was significantly disturbed by the injections.

Large-scale experiments with distances from 50 to 600 m were carried out by injection into surface boreholes. The injection boreholes B 95S and B 132S are situated less than 100 m away from the observation tunnel but in a direction oblique to the axis of the ore dyke. The boreholes B 80E and B 82E are situated at the *Etziboden* more than 500 m south of the production borehole in the direction of the dyke axis. Both boreholes intersect the contact zone of the dyke and showed a hydraulic response to the drainage experiment (see Chapter 4.1.2).

The groundwater samples were taken from the horizontal production borehole Bl. 17 that intersects the ore dyke at depths between 2 and 5 m. Short sampling intervals from 6 to 30 min were applied in the beginning in order to be able to accurately determine the first and peak arrival time of the small-scale tests in the ore dyke. At a later stage, the sampling rate was gradually increased to 8 h. A daily sample was taken after 09 October 1999 and one sample was collected every two days from 01 November 1999 until the end of the sampling campaign on 17 February 2000.

Table 10 Tracer test design

Injection borehole	Tracer	Date of injection	Injected mass [g]	Injection period [min]	Volume of injected fluid [10 ⁻³ m ³]	Ratio V _i / V _b ^{*)} [-]
B 80E	Pyranine	30.06.99 19:52	2500	<15	70	0.6
B 82E	Amidorhodamine	30.06.99 21:01	3000	<15	50	0.3
B 95S	Fluoresceine	30.06.99 18:10	980	<15	100	0.6
B 132S	Na-Naphthionate	30.06.99 16:59	4300	<15	60	1.9
Bl. 15	NaBr	15.07.99 12:01	388	<1	36	3.2
Bl. 18	KCl	15.07.99 11:20	148	<1	58	8.5
Bl. 19	Sulphorhodamine B	15.07.99 10:11	2.0	<1	21	0.6
Bl. 20	Eosine	15.07.99 10:41	2.0	<1	26	0.5
Bl. 19	Sulphorhodamine B	09.09.99 12:56	70	<1	-	-
Bl. 20	Eosine	09.09.99 12:25	80	<1	-	-

^{*)} Ratio of volume of injected fluid to volume of borehole

The fluorescent dyes were analysed using spectrofluorimetry at the chemical laboratories of the Institute of Applied Geology, University of Karlsruhe. The chloride and bromide concentrations of the samples were determined by ionic chromatography at the laboratory of the Environmental Research Centre, University of Karlsruhe.

The average background concentration of chloride amounted to 1.16 ± 0.07 mg/l. These natural fluctuations caused some uncertainties especially during the time of first tracer

arrival and the late time data. The background concentration of bromide was close to or just below the detection limit of the chromatographic analysis. A value of 0.035 mg/l was defined for the evaluation of the TBC. The background of the fluorescent dyes was below the detection limit as expected and assumed to be zero.

Tracer dilution in the injection boreholes

Groundwater samples were carefully taken from the injection boreholes to monitor mixing processes. The chloride and bromide concentrations in Bl. 15 and Bl. 18 reached very low levels within a few hours. The fluorescent dyes in Bl. 19 and Bl. 20, however, were visible for more than 6 weeks after injection and remained partly in the borehole. This observation may be explained by the low ratio of the volume of injected fluid to the volume of borehole, in the order of 0.5, which is much smaller compared to Bl. 15 (3.2) and at Bl. 18 (8.5) - see Table 10. Apparently, a large portion of the tracer fluid was trapped in immobile sections of the boreholes. From the surface boreholes, only B 80E and to a minor degree B 95S showed a good tracer mobilisation. The concentration of naphthionate in B 132S and of pyranine in B 82E decreased slowly, indicating a poor connection of these boreholes with a well-drained fracture zone (Figure 31).

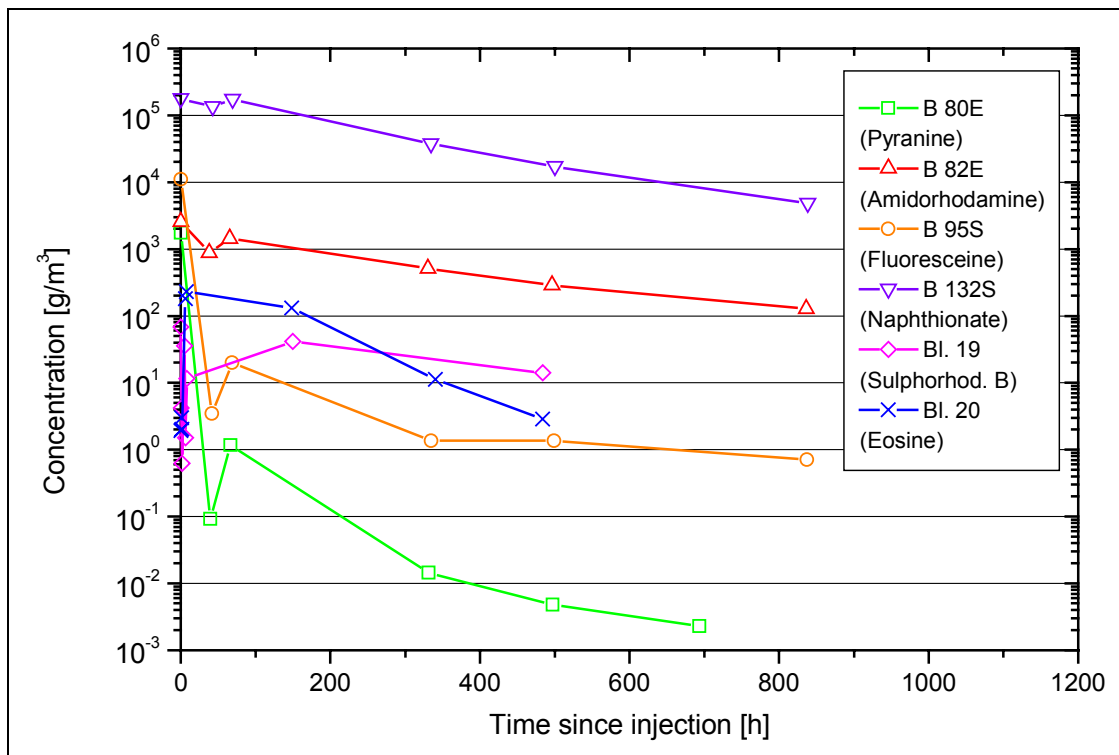


Figure 31 Tracer concentration in the injection boreholes

Evaluation of TBC's

The tracer test results are combined in Table 11. The large-scale tracer experiments were unsuccessful except for the fluoresceine test at B 95S. The tracers injected in B 80E, B 82E and B 132S could not be recovered at the production borehole. Traces of fluoresceine could be observed at Bl. 17 after approximately 25 d corresponding to a maximum flow velocity within the fractured granite of 0.15 m/d. The breakthrough

continued for at least 230 d after which the sampling was stopped. The plateau-like shape of the curve is probably a combined result of multiple flow paths within the fracture network and the retarded release of the tracer from the injection borehole. Due to the very low tracer concentrations and the significant noise in the data, the TBC could not be fitted to an analytical model.

An almost complete recovery (> 90%) of the injected tracer mass has been encountered for the two tests (Bl. 15 and Bl. 18) in the ore dyke section. The second tests at Bl. 19 and Bl. 20 in the porphyritic dyke yielded much lower recovery rates of 12% and 23%, respectively, which shows as pointed out above that a large portion of the tracer has been trapped within the injection borehole. Additionally, a portion of the tracer mass was presumably injected into fracture systems that are not connected to the ore dyke.

Table 11 also gives the tracer first arrival time t_1 , the time of maximum tracer concentration t_{Cmax} and the maximum flow velocity v_{max} for each test. Again, a clear difference between the tests conducted in the ore dyke and the tests with injection in the porphyritic dyke can be recognised. The maximum velocity in the ore dyke was well above 200 m/d whereas maximum velocities between 15 and 30 m/d were determined for the experiments incorporating the porphyritic dyke. It can be concluded that the tested section of the porphyritic dyke is less permeable than the ore dyke.

Table 11 Tracer test results

Injection borehole	Tracer	Distance [m]	Q_{av} [m ³ /h]	Recovered mass [%]	t_1 [h]	t_{Cmax} [h]	v_{max} [m/d]
Bl. 15	NaBr	23	32.9	91	2.71	9.48	213
Bl. 18	KCl	3.0	32.9	99	0.26	0.36	277
Bl. 19	Sulphorhodamine B	14	32.9	no recovery	—	—	—
	Sulphorhodamine B		28.8	3.4	23.1	131	14.5
Bl. 20	Eosine	15	32.9	no recovery	—	—	—
	Eosine		28.8	20	11.6	47.6	31
B 80E	Pyranine	579	32.8	no recovery	—	—	—
B 82E	Amidorhodamine	554	32.8	no recovery	—	—	—
B 95S	Fluoresceine	93	32.8	traces	608 (?)	1464	0.15 (?)
B 132S	Na- Naphthionate	56	32.8	no recovery	—	—	—

Analytical modelling

The normalised TBC's of the fluorescent dyes and salt tracers are presented in Figure 32. The shift of the single graph along the time scale depicts the different flow velocities which can be attributed to different aquifer systems, namely the ore dyke, the porphyritic dyke and the fractured granite. In the chosen log-log scale, small concentrations are better displayed and the tailings of the TBC's can be more easily distinguished from each other. Besides, Tsang (1995) has pointed out that the late time data of the TBC will plot on a straight line with a slope of -1.5 in such a plot if a diffusive flux of the tracer into the adjacent matrix occurs, a finding that is in accordance with the analytical solutions of the SFDM and the SFPFM. Straight-line sections are apparent in the graphs of Figure 32, with B 95 being an exception, and hence may be interpreted as a result of matrix diffusion.

The analytical solutions presented in Chapter 2.4.2 were applied for the modelling of the convergent flow tracer tests. It is generally accepted that the applied dye and salt tracers behave ideally, i.e. that neither sorption nor degradation or chemical reactions have a

considerable impact on the mass transport. Additionally, density effects due to high input concentrations are assumed negligible. The ADM, SFDM and the SFPFM furthermore require that the condition of an instantaneous injection be fulfilled. In order to consider the observed slow release of the tracer solution from the injection borehole into the formation, the EI-ADM and the VI-ADM were additionally included into the analysis.

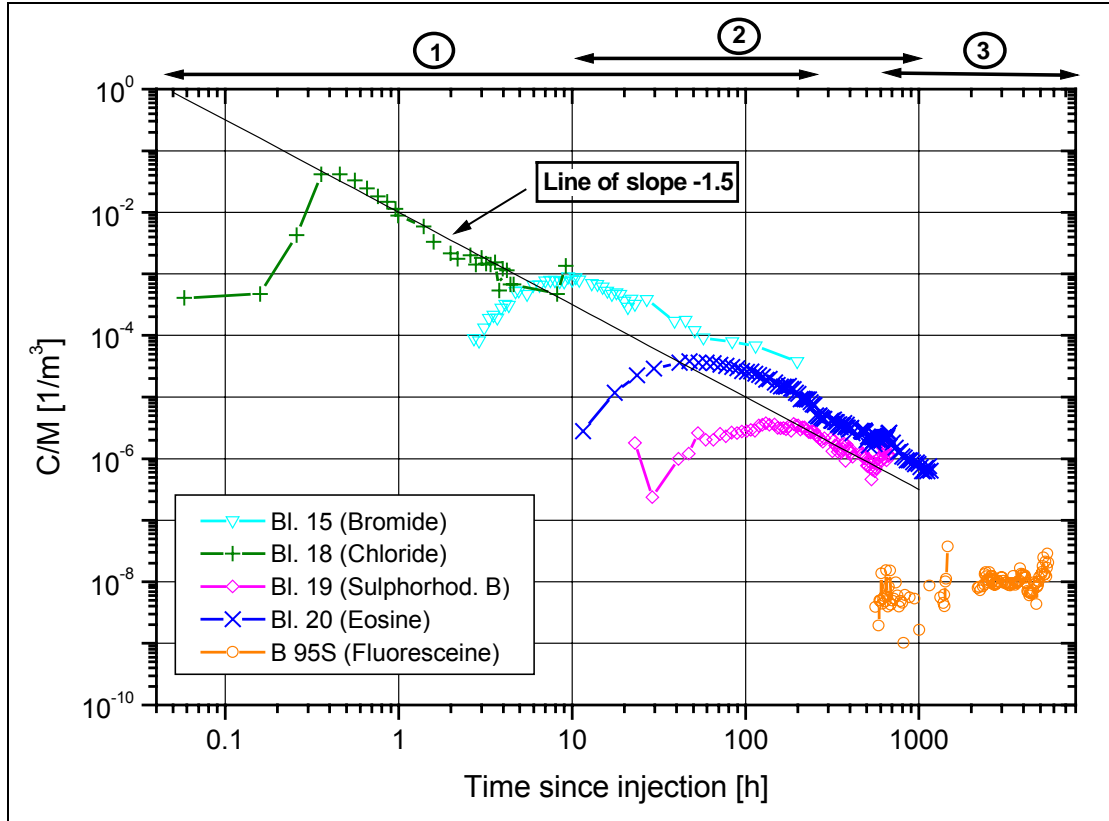


Figure 32 Normalised TBC's of small-scale tracer tests. The numbers refer to the very distinct duration of the tests in the different aquifer systems, namely the ore dyke (no. 1), the porphyritic dyke (no. 2) and the fractured granite (no. 3)

Table 12 contains the parameters obtained from the calibration of the various transport models. The quality of the fitting procedure is expressed in terms of the sum of the square deviations X^2 between measured and calculated concentrations which was obtained from the least squares fit and is defined as:

$$X^2 = \sum_{i=1}^n (C_i^{\text{measured}} - C_i^{\text{calculated}})^2$$

The best fit has been determined using programmed algorithms similar to the codes that have been developed for the pump test analysis (Chapter 4.1.2).

The **bromide TBC** shows a distinct peak after about 3 h. The gradually decreasing concentrations between 50 and 200 h form a noticeable tailing (Figure 33, upper graph). Satisfactory curve fits could be achieved with three different models, the ADM, SFDM and the VI-ADM. Due to the different model assumptions the obtained transport parameters differ significantly from each other. The SFDM yields a higher flow velocity

and Peclet number since diffusion processes instead of dispersive mixing explain the tailing in this model.

The **chloride TBC** is characterised by a narrow peak and a flat tailing (Figure 33, lower graph). Most of the tracer mass was already recovered after 2 h. The calibration of the ADM yielded a much larger value of X^2 compared to other models and is hence inadequate. Instead, the TBC could be nicely fitted with the SFDM. However, it was noticed during the calibration that the sensitivity of X^2 with respect to Pe is extremely weak. Indeed, an almost identical fit could be achieved by application of the SPPFM. Consequently, mixing by dispersion proved to be negligible for this experiment due to the short duration of the test. Since the mean transit time hardly exceeds 0.3 h, the assumption of a significant diffusive flux may also not be justified. Bäumle et al. (2000) therefore suggested that the TBC resembles the shape of the tracer-input function and that advection is the dominant transport mechanism during this short-term and short-distance experiment. Consequently, the TBC may be interpreted as a plug flow type translation of the tracer-input function.

The **sulphorhodamine B TBC** shows the strongest tailing among the small-scale experiments. The **eosine TBC** is similar in shape to the bromide TBC (Figure 34). Compared to the tests conducted in the ore dyke, the experiments incorporating the porphyritic dyke are characterised by considerably larger mean transit times in the order of 100 h and smaller flow velocities in the order of a few meters per day. Once more, several transport models could be successfully applied although these models are based on different assumptions with respect to mass transport processes and injection type. It is certainly reasonable to assume that matrix diffusion plays a noticeable role considering experiments with transit times in the order of magnitude of tens of days. However, low values of the diffusion parameter α of between 0.01 and 0.02 h^{-0.5} were obtained from fitting the SFDM to the measured data. In fact, a sensitivity analysis showed that the influence of α is rather weak which is why the ADM produces an almost identical graph.

By application of the EI-ADM and the VI-ADM, an alternative explanation for the observed tailings other than dispersive mixing and matrix diffusion could be obtained. The EI-ADM yields the best fit to the sulphorhodamine B TBC, i.e. the lowest value of X^2 , of all the models considered. The EI-ADM results in a four times higher flow velocity than the models that assume an instantaneous injection. It also yields a higher Pe since the tailing of the TBC is caused by the slow release from the injection borehole and not by dispersive mixing. The VI-ADM nicely fits the eosine TBC, but it should be pointed out that the t_0 and Pe obtained are almost identical to the values obtained from the ADM. The high value of κ amounting to 1.1 h⁻¹ illustrates that the tracer solution was released within a few hours and that the assumption of an instantaneous injection was at least fulfilled for the portion of the tracer that could be recovered.

It should be stressed again that a radial-convergent flow field towards the well could not develop due to the geometry of the dyke systems. Since two different hydraulic systems are involved along the migration path, i.e. the ore and the porphyritic dyke, mixing may occur at the intersection point of the two dykes. The mixing at the intersection may cause a similar effect to the retarded release from the injection borehole.

Table 12 Transport modelling results

Injection borehole: Bl. 15 Domain: Ore dyke + contact zone Tracer: Bromide						
<u>Transport Model</u>	<u>Fitted</u>					<u>Fit quality</u>
	t_0 [h]	v [m/d]	Pe [-]	α [$\text{h}^{-0.5}$]	κ [1/h]	X^2 [(g/m ³) ²]
ADM	65	8.6	0.9	—	—	0.038
SFDM	38	15	1.5	0.03	—	0.030
VI-ADM	55	10	0.8	—	1.1	0.058
Injection borehole: Bl. 18 Domain: Ore dyke + contact zone Tracer: Chloride						
<u>Transport Model</u>	<u>Fitted</u>					<u>Fit quality</u>
	t_0 [h]	v [m/d]	Pe [-]	α [$\text{h}^{-0.5}$]	λ [1/h]	X^2 [(g/m ³) ²]
ADM	0.82	88	5.0	—	—	14.4
SFDM	0.34	212	62	0.9	—	1.1
SFPFM	0.30	240	—	1.2	—	1.7
Injection borehole: Bl. 19 Domain: Porphyritic dyke Tracer: Sulphorhodamine B						
<u>Transport Model</u>	<u>Fitted</u>					<u>Fit quality</u>
	t_0 [h]	v [m/d]	Pe [-]	α [$\text{h}^{-0.5}$]	λ [1/h]	X^2 [(mg/m ³) ²]
ADM	373	0.9	2.4	—	—	0.087
SFDM	344	1.0	2.6	0.017	—	0.090
EI-ADM	82	4.1	4.1	—	0.004	0.078
Injection borehole: Bl. 20 Domain: Porphyritic dyke Tracer: Eosine						
<u>Transport Model</u>	<u>Fitted</u>					<u>Fit quality</u>
	t_0 [h]	v [m/d]	Pe [-]	α [$\text{h}^{-0.5}$]	κ [1/h]	X^2 [(mg/m ³) ²]
ADM	241	1.5	1.2	—	—	0.71
SFDM	161	2.2	2.0	0.012	—	0.49
VI-ADM	243	1.5	1.2	—	1.1	0.72

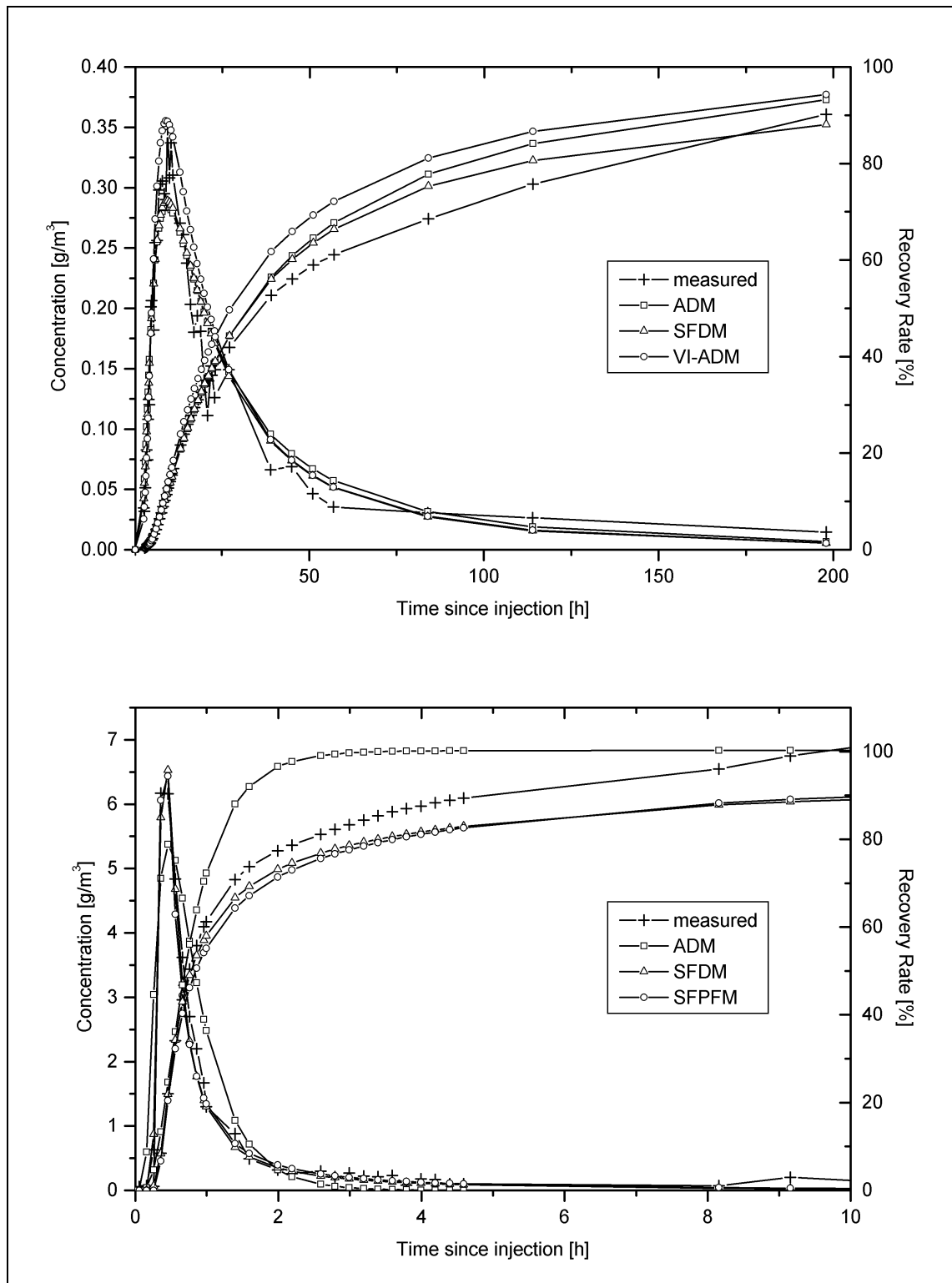


Figure 33 Analysis of tracer breakthrough and recovery curves for the bromide test at Bl. 15 (top), and the chloride test at Bl. 18 (bottom)

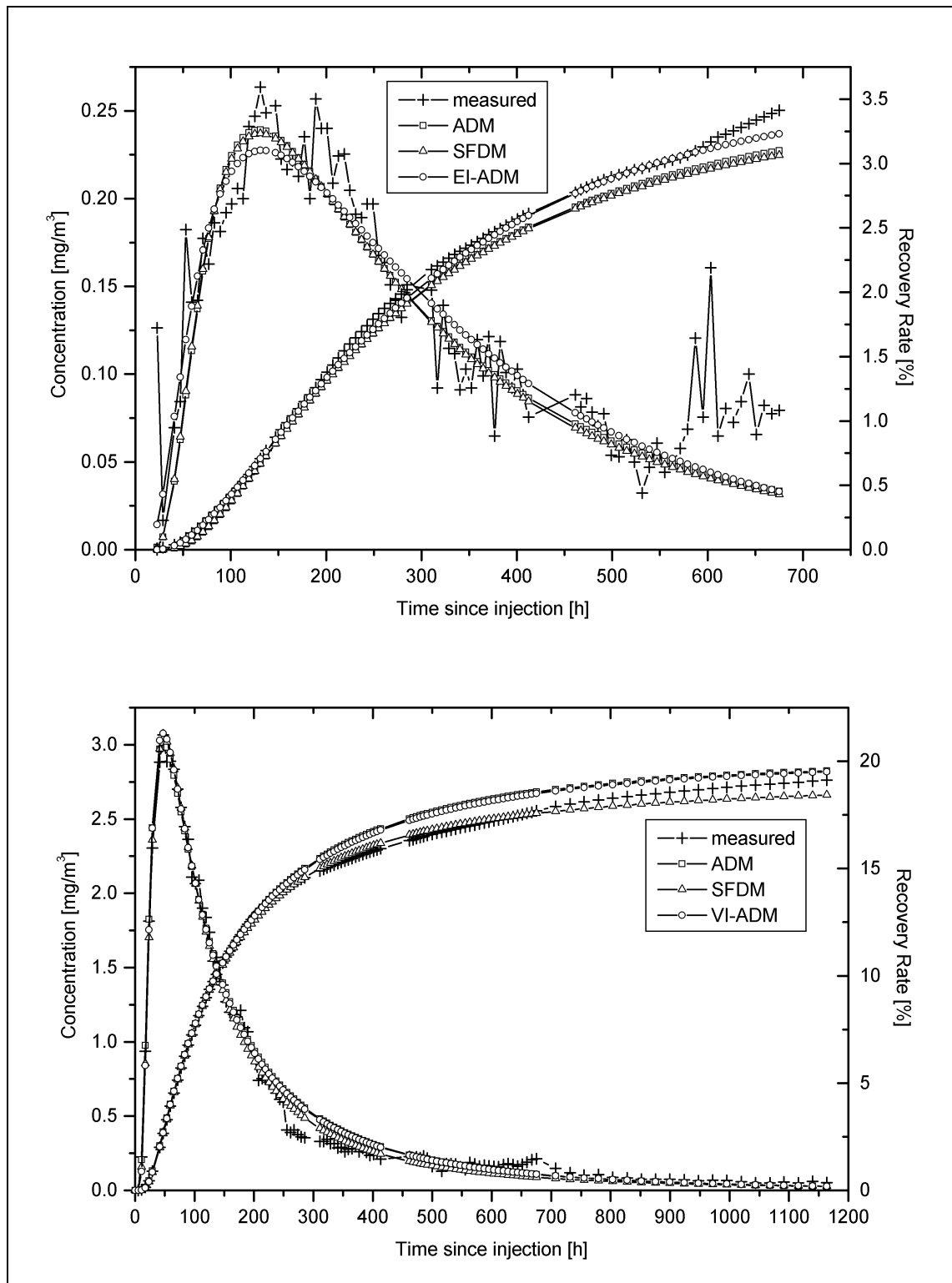


Figure 34 Analysis of tracer breakthrough and recovery curves for the sulphorhodamine B test at BL 19 (top), and the eosine test at BL 20 (bottom)

Conclusions

The evaluation of the tracer tests with the convergent-flow models yielded good fits but significant differences in the transport parameters depending on which model was used.

Generally, it was difficult to distinguish between the effect of dispersive mixing, matrix diffusion and the type of tracer injection. **The application of an inadequate transport model, however, leads to erroneous results with respect to the transport parameters.** The commonly observed tailing of the TBC's can only be partly attributed to the effect of matrix diffusion. The tests at Bl. 18 and Bl. 19 have been largely controlled by the way the tracer entered the formation from the injection borehole. The release of sulphorhodamine B from Bl. 19 was probably considerably hampered, an effect, which could be properly simulated by the EI-ADM. The possible initial spreading of the tracer plume around the injection borehole that depends largely on the volume of chase fluid, as well as the portion of the tracer that may have been injected into dead-end fractures may also have contributed to the observed tailing during the small-scale experiments. Furthermore, mixing at fracture intersections, especially between the ore dyke and the porphyritic dyke may have caused a further spreading of the TBC.

Non-diffusive tailings of the TBC's have already been reported from earlier tracer studies at the Lindau rock test site. Kaselow (1999) performed tracer tests in the northern pit using an injection pipe and proved by numerical modelling that the observed tailing could not be entirely produced by matrix diffusion. Einsiedl et al. (2000) obtained identical tailings of the TBC's for tracer experiments between the boreholes Bl. 10 and Bl. 11 despite the largely differing diffusion coefficients of the injected fluorescent dyes and particle tracers. A similar finding was reported by Bäuml et al. (2001) from a multiple tracer test carried out between Bl. 8 and Bl. 10. Witthüser (2000) concluded from comparative tracer studies using different injection techniques that the tailing of the resulting TBC's, commonly interpreted as a result of dispersion and diffusion, will be remarkably reduced if a double packer injection system is applied.

These results highlight the influence of the injection type on the TBC for small-scale tracer experiments and the need of improved injection techniques. It is furthermore recommended to simultaneously inject tracers with different diffusion coefficients, e.g. soluble and particle tracers, as a tool to distinguish the effect of matrix diffusion from the influence of the injection type.

Table 13 contains a summary of the results of previous and recent tracer tests carried out at the Lindau rock test site. A comparison between the forced-gradient tests and the tests carried out under natural flow conditions is not permitted due to the different hydraulic conditions. It is interesting to note that even under natural flow conditions maximum velocities of above 10 m/d have been observed in the ore dyke. Himmelsbach et al. (1998) concluded from a detailed analysis of tracer tests that were carried out along the ore dyke that dispersivities are small as long as the tracer follows a discrete fracture set but will increase sharply as soon as different fracture sets are involved. The increase in dispersivity was explained by interstitial mixing between different fracture sets. Their dispersivities ranged from 0.17 to 0.30 m for experiments with migration distances of between 11 and 17 m and from 2 to 4 m for experiments with larger distances. The dispersivities obtained from this study exceed 5 m. This implies that different fracture sets are incorporated along the migration path, such as the ore dyke and the porphyritic dyke. Considering the outlined uncertainties regarding the application of the adequate transport model and the potential errors caused by a wrong model selection, the dispersivities have to be looked at with the necessary caution.

Table 13 Comparison of Lindau tracer test results

Test Type	Injection site→ Detection site	i [%]	Q [m ³ /h]	x [m]	v _{max} [m/d]	t ₀ [h]	v [m/d]	a _L [m]	Re- ference
FG-D	Bl. 7→Bl. 8	—	0.46	10.2	179	—	—	—	H
	Bl. 7→Bl. 10	—	0.47	21.4	160	—	—	—	H
	Bl. 8→Bl. 10	186	0.45	11.2	520	0.70	384	0.17	H,H2
	Bl. 8→Bl. 10	93	0.33	11.2	—	1.18	228	0.17	H2
	Bl. 11→Bl. 9	41	0.40	16.2	555	0.78	498	0.25	H
FG-M	B 77E→Bl. 2	0.77	24.7	235	49	161	35	3.9	P,H2
	B 81E→ B 80E	—	0.52	3	92	1.7	42	0.08	R
	Bl. 3→Bl. 4	10	21.6	11.5	1104	0.44	627	0.44	W
	Bl. 5→Bl. 4	16	21.6	10	720	0.97	247	0.66	W
	Bl. 7→Bl. 10	13	0.46	21.4	51	14	37	2.1	H,H2
	Bl. 8→Bl. 10	16-20	0.35	11.2	215-240	2.00-2.13	126-134	0.30	H,H2
	Bl. 8→Bl. 10	8.9	0.48	11.2	—	6.7	40	0.77	Wi
	Bl. 8→Bl. 10	8.9	0.51	11.2	367	15	18	5.6	K, Wi
	Bl. 8→Bl. 10	—	0.60	11.2	179-230	1.6-2.0	131-166	0.04-0.56	B
	Bl. 8→Bl. 11	9.2	0.49	13.0	—	6.5	48	1.3	Wi
	Bl. 10→Bl. 11	16	0.47	6.3	363	0.69	219	0.16	K, Wi
	Bl. 10→Bl. 11	16	0.49	6.2	—	5.8	26	0.21	Wi
	Bl. 11→Bl. 9	48	0.46	16.2	486	1.30	299	0.90	H,H2
	Bl. 12→Bl. 2	3.1	25.2	49	504	5	235	2.5	P,H2
	Bl. 15→Bl. 17	—	32.9	23	213	38	15	15	*)
	Bl. 18→Bl. 17	—	32.9	3	277	0.34	212	—	*)
	Bl. 19→Bl. 17	—	28.8	14	15	344	1.0	5.4	*)
	Bl. 20→Bl. 17	—	28.8	15	31	161	2.2	7.0	*)
	B 95S→Bl. 17	—	32.8	93	25 (?)	—	—	—	*)
NG	B 78E→B 20E	0.44	5.4	346	23	432	19	3.5	H,H2
	B 77E→Q 40	0.5	—	540	3.4	—	—	—	H
	B 79E→Q 41	0.5	—	210	3 (?)	—	—	—	H
	B 80→B 30E	0.5	—	170	14	—	—	—	H

Notes: Test type:

FG-D = forced gradient dipole test

FG-M = forced gradient monopole test

NG = natural gradient test

Reference:

H = Himmelsbach, 1993

H2 = Himmelsbach et al. 1998

P = Pohl, 1994

K = Kaselow, 1999

R = Reinert, 2000

Wi = Witthüser, 2001

W = Witt, 2000

B = Bäuml et al., 2001

*) this study, SFDM

4.1.5 Classification of fractured aquifers

The results of the geohydraulic investigations presented can be combined to classify different fractured aquifer components according to their hydraulic properties, MRT, chemical groundwater composition and regional hydraulic behaviour. The following fractured aquifer components can be distinguished:

The **dyke systems** consisting of the ore dyke *Hermann* and the porphyritic and rhyolitic dykes form the first fractured aquifer component. The ore dyke could be described as a structure with a high transmissivity in the order of 10⁵ m²/d and high storage coefficients in the order of 10⁻¹. The storage coefficients obtained from the hydraulic tests are higher by ½ to 1 order of magnitude than the porosities (2-7%) determined from core samples within the dyke and the contact zone. This illustrates that the values obtained for *T* and *S* only apply to the hydraulically active and interconnected parts within the dyke zone, which carries most of the mobile groundwater. The MRT derived from the WHRA is in the order of a few tens of days. These values accord well with the tracer first arrival times of

between 12 and 15 d and the corresponding maximum flow velocities in the order 14 to 23 m/d that were determined from two tracer tests within the dyke under natural gradient conditions. The groundwater has a low overall mineralisation with an EC in the order of 20 to 40 $\mu\text{S}/\text{cm}$. Fluoride and barium provide a signature to this water type. The increased content of fluoride ($> 0.4 \text{ mg/l}$) and barium ($> 0.2 \text{ mg/l}$) distinguishes the water originating from the dyke from the water of the surrounding aquifers. The dykes act as regional conduits, which drain narrow subterranean catchments. Figure 35 shows a cross section through the dyke with the narrow trough created by the dyke zone. The groundwater flow direction follows the strike of the dykes and often differs from the general regional flow direction.

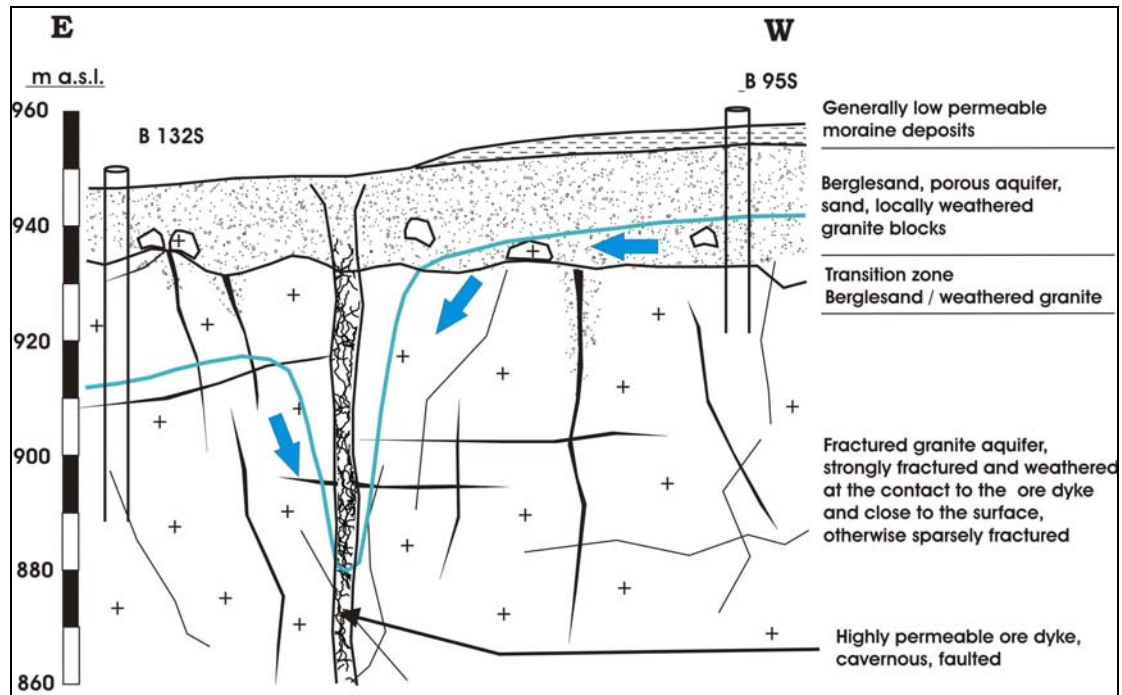


Figure 35 Schematic E-W profile through the ore dyke. The blue line depicts the water table after full recovery from the drainage catchment experiment.

The second fractured aquifer component consists of **highly fractured and weathered granite** along the contact zone of the dykes or close to the surface. The weathered zone close to the surface is probably not strictly separated from the porous aquifers, since the transition from the *Berglesand* to the granite is diffuse. The aquifer is heterogeneous due to the non-uniform degree of fracturing and weathering. An intermediate transmissivity in the order of 1 to 500 m^2/d and a storage coefficient in the order of 10^{-3} to 10^{-4} were obtained from the hydraulic test analysis. The MRT of the groundwater is in the order of 10^2 to 10^3 d. The groundwater chemistry shows a low mineralisation similar to dyke systems but lacks the fluoride and barium signature. The fluoride and barium concentrations are generally less than 0.1 mg/l and 0.2 mg/l, respectively. The highly fractured and weathered granite feeds mostly intermittent springs along the steep slopes. The hydrochemical monitoring during the catchment experiment indicated that the aquifer significantly contributes to the discharge of the dykes. Groundwater of the shallow aquifer within the weathered zone originates predominately from areas in an uphill direction of the lineament and discharges into the dykes with an apparent vertical flow component.

The third fractured aquifer component is formed by **sparsely fractured granite** within the undisturbed and generally deeper sections. The groundwater flow within this aquifer is restricted to the wide-spaced fractures since the rock matrix is virtually impermeable. It is likely that there are blocks and areas with only immobile groundwater (no measurable flow). This explains why large-scale tracer tests in the test site often fail. The aquifer is characterised by a very low permeability (K -value 10^{-6} to 10^{-7} m/d) and a low porosity ($<1\%$). The MRT lies above 10^3 d. The groundwater shows a higher mineralisation than the more mobile groundwater indicated by the EC of above $50 \mu\text{S/cm}$. In particular, it shows a higher sodium and sulphate content. The zone did not noticeably contribute to the discharge at the drainage experiment despite its duration of over one year. This shows that the aquifer is only negligibly incorporated in the hydrological cycle that is otherwise characterised by a high precipitation and recharge, a spontaneous discharge pattern and high groundwater renewal rates.

4.2 Tsumeb Aquifers

4.2.1 Hydraulic tests

Scope of the hydraulic test program

The hydraulic test program included the re-evaluation of available data from former pumping tests during Phase 1 and the performance of additional hydraulic tests during Phase 2 of the study. The purpose of the hydraulic test program was to obtain a hydraulic characterisation of the aquifer systems encountered in the project area. Combining the outcomes of the additional hydrogeological investigations with the results of the hydraulic test program, a conceptual hydrogeological model could be developed. Furthermore, the test evaluation provided transmissivities and storage coefficients as input data for the numerical model (Figure 36).

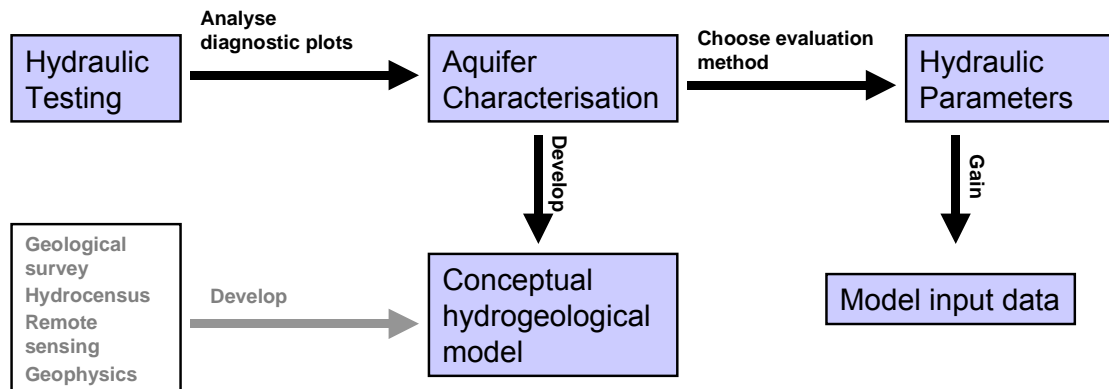


Figure 36 The significance of the hydraulic test program within the study

The rock formations tested in this study comprised the fractured dolomitic rocks of the Abenab and Tsumeb Subgroup, the low permeable clastic sediments of the Nosib and Mulden Group, the Karoo Sequence and the Grootfontein Basement Complex. The hydraulic test sites are displayed in Figure 37.

Eighteen out of the 26 formerly performed pumping tests could be re-evaluated. The hydraulic test program of Phase 2 comprised 2 slug tests, 14 step tests and 18 aquifer tests which were carried out during the period from 23 March 2001 to 09 June 2001. The hydraulic tests are described in full detail in the unpublished Final Report of the TGWS (DWA et al., 2002c).

Slug & bail tests were performed in order to test rock formations with an estimated transmissivity of less than $\sim 1 \text{ m}^2/\text{d}$ according to the lithological interpretation and the observations made during drilling and development of the borehole. Such low transmissivities were expected within the Nosib Group and the Grootfontein Basement Complex).

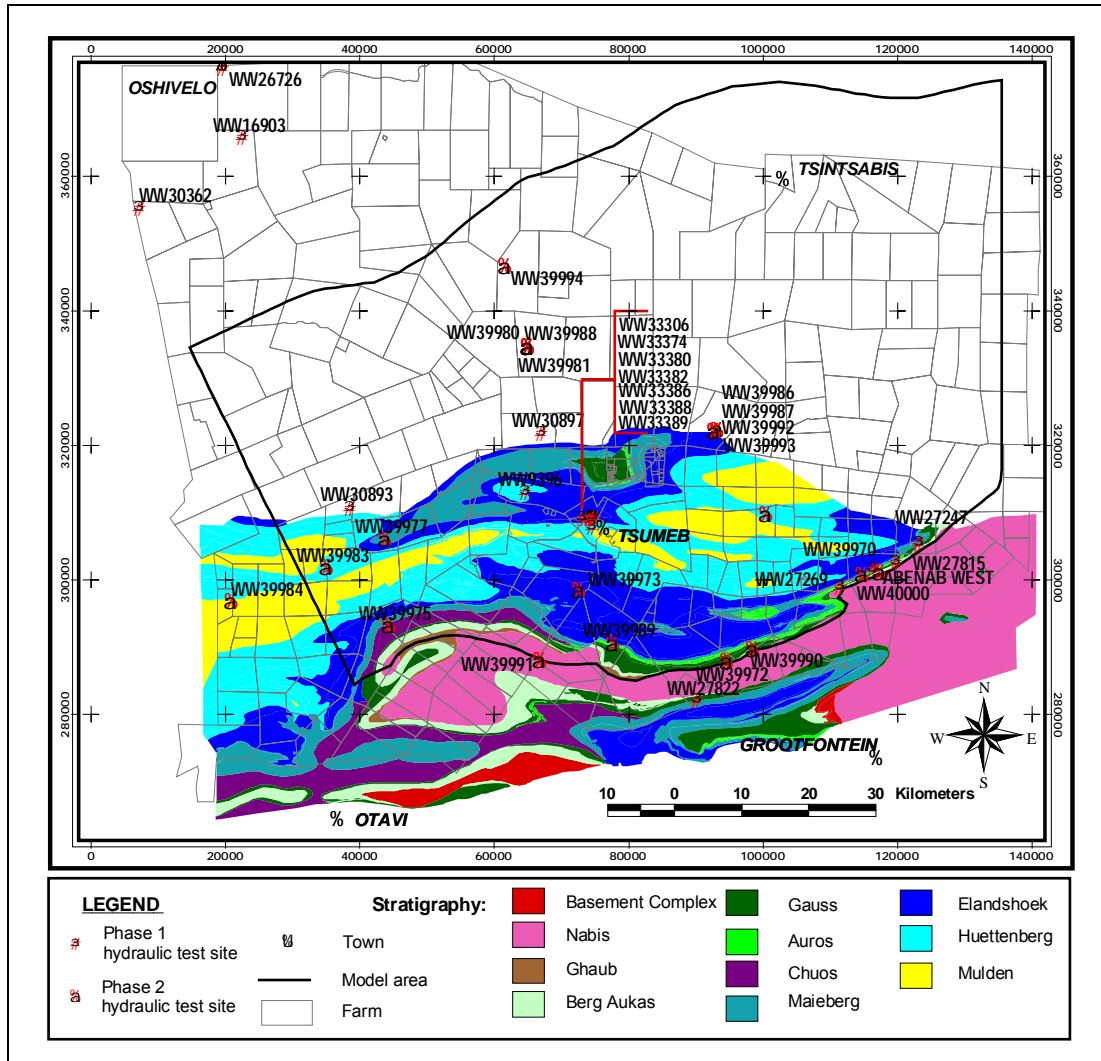


Figure 37 Hydraulic test sites

The objectives of the **step tests** were to:

- ❑ obtain a first estimate of the transmissivity of the formation
- ❑ locate the position of the main water strikes
- ❑ assess the well losses at the varying pumping rates
- ❑ delineate the design of the subsequent aquifer test.

The **aquifer tests** were evaluated in order to

- ❑ provide reliable values for the transmissivity and the storage coefficient of the formations as input parameters for the calibration of the groundwater model;
- ❑ characterise the aquifer systems by detecting leakage, single fracture flow, double porosity properties etc. from diagnostic plots.
- ❑ gain, by the insertion of packers at selected sites, information on the variation of the hydraulic properties with depth and to assess interactions (leakage) between layered aquifer systems.

Hydraulic test procedures

For the slug and bail tests a 6 to 12 m long cylindrical pipe, filled with water or sand, was quickly inserted into or removed from the tested well, thus creating an instantaneous change of at least 3 m in the water table. Subsequently, the **groundwater level** was continuously measured using a water level indicator until the original rest water level (RWL) was obtained.

The step tests were carried out prior to the aquifer test and these consisted of three to four steps with the pumping rates increasing in a step-wise manner. The duration of each step ranged from 1 to 2 hours.

During an aquifer test, the wells were usually pumped for 72 hours. The pumping phase could be shortened if the drawdown had stabilised at an earlier stage. The recovery measurements covered a maximum period of 72 hours.

The drawdown and the recovery of the groundwater levels were measured in both the pumped well and the selected observation well(s) using submersible data loggers. The water levels were also measured with water level indicators to ensure that the test could be evaluated should any of the data loggers not function properly. The groundwater levels were measured at time intervals of 20 s, 1 min and 5 min depending on what stage of the test.

The **pumping rates** were determined by volumetric measurements using a stopwatch and a bucket, by regular flowmeter readings or by readings from a 600 mm rectangular weir.

During the hydraulic test period the **daily rainfall, atmospheric pressure and physical parameters** comprising temperature, EC, pH and O₂ were measured additionally. The rainfall measurements were obtained at each test site for the duration of the hydraulic test. A linear trend analysis was performed to compensate for a gradual rise or fall in the groundwater level during the test period. The atmospheric pressure was measured continuously at the drilling campsite close to Tsumeb. The pressure changes, however, proved to have minimal effect on the results of the evaluation.

Aquifer characterisation and test evaluation methods

Additional to the conventional methods, which assume radial convergent flow towards the pumped well within a homogeneous isotropic formation, analytical solutions considering leakage, single fracture flow and double porosity models were taken into consideration for the hydraulic test evaluation. The adequate analytical solution was found from the analysis of the diagnostic plots. The software package TPA - Test Pumping Analysis (Bardenhagen, 2002) was used for the evaluation of the majority of the pumping tests.

Representative hydraulic parameters

Considering the size of the study area and the heterogeneity of the Tsumeb Aquifers it must be emphasised that only localised results can be obtained from each hydraulic test. The hydraulic parameters gained are only representative for the tested volume of rock (Chapter 2.3.1). From a series of tests within the same formation, however, a range of possible values or most likely values could be determined. Due to the extended period of

pumping, it is assumed that the most reliable results are usually obtained from an aquifer test.

Hydraulic test results

The results obtained from the re-evaluation of former tests during Phase 1 are generally of lower accuracy due to the inferior quality of the data. In particular, apparent fluctuations of the pumping rate were often not recorded. Storage coefficients could not be obtained from these tests since only the groundwater level measurements at the pumped wells were available. From Phase 1 it was therefore recommended that the Phase 2 investigations should include a hydraulic test program that would achieve a reliable hydraulic characterisation of the rock formations. The phase 1 results are not described in detail but are included in the evaluation statistics of the hydraulic tests (Table 15).

The hydraulic parameters obtained from the Phase 2 slug and pumping test analysis and the analytical solutions applied for the curve matching procedure are summarised in Table 14. The representative values for T and S were obtained from either the slug or the step and aquifer test analysis at both the pumped and the observation well(s).

A few remarks are necessary regarding the application of the fracture type analytical solutions:

- For the analyses according to the single fracture models of Gringarten et al. (1974) and Gringarten & Ramey (1974), a fracture half-length of 100 m was assumed although fracture half-lengths of several hundreds of meters, up to above 1000 m, can be derived from geophysical or remote sensing interpretations. The curve matching with a smaller half-length, however, provided better and in most cases more realistic results, indicating that the hydraulically active zone within the lineament is much smaller than its overall length.
- In some cases, the analysis was ambiguous and different analytical solutions could be applied; e.g. a leaky aquifer type behaviour (Hantush-Jacob method) could not be distinguished unequivocally from a double porosity behaviour (Moench's solution) at WW39975.
- Many of the tests proved to be largely affected by **well losses** caused by a negative skin as indicated in Table 14. The early data at the pumped well, which often cover more than 80% of the total drawdown, could not therefore be used for the curve fitting. The late time data of such tests commonly exhibit a shallow curvature on a log-log scale. Fitting a type curve to the late time data depends largely on personal judgement and consequently, less accurate hydraulic parameters may be obtained.

In fact, the hydraulic parameters gained from the pumped well in a fractured rock may be completely wrong if the skin effect is not recognised. The transmissivity may be underestimated by one or more orders of magnitude. One can only obtain reliable results for these tests from the data of the observation well. The largest well loss was typically found at the highest yielding wells. At high pumping rates, turbulent flow will more likely occur. This observation may hence indicate a non-linear well loss caused by turbulent flow in the fractured zone adjacent to the well.

Table 14 Hydraulic test evaluation results

Well	Observation well(s)	T [m ² /d]	S [-]	s _w [-]	s _r [-]	Applied evaluation method(s)
WW39971	WW39970 ¹⁾	0.17	1.3E-03	-	-	Bouwer & Rice (1976) / Cooper et al. (1967)
WW39972	WW38727	3.2	1.0E-03	0.05	0	Gringarten et al. (1974)
WW39973	WW39334	1260	7.0E-04	³⁾	-	Theis (1933) / Cooper & Jacob (1946)
WW39974	WW39310	5560	1.0E-03	³⁾	-	Theis (1933) / Cooper & Jacob (1946)
WW39975	WW39976	2.4	6.0E-06	-	-	Theis (1933) / Hantush & Jacob(1955) / Moench (1982)
WW39977	WW39982	123	8.0E-04	³⁾	-	Gringarten et al. (1974)
WW39980	WW39988	1.5	7.0E-05	-	-	Theis (1933) / Cooper & Jacob (1946)
	WW39981	2.9	3.0E-03	-	-	
WW39983	WW38504	271	5.0E-03	³⁾	-	Hantush & Jacob (1955)
WW39984 (0-224 m)	WW39985 WW38513	3.2	3.0E-04	0.2	0.3	Theis (1933) / Gringarten et al. (1974) / Cinco et al. (1978) ²⁾
WW39984 (224-335m)	WW39985 WW38513 ¹⁾	4.4	2.0E-04	0	-	Theis (1933) / Hantush & Jacob (1955)
WW39986	WW39987	1070	4.0E-04	115	-	Theis (1933) / Cooper & Jacob (1946)/ Hantush & Jacob (1955)
WW39988	WW39980	1.1	7.0E-05	-	-	Theis (1933) / Cooper & Jacob (1946) / Hantush & Jacob (1955)
	WW39981	11	1.0E-03	-	-	
WW39989	WW39300	0.36	3.0E-05	0	0	Theis (1933) / Gringarten et al. (1974)
WW39990	-	<0.005	5.0E-04	-	-	Bouwer & Rice (1976) / Cooper et al. (1967)
WW39991	WW39931	3.3	1.0E-03	-	-	Theis (1933) / Gringarten & Ramey (1974)
WW39992	WW39993	1260	0.016	³⁾	-	Theis (1933) / Cooper & Jacob (1946)/ Hantush & Jacob (1955) / Cinco et al. (1978) ²⁾
WW40000 (0-150m)	WW29331	14	6.0E-04	-	-	Theis (1933) / Cinco et al. (1978) ²⁾
WW40000 (150-400 m)	WW29331 ¹⁾	0.08	-	-	-	Theis (1933) / Cooper & Jacob (1946)

Notes: 1) no response to pumping or slug injection

3) strong well loss

2) quantitative evaluation could not be performed

An example of how the drawdown at the well may be influenced by skin effects is presented in Figure 38. The theoretical drawdown (blue curve) at the pumped well WW39974, that assumes no well loss, is compared to the observed drawdown (red curve). The theoretical drawdown was calculated by inserting the evaluation results obtained from the data of the observation well for T and S into the well function. Without a well loss, the drawdown at the pumped well would amount to about 0.8 m. The actual drawdown at steady state, however, was 5.5 times higher and amounts to 4.5 m.

The **aquifer characterisation** according to the pumping test interpretation is presented in Appendix 4. Fracture zones acting as conduits could be clearly identified at 7 targets (WW39972, WW39991, WW40000 upper section, WW39989, WW38877, WW39984

upper section, WW39983). This indicates that increased groundwater fluxes are commonly associated with faults in the study area.

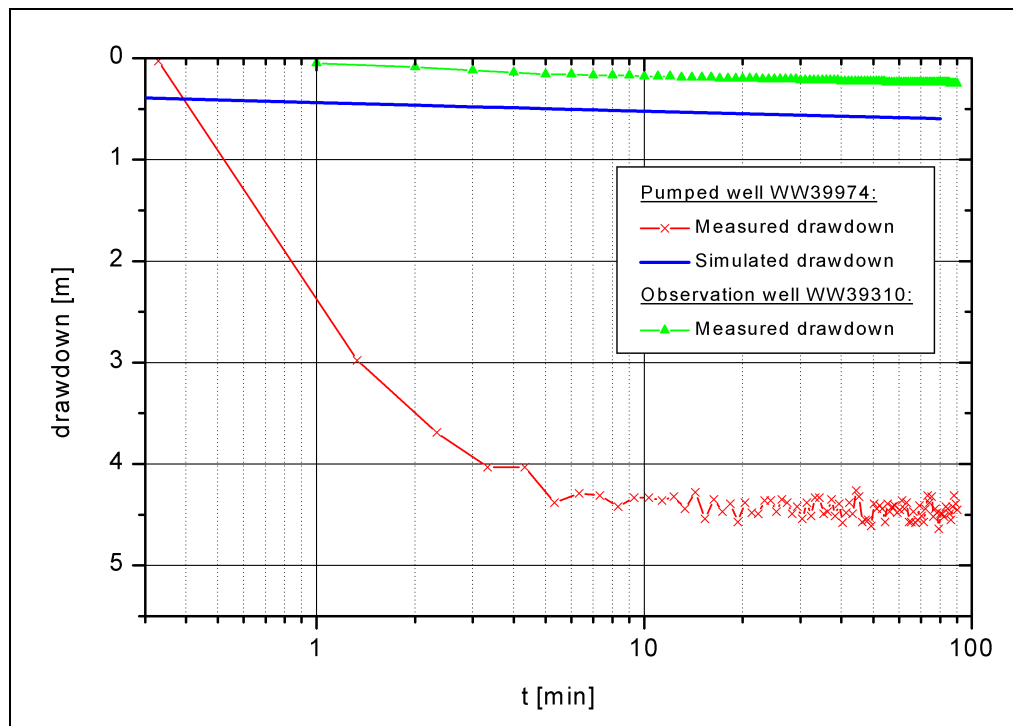


Figure 38 Diagnostic semi logarithmic plot of the aquifer test carried out at WW39974 as an example of severe well losses in fractured rock caused by a negative skin at the pumped well (red curve). The transmissivity of $5560 \text{ m}^2/\text{d}$ and the storage coefficient of $1 \cdot 10^{-3}$ was obtained from the observation well data (green curve) using the Theis method and would result in a much lower drawdown at the pumped well if no well losses occurred (simulated curve).

Leakage from an equivalent or higher permeable rock formation can be assumed at 6 targets (WW39975, WW39983, WW39984 lower section, WW39986, WW39988, WW39992). The storage capacity of the aquitard separating the two aquifers was assumed negligible. Interbedded sections of higher permeable sandstone and low permeable clay within the Mulden Group on top of the pumped Hüttenberg Formation probably form the layered aquifer system at WW39984. The EC measurements at WW39988 indicate that less mineralised groundwater from within the Karoo deposition at greater depths enters the well during pumping. It is less obvious to distinguish such a layered system in the stratigraphical succession for the remaining 4 targets, i.e. for WW39975, WW39983, WW39986 and WW39992. The water contributed by leakage probably comes from a highly permeable layer within the same stratigraphic unit. At WW39986 and WW39992, for example, a water-bearing fractured or even karstified structure within the dolomite may be assumed.

The **transmissivity** and **storage coefficient** of each formation obtained from both the Phase 1 and Phase 2 hydraulic test analyses are summarised in Table 15. In general, a large regional variance in the hydraulic parameters could be observed. A statistical analysis is not feasible since tests are available to represent the heterogeneity of the aquifer systems. The results obtained the hydraulic parameters, nevertheless, provide a

useful range of potential values for groundwater modelling purposes. Furthermore, the formations can be classified according to their hydraulic properties.

According to the test results, the Grootfontein Basement Complex can be regarded as an aquiclude. The Nosib and the Mulden Group are considered as fractured aquitards with transmissivities of less or slightly above $1 \text{ m}^2/\text{d}$. The higher transmissivities seem to be linked to accompanying fault zones (WW39972, WW39984 upper section, WW39990).

The dolomite and the limestone of the Abenab and Tsumeb Subgroup can be classified as fractured aquifers. Both the transmissivities and the storage coefficients, however, vary over a wide range. The ratio of the maximum to the minimum transmissivity of the Elandshoek and the Hüttenberg Formation, for instance, amounts to about 1:80 and 1:50, respectively. The Hüttenberg Formation shows considerably higher transmissivities than the Elandshoek and the Maieberg Formation. The average transmissivity of the Hüttenberg Formation obtained from 8 tests is $1725 \text{ m}^2/\text{d}$ whereas an average of $309 \text{ m}^2/\text{d}$ was calculated for the Elandshoek Formation. The highest transmissivity observed within the Maieberg Formation only amounts to $123 \text{ m}^2/\text{d}$. This formation exhibits considerably lower transmissivities ($T=0.4 \text{ m}^2/\text{d}$ at WW39989) in the southern portion of the study area, which was classified as the “*Disturbed Zone*” (see Chapter 4.2.2.2). The locally karstified Hüttenberg Formation including the Tsumeb dyke was hence identified as the most permeable stratigraphic unit within the study area. The transmissivity of the Chuos Formation at WW39975 amounts to only $2.4 \text{ m}^2/\text{d}$. Consequently, the sandstone and clay of the Chuos Formation act as an aquitard within the surrounding dolomitic aquifers.

The Kalahari is most permeable in the northern portion of the study area. The 3 available test results are all above $400 \text{ m}^2/\text{d}$, but this probably overestimates the average transmissivity of the southern Kalahari Aquifer. According to Dierkes (1996), the average transmissivity of the southern Kalahari Aquifer should be in the order of 10 to $100 \text{ m}^2/\text{d}$.

Transmissivities of between 1 and $10 \text{ m}^2/\text{d}$ were determined for the Karoo sediments at WW39980 and WW39988. The Karoo hence acts as an aquitard separating the Kalahari Aquifer in the North of the study area from the descending Dolomite Aquifer. The more permeable dyke systems, however, may locally intersect the Karoo sediments and connect the two aquifers, which are otherwise vertically separated elsewhere.

Typical storage coefficients range from $3 \cdot 10^{-5}$ to $1 \cdot 10^{-3}$. These values confirm that the Tsumeb Aquifers are generally confined. Unconfined or semi-confined conditions may, however, exist locally within the study area. At WW39992, for instance, an exceptionally high storage coefficient in the order $1 \cdot 10^{-2}$ was obtained for the Hüttenberg Formation. This borehole is located within the highly fractured zone accompanying the Tsumeb dyke.

Only limited information on the **vertical variation of the hydraulic parameters** can be derived from the pumping test evaluation, as results of only two packer tests are available. The Hüttenberg Formation exhibits unexpected low transmissivities ($T=4 \text{ m}^2/\text{d}$) below about 300 m b.g.s. at WW39984. The dolomite of the Abenab Subgroup at WW40000 shows a very low transmissivity ($T=0.08 \text{ m}^2/\text{d}$) at a depth $>200 \text{ m}$ b.g.s. compared to $14 \text{ m}^2/\text{d}$ above this level. A sharp drop in the groundwater level was observed during the step tests at WW39975, WW39984, WW39991 and WW40000. This drop usually occurred once the water table fell below the main water strike, which was

frequently encountered at depths between 60 to 100 m b.g.s. These observations indicate that a large amount of the total groundwater flux is restricted to depths down to about 200 m b.g.s.

Table 15 Hydraulic test evaluation statistics (Phase 1 & Phase 2 results)

Stratigraphic Unit	T [m ² /d]	S [-]	Characterisation
Basement Complex	n = 1 T < 5·10 ⁻³ m ² /d	n = 0	Aquiclude
Nosib	n = 3 T ~ 3 m ² /d along fault zones T = 0.2 m ² /d undisturbed zones	n = 3 1.0·10 ⁻³ < S < 1.3·10 ⁻³	Aquitard
Abenab Subgroup	n = 5 14 m ² /d < T < 466 m ² /d T = 0.08 m ² /d at depth > ~200m	n = 1 S = 6·10 ⁻⁴	Aquifer
Chuos	n = 1 T = 2.4 m ² /d	n = 1 S = 6·10 ⁻⁶	Aquitard
Maieberg	n = 4 87 m ² /d < T < 123 m ² /d T = 0.4 m ² /d in the south	n = 2 3.0·10 ⁻⁵ < S < 8.0·10 ⁻⁴	Aquitard or Aquifer
Elandshoek	n = 8 15 m ² /d < T < 1260 m ² /d average T = 309 m ² /d	n = 1 S = 7·10 ⁻⁴	Aquifer
Hüttenberg	n = 8 121 m ² /d < T < 5565 m ² /d average T = 1725 m ² /d T = 4 m ² /d at depth > ~300m	n = 5 4.0·10 ⁻⁴ < S < 1.6·10 ⁻² S = 2.0·10 ⁻⁴ at depth > ~300m	Aquifer
Mulden	n = 1 T = 3.2 m ² /d	n = 1 S = 3·10 ⁻⁴	Aquitard
Karoo	n = 4 1.1 m ² /d < T < 11 m ² /d	n = 4 7.0·10 ⁻⁵ < S < 3.0·10 ⁻³	Aquitard
Kalahari	n = 3 434 m ² /d < T < 10367 m ² /d	n = 0	Aquifer

4.2.2 Groundwater Model

4.2.2.1 General outline

The general outline of the modelling approach is depicted in Figure 39. The study was separated in two phases. **In Phase 1, a preliminary conceptual hydrogeological model was developed based on existing data and reports. This exceptional approach is considered necessary in order to cope with the complexity of the geological structure in the study area.** The overall aim of the Phase 1 modelling was to elaborate a detailed work program for the up-coming studies including a major exploration drilling and hydraulic test program based on the preliminary modelling results (Tordiffe et al., 2001).

Due to the complexity of the geological structure, it would have been inefficient to construct a 3-D model at first hand. Instead, the 2-dimensional horizontal (2-DH) and two 2-dimensional vertical models (2-DV) of the Tsumeb Aquifers were established. The main target of the 2-DH models consisted in the definition of the hydraulic boundary conditions and in the numerical implementation of the complex geological structure into the model. The 2-DV models were included in order to assess the groundwater flow variations with depth. The 2-DV models were aligned in South-North direction, which corresponds to the regional groundwater flow direction. Geological profiles were developed prior to the construction of the 2-DV models. The profiles were located at 17°30' E (⁵²556) close to Lake Otjikoto and at 17°45' E (⁷⁸864) close to Tsumeb (see map of study area depicted in Figure 10). The 2-DV models were calibrated with the simulated groundwater levels obtained from the 2-DH model (Bäumle et al., 2001).

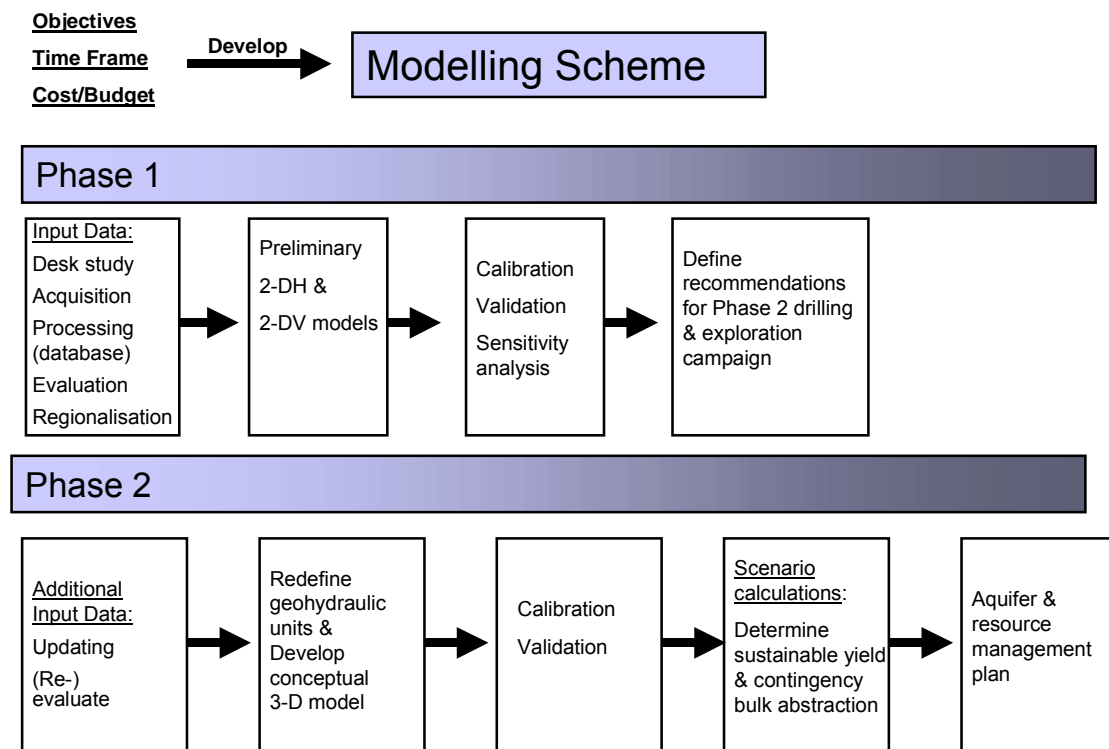


Figure 39 Modelling scheme

The 2-D models could be successfully calibrated despite the incomplete database input. From the preliminary groundwater balance calculated by the models it could already be concluded that the Tsumeb Aquifer systems represent a substantial groundwater resource which was worth further investigation (Bufler et al. 2000). Sensitivity studies were carried out to investigate the impact of varying boundary conditions and model input parameters such as recharge factors or hydraulic properties of the various rock formations on the groundwater flow and balance. By means of the sensitivity studies, the understanding of the complex hydrogeological situation of the study area was improved stepwise. Based on the results of the model scenario calculations, recommendations were made to redefine and optimise the exploration drilling and the field survey during the forthcoming Phase 2 of the investigation program. The following 6 major conclusions and the corresponding recommendations and proposed measures could be defined from the modelling results:

1. The type of the southern boundary conditions needs to be specified.

The influx of groundwater over the Nosib anticline should be investigated by drillings and hydraulic testing as well as precise groundwater level measurements.

2. The hydraulic impacts of the lineaments (dykes/faults) and the karst features on the hydraulic regime are only known from few locations.

Details of the nature of the dykes (depth of weathering zone, dip, thickness), in particular of the Tsumeb dyke, should be investigated by drilling and hydraulic tests.

3. The distribution and hydraulic character of the Karoo deposits, which might separate the Kalahari from the Dolomite Aquifer at depth, needs to be investigated.

The Karoo deposits have to be investigated in detail by geophysics, drilling and hydraulic testing.

4. The groundwater level database needs to be improved to facilitate a more accurate steady state and transient model calibration.

A revised groundwater contour map based upon DGPS measurements of approximately 50 wells should be constructed. Water level recorders should be installed at selected wells and daily precipitation records should be evaluated at selected gauging stations.

5. Existing values for the recharge of the study area show discrepancies. The recharge must be known in more detail and with a higher reliability.

Environmental tracer methods should be applied to quantify the recharge. Groundwater samples should be taken and analysed for chemical parameters, for stable isotopes $^{18}\text{O}/^2\text{H}$ and for radioisotopes ^3H and $^{13}\text{C}/^{14}\text{C}$.

6. More and reliable transmissivity values and storage coefficients are required.

The drilling and hydraulic testing at approximately 18 selected sites is necessary. To be able to obtain storage coefficients from the hydraulic test evaluation, the drill sites must be located close to existing wells or piezometers.

The **Phase 2** of the groundwater modelling incorporates the new findings from the geological and the detailed geophysical surveys as well as from the results of the drilling, aquifer testing and recharge study. **The conceptual hydrogeological model was**

refined and a numerical 3-D model was established and calibrated. Scenario calculations were performed to determine the sustainable yield and the permissible contingency bulk abstraction. With the modelling of the aquifer responses for varying abstraction scenarios, recommendations for a sustainable management of the groundwater resources in the study area were developed.

The unpublished Final Report of the TGWS (DWA et al., 2002e) comprises a more detailed description of the modelling approach and the modelling results.

4.2.2.2 Conceptual hydrogeological model

The assessment of the hydrogeological situation (Chapter 3.2) showed that the Tsumeb aquifer systems could be treated as hydraulically equivalent porous aquifers. The karstification and most of the fault patterns seem to be only a local phenomenon and will be of minor importance in the regional scale considered of 100 km in an E-W direction and 70 km in N-S direction. **Hence, an equivalent continuum model could be applied.** This finding is in accordance with the work of Schmidt & Plöthner who developed a numerical model for the southern part of the OML (BGR, 1996; Schmidt & Plöthner, 1999). Areally extensive faults and fracture zones, however, had to be treated as individual geohydraulic units with distinct permeability and porosity.

The finite element code of FEFLOW was used to simulate the groundwater flow within the Tsumeb Aquifers. The 3-D model developed incorporates seven major geohydraulic units to match the complex lateral alternation of the geological structure and 5 vertical layers to account for the vertical succession of the aquifers and aquitards.

Model boundaries

All model boundaries were established by interpreting groundwater contour maps that were based on the groundwater levels measured in October 2000 and in June/July 2001.

The eastern and western margins of the model are considered as no-flow boundaries. Since they are aligned parallel to the major flow patterns, any exchange of groundwater across the eastern and western margin of the model is negligible.

The northern model boundary is defined by a hydraulic head boundary condition. It corresponds to the most northerly groundwater level data available, where no significant fluctuations of the groundwater level (1140 m a.s.l.) over long-term periods could be observed. These insignificant fluctuations, in the order of a few meters, will only have little influence on the regional flow pattern within the Tsumeb Aquifers.

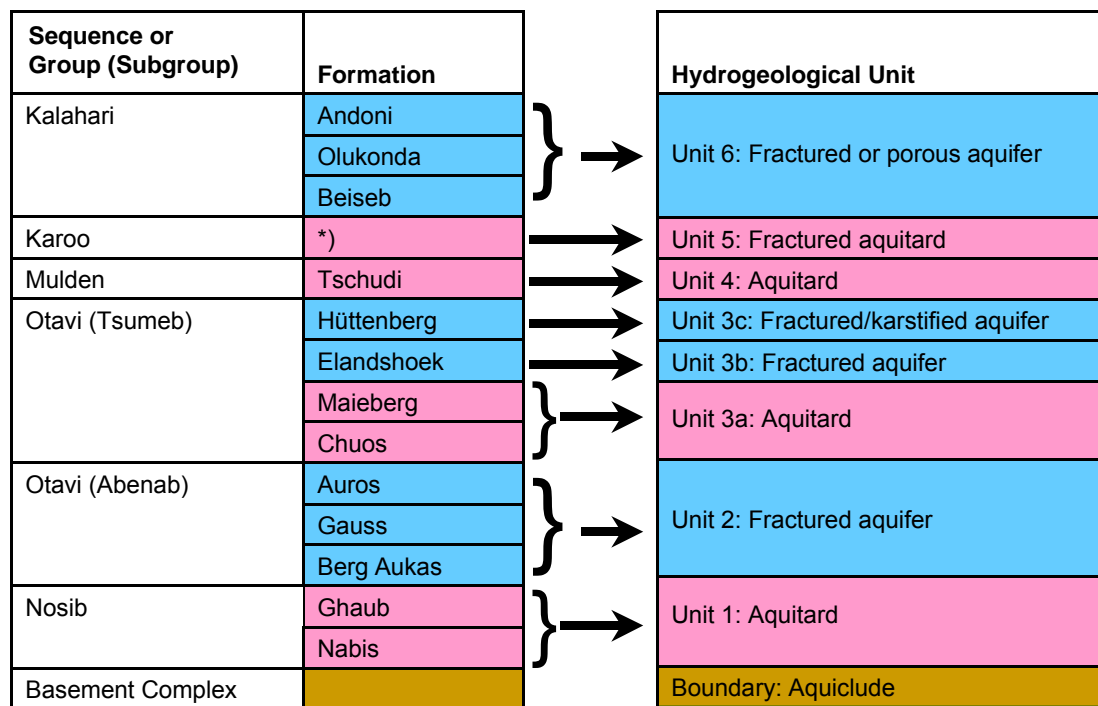
The southern model boundary comprises a constant flux boundary condition for the Nosib Group in the west, whereas a no-flow boundary was defined in the east for the contact between the Grootfontein Basement Complex and the Abenab Subgroup. The inflow across the Nosib Group was estimated by using Darcy's Law. Assuming an average K -value of $9 \cdot 10^{-3}$ m/d, an aquifer thickness of 450 m and a hydraulic gradient of 1.5%, as obtained from the groundwater contour plan, an inflow of $0.8 \text{ Mm}^3/\text{a}$ was calculated.

The model delineated in Figure 41 covers an area of $7,693 \text{ km}^2$. The resulting finite element mesh comprises 89,928 elements for each layer, which totals to 449 640 elements for the entire model. The average element size equals approximately

8.5 ha. The model discretisation is, however, strongly refined around abstraction wells and areas with sharp permeability contrasts.

Horizontal differentiation of aquifer properties: Geohydraulic units

In order to implement the complex geological setting in a numerical model, geohydraulic units had to be defined. The geohydraulic units combine different litho-stratigraphic and lithological sequences of comparable hydraulic properties (Figure 40). The stratigraphical succession could be largely simplified by this conceptional approach. Nevertheless, the model is still able to delineate the hydrogeological characteristics of the study area.



*) undifferentiated

Figure 40 Geohydraulic units: The dyke systems that crosscut the formations form the additional 7th unit and are omitted in this figure.

According to the hydraulic characteristics of the rock formations, 7 geohydraulic units have been defined (see Figure 41), and these comprise the following:

Unit 1: Nosib Group

The bedrock formations of the Nosib Group are considered as a fractured aquitard with transmissivities less than or slightly above $1 \text{ m}^2/\text{d}$ (refer to Table 15).

Unit 2: Abenab Subgroup

The Gauss, Berg Aukas and Auros Formations represent the major lower dolomitic aquifer of the Tsumeb Synclinorium. The shale of the lower Auros Formation that is approximately 50 m thick is regarded as an aquitard separating the dolomites within the Abenab Subgroup. In the 3-D model, however, the stratigraphy had to be simplified and the lower Auros Formation was not considered as a separate unit within the Dolomite

Aquifer. According to the pumping test analysis the transmissivity of the Abenab Subgroup ranges from 14 to 144 m²/d. The only available storage coefficient for the Abenab Subgroup amounts to $6 \cdot 10^{-4}$.

Unit 3: Tsumeb Subgroup

The rock formations of the Tsumeb Subgroup are allocated to the geohydraulic unit 3. This unit has to be subdivided into four sub-units according to the different hydrogeological properties of the formations.

Unit 3a: Maieberg and Chuos Formation (Aquitard)

The tillite and shale of the Chuos Formation and the steep dipping sediments of the Maieberg Formation in the south of the study area are considered to be low permeable ($T \approx 2 \text{ m}^2/\text{d}$). The Maieberg formation hence divides the two major dolomitic aquifers (Abenab and Tsumeb Subgroup) in the SE of the study area and hampers the groundwater flow from following the general northerly direction. The model has to account for the comparatively high T -values ranging from 87 to 127 m²/d encountered in the area north of Lake Otjikoto.

Units 3b & 3c: Elandshoek and Hüttenberg Formation (Aquifers)

The outcrop area of the Elandshoek and Hüttenberg Formations cover most of the southern part of the study area. These formations are also considered to underlie most of the Kalahari Sequence in the northern part of the study area and are generally characterised by a high permeability. The Hüttenberg dolomite is locally karstified. The units 3b and 3c hence represent the most productive aquifers within the investigation area. The pumping test analysis yields an average transmissivity of 1725 m²/d for the Hüttenberg Formation and of 309 m²/d for the Elandshoek Formation. Typical storage coefficients are in the order of $5 \cdot 10^{-4}$ to $1 \cdot 10^{-3}$.

Unit 3d: Disturbed Zone (Aquitard)

In the southern central model area, the groundwater flow within the Abenab Subgroup is deflected towards the north-east due to an impermeable barrier formed by the steep dipping Maieberg limestone in combination with the outcropping Remnant dyke and a major NE trending fault. These low permeable rock formations ($T = 0.4 \text{ m}^2/\text{d}$) combine in the so-called "*Disturbed Zone*".

Unit 4: Mulden Group (Aquitard)

The Tschudi Formation was affected by metamorphism and consists therefore of slightly permeable to impermeable phyllite and quartzite. The Mulden Group is considered an aquitard with a transmissivity in the order of 1 to 10 m²/d.

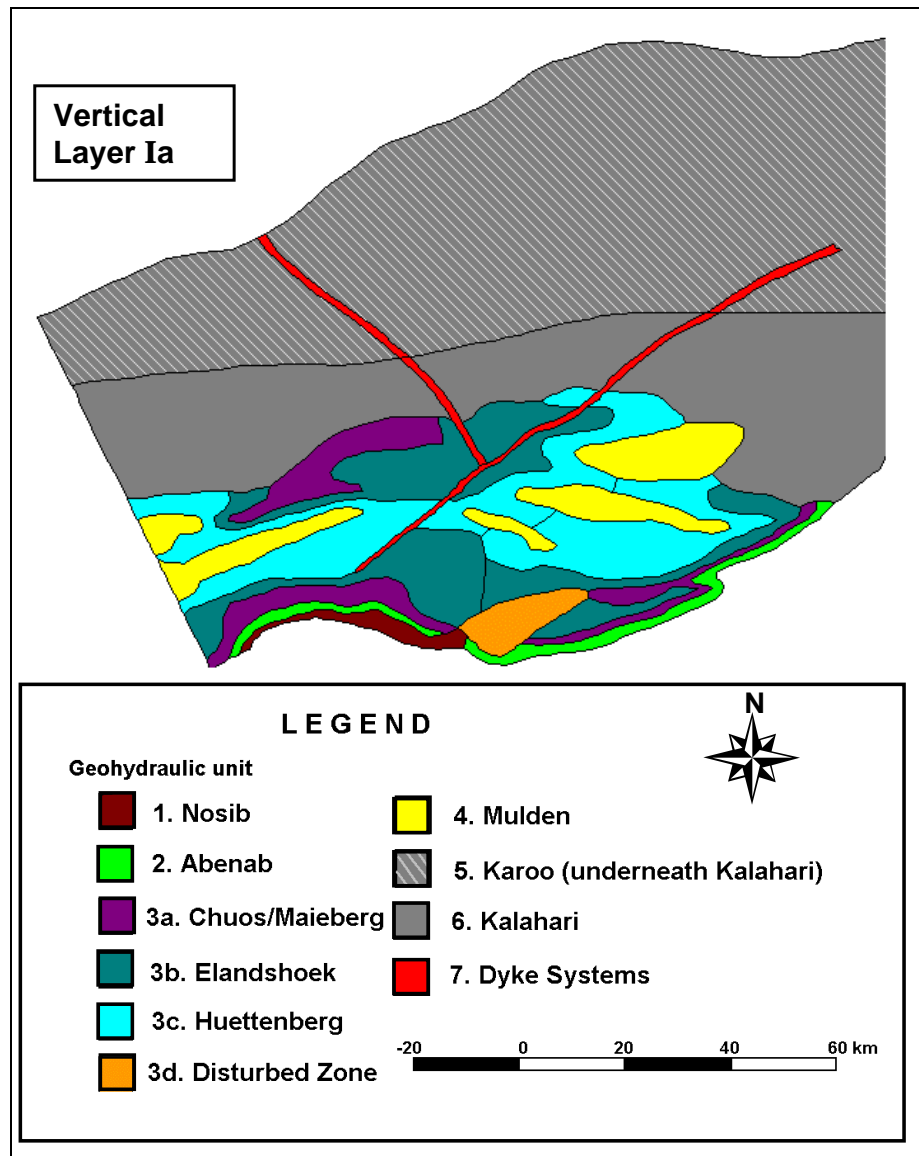


Figure 41 Geohydraulic units as defined for the top layer (no. Ia) of the 3-D model

Unit 5: Karoo Sequence (Aquitard)

The Otavi dolomite is covered in the north of the study area by the widely distributed shale and the intercalated basalt of the Karoo Sequence. The unit is regarded as an aquitard with transmissivities in the order of 1 to 10 m²/d. The Karoo deposition forms a unit which hydraulically separates the dolomite series from the overlying Kalahari Sequence.

Unit 6: Kalahari Group (Aquifer)

The sedimentary, semi-consolidated Kalahari Aquifer extends between Tsumeb and Oshivelo and covers almost the entire Tsumeb foreland. The transmissivities of the heterogeneous Kalahari sediments are moderate in the south according to the lithological characterisation of the phase 2 drilling. In the north of the study area at Oshivelo, high

transmissivities ranging from 400 to $>10^5 \text{ m}^2/\text{d}$ are encountered due to a lithological change towards coarser-grained sands (Dierkes, 1996; DWA 2002).

Unit 7: Dyke and fault systems (Aquifer, vertical conduits)

The geophysical reconnaissance gave evidence that, apart from a number of regional fault and fracture zones, a series of different dyke systems might exist. Considering the hard and software restrictions however, only the most prominent features were added into the model. The lineaments include the north-east trending Tsumeb dyke and a regional, NW-SE striking fault zone. Both lineaments intersect large parts of the study area. The Tsumeb dyke represents the doleritic dykes, which have intruded during the Jurassic, whereas the fault zone presumably belongs to the open tensional, conjugate structures, which, after emplacement during the Cambrian, were rejuvenated in the Jurassic (see Chapter 3.2.3). It can be assumed that these vertically orientated conduits intersect all layers within the model. The dyke and fault systems are characterised by a high permeability and are considered to act as regional conduits, which can transfer groundwater between different aquifers. Transmissivities of $>1000 \text{ m}^2/\text{d}$ and storage coefficients between $4 \cdot 10^{-4}$ and $2 \cdot 10^{-2}$ were evaluated from the pumping test analysis (WW39986, WW39992).

Vertical differentiation of aquifer properties: Layers

The main issue in the design of the 3-D model is the uncertain variation of the hydraulic parameters with depth. In Karst areas, the permeability and the porosity of the rock are often correlated with depth and orientation of the actual or ancient karst levels and are not necessarily coupled to the geological structure such as folding and bedding planes. In general, it can be assumed that the transmissivity and the storage coefficient decrease with increasing depth. The hydraulic packer tests, which were carried out in the study area, indicate a sharp decrease in transmissivity already at depths below 200-300 m b.g.s. From the vertical distribution of oxygen and sulphate, different zones with varying redox-state were derived. A reducing environment prevails at depths below 900 m b.g.s. (see Chapter 3.2.5). Accordingly, the lower boundary of active convection was placed at a depth of 900 m.

The model subdivides the entire aquifer system into different vertical layers with distinct hydraulic properties. Three different layers I to III up to the maximum depth of 900 m b.g.s. are considered. The groundwater flow below 900 m b.g.s. is presumably related to very large mean residence times and is hence of little significance for the purpose of this study. The thickness of the layers and the principal reduction of the transmissivity, the hydraulic conductivity and the storage coefficient with depth are depicted in Table 16. If for example a transmissivity of $100 \text{ m}^2/\text{d}$ and a storage coefficient of $5 \cdot 10^{-3}$ is allocated to the top layer I of one unit, the transmissivity will be reduced to $30 \text{ m}^2/\text{d}$ for layer II and to $10 \text{ m}^2/\text{d}$ for layer III. The storage coefficient will be reduced to $1 \cdot 10^{-3}$ for layer II and to $1 \cdot 10^{-4}$ for layer III according to this concept.

Table 16 Thickness of the model layers and the vertical differentiation of T , K and S in terms of ratios with respect to the bottom layer.

Layer no.	Thickness [m]	T- ratio [-]	K – ratio [-]	S- ratio [-]
I (Top)	150	10	30	50
II	300	3	4.5	10
III (Bottom)	450	1	1	1

Figure 46 shows a schematic N-S profile of the 3-D model at 17°45'E. The Kalahari and the Karoo units are delineated as wedges with increasing thickness towards the north. To implement these units in the numerical FEFLOW model, the layers I and II had to be subdivided. The Kalahari and the Karoo unit could then be assigned to the top layer Ia and layer Ib, respectively. A rectangular trough represents the Mulden Group that reaches only down to layer IIa and is underlain by the Hüttenberg unit at greater depths. The downward dip of the formations in the south and the upward dip in the Tsumeb area are considered by a step-wise shift of the units from the top to the bottom layer.

4.2.2.3 Model input data

Apart from the geological, structural and lithological characterisation of the study area and the geophysical interpretation, the following additional input data were utilised for the construction of the 3-D model:

- ❑ rainfall data
- ❑ recharge factors
- ❑ groundwater abstraction rates
- ❑ groundwater level measurements
- ❑ aquifer parameters (T , S)

Rainfall data

Rainfall data over a 30-year period are available at 29 rainfall gauges within or in the vicinity of the model area (see Chapter 3.2.1). The Kriging regionalisation method was used to calculate the regional rainfall distribution for the steady state calibration.

The rainfall records at Tsumeb cover a period of 90 years. A statistical analysis was performed using these records in order to define realistic average and below-average rainfall conditions for the prediction models. The average annual rainfall at Tsumeb amounts to 527 mm/a with a standard deviation of 180 mm.

The frequency of a certain rainfall amount can be best fitted to a log Pearson-3 distribution (Figure 42). All single rainfall data lie well within the narrow 95% confidence interval. From the cumulative density function CDF, the probability p that the annual rainfall falls below a certain threshold rainfall can be calculated. The return period of a threshold rainfall is then given by $1/p$. The specific probability plot depicted in Figure 42 can be used to determine p and $1/p$ for any given threshold rainfall. The probability that the annual rainfall is less than 400 mm, e.g., is 0.25 or 25%. The return period is hence 4 years, i.e. statistically, the rainfall will not exceed 400 mm every 4th year.

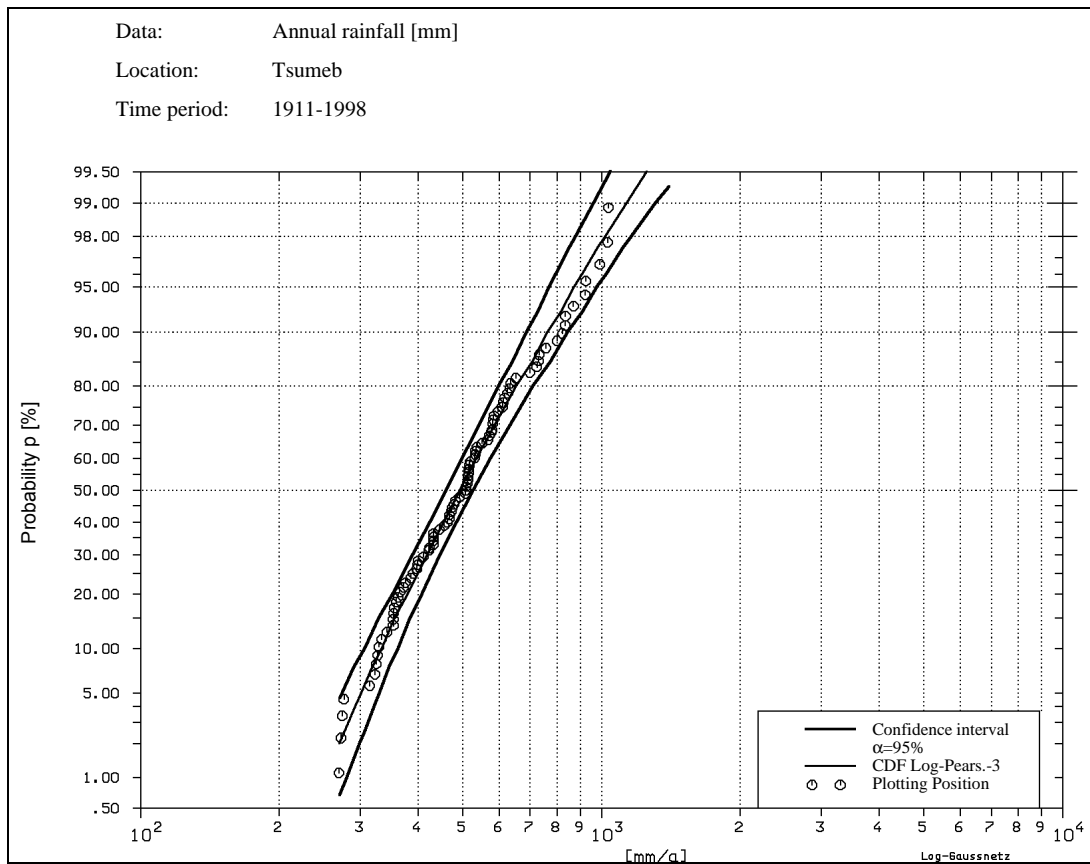


Figure 42 Cumulative density function (CDF) fitted to the annual rainfall at Tsumeb

Recharge factors

The recharge R over a time period or time step was calculated from the rainfall P as follows:

$$R = RF \cdot P, \text{ with}$$

RF recharge factor, i.e. percentage of rainfall that contributes to the groundwater recharge.

It was assumed that the recharge factors are highest for areas where the dolomite outcrops (Figure 43). This area encounters comparatively high rainfall that can more easily infiltrate through fractures within the exposed rock. The recharge factors are expected to be lowest for the Kalahari and the Mulden Group due to high evapotranspiration losses. The Kalahari and the Mulden Group are characterised by a complete vegetation cover and low permeable layers consisting of calcrete, silt and clays. Water ponds commonly observed after rainfall events indicate slow infiltration in these areas. Intermediate recharge factors are assumed for the so-called transition zone, which comprises dolomites covered usually by less than 20 m of pedogenetic deposits. Possible values of recharge in the OML and the Kalahari have been discussed in detail in Chapter 3.2.2.

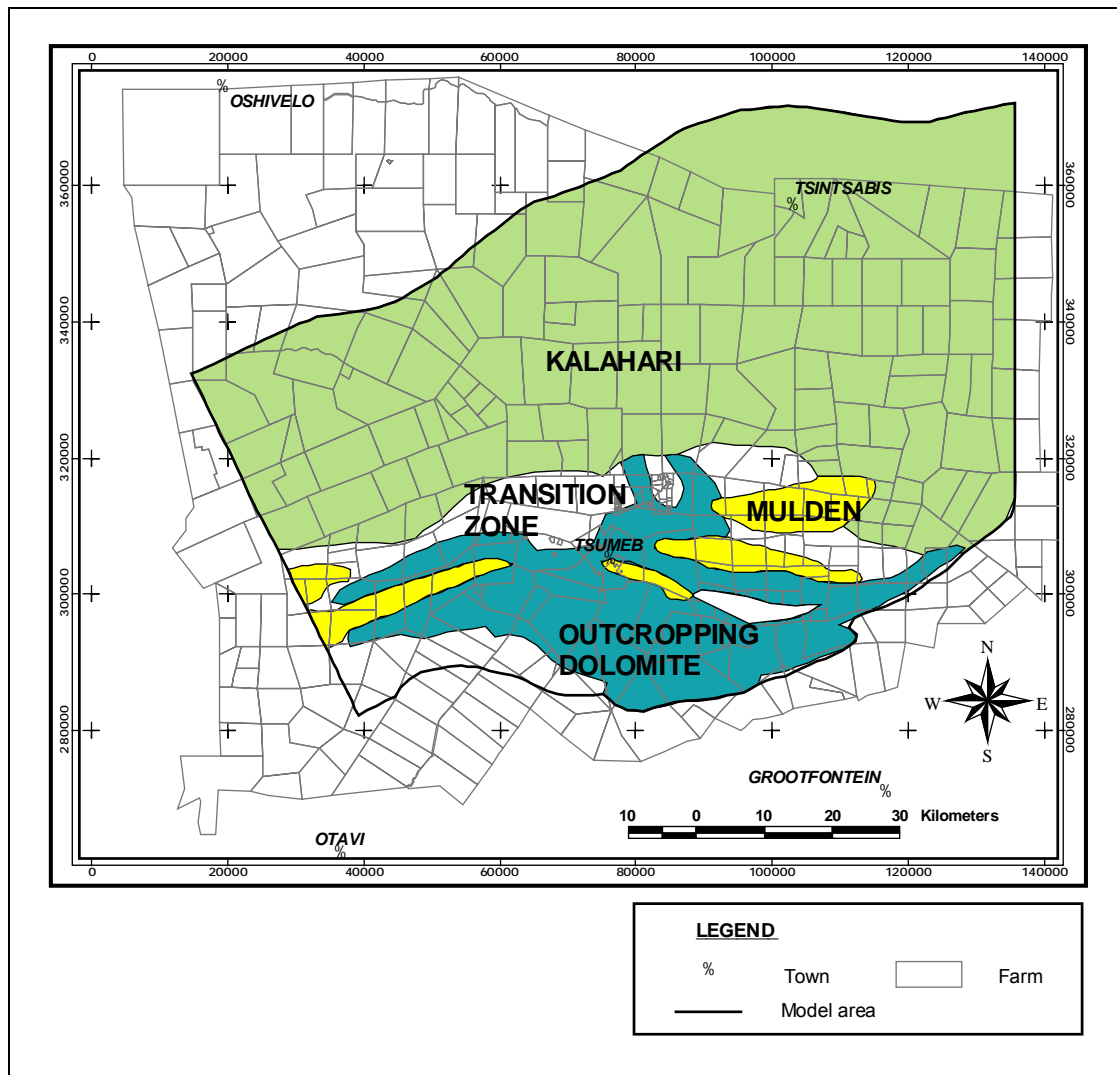


Figure 43 Recharge areas

Groundwater abstraction rates

The groundwater abstraction considered in the model includes the supply to the municipalities of Tsumeb and Tsintsabis amounting to $3.6 \text{ Mm}^3/\text{a}$ and the abstraction for irrigation purposes amounting to $5.7 \text{ Mm}^3/\text{a}$. The main irrigation areas comprise the farms *Mannheim*, *Ludwigshafen* and *Heidelberg* north-east of Tsumeb and the Lake Guinas area (see Figure 10). Unfortunately, no records of the abstraction history over the last 30 years, which corresponds to the calibration period, were obtainable.

The domestic and stock water consumption amounts to approximately $3 \text{ Mm}^3/\text{a}$. Since the abstraction for domestic and stock watering purposes are almost evenly distributed over the whole study area, it was not necessary to incorporate additional abstraction sites in the model. Instead, this abstraction was combined with the recharge as one groundwater balance component.

Groundwater level measurements

The steady state and the transient calibration of the model is based on the following groundwater level measurements (see Figure 44):

- ❑ Measurements of high accuracy (± 1 cm) taken in Oct. 2000 and in June/July 2001 at 61 wells that were levelled using differential GPS.
- ❑ 1415 less accurate measurements (approximately ± 5 m) obtained from the existing groundwater database.

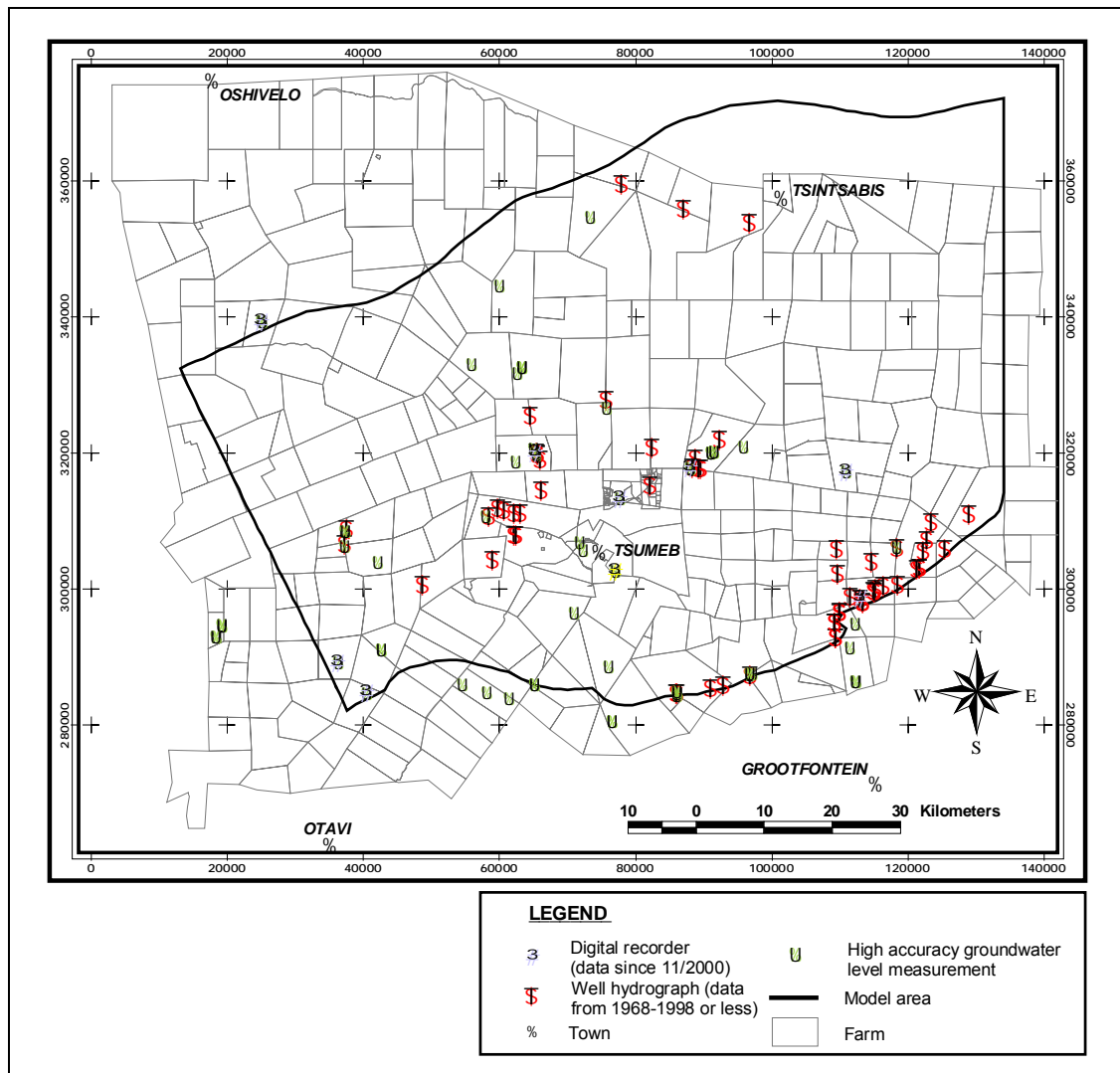


Figure 44 Location of the calibration wells and hydrographs

- ❑ Hydrograph series at 20 wells covering 10 to 30 consecutive years over the calibration period 1968-1998; The accuracy of the water level measurements is approximately ± 1 cm; The elevation of the wells, however, is less precise (approximately ± 5 m) since it had to be determined from the topographic map 1:50,000.
- ❑ Continuous groundwater level measurements at 8 wells of high accuracy (± 1 cm) recorded by the recently installed data loggers covering the period from Nov. 2000 to June 2001.

Aquifer parameters

The available transmissivities and storage coefficients were obtained from the hydraulic test analysis described in Chapter 4.2.1.

4.2.2.4 Steady state calibration

The transmissivities of the geohydraulic units and the recharge factors of the different recharge areas are modified within the frame of the values obtained from the literature and the field studies. The aim of the steady state calibration is to minimise the differences between the simulated and the measured groundwater levels.

The model adequately simulates the **general groundwater flow** from south to north. The hydraulic head exceeds 1400 m a.s.l. in the Otavi Mountainland and declines to 1140 m a.s.l. towards the northern boundary of the model area. The Kalahari is characterised by generally low hydraulic gradients. Steep hydraulic gradients occur as an east-west trending belt in the Otavi Mountain Land, where the infiltration rates are highest and the northward flow is hampered by the low permeable sediments within the Chuos and the Maieberg Formation. In the south-east, a striking eastward-directed flow towards the Abenab mines can be observed. The eastward flow is caused by the hydraulic separation of the area located south of the Maieberg Formation from the rest of the investigation area.

Figure 45 shows that the differences between **the simulated and the measured groundwater levels** are generally less than 10 m. In areas with low hydraulic gradients such as the Kalahari, the deviation is usually less than 5 m. These differences are acceptable considering the size of the model area and the heterogeneity of the rock formations. Comparatively high deviations are encountered in the south-east on the farm *Abenab* and in the south-west on the farm *Finsterbergen*. These farms fall within the zone of the steep hydraulic gradients, which is slightly shifted towards the south in the model. The large deviations at the farms *Hurisib* and *Varianto* are due to perched or locally stratified aquifers. The small-scaled lateral and vertical local heterogeneity of the rock formations has to be accounted for by smaller-scaled models.

The calibration resulted in a **recharge factor** of 4% (21 mm/a) for the dolomite outcrops. A recharge factor of 1.6% (8 mm/a) was allocated to the transition zone. A very small recharge factor of 0.33% (1.7 mm/a) had to be applied to the Kalahari and the Mulden unit. Higher recharge factors in these areas would result in a denser spacing of the contour lines towards the northern part of the model area, which field measurements, however, could not confirm. The low recharge within the Kalahari was somewhat surprising but reflects the high evapotranspiration losses in this area. Consequently, a large portion of the groundwater in the Kalahari Aquifer must originate from the dolomitic areas further to the south.

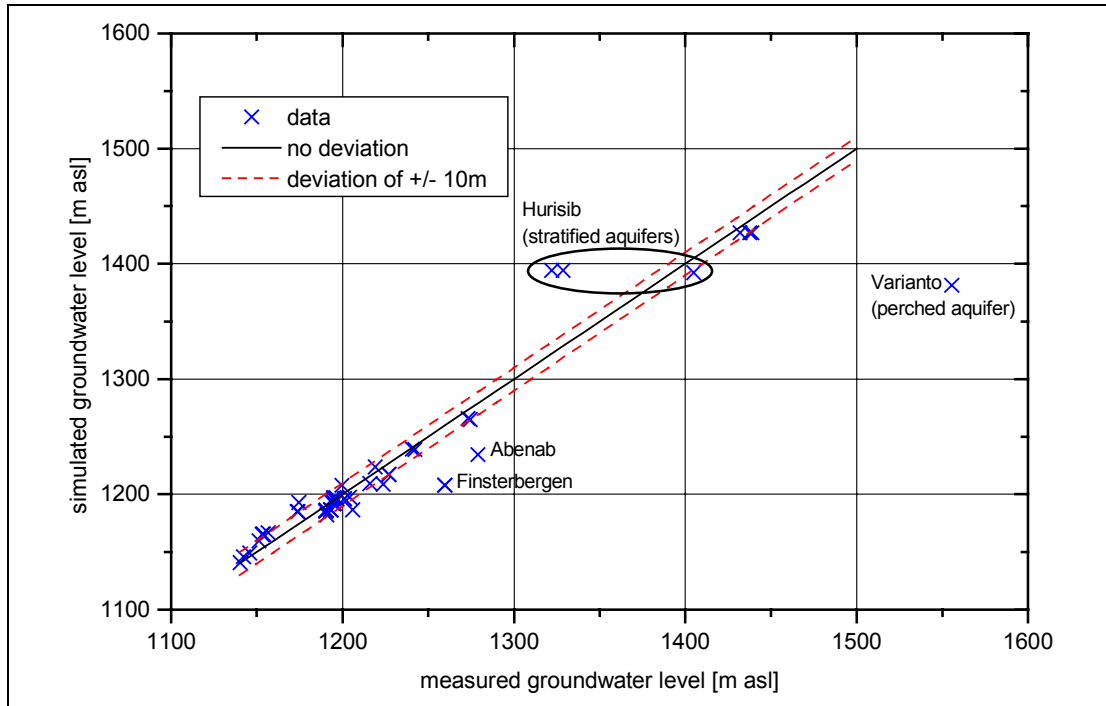


Figure 45 Correlation between simulated and measured groundwater levels at wells with high-accuracy measurements

Table 17 shows the good conformity between the **calibrated transmissivity values**, which were allocated to the seven geohydraulic units, and the hydraulic test results. Figure 46 schematically depicts how the T -values are vertically distributed. The total transmissivity, i.e. the sum of the T -values from the top to the bottom layer, is highest in the central study area around Tsumeb, Lake Otjikoto and Lake Guinas, but decreases towards the North where the lower permeable Kalahari and Karoo sediments bury the dolomites. Only in the very north of the model area the total transmissivity increases again due to higher transmissivity assigned to the coarser-grained Kalahari sediments.

Table 17 Comparison of the hydraulic parameters obtained from the hydraulic tests and the model calibration for the top layer I (depth 0 - 150 m)

Geohydraulic Unit (Formation)	T [m ² /d]		S [-]	
	Hydraulic tests	Model	Hydraulic tests	Model
1 (Nosib)	0.2 – 3	2	$1 \cdot 10^{-3}$	$1 \cdot 10^{-4}$
2 (Abenab)	14 – 466	160	$6 \cdot 10^{-4}$	$1 \cdot 10^{-3}$
3a (Chuosi/ Maieberg)	2.4	3	$3 \cdot 10^{-6} - 8 \cdot 10^{-4}$	$3 \cdot 10^{-4}$
3b (Elandshoek)	15 – 1260 (\bar{T}^*) = 309)	300	$7 \cdot 10^{-4}$	$1 \cdot 10^{-3}$
3c (Hüttenberg)	121 – 5565 (\bar{T}^*) = 1725)	700	$4 \cdot 10^{-4} - 2 \cdot 10^{-2}$	$1.5 \cdot 10^{-3}$
3d (Disturbed Zone)	0.4	2	-	$1 \cdot 10^{-4}$
4 (Mulden)	3.2	4	$3 \cdot 10^{-4}$	$1 \cdot 10^{-4}$
5 (Karoo)	1 – 11	15	$7 \cdot 10^{-5} - 3 \cdot 10^{-3}$	$1 \cdot 10^{-4}$
6 (Kalahari)	434 – 10367	50 – 500	-	$1 \cdot 10^{-4}$
7 (Dyke systems)	1065 – 1260	800	$4 \cdot 10^{-4} - 2 \cdot 10^{-2}$	$1 \cdot 10^{-3}$

*) average transmissivity (arithmetic mean)

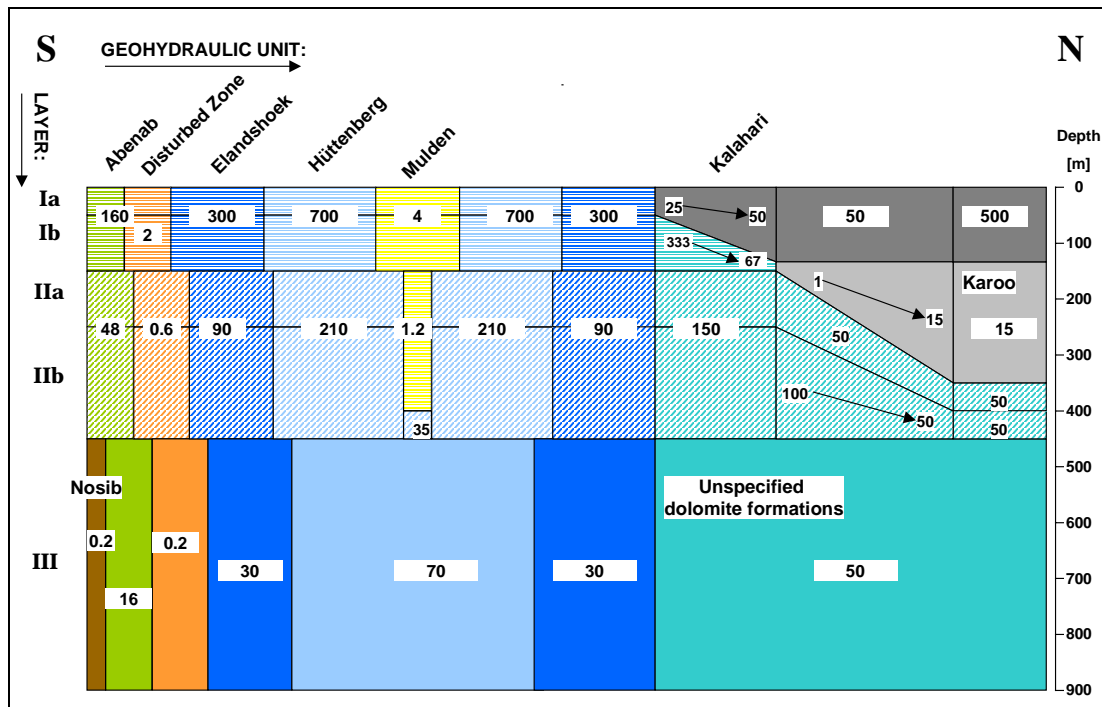


Figure 46 Schematic N-S profile. Inserted numbers give the transmissivity [m^2/d] of each geohydraulic unit and layer. Note that the horizontal distance is not to scale.

Figure 47 depicts the **groundwater balance** of the model area. The total recharge due to infiltration of precipitation amounts to $42.6 \text{ Mm}^3/\text{a}$. The inflow into the model from the south-east amounts to $0.8 \text{ Mm}^3/\text{a}$. Together with a total abstraction rate of $12.3 \text{ Mm}^3/\text{a}$, this leads to a net outflow of $31.1 \text{ Mm}^3/\text{a}$. Since these figures describe steady state conditions, the net balance between input and outflow equals zero.

4.2.2.5 Transient calibration

The transient calibration is performed in order to assess the influence of varying hydrological conditions on the groundwater flow regime. It uses the transmissivity values and the recharge factors obtained from the steady-state calibration, i.e. neither the T -values nor the recharge factors were further modified. From the transient calibration, which includes both the long-term monitoring period from 1968 to 1998 and the short-term monitoring period (daily measurements) from November 2000 to June 2001, the storage characteristics of the aquifer systems can be determined.

The calibrated water levels from 1970 to 1998 at the Lake Otjikoto area are shown in Figure 48 as an example. The 3-D groundwater model adequately simulates the increase in the groundwater table during the mid-1970's following several years of above-average rainfall at the lake hydrograph (WW39427) and the surrounding well WW10317. The overall rise in the groundwater table from 1970 to 1980, however, is underestimated by 2-3 m. This indicates that the abstraction rate during the 1970's was not as high as presumed in the model, or that the recharge factors are higher in years with exceptionally high rainfall.

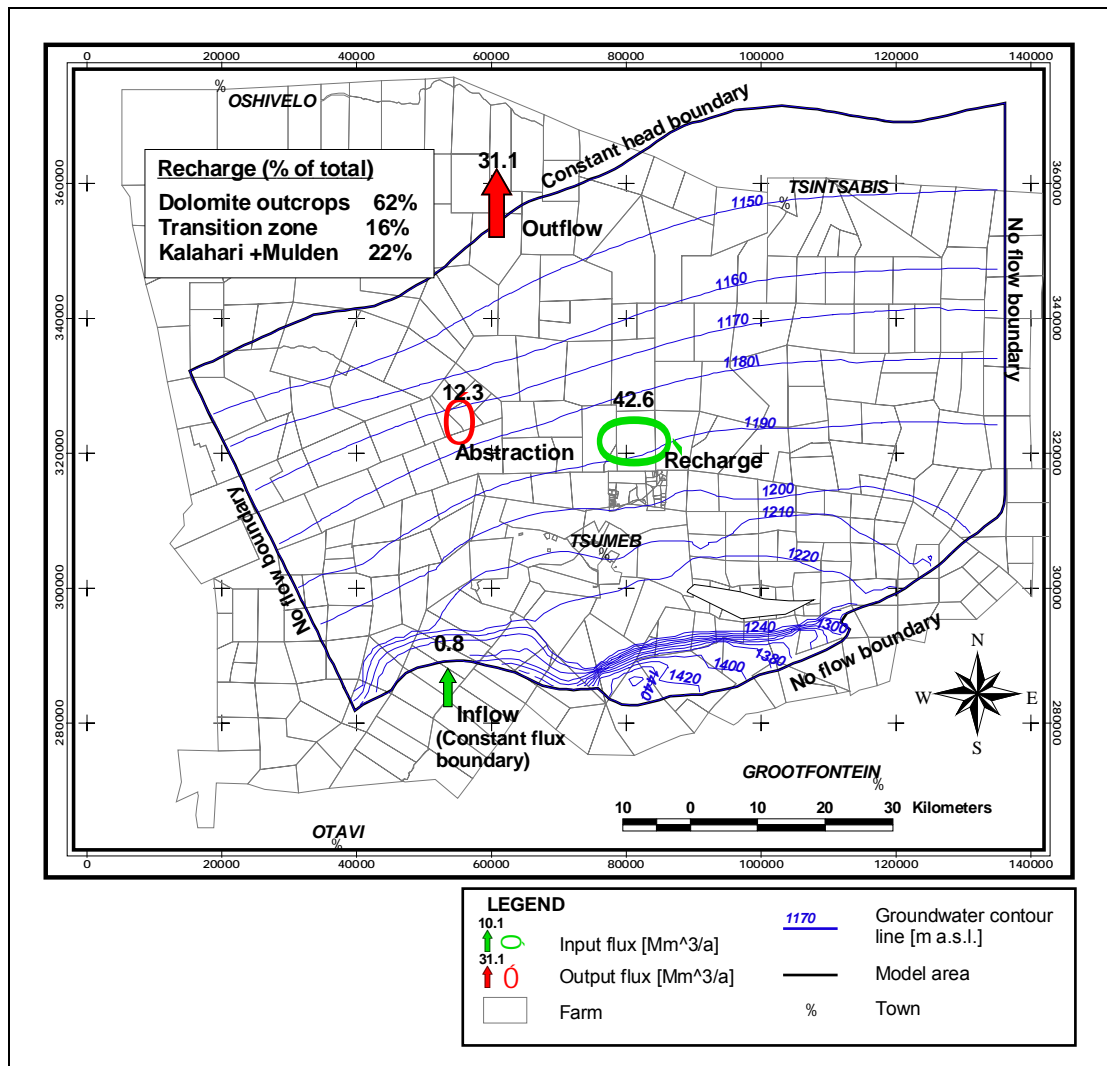


Figure 47 Groundwater balance and levels as obtained from the steady state model calibration

The transient calibration yielded plausible **storage coefficients** which could be verified by the pumping test analyses despite the uncertainties regarding the climatological input, recharge data and the former abstraction rates (Table 17). One should bear in mind when assessing the modelling results that only very few storage coefficients are available for some of the rock formations. Therefore, the modelling provides the most representative storage coefficients at the current state of knowledge.

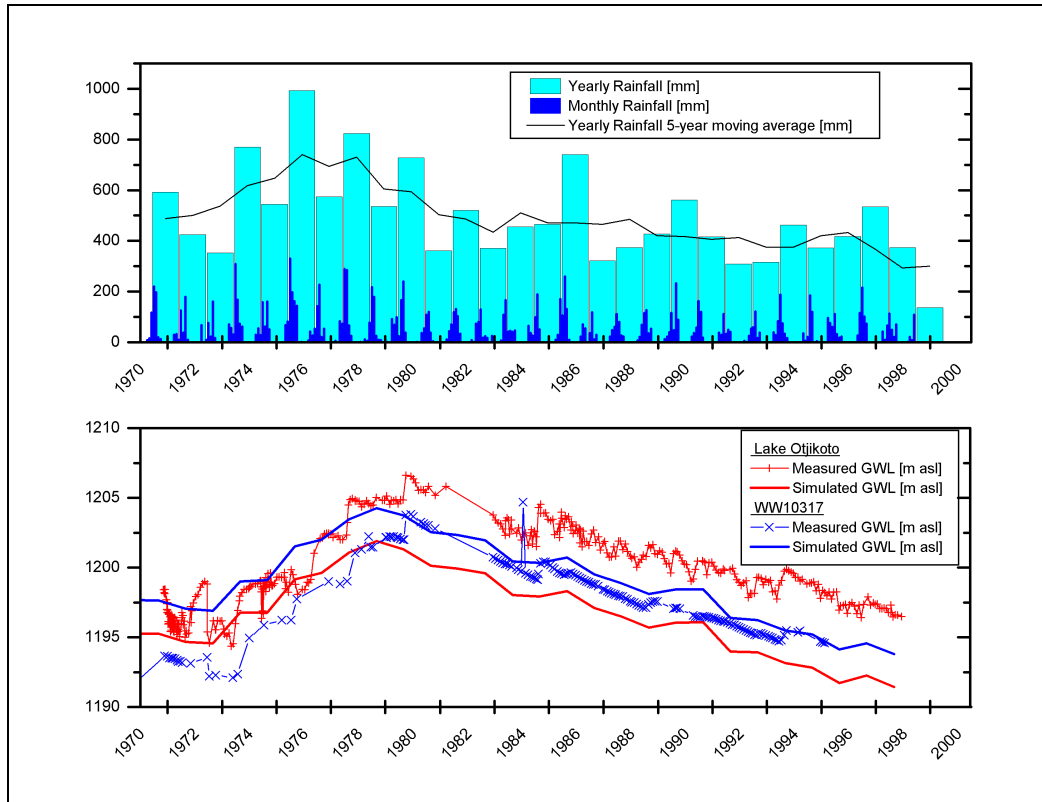


Figure 48 Rainfall data at Tsumeb and Transient calibration of groundwater levels (GWL) at Lake Otjikoto and WW10317

4.2.3 Assessing the groundwater potential

The calibration results prove that the regional numerical 3-D model enables simulation of the long-term development of groundwater resources under the influence of varying climatological conditions in a representative way. The model can hence be used as a reliable tool to calculate the effects on the groundwater balance and the regional flow pattern for different abstraction scenarios and predefined climatological conditions.

It clearly follows from the element size that a regional model can not be applied to small-scale problems, such as the precise simulation of a well field abstraction and the resulting drawdown at observation wells nearby. On the other hand, only a regional model enables regional identification of hydraulic interactions and helps to understand how varying climatic conditions influences them.

Scenario calculations with varying abstraction schemes were performed to match the available groundwater resources with future demands. Average rainfall conditions and below average rainfall conditions were considered for the predictions. The below-average rainfall was defined by a return period of 4 years and amounts to 400 mm/a compared to 527 mm/a for average conditions at Tsumeb. The overall objectives of the prediction models are

1. to quantify the permissible safe yield of the investigation area,
2. to assess the available amount of contingency groundwater that can be directed towards the Central Area of Namibia

3. to provide essential information for the environmental assessment,
4. to provide guidelines for the improvement of criteria used to allocate permits for groundwater abstraction and
5. to establish an aquifer management plan.

Scenario 1 considers an annual increase in the groundwater abstraction for irrigation and municipal purposes of 0.75% per annum over the next 15 years. This increase is considered inevitable due to the expected population growth and the intensification of agricultural use. This scenario is therefore considered to represent the **status quo**. The total abstraction in the model area will increase from 12.3 to 13.3 Mm³/a over 15 years. No further increase in the abstraction is allowed after this period (Figure 49).

A series of simulation runs were carried out to determine the **permissible safe yield** of the model area. The determination of the permissible safe yield should prevent **overexploitation** of the aquifer systems. Overexploitation takes place in (Custodio, 2002: 254)

“the situation in which, for some years, average aquifer abstraction rate is greater than, or close to the average recharge rate.”

This definition, however, does not consider the possible negative influence of an additional regional drawdown. The permissible safe yield was therefore defined as

“the abstraction rate at which the regional drawdown will stabilise at a level (below the current levels) that is acceptable with respect to both environmental concerns and eventual compensation payments to farmers.”

It was suggested that such a drawdown should not exceed 15 m regionally. The scenarios considered the Lake Guinas in the west, the Tsumeb area in the central parts and the Abenab area in the south-east as possible future abstraction sites.

The **scenario 2** presented in this report was defined from several model runs with varying abstraction rates and fulfils the definition of the permissible safe yield. It considers an additional abstraction of 2 Mm³/a from the Tsumeb Mine as well as from Lake Guinas over and above the annual increase of 0.75%/a defined above. The total abstraction in the model area hence increases from 16.3 Mm³/a at the beginning of the simulation to 17.3 Mm³/a over 15 years.

Scenario 3 was established in order to investigate the impact of a **bulk contingency abstraction** on the Tsumeb Aquifers. It defines the amount of water that can be supplied to the Central Area of Namibia to meet a temporary demand during drought conditions. The following criterion is set up for the determination of the bulk contingency abstraction: After a period of not more than three subsequent years the contingency bulk abstraction will be interrupted and the groundwater levels are allowed to recover. The recovery period must be sufficiently long so that the groundwater levels and the stored groundwater volume reach levels, which are equal to or higher than in scenario 2. This guarantees that the bulk contingency abstraction will not exceed the long-term sustainable management. Compared to scenario 1, an additional abstraction of 8 Mm³/a from the Tsumeb Mine and of 4 Mm³/a from the Abenab Mine for three subsequent years is implemented in scenario 3. After this period, the recovery from the contingency bulk abstraction is ascertained. This abstraction scheme is repeated for two additional 15-year

cycles, i.e. for the years 16 - 30 and 31 - 45. According to scenario 3, 36 Mm³/a can be supplied to the Central Area every 15 years (Figure 49).

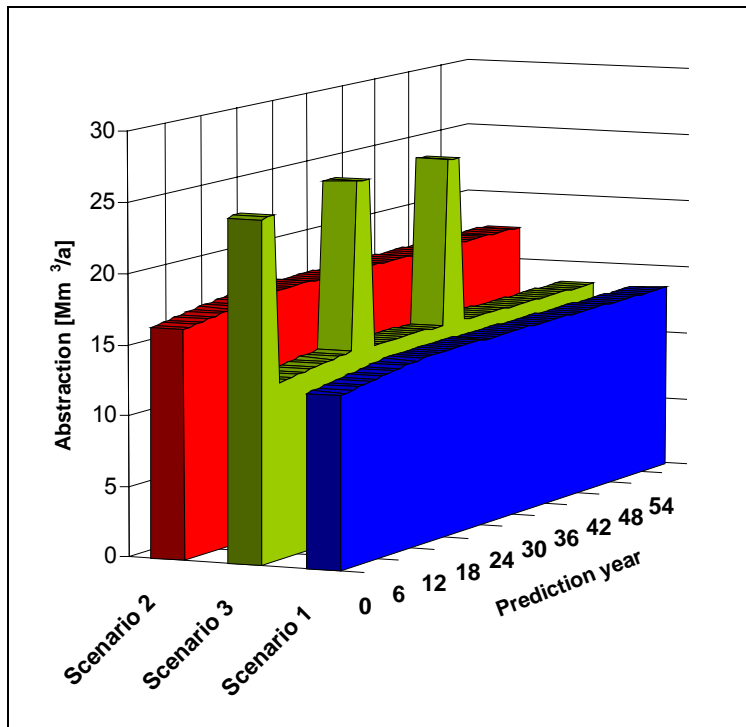


Figure 49 Total abstraction according to scenarios

Figure 50 shows the predicted drawdown at four characteristic sites. Lake Otjikoto is situated within the Dolomite Aquifer about 20 km north-west of Tsumeb. Since the lake is a major tourist attraction and was declared a National Document, any changes in the current water levels will be of specific environmental concern. The well WW39974 also falls within the Dolomite Aquifer but is situated about 25 km east of Tsumeb (see Figure 37). The current irrigation is concentrated in an area 10 to 15 km north-east of Tsumeb. The dolomites are covered with a relative thin sequence of Kalahari sediments. *Heidelberg* is one of the most important irrigation farms within this area. Lowering of the groundwater table within the irrigation area may result in high compensation payments being incurred. The well WW27269 is situated within the Abenab Subgroup approximately 15 km west of the Abenab Mine shafts.

The graphs for scenarios 1 and 2 show that the groundwater levels stabilise after a period of at least 60 years from the start of the supplementary abstraction. This time lag is due to the storage properties of the Tsumeb aquifers. It can be assumed that the complete recovery from an over-exploitation of the aquifers will take a similarly long period.

The gradual increase in abstraction over the next 15 years leads to a regional drawdown in the range of 2 to 4 m (Scenario 1). The additional abstraction of 4 Mm³/a as defined by scenario 2 creates a regional lowering in the groundwater table of between 9 and 12 m. After 60 years the water levels will only slightly decline further. Only in the vicinity of the chosen abstraction sites, a considerably larger drawdown is to be expected. The expected fall in the groundwater levels is considered permissible if an appropriate monitoring scheme, which covers the whole study area, is implemented. The contingency

bulk abstraction (scenario 3) leads to a maximum drawdown of 7 m at Lake Otjikoto, 11 m at WW39972 and 14 m at *Heidelberg*. The maximum drawdown at WW27269 reaches 35 m. The fact that the water bearing Abenab Subgroup is bounded by low permeable rock formations explains the large drawdown constricted to the south-eastern part of the model area. The higher drawdown created by the bulk contingency abstraction, however, recovers to a large extent over the 12 year recovery period. The residual drawdown after each 15-year cycle (difference in drawdown compared to scenario 1) is generally less than 5 m. The graphs also show that the groundwater levels lie above the levels simulated by scenario 2 at the end of each 15-year cycle.

Figure 51 shows the change of the stored groundwater volume for each of the three scenarios. The flattening out of the curves once more indicates that steady-state conditions are reached after about 60 years for scenarios 1 and 2. The depletion of the aquifer systems amounts to 20 Mm³ for scenario 1 and to, say 90 Mm³ for scenario 2. With scenario 3, the depletion only temporarily exceeds the values of scenario 2, a fact that justifies the proposed bulk abstraction of 36 Mm³ every 15 years.

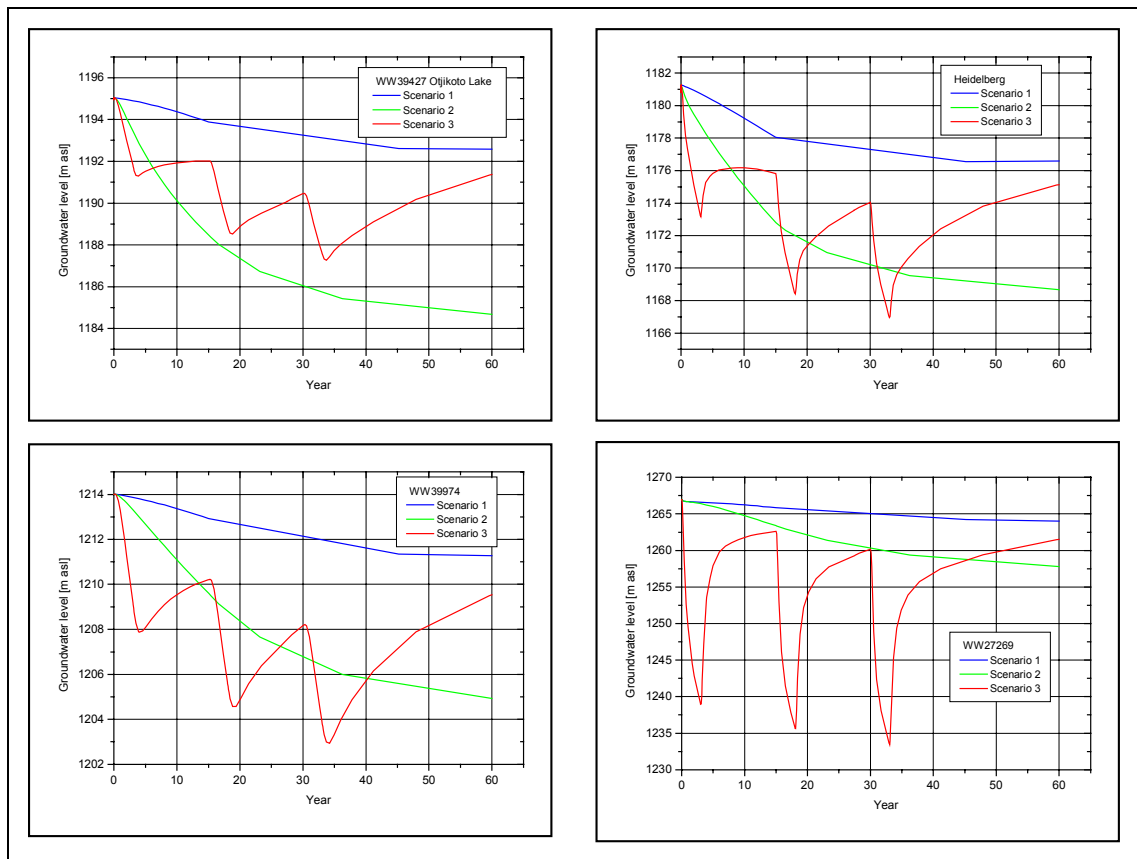


Figure 50 Predicted decline of groundwater levels in the model area

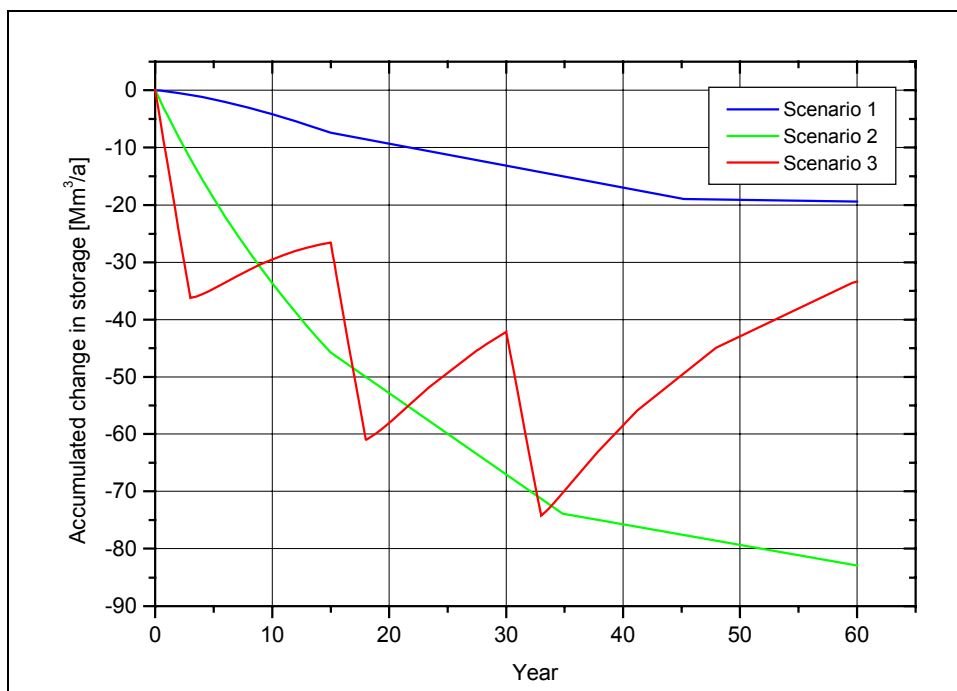


Figure 51 Predicted accumulated change in groundwater storage

5 Summary and discussion

The regional study of the Lindau fractured rock test site and the Tsumeb Aquifers included different geohydraulic methods. The synthesis of the results from different geohydraulic methods has been an important aspect and constitutes the principal methodological approach of this thesis. The results were combined in a hydraulic characterisation of the fractured rock aquifer systems. The investigations resulted in the development of conceptual hydrogeological models and focussed on the assessment of the hydraulic impact of dominant fault and dyke structures, the regional distribution of different aquifer systems and the quantification of groundwater flow parameters and fluxes. The importance and necessity of incorporating results of interdisciplinary studies in the process of developing such a conceptual model, in particular geological exploration and geophysical investigations, has been emphasised throughout this work.

The investigations at the Lindau test site focussed essentially on the assessment and evolution of geohydraulic methods whereas the TGWS is to be considered as the first comprehensive hydrogeological investigation of the Tsumeb Aquifers with the primary objective to determine the groundwater potential of this area.

5.1 Assessment of potential and constraints of geohydraulic methods

Well hydrograph recession analysis

The WHRA was first proposed by Shevenell (1996) as a tool to analyse well hydrographs in a Karst environment. Contrary to streamflow recession analysis, for which the base level of the recession is that of zero flow, the base level or “*static water level*” for the WHRA can not be readily quantified. The accuracy of the WHRA, however, strongly relies on the proper determination of the static water level. Two different methods for the evaluation of hydrographs described in the streamflow recession literature help to overcome this problem, and were introduced into the WHRA in this thesis. Furthermore, the WHRA was applied for the first time to groundwater level data from wells in granitic rock. Applying these new evaluation methods, the static water level is no longer needed for the determination of the recession coefficient and MRT. In fact, it was shown how the methods could be extended in order to calculate the static water levels, once the recession coefficient has been determined from the analysis.

Most of the well hydrographs in the fractured granite unquestionably followed a recession of exponential type decay. Contrary to hydrographs in karstified dolomite for which recession limbs after storm events are analysed, the seasonal decline of the water levels over the drier summer period were evaluated due to the low permeability of the granite. The WHRA applied at the Lindau test site proved to be an effective tool to obtain a regional distribution of the MRT and the permeability from groundwater level data. A small MRT corresponds to a high permeability. The analysis was also useful for the determination of static water levels, which are likely to correspond with the elevation of spring outlets. Since the springs occur as diffuse outlets along the steep slopes and are generally covered by debris at Lindau, the WHRA can provide a better indication of the actual elevation than can topographic maps.

Problems encountered during the analysis included the high sensitivity of the results with respect to noise in the data, and the dependence of the results on subjective judgements. Furthermore, the analysis is tedious and time consuming. The variations in the results between individual years may sometimes exceed 100% although they are mostly smaller. Years with recurrent recharge events during the recession period will most likely cause a higher uncertainty. The main advantage of the availability of long time series is therefore that they offer a greater chance that the records contain years with little summer precipitation.

Hydraulic tests

Hydraulic tests are a classical and indisputable tool to determine aquifer parameters and to characterise aquifer systems. Hydraulic tests were therefore implemented in both aquifer studies. The catchment drainage experiment at Lindau, however, differed from the conventional pump and slug tests carried out in the Tsumeb Aquifers by its extraordinary duration of almost 14 months. In both study areas, fracture-type flow pattern prevailed. The thesis includes a state of the art of analysis methods for hydraulic tests in fractured rock and highlights the importance of diagnostic plots for the detection of the aquifer type and the choice of the correct analysis method.

It is well known that single well tests can at best provide an estimate of the storage coefficient. As an important result of this study, single well tests proved also to be inappropriate for the determination of the transmissivity, if very high well losses occurred. The design of aquifer tests should therefore always consider observation wells. The main shortcomings of hydraulic tests are the high costs and the limited representativeness of the aquifer parameters gained in a heterogeneous media. Additional results from a WHRA may help to close this gap. It was expected that the catchment drainage experiment would provide parameters that are more representative as it incorporated a huge volume of rock due to the large test duration. However, the occurrence of episodic recharge events and a seasonal trend impeded an accurate analysis of the complete data set.

Hydrochemical analysis

The analysis of hydrochemical data was used to distinguish groundwater of different provenance at Lindau. Barium and fluoride provided a signal to water originating from the ore dyke. Time series of the chemical composition of the groundwater at the production well could be used to detect a vertical flow component within the dyke zone, originating from the shallow aquifer within the *Berglesand* and the weathered upper zone of the granite. Analysis of isotope data gathered during the TGWS provided recharge estimates that could be used for the validation of the groundwater model. The isotope and hydrochemical data generally sustain the conceptual hydrogeological model, which defined the Otavi Mountainland with its outcrops of dolomite as the primary source of direct groundwater recharge.

Tracer tests

Tracer tests can be applied in small-scaled investigations to determine flow paths, flow velocities and transport mechanisms within different aquifer systems. At Lindau, three

different zones with very characteristic flow velocities and transit times could be distinguished from tracer tests. These systems comprised the ore dyke, the porphyritic dyke and the undisturbed granite. Tracer tests are often unsuccessful in sparsely fractured rock for distances of, say, more than 100 m due to large transit times and poor recovery caused by mixing processes within the borehole and incomplete or retarded release of the tracer into the formation. Therefore, tracer tests are of limited use for large investigation areas in fractured rock such as in the TGWS.

The estimation of transport parameters from tracer tests is generally difficult, since the transport models inevitably have to simplify the real flow and transport mechanism in fractured rock. Experience from tracer tests carried out at Lindau over the past decade show that the assumption of an instantaneous injection is difficult to fulfil in fractured rock. Recent analytical solutions, which consider a retarded release of the tracer into the formation, were applied for the analysis of the TBC's and resulted in good curve fits. The quality of the curve fit by itself, however, does not justify the model selection. It was shown in the analysis of the TBC's that several models, though based on different assumptions with respect to flow and injection type, can generate similar TBC's. The tailing of the TBC's can be attributed to dispersive mixing, matrix diffusion or the retarded tracer release. It is hence obvious that the gained flow and transport parameters differ largely from each other depending on the model that has been applied. It followed by comparison of the results from the different analytical models that the flow velocities will be underestimated whilst the effect of dispersion or diffusion will be overvalued if the retarded tracer release is not considered in the analysis.

As a conclusion, a better insight on the transport processes and refined injection methods, by which the release of the tracer plume is better controlled, are urgently needed. The latter will be of particular importance for small-scale experiments for which the transit time is small compared to the release time of the tracer. Laboratory tests to determine diffusion and sorption coefficients, multi-tracer tests incorporating tracers with different diffusion and sorption characteristics as well as the use of double packers and measuring devices, which monitor the tracer release into the formation, are therefore encouraged.

Groundwater modelling

Groundwater modelling on the one hand integrates the results of geohydraulic, geophysical and geological methods. On the other hand, the success of groundwater modelling largely depends on the information provided from these independent studies. The 3-D Tsumeb groundwater model has been established as a tool for the assessment of the groundwater resources of the Tsumeb Aquifers and for the development of an aquifer management plan. In order to cope with the complex vertical and lateral succession of stratigraphic units and the occurrence of dyke and fault zones it was necessary to apply a specific modelling scheme. This conceptual approach comprised the development of 2-D horizontal and 2-D vertical models prior to the development of the comprehensive 3-D model. The 2-D models helped to improve the understanding of the complex hydrogeological situation in a stepwise manner and to set up a revised and optimised program for additional field investigations. It was furthermore essential to group stratigraphic units laterally into geohydraulic units and vertically into layers according to their hydrogeological behaviour. An equivalent continuum model proved to be adequate

due to the large size of the study area. Two major lineaments, the Tsumeb dyke and a NW-SE striking open tensional fault, were considered as individual geohydraulic units.

5.2 Characteristics of fractured aquifers with dominant fault/dyke zones

Two fractured aquifer systems, the Lindau fractured rock test site in the Southern Black Forest, Germany, and the Tsumeb Aquifers in the semi-arid region of northern Namibia have been described and the differences of the climate, lithology and scale of the investigations have been outlined. What links the two study areas is the low primary porosity of the host rock consisting of granite (Lindau) and fractured dolomite (Tsumeb Aquifers). The low primary porosity is the reason why groundwater flow in both areas is mainly restricted to fractures, which are only abundant along dykes, faults and contact zones.

For both sites, the role of intrusive dykes and faults as conduits of groundwater flow could be demonstrated. In the north of the Tsumeb study area, these structures cut through the Karoo and locally connect the Kalahari Aquifers with the Dolomite Aquifers. The impact of these structures on the flow regimes is otherwise less striking compared to the ore dyke at Lindau. The reason for this is the much larger size of the Tsumeb study area. For smaller-scaled investigations, such as the development of a well field, the significance of these structures with respect to groundwater flow would largely increase. The importance of structures and the way they need to be considered in a conceptual hydrogeological model hence depends on both the scale and objectives of a study.

The assessment of the regional distribution of permeability was an integral part of both hydrogeological studies. Besides the lateral differences in permeability, which can be attributed to changes in the stratigraphy, vertical zones could be defined in both areas according to the degree of weathering and fracturing. The lateral and vertical distribution of the zones with varying permeability could be delineated by a synthesis of results from geological interpretation, hydraulic tests, tracer experiments and the WHRA. The groundwater flow in the Tsumeb Aquifers occurs essentially within the upper 150 m b.g.s. Groundwater flow at depths below 900 m was considered negligible. The groundwater circulation at Lindau seems to be largely associated with the weathering zone in the upper 30 m of the rock. Along the ore dyke, however, the groundwater circulation reaches a depth of at least 100 m. Efficient deep circulation is hence restricted to the dyke zones. The seepage of rainfall is facilitated by the fact that the ore dyke outcrops at various places throughout the study area. Surface-related water can access the dyke either by direct recharge or, more important by impounding interflow originating from higher elevated areas and perpendicular to the dyke axis. The highly permeable and interconnected sections of the ore dyke, and its contact zone, therefore carry mostly recent groundwater and form an efficient subterranean drainage system.

As a result of the comprehensive hydrogeological study of the Tsumeb Aquifers, the regional groundwater potential of the area could be quantified for the first time. The groundwater model revealed the eminent importance of the dolomitic outcrops of the Otavi Mountainland for the replenishment of the groundwater resources. The direct recharge within the area of outcrops amounts to 4% of the MAR or 21 mm/a according to the modelling results and is hence 12 times higher than the direct recharge in the Kalahari foreland. With 21% of the direct recharge, the Kalahari nevertheless constitutes

an important component of the overall water balance due to the huge area covered by Kalahari sediments. A total amount of 18 Mm³/a was defined as the sustainable yield of the area of which 12 Mm³/a are currently used. 36 Mm³/a could be supplied additionally to the Central Area over a period of three years as a bulk contingency abstraction, but the aquifers must be allowed to recover over a period of at least 12 years after such an abstraction. It must be stressed that the values presented assume that average hydraulic conditions persist. Scenario calculations using below-average rainfall indicate that the groundwater resources may soon be exhausted if drought conditions prevail. Any increase in groundwater abstraction must therefore be controlled by a continuous monitoring of regional rainfall and groundwater levels.

5.3 Suggestions for future investigations

To conclude the following suggestions and challenges for future work at the two test sites should be mentioned:

Considering the available hydraulic information and the elaborated characterisation of the hydraulic system comprising the intrusive dykes and host rock, the next step at Lindau should be the establishing of a groundwater model. An equivalent continuum approach as applied to the Tsumeb Aquifers seems acceptable, but considering the smaller size of the study area and the dominant hydraulic influence of the ore dyke *Hermann*, a hybrid model is more promising. The hybrid model would consider the host rock as an equivalent continuum. The dyke system would have to be incorporated as a distinct set of fractures and the flow within the structures is expressed by means of the Cubic Law. In order to consider the vertical succession of *Berglesand*, weathered granite and sparsely fractured granite, the model should be composed of layers of which each corresponds to a zone with distinct permeability and MRT.

Further investigations required include the assessment of the hydraulic characteristic of the porphyritic dykes. The interaction between these dykes with the ore dyke, in particular, needs to be quantified. Another major issue is the ratio of surface runoff to interflow and groundwater discharge. This requires an assessment of the water balance, which includes surface water and groundwater flow components. The area is characterised by high amounts of rainfall and little winter evaporation, which indicates a high recharge and a fast turnover time for groundwater. A large amount of the precipitation, however, will presumably not reach the deep aquifer except in the vicinity of the dykes, but will flow into the rivers by surface runoff or interflow within the unconsolidated rocks along the steep slopes. An estimation of the recharge, i.e. the amount of water that percolates into the deep aquifer, is therefore needed prior to the development of the groundwater model. A first estimate for the rainfall that directly enters the dyke could be obtained from hydrochemical data using a simple mixing calculation. Accordingly, the amount of young water after strong rainfall events yields a percentage of 25-40% of the total flow within the dyke.

The conceptual hydrogeological model of the Tsumeb Aquifers is considered appropriate in principle. However, the available data for the transient calibration was comparatively sparse. The calibration should be refined after approximately five years using groundwater level data obtained from the recently installed data loggers. Furthermore, an improved recharge assessment is encouraged as direct recharge forms the predominant inflow into the system. The recharge should be investigated on an event-scale rather

than on the basis of annual averages. The investigation could lead to the definition of threshold values, which need to be exceeded before direct recharge occurs. Finally, a more precise assessment of the vertical interaction between the Kalahari Aquifer and the Dolomite Aquifer in the north of the study area, where the intercalated Karoo separates the two systems, is required. This could give further insight into the recharge of the Oshivelo Artesian Aquifer (OAA) which adjoins the study area at its northern margin. The OAA is a valuable groundwater resource and it is believed that it is largely fed by the Dolomite Aquifer underneath. It might therefore be of interest to include the OAA into the groundwater model.

6 References

- Ackermann, G. (1981): Geologie und Hydrogeologie der Sperrenstelle des geplanten Stausees Lindau (Hotzenwald).- unpublished M.Sc. Thesis at the Department of Applied Geology, University of Karlsruhe, 216 pp; Karlsruhe.
- Agarwal, R.G., Al-Hussainy, R. & H.J. Ramey JR (1970): An investigation of well-bore storage and skin-effect in unsteady liquid flow: 1. Analytical treatment.- *AIME* **249**: 279-290, New York.
- Annau, R., Bender, S. & S. Wohnlich (eds.) (1998): Hard rock hydrogeology of the Bohemian Massif.- (3rd International Workshop, Windischeschenbach, Germany, Oct. 1998) *Münchner Geologische Hefte Reihe B, Band 8*: 184 pp; München.
- Armbruster, V. (2002): Grundwasserneubildung in Baden-Württemberg.- *Freiburger Schriften zur Hydrologie*, Band **17** [in preparation]; Institut für Hydrologie; Freiburg.
- Bardenhagen, I. (1999): Skin localization at wells drilled in a vertical fault zone.- *Ground Water* **37(5)**: 764-769.
- Bardenhagen, I. (2000): Groundwater reservoir characterization based on pumping test curve diagnosis in fractured formation.- in: Silio et al. (eds.): Groundwater: Past achievements and future challenges (Proc. of IAH Congress held in Cape Town, Nov. 26- Dec. 01, 2000): 81-86; Rotterdam (Balkema).
- Bardenhagen, I. (2002): Test pumping analysis for fractured aquifers – TPA.- www.geocities.com.bardenhageni.
- Barenblatt, G.E., Zheltov, I.P. & I.N. Kochina (1960): Basic concepts in the theory of seepage of homogeneous liquids in fissured rocks.- *J. of Applied Mathematics* **24(5)**: 1286-1303.
- Barnes, B.S. (1940): Discussion of analysis of runoff characteristics.- *Trans. ASCE* **105**: 106.
- Bäumle, R. (2001): Berücksichtigung zeitlich verzögerter Tracereingaben bei der Ermittlung der Stofftransportkennwerte aus Markierungsversuchen im Raum Stuttgart.- *Schriftenreihe des Amtes für Umweltschutz*, Heft **1/2001**, Kombinierte Markierungsversuche im Mineralwasseraquifer Oberer Muschelkalk, Stadtgebiet Stuttgart: 81-101 ; Stuttgart.
- Bäumle, R., Einsiedl, F., Hötzl, H., Käss, W., Witthüser, K. & S. Wohnlich (2001): Comparative tracer studies in a high permeable fault zone at the Lindau fractured rock test site (SW Germany).- in: Association of Tracer Hydrology (ATH) (eds.): Tracer studies in the unsaturated zone and Groundwater (Investigations 1996-2001). (8th International Symposium on Water Tracing, Munich 2001); *Beiträge zur Hydrogeologie* **52/2001**:136- 145; Graz.
- Bäumle, R., Himmelsbach, T. & R. Bufler (2001): Conceptual hydrogeological models to assess the groundwater resources of the heterogeneous fractured aquifers at Tsumeb (Northern Namibia).- in: Seiler, K.-P. & S. Wohnlich (eds.): New approaches characterizing groundwater flow (Proc. of the XXXI IAH Congress held in Munich, Sep. 10-14, 2001), Vol. **1**: 245-249; Lisse, The Netherlands (Balkema).

- Bäumle, R., Hötzl, H. & K. Witthüser (2000): Flow pattern and transport behaviour of granitic rock intersected by a highly permeable fault zone.- in: Tracers and Modelling in hydrogeology (Proc. Of the TraM' 2000 Conference held at Liege, Belgium, May 2000); *IAHS Publ.* No. **262**, 2000: 283-288; Wallingford, UK (IAHS Press).
- Beekmann, H.E., Gieske, A. & E.T. Selaolo (1996): GRES: Groundwater Recharge Studies in Botswana 1987-1996.- *Botswana J. of Earth Science* Vol. **III**: 1-7.
- BGR - Bundesanstalt für Geowissenschaften und Rohstoffe (1995): Otavi Mountain Land: Considerations on the use of groundwater abstracted from mines for drinking water purposes.- Technical Cooperation Project no. 89.2034.0, German-Namibian Groundwater Exploration Project - Reports on geohydraulic investigations and groundwater modelling (unpublished); Vol. **E-V**: 7 pp, BGR file no. 2367/95, BGR archive no. 113827, DWA file no. 12/1/1/16/1; Windhoek.
- BGR - Bundesanstalt für Geowissenschaften und Rohstoffe (1996): Otavi Mountain Land data base evaluation and conceptual model KARST_01 and KARST_02.- Technical Cooperation Project no. 89.2034.0, German-Namibian Groundwater Exploration Project - Reports on geohydraulic investigations and groundwater modelling (unpublished); Vol. **E-II**: 38 pp, BGR file no. 11267/95, BGR archive no. 113752, DWA file no. 12/1/1/16/1; Windhoek.
- BGR - Bundesanstalt für Geowissenschaften und Rohstoffe (1997a): Hydrogeology and isotope hydrology of the Otavi Mountainland and its surroundings (KARST_01 and KARST_02).- (unpublished); Vol. **D-III**: 65 pp.; BGR file no. 10793/97, BGR archive no. 116049; Windhoek.
- Biehler, D. (1995): Kluftgrundwässer im kristallinen Grindgebirge des Schwarzwaldes - Ergebnisse von Untersuchungen in Stollen.- *Tübinger Geowissenschaftliche Arbeiten*, **C22**, 1995; 103 pp; Tübingen.
- Boehmer, W.K. & J. Boonstra (1987): Analysis of drawdown in the country rock of composite dike aquifers.- *J. of Hydrology* **35** (1987): 199-214; Amsterdam (Elsevier).
- Boonstra, J. & W.K. Boehmer (1986): Analysis of data from aquifer and well tests in intrusive dikes.- *J. of Hydrology* **88** (1986): 301-317; Amsterdam (Elsevier).
- Bourdet, D. & A.C. Gringarten (1980): Determination of fissure volume and block size in fractured reservoirs by type -curve analysis.- Paper **SPE 9293** presented at the SPE-AIME 55th Annual fall technical conference and exhibition, Sept. 21-24 1980; Dallas.
- Bouwer, H. & R.C. Rice (1976): A slug test method for determining hydraulic conductivity of unconfined aquifers with completely or partially penetrating wells.- *Water Resources Research* **12** (3): 423-428.
- Bredenkamp, D.B., Botha, L.J., van Tonder, G.J. & H.J. van Rensburg (1995): Manual on quantitative estimation of groundwater recharge and aquifer storativity.- 363 pp.; Water Research Commission; Pretoria.
- Brouyère, S. (2000): Modelling the injection of a tracer in a well: a new mathematical approach.- in: Dassargues, A. (ed.): Tracers and Modelling in hydrogeology (Proc. of the TraM' 2000 Conference held at Liège, Belgium, May 2000); *IAHS Publ.* **262**: 25-31; Wallingford, UK (IAHS Press).

- Buch, M.W. & C. Trippner (1997): Overview of the geological and geomorphological evolution of the Etosha region, northern Namibia.- *MADOQUIA* 1997, **20(1)**: 65-74.
- Bufler, R., Ambs, P., Himmelsbach, T., Tordiffe, E. & R. Bäumle (2000): Preliminary assessment of the groundwater potential of the Tsumeb aquifers in northern Namibia.- in: Silio et al. (eds.): Groundwater: Past achievements and future challenges (Proc. of IAH Congress held in Cape Town, Nov. 26- Dec. 01, 2000): 103-107; Rotterdam (Balkema).
- Carrera, J. & G.R. Walter (1989): Convergent flow tracer tests: numerical study of design parameters and sensitivity.- unpublished manuscript, 35 pp.
- Christelis, G. & W. Struckmeier (eds.) (2001): Groundwater in Namibia – an explanation to the hydrogeological map.- 128 pp.; Windhoek (John Meinert Printing).
- Cinco, L.H. & F.V. Samaniego (1981): Transient pressure analysis for fractured wells.- *J. of Petroleum Technology* (Sep. 1981): 1749-1766.
- Cinco, L.H. & F.V. Samaniego (1981): Transient pressure analysis for fractured wells.- *J. of Petroleum Technology* (Sep. 1981): 1749-1766.
- Cinco, L.H., Samaniego, F.V. & N.A. Dominguez (1978): Transient pressure behaviour for a well with a finite conductivity vertical fracture.- *Society of Petroleum Engineers J.* (Aug. 1978): 253 – 264.
- Cinco, L.H., Samaniego, F.V. & N.A. Dominguez (1978): Transient pressure behaviour for a well with a finite conductivity vertical fracture.- *Society of Petroleum Engineers J.* (Aug. 1978): 253 – 264.
- Cooper, H.H. and C.E. Jacob (1946): A generalized graphical method for evaluating formation constants and summarizing well field history.- *American Geophysical Union Trans.* **27**: 526-534.
- Cooper, H.H., J.D. Bredehoeft and S.S. Papadopoulos (1967): Response of a finite-diameter well to an instantaneous charge of water.- *Water Resources Research* **3(1)**: 263-269.
- Custodio, E. (2002): Aquifer overexploitation: what does it mean?- *Hydrogeology J.* (2002) **10**: 254-277; Heidelberg (Springer).
- Dachroth W. & Sonntag C. (1983): Grundwasserneubildung und Isotopendatierung in Südwestafrika/Namibia.- *Zeitschrift deutsche geologische Gesellschaft* **134**: 1013-1041.
- De Swaan, O.A. (1976): Analytical solutions for determining natural fractured reservoir properties by well testing.- *Society of Petroleum Engineers J.* (June 1976): 117-122.
- Dierkes, K. (1996): Hydrogeographical and hydrogeological investigations at the southern margin of the Etosha-Kalahari Basin/Namibia.- unpublished M.Sc. thesis, University of Regensburg; 115 pp.; Regensburg.
- DWA - Republic of Namibia - Ministry of Agriculture, Water and Rural Development/ Department of Water Affairs (1990): An evaluation of the groundwater resources of the Grootfontein Karst area.- Unpublished report by K.G. Seeger; file no. 12/5/1/3; 187 pp.; Windhoek.

- DWA - Republic of Namibia - Ministry of Agriculture, Water and Rural Development/ Department of Water Affairs (1992): Criteria to be considered when allocating permits for the abstraction of groundwater for irrigation purposes in the Karst area.- Unpublished report by N. Hoad, file no. 12/1/B; 14 pp.; Windhoek.
- DWA - Republic of Namibia - Ministry of Agriculture, Water and Rural Development/ Department of Water Affairs (1993): An overview of groundwater investigations in the Tsumeb and Oshivelo areas.- Unpublished report, File No.: 12/4/2/18, 65 pp., Windhoek.
- DWA - Republic of Namibia - Ministry of Agriculture, Water and Rural Development/ Department of Water Affairs (2002): Groundwater investigations of the Oshivelo Artesian Aquifer: Results of the 2002 drilling and pump test campaign.- Unpublished report by R. Bäumle, File No.: 12/1/2/16/7, 9 pp., Windhoek.
- DWA - Republic of Namibia - Ministry of Agriculture, Water and Rural Development/ Department of Water Affairs, Kreditanstalt für Wiederaufbau & GKW/Bicon (2000): Phase 1 Final Report.- Unpublished report, File no. 12/1/2/16/2, 109 pp, Windhoek.
- DWA - Republic of Namibia - Ministry of Agriculture, Water and Rural Development/ Department of Water Affairs, Kreditanstalt für Wiederaufbau & GKW/Bicon (2002a): Tsumeb Groundwater Study Final Report Vol. 1 – Main Report.- Unpublished report, File no. 12/1/2/16/2 [in preparation], Windhoek.
- DWA - Republic of Namibia - Ministry of Agriculture, Water and Rural Development/ Department of Water Affairs, Kreditanstalt für Wiederaufbau & GKW/Bicon (2002b): Tsumeb Groundwater Study Final Report Vol. 2 –Geological / geophysical surveys and borehole siting.- Unpublished report, File no. 12/1/2/16/2 [in preparation], Windhoek.
- DWA - Republic of Namibia - Ministry of Agriculture, Water and Rural Development/ Department of Water Affairs, Kreditanstalt für Wiederaufbau & GKW/Bicon (2002c): Tsumeb Groundwater Study Final Report Vol. 4 – Hydraulic test evaluation.- Unpublished report, File no. 12/1/2/16/2 [in preparation], Windhoek.
- DWA - Republic of Namibia - Ministry of Agriculture, Water and Rural Development/ Department of Water Affairs, Kreditanstalt für Wiederaufbau & GKW/Bicon (2002d): Tsumeb Groundwater Study Final Report Vol. 6 – Report of the groundwater quality and isotope hydrology/recharge.- Unpublished report File no. 12/1/2/16/2 [in preparation], Windhoek.
- DWA - Republic of Namibia - Ministry of Agriculture, Water and Rural Development/ Department of Water Affairs, Kreditanstalt für Wiederaufbau & GKW/Bicon (2002e): Tsumeb Groundwater Study Final Report Vol. 7 – Groundwater modelling.- Unpublished report, File no. 12/1/2/16/2 [in preparation], Windhoek.
- Edmunds, W.M. & B.T. Verhagen (2000): Isotope based assessment of groundwater renewal: An international study of the unsaturated zone.- in: Silio et al. (eds): Groundwater: Past achievements and future challenges (Proc. of IAH Congress held in Cape Town, Nov. 26- Dec. 01, 2000): 487-492; Rotterdam (Balkema).
- Einsiedl, F., Langhals, H., Maloszewski, P., Witthüser, K. & S. Wohnlich (2000): Application of two new fluorescent dyes and fluorescent particles in a horizontal and vertical fracture.- in: Dassargues, A. (ed.): Tracers and Modelling in hydrogeology

- (Proc. of the TraM' 2000 Conference held at Liege, Belgium, May 2000); *IAHS Publ.* 262: 175 - 179; Wallingford, UK (IAHS Press).
- Emmermann, R. (1977): A petrogenetic model for the origin and evolution of the Hercynian granite series of the Schwarzwald.- *Neues Jahrbuch Mineralogischer Abhandlungen* **128** (3): 219-253; Stuttgart.
- FH-DGG - Deutsche Geologische Gesellschaft - Fachsektion Hydrogeologie (ed.) (1999): Hydrogeologische Modelle - Ein Leitfaden für Auftraggeber, Ingenieurbüros und Fachbehörden.- Hydrogeologische Beiträge der FH-DGG; *Schriftenreihe der Deutschen Geologischen Gesellschaft*, Heft **10**: 36 pp.; Hannover.
- Geyh, M.A. (1995): Geochronologische Aspekte paläohydrologischer und paläoklimatischer Befunde in Namibia. *Geomethodica* **20**: 75-99.
- Gieske, A., Selaolo, E.T. & H.E. Beekman (1995): Application of tracers in arid zone hydrology.- (Proc. of the Vienna Symposium, Aug. 1994), *IAHS Publ.* no. **232** (1995): 373-382; Wallingford, UK (IAHS Press).
- Goldscheider, N., Hötzl, H., Käss, W., Kottke, K. & W. Ufrecht (2000): Kombinierte Markierungsversuche zur Klärung der hydrogeologischen Verhältnisse und Abschätzung des Gefährdungspotentials im Mineralwasseraquifer Oberer Muschelkalk.- *Schriftenreihe des Amtes für Umweltschutz*, Heft **1/2001** Kombinierte Markierungsversuche im Mineralwasseraquifer Oberer Muschelkalk, Stadtgebiet Stuttgart:7-80 ; Stuttgart.
- Gringarten, A.C. & H.J. Ramey JR (1974): Unsteady state pressure distributions created by a well with a single horizontal fracture, partial penetration or restricted entry.- *Society of Petroleum Engineers J.* (Aug. 1974): 413-426.
- Gringarten, A.C. & P.A. Witherspoon (1972): A method of analyzing pump test data from fractured aquifers.- in: Int. Soc. Rock Mechanics and Int. Ass. Eng. Geol., (Proc. Symposium Rock Mechanics, Stuttgart), Vol. **3-B**: 1-9; Stuttgart.
- Gringarten, A.C. (1984): Interpretation of tests in fissured and multi-layered reservoirs with double-porosity behaviour: theory and practice.- *J. of Petroleum Technology* (Apr. 1984): 549-564.
- Gringarten, A.C., Ramey JR., H.J. & R. Raghavan (1974): Unsteady state pressure distributions created by a well with a single infinite-conductivity vertical fracture.- *Society of Petroleum Engineers J.* (Aug. 1974): 347-360.
- Grisack, G.E. & J.F. Pickens (1981): An analytical solution for solute transport through fractured media with matrix diffusion.- *J. of Hydrology*, **52**: 47-57.
- Guvanasen, V. & V.M. Guvanasen (1987): An approximate semianalytical solution for tracer injection tests in a confined aquifer with radially converging flow field and finite volume of tracer and chase fluid.- *Water Resources Research* **23**(8): 1607-1619; Washington, DC.
- Hantush, M.S. and C.E. Jacob (1955): Non-steady radial flow in an infinite leaky aquifer.- *American Geophysical Union Trans.* 36: 95-100.

- Hedberg, R.M. (1979): Stratigraphy of the Ovamboland Basin, South West Africa.- *Bull. Precambria Res. Unit*, University Cape Town, **24**: 325 pp. (Ph.D. Thesis Univ. Cape Town).
- Hekel, U. (1994): Hydrogeologische Erkundung toniger Festgesteine am Beispiel des Opalinustons (Unteres Aalenium).- *Tübinger Geowissenschaftliche Arbeiten (TGA)*, Reihe **C** No. **18**, 1994; 170 pp.; Tübingen.
- Himmelsbach, T. (1993): Untersuchungen zum Wasser- und Stofftransportverhalten von Störungszonen im Grundgebirge (Albtalgranit, Südschwarzwald).- *Schriften Angewandte Geologie Karlsruhe* **23**, 238 pp.; Karlsruhe.
- Himmelsbach, T., Hötzl, H. & P. Maloszewski (1998): Solute transport processes in a highly permeable fault zone of Lindau fractured rock test site (Germany).- *Ground Water* **36** (5): 792-800.
- Himmelsbach, T., Hötzl, H., Käss, W., Leibundgut, C., Maloszewski, P., Meyer, T., Moser, H., Rajner, V.; Rank, D.; Stichler, W., Trimborn, P., Veulliet, E. (1992): Transport phenomena in different aquifers (Investigations 1987-1992). Fractured Rock test site Lindau/Southern Black Forest (Germany).- *Steirische Beiträge zur Hydrogeologie* **43**: 159-228; Graz.
- Hoehn, E. (1979): Hydrogeologische Untersuchungen im Gebiet westlich von Frick (Aargauer Tafeljura).- *Beiträge zur Geologie der Schweiz - Hydrogeologie* No. **26**; 55 pp.; Bern (Kümmerly + Frei).
- Hötzl, H. & K. Witthüser (1999): Methoden für die Beschreibung der Grundwasserbeschaffenheit. - DVWK Schriften, **125**; Bonn (Wirtschafts- und Verlagsgesellschaft Gas und Wasser).
- Huyser, D.J. (1982): Chemiese kwaliteit van de grondwater in Suidwes-Afrika/Namibie.- Nasionale Instituut vir Waternavorsing / Departement van Waterwese Suidwes-Afrika/Namibie; Vol. 1, Voorkepelende verslag: 144 pp., Pretoria, Windhoek (Kontrakverslag).
- JICA - Japan International Cooperation Agency (2002): The study on the groundwater potential evaluation and management plan in Southeast Kalahari (Stampriet) Artesian Basin in the Republic of Namibia.- Final Report – Main Report (March 2002); unpublished; 175 pp; Windhoek.
- Kaselow, A. (1999): Analytische und numerische Modellierung von Stofftransport in einer Störungszone im Grundgebirge.- unpublished M.Sc. Thesis at the Department of Applied Geology, University of Karlsruhe, 132 pp.; Karlsruhe.
- Klock, H., Külls, C. & P. Udluft (2001): Estimating recharge values using hydrochemical and geological data: a case study from the semiarid Kalahari catchment of northern Namibia.- Impact of human activity on groundwater dynamics (Proc. of a symposium held during the 6th IAHS Scientific Association at Maastricht, The Netherlands, July 2001); *IAHS Publ.* No. **269** (2001): 25-31; Wallingford, UK (IAHS Press).
- Kolditz, O. (1997): Flow, contaminant and heat transport in fractured rock.- 263 pp.; Berlin, Stuttgart (Borntraeger).

- Kruseman, G.P. & N.A. de Ridder (1991): Analysis and evaluation of pumping test data.- International Institute for Land Reclamation and Improvement Publ. no. **47**, 2nd ed., 377 pp.; Wageningen.
- Külls, C. (1999): Groundwater of the North-Western Kalahari, Namibia –Estimation of recharge and quantification of the flow systems.- Doctorate Thesis at the Julius-Maximilian University of Würzburg, 165 pp; Würzburg.
- Landesvermessungsamt Baden-Württemberg (1998): Rasterdaten digitaler Karten - Ausschnitt aus der Topografischen Karte im Maßstab 1:25 000, Blatt Nr. TK 8214.- Stuttgart.
- Langguth, H.-R. & R. Voigt (1980): Hydrogeologische Methoden.- 486 pp; Berlin, Heidelberg (Springer).
- Lenda, A. & A. Zuber (1970): Tracer dispersion in groundwater experiments.- in: Isotope techniques in groundwater hydrology Vol. **II**; **IAEA-SM-129/7**: 619 - 641; Vienna.
- Linsley, R.K., Kohler, M.A. & J.L.H. Paulhus (1982): Hydrograph analysis.- In: Hydrology for Engineers, pp. 223-233; New York (McGraw-Hill).
- Lloyd J.W. & J.A. Heathcote (1985): Natural inorganic hydrochemistry in relation to groundwater.- 296 pp.; Oxford UK (Oxford University Press).
- Lombaard, A.F.; Günzel, A.; Innes, J. & T.L. Krüger (1986): The Tsumeb Lead-Copper-Zinc-Silver deposit, South West Africa/Namibia.- in: Anhaeusser, C.R. & Maske, S. (eds.) (1986): Mineral Deposits of Southern Africa, pp. 1761-1787; Johannesburg (Geological Society South Africa).
- Mainardy, H. (1999): Groundwater recharge in the transition zone between rock ridges and the cover of loose Kalahari sediments.- HU-Forschungsergebnisse aus dem Bereich Hydrogeologie und Umwelt **17**, 145 pp.; Würzburg.
- Maloszewski, P. & A. Zuber (1985): On the theory of tracer experiments in fissured rocks with a porous matrix.- *J. of Hydrology* **79**: 333-358; Amsterdam (Elsevier).
- Maloszewski, P. & A. Zuber (1990): Mathematical Modeling of Tracer Behaviour in Short-Term Experiments in Fissured Rocks.- *Water Resources Research* **26 (7)** : 1517-1528.
- Maloszewski, P. (1994): Mathematical modelling of tracer experiments in fissured aquifers.- *Freiburger Schriften zur Hydrologie*, Band **2**, 107 pp.; Freiburg i. Br.
- Marchant, J.W. (1980): Hydrogeochemical exploration at Tsumeb.- Unpublished PhD Thesis, Cape Town University, 222 pp; Cape Town.
- Mavor, M.J. & H. Cinco (1989): Transient pressure behaviour of naturally fractured rock reservoirs.- paper SPE 7977 presented at the 1979 SPE California Regional Meeting, Ventura, April 18-20, 1979.
- Metz, E. (1980): Geologische Landeskunde des Hotzenwaldes.- 1116 pp; Lahr, Germany (Schauenburg).
- Miller, R. McG. (1992): Stratigraphy.- in: Republic of Namibia - Ministry of Mines and Energy, Geological Survey: The Mineral resources of Namibia: pp. 1.2 (1-34); Windhoek.

- Miller, R. McG. (1997): The Owambo Basin of northern Namibia.- in: Selley, R.C. (ed.): African basins. Sedimentary basins of the world; Chapter 11, pp 237-268; Amsterdam (Elsevier).
- Miller, R.McG. (1983): The Pan-African Damara Orogen of South West Africa/Namibia.- in: R.McG. Miller (ed.): Evolution of the Damara Orogen; Special Publ. of the Geological Society of South Africa no. **11**: 431-515; Johannesburg.
- Moench, A.F. (1984): Double-porosity models for a fissured groundwater reservoir with fracture skin.- *Water Resources Research* **20**(7): 831-846.
- Moench, A.F. (1995): Convergent radial dispersion in a double-porosity aquifer with fracture skin: Analytical solution and application to a field experiment in fractured chalk.- *Water Resources Research* **31**(8): 1823-1835.
- Moser, H. (1979): Isotopenhydrologische Methoden zur Bestimmung der Durchlässigkeit des Grundwasserleiters.- *Mitteilungen der Ingenieur- und Hydrogeologie* **9**: 79-103.
- Moser, H. & Rauert, W. (1982): Lehrbuch der Hydrogeologie Band **8**: Isotopenmethoden in der Hydrologie.- 400 pp.; Berlin, Stuttgart (Bornträger).
- Mühr, B. (2002): www.klimadiagramme.de.- Based on data of DWD - Deutscher Wetterdienst.
- National Research Council (1996): Rock fractures and fluid flow - Contemporary understanding and applications.- 525 pp; Washington, D.C (National Academy Press.)
- Novakowski, K. (1992): An evaluation of boundary conditions for one-dimensional solute transport, 1. Mathematical development.- *Water Resources Research* **28**(9): 2399-2410.
- Ogata, A. & R.B. Banks (1961): A solution of the differential equation of longitudinal dispersion in porous media.- in: Geological Survey professional paper **411-A**: Fluid movement in earth materials, 7 pp.; Washington, D.C. (United States Government Printing Office).
- Parkhurst D.L (1996): User's guide to PHREEQC - A computer program for speciation, reaction path, advective transport, and inverse geochemical calculation.- U.S. Geological Survey Water Resource Investigations 95-4227.
- Pohl, A. (1994): Quantifizierung der hydraulischen Eigenschaften eines hochdurchlässigen Ganges im Grundgebirge mittels Lauf- und Tracerversuchen (Albtalgranit, Südschwarzwald).- unpublished M.Sc. Thesis at the Department of Applied Geology, University of Karlsruhe (part II), 77 pp.; Karlsruhe.
- Pointet, T. (ed.) (1997): Hard rock hydrosystems.- (Proc. of Rabat Symposium S2, May 1997), *IAHR Publ. No.* **241**; 168 pp.; Wallingford, UK (IAHS Press).
- Powers, J. G. & L. Shevenell (2000): Transmissivity Estimates from Well Hydrographs in Karst and Fractured Aquifers.- *Ground Water*, **38**(3): 361-369.
- Reinert, F. (1999): Durchführung und Auswertung von Pump- und Markierungsversuchen in stark heterogenen Kluftgrundwasserleitern (Albtalgranit, Südschwarzwald).- unpublished M.Sc. Thesis at the Department of Applied Geology, University of Karlsruhe, (part 2); 100 pp.; Karlsruhe.

- Renk, A. (1981): Zum Mineralgehalt des Hermanngangs (Südschwarzwald).- unpublished report GLA Baden-Württemberg; 39 pp.; Freiburg i. Br.
- Ritter, J. (1994): Genese der Mineralisation Hermanngang in Albtalgranit (SE-Schwarzwald) und Wechselwirkungen mit dem Nebengestein.- Doctorate Thesis at the University of Karlsruhe, 177 pp; Karlsruhe.
- Rorabaugh M.I. (1964): Estimating changes in bank storage and groundwater contribution in streamflow.- *International Association Scientific Hydro. Publ.* **63**: 432-441.
- Scanlon, B.R., Healy, R.W. & P.G. Cook (2002): Choosing appropriate techniques for quantifying groundwater recharge.- *Hydrogeology J.* (2002) **10**: 18-39; Heidelberg (Springer).
- Schaltegger, U. (2000): U-Pb geochronology of the Southern Black Forest (Central Variscan Belt): timing of exhumation and granite emplacement.- *International J. Earth Sciences* **88**: 814-828.
- Schleicher, H. (1978): Petrologie der Granitporphyre des Schwarzwaldes.- *N. Jahrbuch Mineralogische Abhandlungen* **132/2**: 153-181; Stuttgart.
- Schmidt, G. & D. Plöthner (1999): Grundwasserstudie zum Otavi-Bergland, Namibia.- *Zeitschrift für Angewandte Geologie* **45(3)**-1999: 114-123.
- Schräber, D. & P. Szymak (1984): Zur Ermittlung des Basisabflusses und der Abschätzung dräner Kluftvolumina aus Quellschüttungsmessungen in Festgesteinen.- *Zeitschrift für Angewandte Geologie* **30(3)**-1984: 135-139.
- Schulze-Makuch, D., Carlson, D.A., Cherkauer, D.S. & P. Malik (1999): Scale dependency of hydraulic conductivity in heterogeneous media.- *Ground Water* **37(6)**: 904-919.
- Sealolo, E.T. (1998): Tracer studies and groundwater recharge assessment in the eastern fringe of the Botswana Kalahari – The Letlhakeng – Botlhapatlou area.- 229 pp.; Gaborone, Botswana (Printing & Publishing Company Botswana (Pty) Limited).
- Seiler, K.-P. & S. Wohnlich (eds.): New approaches characterizing groundwater flow Vol. 2, Section Hard rock hydrogeology.- (Proc. of the XXXI IAH Congress held in Munich, Sep. 10-14, 2001), Vol. **2**: 883-1096; Lisse, The Netherlands (Balkema).
- Shevenell, L. (1996): Analysis of well hydrographs in a karst aquifer: estimates of specific yields and continuum transmissivities.- *J. of Hydrology* **174** (1996): 331-355; Amsterdam (Elsevier).
- Stenzel, U. (1997): Hydrochemische Untersuchug und Modellierung im geklüfteten Albtalgranit im Bereich des Erzanges Hermann (Südschwarzwald, Testfeld Lindau).- unpublished M.Sc. Thesis at the Department of Applied Geology, University of Karlsruhe, 86 pp; Karlsruhe.
- Stober, I. & K. Bucher (2000): Herkunft der Salinität in Tiefenwässern des Grundgebirges unter besonderer Berücksichtigung der Kristallinwässer des Schwarzwaldes.- Grundwasser - *Zeitschrift der Fachsektion Hydrogeologie* **3(5)**: 125-140; Heidelberg (Springer).

- Stober, I. (1986): Strömungsverhalten von Festgesteinsaquiferen mit Hilfe von Pump- und Injektionsversuchen.- *Geologisches Jahrbuch Reihe C*, Heft **42**: 3-204.
- Strayle, G., Stober, I. & W. Schloz (1994): Ergiebigkeitsuntersuchungen in Festgesteinsaquiferen.- Geologisches Landesamt Baden-Württemberg (eds.) *GLA-Informationen* **6/94**;114 pp.; Freiburg i. Br.
- Streltsova, T.D. (1988): Well Testing in heterogeneous formations.- Axxon Monograph, 413 pp.; New York. (J. Wiley & Sons).
- Sudicky, E.A. & E.O. Frind (1982): Contaminant transport in fractured porous media: Analytical solutions for a system of parallel fractures.- *Water Resources Research* **18(6)**: 1634 - 1642.
- Tallaksen, L.M. (1995): A review of baseflow recession analysis.- *J. of Hydrology* **165** (1995): 395-370; Amsterdam (Elsevier).
- Tang, D.H., Frind, E.O., Sudicky, E.A. (1981): Contaminant transport in fractured porous media: Analytical solution for a single fracture.- *Water Resources Research* **17(3)**: 555-564.
- TCL - Tsumeb Corporation Limited (1979): Geological map of the Otavi Mountainland on scale 1:100.000.- Ministry of Agriculture, Water and Rural Development/ Department of Water Affairs (archives); Windhoek.
- Theis, C.V. (1935): The relation between the lowering of the piezometric surface and the rate and duration of discharge of a well using groundwater storage.- *American Geophysical Union Trans.* **16**: 519-524.
- Toebe C & D.D. Strang (1964): On recession curves, 1 – recession equations.- *J. Hydrology New Zealand* **3(2)**: 2-15.
- Tordiffe, E., Bufler, R. & R. Bäumle (2001): Groundwater modelling approach to an optimisation of the investigation scheme and first assessment of the groundwater potential of the Tsumeb aquifers, northern Namibia.- (Conference of the Water Association of Namibia: Recent Developments in the Water Sector held in Windhoek, 5th June, 2001), Conference papers: 9-14; Windhoek.
- Toussaint, B. (1981): Ermittlung der Leerlaufkoeffizienten nach Maillet und des effektiv nutzbaren Gesteinhohlraumes in hessischen Flußgebieten durch Auswertung der Abflüsse im Trockenjahr 1976.- *Deutsche Gewässerkundliche Mitteilungen (DGM)* **25**, **3/4**: 70 -83; Koblenz.
- Tsang, C.F., Tsang, Y.W. & F.V. Hale (1991): Tracer transport in fractures: Analysis of field data based on a variable-aperture channel model.- *Water Resources Research* **27(12)**: 3095-3196.
- Tsang, Y.W. (1995): Study of alternative tracer tests in characterising transport in fractured rocks.- *Geophysical Research Letters* **22(11)**: 1421-1424, Washington, D.C.
- Van der Westhuizen, W.A., Tordiffe, E.A., Looek, J.C. & H. de Bruijn (1988): Quaternary karstification and vanadium mineralization in the Otavi Mountain Land, South West Africa/Namibia.- *Palaeocology of Africa and the Surrounding Islands* **19**: 391-403; Rotterdam (Balkema).

- Van Genuchten, M. TH. & W.J. Alves (1982): Analytical solutions of the one-dimensional convective-dispersive solute transport equation.- United States Department of Agriculture - *Agricultural Research Service Technical Bulletin* No. **1661**; 149 pp.; Washington, DC (United States Government Printing Office).
- Verhagen, B.T. (1995): Semiarid zone groundwater mineralization processes as revealed by environmental isotope studies.- (Proc. of the Vienna Symposium, Aug. 1994), *IAHS Publ. no. 232* (1995): 245-266; Wallingford, UK (IAHS Press).
- Verhagen, B.T. (1999): Recharge quantification with radiocarbon: Independent corroboration in three Karoo aquifer studies in Botswana.- Isotope techniques in water resources development and management (Proc. of International Symposium held in Vienna, May 1999): 2-12.
- Veulliet, E.J. (1994): Simulation von Schadstoffmigration im geklüfteten Grundgebirge.- *Schriften Angewandte Geologie Karlsruhe* **28**, 192 S.; Karlsruhe.
- Vogel, J.C., Thilo, L. & M. Van Dijken (1974): Determination of groundwater recharge with tritium.- *J. of Hydrology* **23** (1974): 131-140; Amsterdam (Elsevier).
- Witt, P. (2000): Untersuchung des Fließverhaltens in einem geklüfteten Gestein mittels Laufversuchen, markierungsversuchen und Hydrochemie.- unpublished M.Sc. Thesis at the Department of Applied Geology, University of Karlsruhe, 80 pp.; Karlsruhe.
- Wittenberg, H. & M. Sivapalan (1999): Watershed groundwater balance estimation using streamflow recession analysis and baseflow separation.- *J. of Hydrology* **219** (1999): 20-33; Amsterdam (Elsevier).
- Witthüser, K. (2000): Untersuchungen zum Stofftransport in geklüfteten Festgesteinen unter besonderer Berücksichtigung der Matrixdiffusion.- Doctorate Thesis at the University of Karlsruhe, 145 pp.; Karlsruhe.
- Wrabel, J. (1999): Ermittlung der Grundwasserneubildung im semiariden Bereich Namibias mittels der Chlorid-Bilanz-Methode.- *HU-Forschungsergebnisse aus dem Bereich Hydrogeologie und Umwelt* **6**; 155 pp.; Würzburg.

APPENDICES

Appendix 1 Results of well hydrograph recession analysis according to Method 1

Borehole	Elevation of spring outlet [m a.s.l.]					Mean residence time τ [d]				
	n	Min	Max	Mean	σ	n	Min	Max	Mean	σ
Bl. 12	2	875.3	878.4	876.9	1.6	2	8	13	11	3
Bl. 3	1	874.6	874.6	874.6	N/A	1	18	18	18	N/A
B 42S	1	868.4	868.4	868.4	N/A	1	21	21	21	N/A
B 77E	1	870.8	870.8	870.8	N/A	1	23	23	23	N/A
Östu I	1	870.8	870.8	870.8	N/A	1	23	23	23	N/A
Bl. 11	0	N/A	N/A	N/A	N/A	0	N/A	N/A	N/A	N/A
B 74E	2	878.0	878.4	878.2	0.2	2	24	48	36	12
B 68E	2	887.5	891.0	889.3	1.8	2	25	83	54	29
B 64S	4	919.3	926.9	921.7	3.0	4	20	74	48	22
B 64E	5	875.5	876.2	875.9	0.3	5	29	72	45	16
B 62E	5	874.2	876.5	875.4	1.0	5	25	96	59	27
B 63E	6	875.3	876.4	875.8	0.4	6	22	85	52	22
B 67S	3	901.9	903.0	902.5	0.5	3	48	65	57	7
B 69S	3	913.2	914.8	914.0	0.7	3	45	125	80	33
B 70E	1	876.6	876.6	876.6	N/A	1	66	66	66	N/A
B 69E	3	878.8	879.1	879.0	0.1	3	55	87	74	13
B 65S	5	915.2	921.1	917.5	2.0	5	32	89	67	25
B 66S	1	907.4	907.4	907.4	N/A	1	113	113	113	N/A
B 94S	4	930.4	935.7	933.4	2.0	4	68	149	107	32
Bl. West	2	923.6	93N/A	926.8	3.2	2	118	142	130	12
B 129S	2	879.1	920.9	N/A	20.9	2	60	161	110	51
B 81E	3	892.2	895.6	893.6	1.5	3	85	188	140	42
B 95S	4	916.9	938.9	932.5	9.1	4	65	452	176	160
B 82E	3	887.2	890.7	888.7	1.5	3	189	321	240	58
B 80E	4	890.7	893.0	891.9	0.9	4	149	232	198	31
B 127S	4	927.3	932.3	930.1	2.0	4	208	343	275	57
B 130S	6	915.6	920.9	918.7	2.0	6	178	434	280	89
B 4S	3	872.9	883.8	878.6	4.5	3	315	460	371	64
B 131S	5	911.6	922.3	916.0	4.4	5	187	639	420	174
B 132S	5	855.7	913.8	887.3	23.4	5	56	1026	393	351
B 128S	3	908.3	932.9	919.9	10.1	3	112	783	506	286
B 30E	1	N/A	N/A	N/A	N/A	1	637	637	637	N/A

Appendix 2 Results of well hydrograph recession analysis according to Method 2

Borehole	Elevation of spring outlet [m a.s.l.]					Mean residence time τ [d]				
	n	Min	Max	Mean	σ	n	Min	Max	Mean	σ
Bl. 12	1	875.0	875.0	875.0	N/A	1	18	18	18	N/A
Bl. 3	0	N/A	N/A	N/A	N/A	0	N/A	N/A	N/A	N/A
B 42S	1	868.4	868.4	868.4	N/A	1	28	28	28	N/A
B 77E	1	870.7	870.7	870.7	N/A	1	27	27	27	N/A
Östu I	1	875.4	875.4	875.4	N/A	1	42	42	42	N/A
Bl. 11	1	874.9	874.9	874.9	N/A	1	39	39	39	N/A
B 74E	3	877.7	878.5	878.0	0.4	3	24	57	45	15
B 68E	2	888.9	889.5	889.2	0.3	2	28	32	30	2
B 64S	4	917.7	920.4	919.5	1.0	4	21	62	47	16
B 64E	6	875.3	876.1	875.8	0.3	6	31	82	50	17
B 62E	7	875.5	876.9	876.3	0.5	7	28	69	42	14
B 63E	6	874.6	876.4	875.8	0.6	6	30	90	52	20
B 67S	6	901.1	906.7	903.0	1.8	6	29	68	54	13
B 69S	6	913.6	916.0	914.8	0.8	6	18	114	51	34
B 70E	1	876.6	876.6	876.6	N/A	1	64	64	64	N/A
B 69E	4	877.7	879.4	878.9	0.7	4	57	83	71	11
B 65S	5	912.9	921.1	916.6	2.8	5	33	128	79	36
B 66S	3	898.9	908.5	904.9	4.3	3	52	136	102	36
B 94S	4	923.9	933.6	930.7	3.9	4	96	220	141	48
Bl. West	0	N/A	N/A	N/A	N/A	0	N/A	N/A	N/A	N/A
B 129S	1	N/A	N/A	N/A	N/A	1	195	195	195	N/A
B 81E	3	891.4	893.2	892.3	0.7	3	136	201	175	28
B 95S	4	916.7	938.7	930.4	8.5	4	74	411	172	138
B 82E	3	891.3	893.3	892.3	0.8	3	109	228	159	51
B 80E	4	890.8	892.6	891.8	0.7	4	162	284	211	51
B 127S	4	928.9	934.8	931.9	2.1	4	106	329	222	79
B 130S	4	915.5	923.3	92N/A	3.3	4	117	426	248	128
B 4S	4	874.3	894.4	882.0	7.9	4	102	437	317	131
B 131S	4	916.8	920.4	918.0	1.4	4	247	366	324	48
B 132S	4	826.8	911.9	886.7	34.8	4	64	1338	433	524
B 128S	1	932.3	932.3	932.3	N/A	1	132	132	132	N/A
B 30E	0	N/A	N/A	N/A	N/A	0	N/A	N/A	N/A	N/A

Appendix 3 Hydrochemical data

Site	Date	T [°C]	pH	EC [µS/cm]	O ₂ [mg/l]	Na [mg/l]	K [mg/l]	Mg [mg/l]	Ca [mg/l]	Sr [mg/l]	Fe [mg/l]	Ba [mg/l]	F [mg/l]	Cl [mg/l]	SO ₄ [mg/l]	NO ₃ [mg/l]	PO ₄ [mg/l]
Bl. 15	15.07.1999					2.44	0.30	0.50	6.88	0.228		0.05	0.90	0.94	1.59	<0.02	<0.03
Bl. 17	08.04.1999	6.1	6.3		11.3	2.00	0.65	0.44	4.76	0.038	<0.25	0.23	0.27	0.94	1.80	2.95	<0.03
Bl. 17	09.04.1999	6.1	6		10.9	2.02	0.59	0.41	4.76	0.030		0.18	0.25	0.87	1.47	4.95	<0.03
Bl. 17	10.04.1999	6.1	5.9		11.5	2.06	0.59	0.41	4.70	0.029		0.17	0.23	0.87	1.46	5.27	<0.03
Bl. 17	13.04.1999	6.1	5.9	27.3	11.1	1.98	0.81	0.40	4.56	0.029		0.17	0.23	0.92	1.47	5.25	<0.03
Bl. 17	14.04.1999	6.1	5.9	24.8	10.8	1.90	0.54	0.38	4.00	0.026		0.17	0.23	0.81	1.50	4.28	<0.03
Bl. 17	15.04.1999	6.1	5.9	24.7	11.3	1.78	0.57	0.36	3.78	0.026	<0.25	0.17	0.29	0.81	1.84	4.47	<0.03
Bl. 17	20.04.1999	6.5		30.9	10.4	1.92	0.60	0.41	4.70	0.030		0.20	0.25	0.87	1.54	5.22	<0.03
Bl. 17	21.04.1999	6.1	5.7	25.6	10.4	2.00	0.66	0.39	4.18	0.027		0.18	0.26	0.99	1.58	4.35	<0.03
Bl. 17	22.04.1999	6.1	5.3	25.2	11.4	1.94	0.53	0.38	4.10	0.025		0.18	0.28	0.84	1.58	3.52	<0.03
Bl. 17	23.04.1999	6.1	5.2	25	10.9	2.08	0.60	0.38	4.02	0.026		0.18	0.29	0.97	1.59	3.07	<0.03
Bl. 17	24.04.1999	6.1	5.3	24.9	10.6	2.28	0.68	0.38	3.94	0.025		0.18	0.31	1.02	1.53	3.07	<0.03
Bl. 17	25.04.1999	6.1	5.3	24.8	10.2	1.88	0.61	0.36	3.80	0.025	<0.25	0.18	0.37	0.89	1.74	3.53	<0.03
Bl. 17	26.04.1999	6.1	5.2	24.7	10.3	2.18	0.62	0.37	3.80	0.025		0.18	0.32	0.92	1.44	3.11	<0.03
Bl. 17	28.04.1999	6.1	5	24.8	10	2.24	0.68	0.37	3.86	0.024		0.18	0.34	1.01	1.52	2.60	<0.03
Bl. 17	02.05.1999	6.1	5.5	24.9		2.26	0.58	0.37	3.78	0.024		0.18	0.34	0.87	1.50	2.76	<0.03
Bl. 17	06.05.1999	6.1	6.1	24.9		2.24	0.57	0.36	3.84	0.024		0.19	0.34	0.88	1.55	2.56	<0.03
Bl. 17	14.05.1999	6.1	5.8	25.4	11.5	2.39	0.65	0.36	3.78	0.023	<0.25	0.19	0.44	1.10	1.67	3.07	<0.03
Bl. 17	16.05.1999	6.1				2.38	0.57	0.36	3.94	0.024		0.20	0.35	0.86	1.49	2.72	<0.03
Bl. 17	17.05.1999	6.1	6	25.4	11.4	2.46	0.59	0.37	4.00	0.023		0.20	0.35	0.87	1.44	2.59	<0.03
Bl. 17	20.05.1999	6.1	6.1	25.6	11.8	2.20	0.58	0.37	4.00	0.024		0.21	0.36	0.84	1.49	2.46	<0.03
Bl. 17	25.05.1999	6.1	5.7	25.2	9.4	2.32	0.58	0.36	3.82	0.023		0.21	0.35	0.87	1.49	2.52	<0.03
Bl. 17	01.06.1999	6.1	6.3	25.2	11.7	2.38	0.57	0.36	3.86	0.022		0.22	0.38	0.89	1.53	2.57	<0.03
Bl. 17	17.06.1999	6.2		26.7	10.6	2.54	0.57	0.38	4.20	0.023		0.23	0.48	0.92	1.45	2.23	<0.03
Bl. 17	25.06.1999	6.2		27.7		2.50	0.57	0.38	3.78	0.025	<0.25	0.27	0.58	0.87	1.59	1.99	<0.03
Bl. 17	30.06.1999	6.3		28.1		2.58	0.55	0.40	4.46	0.025		0.26	0.56	0.92	1.46	2.25	<0.03
Bl. 17	10.07.1999	6.3	6.3	28.6	10.8	2.66	0.56	0.41	4.56	0.025		0.28	0.59	0.92	1.49	2.20	<0.03
Bl. 17	15.07.1999	6.3	6.4	29	10.7	2.66	0.58	0.40	4.52	0.025		0.29	0.59	0.91	1.41	1.83	<0.03
Bl. 17	22.07.1999	6.3	6.2	28.4	10.7	2.70	0.64	0.41	4.62	0.025		0.29	0.57	0.90	1.43	2.32	<0.03
Bl. 17	28.07.1999	6.1	6.2	28.5		2.70	0.59	0.40	4.58	0.024		0.27	0.57	0.91	1.44	1.97	<0.03
Bl. 17	04.08.1999	6.2				2.72	0.59	0.40	4.48	0.024		0.28	0.58	0.94	1.40	1.48	<0.03
Bl. 17	17.08.1999	6	6.2	29.5		2.66	0.57	0.41	4.74	0.025		0.30	0.62	0.90	1.45	1.93	<0.03
Bl. 17	30.08.1999	6.2		30	11.1	2.72	0.54	0.45	5.24	0.028		0.33	0.76	0.92	1.71	2.36	<0.03
Bl. 17	09.09.1999	6.5	6.3	30.5	10.7	2.81	0.56	0.41	4.86	0.026	<0.25	0.33	0.64	0.94	2.18	2.55	<0.03
Bl. 17	08.10.1999	7				2.80	0.53	0.46	5.44	0.027		0.38	0.76	0.92	1.71	2.36	<0.03
Bl. 17	28.10.1999					3.64	0.64	0.49	5.33	0.033		0.38	0.77	1.09	2.04	1.53	<0.03
Bl. 17	05.11.1999					2.97	0.72	0.54	7.56	0.038		0.40	0.72	1.06	1.76	<0.02	<0.03
Bl. 17	16.11.1999					4.52	0.78	0.50	5.36	0.035		0.39	0.73	1.19	2.63	<0.02	<0.03
Bl. 17	08.12.1999					2.91	0.61	0.49	5.29	0.035		0.40	0.82	1.01	1.80	<0.02	<0.03
Bl. 17	20.12.1999					2.62	0.57	0.46	4.58	0.031		0.33	0.52	0.80	1.66	<0.02	<0.03
Bl. 17	29.12.1999					2.44	0.55	0.41	4.10	0.032		0.30	0.46	0.88	1.66	<0.02	<0.03
Bl. 17	06.01.2000					2.40	0.57	0.40	3.97	0.030		0.28	0.44	0.94	1.67	<0.02	<0.03
Bl. 17	12.01.2000					2.40	0.57	0.39	3.95	0.027		0.27	0.43	0.94	1.72	<0.02	<0.03
Bl. 17	19.01.2000					2.42	0.55	0.40	3.90	0.026		0.27	0.50	1.00	1.65	<0.02	<0.03
Bl. 17	04.02.2000					2.58	0.61	0.42	4.11	0.028		0.29	0.56	1.01	1.61	<0.02	<0.03
Bl. 17	17.02.2000					2.49	0.68	0.40	3.84	0.028		0.27	0.47	1.03	1.85	0.27	<0.03
Bl. 17	23.02.2000					2.40	0.59	0.39	3.94	0.025		0.26	0.43	0.91	1.75	<0.02	<0.03
Bl. 17	17.03.2000					2.47	0.64	0.38	3.88	0.025		0.26	0.40	0.99	1.92	1.73	<0.03
Bl. 17	24.03.2000					2.73	0.85	0.39	3.86	0.028		0.29	0.41	1.23	1.75	2.18	<0.03
Bl. 17	18.05.2000					2.69	0.58	0.43	4.26	0.028		0.30	0.53	0.99	2.46	2.08	<0.03
Bl. 18	15.07.1999					2.56	0.32	0.43	5.64	0.198		0.05	0.74	0.88	1.39	0.37	<0.03
Bl. 19	15.07.1999					3.18	0.26	1.24	14.00	0.157		0.08	0.37	0.84	2.53	<0.02	<0.03
Bl. 20	15.07.1999					3.18	0.26	2.96	18.40	0.138		0.10	0.25	0.99	2.11	0.68	<0.03
Bl. West	15.07.1999					3.75	0.18	0.99	16.40	0.226		0.18	0.57	0.91	3.60	1.51	<0.03
Pluviograph	20.05.1999					0.35	0.03	0.04	0.29				0.03	0.95	0.82	1.44	<0.03
Pluviograph	25.05.1999					0.22	0.01	0.04	0.26				0.06	0.63	1.21	2.01	<0.03

Note: Pluviograph was installed at Lindau near the *Schwarze Säge*

Appendix 4 Aquifer characterisation from pumping test analysis

Well	Stratigraphy	Lithology	Aquifer characterisation
WW39971	Nosib Group	Sand-/siltstone, pyroclastics, quartzite, weathered volcanics	Fractured Aquitard. Low permeable fractured rock.
WW39972	Nosib Group	Faulted and weathered quartzite	Fractured Aquitard. Fault zone acts as a vertical conduit within low permeable fractured rock. Permeability of adjacent formation presumably increased due to fracturing compared to undisturbed rock.
WW39973	Elandshoek Formation	Fractured dolomite	Homogeneously fractured aquifer. High yielding and high permeable formation.
WW39974	Hüttenberg Formation	Fractured, locally karstified dolomite	Homogeneously fractured and locally karstified aquifer. High yielding and high permeable formation.
WW39975	Chuoss Formation	Fractured partially weathered sandstone, clay	Fractured aquitard. Evaluation suggests leakage from higher permeable dolomitic rock. Double porosity characteristic is less plausible but cannot be fully disregarded. Sharp decrease in permeability below ~60 m b.g.s.
WW39977	Maieberg Formation	Mainly fractured limestone	Fractured Aquifer. Fault zone acts as a vertical conduit. Length of hydraulically active zone appears to be much smaller than the length of the lineament determined from geophysical data.
WW39980	Kalahari Group/ Karoo Sequence	Weathered sandstone/ arkose, minor: shale and clay	Aquitard, but evidence of lateral heterogeneity.
WW39983	Hüttenberg Formation	Fractured dolomite, fracture/ fault zone.	Fractured aquifer. Evaluation assuming leakage (possibly from adjacent water-bearing fractured or karstified layer or zone) results in best fitting. Alternatively, a single fracture or a double porosity model with considerable fracture skin may be assumed
WW39984	Mulden Group (0-224m)	Fractured sandstones, siltstone, clay(?)	Fractured aquitard. Fault zone acting as a vertical conduit within low permeable fractured rock. Evaluation suggests bilinear rather than linear flow field indicating a finite conductive vertical fracture zone.
WW39984	Hüttenberg Formation (256-335m)	Fractured dolomite	Homogeneously fractured aquitard. Transmissivity of Hüttenberg at this depth reduced by a factor of >100 compared to surface exposed dolomite. Evaluation suggests leakage from overlying Mulden Group sediments.
WW39986	Hüttenberg Formation	Intensively fractured dolomite ("cave breccia") with karstified zones, on top of Tsumeb dyke	Intensively fractured and locally karstified aquifer. High yielding and high permeable formation. Evaluation assuming leakage, possibly from adjacent water bearing fractured or karstified layer or zone.
WW39988	Kalahari Group/ Karoo Sequence	Weathered sandstone/ arkose and mudstone/ claystone	Aquitard, but evidence of lateral heterogeneity.

Well	Stratigraphy	Lithology	Aquifer characterisation
WW39989	Maieberg Formation (0-247m)/ Auros Formation (247-280m)	Fractured dolomite and limestone with interbedded shale	Fractured Aquitard. Fault zone acting as a vertical conduit within low permeable fractured rock. Strongly dipping layers consisting of shale in the vicinity (~120m southward) may act as a barrier boundary.
WW39990	Grootfontein Basement Complex	Quartzite, gneiss (?)	Aquiclude. Virtually impermeable rock.
WW39991	Nosib Group	Fractured and slightly weathered sandstone, shale	Fractured Aquitard. Evaluation suggests a horizontal fracture zone, which acts as a conduit. Permeability of adjacent formation presumably increased due to fracturing compared to undisturbed rock. Sharp decrease in yield (and permeability) below the main water strike.
WW39992	Hüttenberg Formation	Intensively fractured dolomite, fault zone hosting water strike (on top of Tsumeb dyke)	High permeable fractured aquifer. High yielding formation with large storage coefficient. Bilinear flow indicating fracture zone at early times. Evaluation suggests leakage at late times (possibly from another (adjacent) water-bearing fractured or karstified zone.
WW40000	(Upper) Auros Formation, 0-150m	Fractured dolomite, interbedded shale and limestone	Fractured Aquifer. Either homogeneously fractured rock or finite conductive fracture zone with considerable storage properties (no clear distinction possible from evaluation)
WW40000	(Lower) Auros Formation, 187-400m	Fractured dolomite, limestone and shale	Fractured Aquitard. Permeability of Abenab Subgroup sediments considerably decreases with depth.

Roland Bäumle

geboren am 8. September 1967 in Kehl

Abriß des Lebens- und Bildungsganges

Sept. 1974 – Mai 1987	Schulausbildung mit Abschluss der Allgemeinen Hochschulreife am Einstein- Gymnasium in Kehl
Okt. 1987 – Sept. 1988	Wehrdienst
Okt. 1988 – Apr. 1995	Studium in Fachrichtung Hydrologie mit Abschluss Diplom-Hydrologe am Lehrstuhl für Hydrologie der Universität Freiburg i.Br.
Sept. 1991 – Aug. 1992	Auslandsstudienaufenthalt an der <i>University of British Columbia</i> , Vancouver (Kanada).
Mai 1995 – Juli 1995	Wissenschaftliche Hilfskraft am Lehrstuhl für Hydrologie, Universität Freiburg i.Br.
Aug. 1995 – Apr. 1997	Mitarbeiter der Abteilung Hydrogeologie, igi Niedermeyer Institute (Beratende Ingenieure), Westheim
Mai 1997 – Apr. 2000	Promotionsstudent im Rahmen des Graduiertenkollegs <i>Ökologische Wasserwirtschaft</i> an der Universität Kalsruhe (TH)
Mai 2000 – Aug. 2001	Wissenschaftlicher Angestellter am Lehrstuhl für Angewandte Geologie, Universität Karlsruhe (TH)
seit Sept. 2001	Mitarbeiter in der <i>Geohydrology Division</i> am <i>Ministry of Agriculture, Water and Rural Development</i> in Windhoek, Namibia